



Bottlebrush polymers: From controlled synthesis, self-assembly, properties to applications

Zili Li^{a,b}, Miao Tang^b, Shuang Liang^a, Mingyue Zhang^a, Gill M. Biesold^a, Yanjie He^a,
Shu-Meng Hao^a, Woosung Choi^a, Yijiang Liu^a, Juan Peng^{b,*}, Zhiqun Lin^{a,*}

^a School of Materials Science and Engineering, Georgia Institute of Technology, Atlanta, GA 30332, United States

^b State Key Laboratory of Molecular Engineering of Polymers, Department of Macromolecular Science, Fudan University, Shanghai 200438, China

ARTICLE INFO

Article history:

Received 11 September 2020

Revised 3 December 2020

Accepted 8 March 2021

Available online 10 March 2021

Keywords:

Bottlebrush polymer

Controlled radical polymerization

1D Cylindrical morphology

Grafting density

Self-assembly

Structure-property relationship

ABSTRACT

Bottlebrush polymers (BBPs) have emerged as intriguing class of materials for an array of applications, including supersoft elastomers, organic optoelectronics, templates for crafting one-dimensional (1D) nano-materials, energy storage, and biomedical devices. The densely-grafted side chains along the linear backbones afford BBPs with extended cylindrical shapes and the absence of entanglements. The architectures of BBPs can be readily tuned by manipulating the chemical structures and compositions, both of which govern the viscoelastic properties, melt processability, and alignment of BBPs. This enables the crafting of BBPs with controlled dimensions, compositions, and architectures by capitalizing on advanced synthetic techniques. However, challenges remain in the synthesis and applications of BBPs with precisely controlled architectures. This review aims to provide a comprehensive and critical summary that highlights the recent advances in BBPs in terms of their controlled syntheses, self-assembly, properties, and applications. In addition, challenges facing the syntheses and applications of BBPs will be underscored, with the corresponding solutions to these issues for improving the control over chemical structures (e.g., introducing conjugated side chains), compositions (e.g., other than the widely used polynorbornene or polyacrylate backbone), and utilities (e.g., as solid-state electrolyte in energy storage devices) of BBPs.

© 2021 Elsevier B.V. All rights reserved.

Abbreviations: AGET, activators generated by electron transfer; ATRP, atom transfer radical polymerization; AFM, atomic force microscopy; APTS, 3-acryloylpropyltrimethoxysilane; BCPs, block copolymers; BBPs, bottlebrush polymers; BBCPs, bottlebrush block copolymers; CTA, chain transfer agent; CRP, controlled radical polymerization; CTC, charge-transfer complex; cryo-TEM, Cryogenic transmission electron microscopy; CESA, controlled evaporative self-assembly; CANS, covalent adaptable networks; DP, degree of polymerization; CuAAC, Copper(I)-catalyzed azide-alkyne cycloaddition; ETL, electron-transport layers; EML, emissive layer; FRET, fluorescence resonance energy transfer; GI-SAXS, grazing-incidence small-angle X-ray scattering; GI-WAXS, Grazing-incidence wide-angle X-ray scattering; HTL, hole-transport layers; IPEC, ionic polyelectrolyte complexation; LB, Langmuir Blodgett; LCST, lower critical solution temperature; LUB, lubricin; MW, molecular weight; MASA, meniscus-assisted self-assembly; NMP, nitroxide-mediated radical polymerization; NMR, nuclear magnetic resonance; NCA, N-carboxyanhydride; NHS, N-hydroxysuccinimide; NVP, N-vinylpyrrolidone; OLEDs, organic light-emitting diodes; ORR, oxygen reduction reaction; 1D, one-dimensional; PCs, photonic crystals; POSS, polyhedral oligomeric silsesquioxane; PS, polystyrene; PNB, polynorbornene; PBA, poly(butyl acrylate); PLL, poly(L-lysine); PLA, poly(lactic acid); PNIPAM, poly(N-isopropylacrylamide); PCL, poly(ϵ -caprolactone); PrBA, Poly(*t*-butyl acrylate); PDMAEMA, poly(dimethylaminoethyl methacrylate); PAA, polyacrylic acid; PPFA, poly(pentafluoropropyl acrylate); PEGMEMA, poly(ethylene glycol) methyl ether methacrylate; PCMS, poly(*p*-chloromethylstyrene); PDMA, poly(dimethylacrylamide); PANI, polyaniline PLG, poly(L-glutamic acid); P4VP, poly(4-vinylpyridine); PG, polyglycidol; PEG, polyethylene glycol; PDMS, poly(dimethylsiloxane); PDA, polydopamine; PET, photo-electron

1. Introduction

Bottlebrush polymers (BBPs) represent an important class of high-density side-chain-grafted polymers with high molecular weights (MWs), in which one or more polymeric side chains are tethered to each repeating unit of a linear polymer backbone, such that these macromolecules look like “bottlebrushes” [1]. BBPs with various architectures (e.g., random (heterografted), bottlebrush block copolymers (BBCPs), cor-shell, Janus, brush-on-brush, etc.) have been created with commonly used the “grafting-from,” “grafting-through,” and “grafting-to” approaches (Fig. 1). Notably,

transfer; P3HT, poly(3-hexylthiophene); ROP, ring-opening polymerization; ROMP, ring-opening metathesis polymerization; RDRP, reversible deactivation radical polymerization; RAFT, reversible addition-fragmentation chain transfer; SAXS, small angle X-ray scattering; SAM, sequential-addition of macromonomers; SPE, solid polymer electrolyte; TEMPO, 2,2,6,6-tetramethylpiperidine-1-oxyl; TAD, triazolinodione; TMOS, tetramethyl orthosilicate; TFA, trifluoroacetic acid; TSCT, through-space charge transfer; 2D, two-dimensional; VOAc, vinyl acetate; 0D, zero-dimensional.

* Corresponding authors.

E-mail addresses: juanpeng@fudan.edu.cn (J. Peng), zhiqun.lin@mse.gatech.edu (Z. Lin).

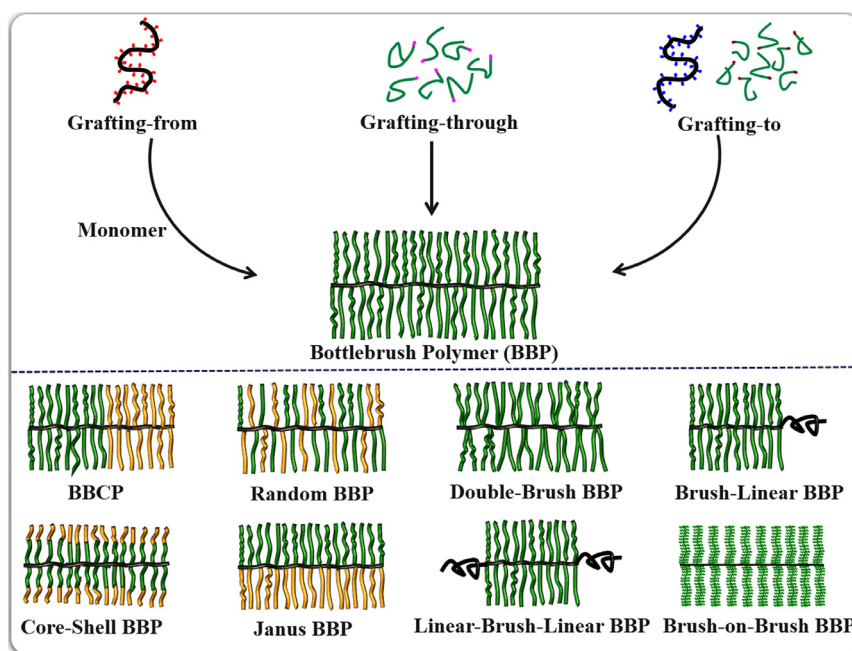


Fig. 1. An illustration of the main approaches for the synthesis of BBPs and advanced architectures of BBPs.

both BBCPs and cor-shell BBPs can be regarded as bottlebrush copolymers, while homopolymer BBPs contain one type of backbone and side chain. In cases where grafting does not occur at every repeating unit, BBP-like polymers with low grafting density (σ) are considered as comb-like polymers [2]. In particular, Janus BBPs can be crafted by asymmetrically attaching two different polymer chains to one repeating unit along a polymer backbone [3]. Notably, cylindrical micelles can be obtained by self-assembly of linear block copolymers (BCPs) in selective solvents [4–7]. Although in some reviews, the latter two types of brush polymers (i.e., comb-like polymers (with the crowding parameter, $\Phi < 1$), [8] and cylindrical micelles assembled by linear polymers) are also referred as BBPs, they are beyond the scope of this review. In this review, the discussion is limited to “ideal” BBPs. It is noteworthy that the side chain length (i.e., degree of polymerization (DP) of side chain, n_{sc}) of the BBP should be shorter than the backbone length (DP of backbone, n_{bb}), such that it can exhibit a one-dimensional (1D) cylindrical morphology [9]. It is possible to visualize this single molecular bottlebrush (i.e., cylindrical morphology) with atomic force microscopy (AFM) [1,10]. The densely-packed polymeric side chains of the BBPs experience significant steric repulsion, because of which the BBPs form extended cylindrical shapes (i.e., rigid backbone, $n_{bb} < b/l_m$, see Section 3.2) [8]. This steric repulsion renders a unique feature to the BBPs, i.e., the absence of entanglement (much lower backbone entanglement density that can be ignored), which dictates the viscoelastic properties and molecular alignment of BBPs. In addition, this intriguing characteristic also endows BBPs with distinctive mechanical and rheological performances (e.g., low entanglement plateau modulus), crystalline abilities (e.g., fast crystal nucleation and slow growth), and stimuli-responsive behaviors (e.g., various morphological transformation).

The distinct molecular architectures and tunable structural parameters (e.g., grafting density and, DP of the backbone and side chain) of BBPs impart them with substantially different properties and behaviors from those of the linear polymers, which lead to unique self-assembly behaviors in solution and bulk states. BBPs have been observed to self-assemble into spherical, [11] worm- or rod-like, [12,13] lamellar, [14,15] and other structures [16,17]. These self-assembled conformations can also be tailored by various exter-

nal stimuli. BBPs have been widely used as unimolecular templates to prepare 1D organic nanotubes, [18] inorganic nanostructures (e.g., nanorods, core-shell nanorods, and nanotubes), [12,19] and hybrid nanocomposites [20]. In addition, lack of entanglements significantly reduces the entanglement plateau modulus, which renders the BBPs as excellent alternative polymers to yield superelastic elastomers [21]. Optoelectronic materials based on diblock BBPs have been achieved by engineering the branches with hole- and electron-transporting moieties on their blocks respectively, affording 1D nanoobjects with two different transporting parts that resemble the device configuration in advanced white organic light-emitting diodes (OLEDs) [22]. Additionally, the intrinsic 1D conformations of BBPs and the corresponding shape-regulated materials can facilitate electron/charge transport, and therefore, these have been used as solid electrolytes to improve the transference numbers and electrochemical performances [23,24]. Furthermore, owing to their high MWs and highly extended backbones, bottlebrush block copolymers have been observed to self-assemble into large-domain lamellar nanostructures in films or confined spaces, which have been used as photonic crystals (PCs) [15]. Notably, most of these applications are based on the unique 1D cylindrical shapes of BBPs. Controlled radical polymerization (CRP) of highly tailorable functional building blocks is a highly effective strategy to craft BBPs with well-defined 1D cylindrical architectures [25,26].

This review highlights the recent achievements of BBPs including their controlled syntheses, self-assembly, properties, and applications. First, the design principles of BBPs are presented to introduce the BBPs with a variety of intriguing morphologies. Subsequently, the construction of well-controlled BBPs with diverse sub-architectures via the current synthetic techniques and strategies is critically examined. Particularly, the emerging strategies that are simple as well as time- and cost-effective are described, including (i) photo-mediated reversible deactivation radical polymerization and (ii) programmable flow chemistry. Then, self-assembled architectures of BBPs, and their unique physical (e.g., crystalline and stimuli-responsive), mechanical, and rheological properties in both solution and bulk states are reviewed. Thereafter, the applications (e.g., templates, elastomers, organic optoelectronic materials, energy storage, biomedical fields, etc.) of BBPs with dif-

ferent compositions and structures are described. Finally, after a brief summary, an outlook for the prospective studies on BBPs is presented. The challenges facing the synthesis and applications of BBPs are discussed, followed by the corresponding solutions to improve the control over chemical structures, compositions, and utilities of BBPs.

2. Synthesis of bottlebrush polymers

2.1. Design principle of bottlebrush polymers

The DP of the backbone and side chain, as well as grafting density, are crucial to controlling the sizes of the BBP macromolecules; these can form cylindrical morphology because of the steric repulsions among the attached brushes. Specifically, the BBP backbone should be significantly longer than that of its side chain to yield a cylindrical morphology [27–29]. Inversely, if the size of side chain is comparable to that of the backbone, a spherical topology resembling a star-like polymer is obtained [28,30]. Grafting density is the number of side chains per repeating unit. For clarification, each monomeric unit can theoretically carry one side chain with 100% grafting density. It is worth noting that grafting density should have the same value as initiation efficiency in the “grafting-from” approach. Grafting density affects the crowding among the side chains which determines the steric repulsions. Therefore, appropriate control of all parameters during BBP synthesis is key to controlling the final architecture. BBPs with well-defined structures, desired functional groups, and controlled MWs have been synthesized using various advanced controlled/living polymerization techniques (e.g., CRP, [26] controlled anionic/cationic polymerization, [31,32] ring-opening polymerization (ROP), [33] ring-opening metathesis polymerization (ROMP), [34] and click reactions [35]). BBPs can be typically obtained through three main synthetic approaches (Fig. 1): (1) “grafting-from” (polymerization of monomers from the polyinitiators in the backbone), (2) “grafting-through” (polymerization of the macromonomers), and (3) “grafting-to” (attachment of the pre-prepared side chains to the backbone).

While each of the three strategies possesses inherent advantages and disadvantages, no single approach can effectively control all structural parameters such as the grafting density, length, and composition. By combining different CRP techniques with other strategies, novel BBPs with advanced molecular architectures have been constructed (Table 1). An array of BBP molecular architectures bearing two different side chains can be produced to form BBCPs or random bottlebrush copolymers. Generally, each repeating unit contains a single side chain. However, it is possible to attach two polymeric side chains on each backbone repeating unit, generating double-brush (sometimes called barbwire [36]) copolymers with identical or different characteristics (Janus BBPs) [3]. The doubly substituted side chains have bulky volumes which dramatically enhance the stiffness of the backbone [1]. Linear polymer chains can be covalently bonded to the bottlebrush backbone end(s) to form brush-linear (attached at one end) or linear-brush-linear (attached at both ends) block copolymers. Core-shell BBPs can also be synthesized by attaching diblock copolymer side chains to the backbone. Most BBPs contain side chains with a spacing of two C-C bonds in the backbone owing to the characteristics of vinyl-based (macro)monomers. To further increase the steric repulsion among the side chains, brush polymers have been grafted onto the side chains to form brush-on-brush copolymers.

2.2. Synthetic techniques for bottlebrush polymers

Conventional radical polymerization is a widespread and robust technique to synthesize polymers because of its facile implementation, low cost, good tolerance to polar and active func-

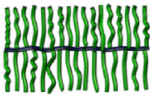
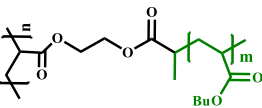
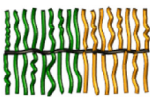
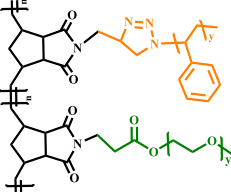
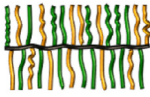
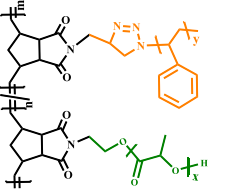
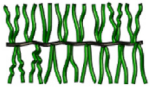
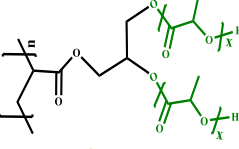
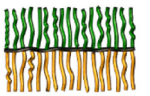
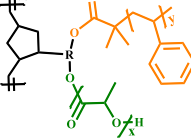
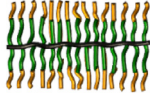
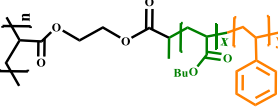
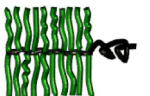
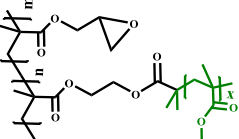
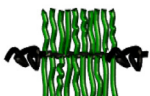
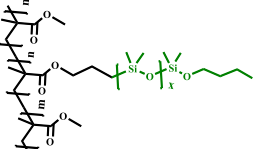
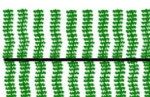
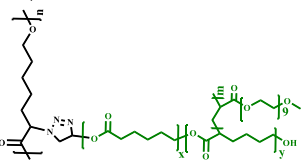
tional groups or impurities, and mild reaction conditions [37]. BBPs have been prepared by free radical polymerization of acrylate macromonomers [38]. However, the relatively poor control over the MW, molecular weight distribution of polymers, termed dispersity ($\bar{D} = M_w/M_n$), and chain-end functionality hindered further applications of these BBPs. MW and \bar{D} are the key factors regulating the structures and performances of the polymers. CRP is based on reversible deactivation radical polymerization (RDRP), forming active and dormant states during the polymer propagation process [26]. CRP techniques (i.e., atom transfer radical polymerization (ATRP), reversible addition-fragmentation chain transfer (RAFT) polymerization, and nitroxide-mediated radical polymerization (NMP)) have been extensively employed to prepare various state-of-the-art well-defined molecular architectures that are beneficial for the synthesis of precisely designed BBPs [26].

ATRP typically involves chain initiation and propagation from the end halide groups via a radical mechanism with catalysis using transition metal halides and organic ligands. The periodical transformation of active and dormant species are generated by the reaction with activators (i.e., CuX) and produced deactivators (i.e., CuX₂), achieving the control of polymerization [39]. RAFT polymerization proceeds through a degenerative chain transfer process, in which the propagating species equilibrate with the dormant species [40]. Generally, the RAFT chain transfer agents (CTAs) could be tethered onto polymer backbone through the Z-group approach where the stabilizing CTA group is covalently bonded to the backbone or the R-group approach where the CTAs are attached to the main chain via the reinitiating group [41]. Notably, the direction of attachment of the CTA leads to very different outcomes in the grafting step (e.g., attachment of the R group leads to the “grafting-from” approach, and attachment of the Z-group results in the “transfer-to” approach). NMP is governed by the reversible termination process between the propagating (macro)radicals and predominant species (e.g., 2,2,6,6-tetramethylpiperidine-1-oxyl (TEMPO)). The polymerization rate is dominated by the excess nitroxide radicals after the initiation process because of the dynamic balance of polymerization [42]. Living anionic/cationic polymerization is achieved via the long-lived anionic/cationic species [32,43]. The key to achieving living ionic polymerization is controlling the equilibria between the active (ionic) and dormant (covalent) species [32]. ROMP involves the opening of cyclic olefin and the recombination of unsaturated bonds. The obtained polymer has unsaturated bonds in every repeating unit of the main chain, this key feature is different from the conventional polymers synthesized via radical polymerization [34]. A decrease in the ring strain of the cyclic monomer promotes the occurrence of ROMP and it is beneficial to prepare BBPs via the “grafting-through” approach [44]. Those reactions are commonly used in pre-polymerization and post-modification. Click reactions constitute a set of reactions that are can efficiently and reliably link certain moieties [45]. These reactions such as azide/alkyne cycloadditions, Michael addition, and nucleophilic substitution have been widely used in organic chemistry and polymers for post-modification, particularly for the preparation of BBPs via the “grafting-to” approach [46–48]. The mechanism, advantages and disadvantages of these synthetic techniques for the preparation of BBPs are summarized in Table 2.

2.3. Strategies for bottlebrush polymer synthesis

The synthesis of BBPs can be categorized into three basic approaches (e.g., “grafting-from”, “grafting-through”, and “grafting-to”) according to the formation of their side chains as shown in Fig. 1. Each of these strategies exhibits characteristic features and limitations in determining the structural parameters of the BBPs

Table 1
Selected representative BBPs with various sub-architectures.

Types	Schematic illustration	Chemical structure	Name abbreviation	Ref.
BBP			PBPEM-g-PBA	[13]
BBCP			[PNB-g-PS]-b-[PNB-g-PEO]	[244]
Random BBP			[PNB-g-PS]-r-[PNB-g-PLA]	[177]
Double-Brush BBP			PGMA-g-vPLA	[266]
Janus BBP			PNB-g-PS/PLA	[184]
Core-Shell BBP			PBPEM-g-[PBA-b-PS]	[13]
Brush-Linear BBP			[PBIEM-g-PMMA]-b-PGMA	[242]
Linear-Brush-Linear BBP			PMMA-b-bbPDMS-b-PMMA	[424]
Brush-on-Brush BBP			PCL-g-(PCL-b-(P(CL-Br)-g-POEGA))	[229]

from molecular engineering and synthetic perspectives. Selected representative examples of BBPs with different architectures prepared using the corresponding synthetic strategies are summarized in Table 3. Notably, it is challenging to craft densely grafted macromolecules with cylindrical morphologies owing to the intrinsic limitations of the approaches and techniques. Therefore, significant efforts and scientific investigations are required to gain insights into the distinct macromolecular architectures prepared using these approaches.

2.3.1. Grafting-from

The growth of the polymer brushes starts from initiating sites on the polymer backbone in the “grafting-from” approach. The polyinitiators are introduced by the polymerization of an iminer or through post-modification to introduce the initiating moieties [1]. High-MW side chains can be obtained through the “grafting-from” approach because the monomers can readily diffuse to the initiator sites as the polymers gradually grow from the active centers. One of the key features of this strategy is the high graft-

Table 2
Summary of the synthetic techniques for the preparation of BBPs.

Techniques	Basic Compositions	Advantages	Disadvantages
ATRP	Halide compound, CuX, and ligands	Good tolerance to functional moieties, commercial initiators, and easily end-group transformation	Transition metal usage
RAFT	CTA and radical initiator	Various monomers, diverse of reaction media, and easily end-group transformation	Colour- and odor-containing product
NMP	Nitroxide initiator	Good tolerance to impurities	Limited monomers
Anionic/Cationic Polymerization	Associate monomer and catalyst	Easily end-group transformation and grafting reaction	Harsh conditions and high sensitivity
ROMP	Cyclic olefin and Grubbs' catalyst	Great tolerance to impurities and high reactivity for macromonomers	Low packing density of side chains
Click Reactions	Functional end moieties	Mild reaction condition and high efficiency	Pre-preparing process for functional groups

Table 3
Selected representative BBPs prepared with different synthetic strategies.

Backbone Type	DP	Side chain Type	DP	Grafting density	Techniques	Strategy	Ref.
Polymethacrylate	514	PBA, PBA- <i>b</i> -PS	15–27	100%	ATRP	Grafting-from	[13]
Polymethacrylate	1500	PDMAEMA	32–40	50%	ATRP	Grafting-from	[90]
Polymethacrylate	360	PAA	57	100%	ATRP	Grafting-from	[88]
Cellulose	-	PtBA, P4VP, PtBA- <i>b</i> -PS, PS- <i>b</i> -PtBA- <i>b</i> -PS	68–153	100%	ATRP	Grafting-from	[12]
Polypeptide	120	PS	100–400	100%	ROP/ATRP	Grafting-from	[58]
Poly(ϵ-caprolactone)	700	PBA- <i>b</i> -POEGA	28–35	80–98%	ROP/ATRP	Grafting-from	[62]
Polystyrene	120	PS	41–46	95%	RAFT	Grafting-from	[56]
Polynorbornene	50	PS	77	77%	RAFT/ROMP	Grafting-from	[176]
Polymethacrylate	-	PS/PLA	-	PS(>90%)/PLA(86%)	ATRP/ROP	Grafting-from	[96]
Polymethacrylate	425	PEG	45	100%	ATRP	Grafting-through	[28]
Polymethacrylamide	27–151	polypeptide	20	100%	PET-RAFT	Grafting-through	[127]
Polynorbornene	130	PMMA	72	100%	ROMP/ATRP	Grafting-through	[63]
Polynorbornene	57–578	PS	19–66	100%	ROMP/Click	Grafting-through	[177]
Polynorbornene	56–151	PS/PLA	23/21	100%	ROMP/RAFT/ROP	Grafting-through	[184]
Polynorbornene	25–200	P3HT	12	100%	ROMP/Click	Grafting-through	[181]
Polynorbornene	95	PS- <i>b</i> -PMA- <i>b</i> -PtBA	132	100%	ROMP/RAFT	Grafting-through	[240]
Polynorbornene	48	DNA	-	32%	ROMP/Nucleophilic substitution	Grafting-to	[193]
Polymethacrylate	210	PEO, PS, PBA, PBA- <i>b</i> -PS	7–46	20–100%	CuAAC	Grafting-to	[201]
Polystyrene	19	PS	22	55%	Thiol-yne	Grafting-to	[219]

ing density because of the significantly decreased steric hindrance among the side chains during the growth [1]. However, intermolecular termination and macroscopic gelation can occur due to the intramolecular coupling of the densely packed initiator sites on the backbone during radical polymerization. This can be mitigated by the CRP techniques that rely on RDRP to lower the concentrations of radical species. This key characteristic is important in reducing the radical termination events during the BBPs synthesis. Long-backbone BBPs with high grafting density and low \bar{D} can be readily obtained via the “grafting-from” approach. A variety of backbones have been used to construct BBPs including poly(meth)acrylate (P(M)MA), [49–53] polystyrene (PS), [54–56] polymethacrylamide, [57] polypeptides, [58,59] polythiophene, [60,61] polylactone, [62] polynorbornene (PNB), [63,64] polysaccharides, [12] and other compounds [65–69]. Side chains are then attached to these backbones using ATRP, [12,49,50,54,58,60–63] RAFT, [51,56,64,65] ROP, [55,57,59] NMP, [53,67] and ionic polymerization [66]. ATRP is the most widely applied technique in the “grafting-from” approach to control the growth of the brushes because of the aforementioned advantages. Initiators can easily be attached onto the main chain via a facile esterification reaction because of the abundant hydroxyl groups in natural and artificial polymers. Notably, as the esterification of the backbone requires a

high amount of initiator, the commercial alkyl halides (ATRP initiators) afford significant advantages over other labor-intensive initiators (RAFT, NMP, and ROP).

To better understand the brushes' distribution along the polymer backbone, it is important to determine the initiation efficiency during polymerization. In the “grafting-from” approach, the polyinitiators that are intrinsically present in the template initiate the side chain growth. In general, a fast initiation rate and deactivation, based on the mechanism of the CRP techniques ensure that all side chains to grow simultaneously and have approximately equal lengths because of the high initiation efficiency at the early stage [26]. Unfortunately, initiation efficiency is not always 100% because a fraction of the side chains grow faster in the early stage of polymerization and sterically hinder the adjacent initiating sites that result in incomplete initiation on the backbone [70,71]. In addition, this hindrance can negatively affect the formation of uniform side chains, particularly, in the core-shell BBPs. Therefore, it is desirable to gain insights into the factors affecting initiation efficiency (this value is also considered as the grafting density in this strategy). The unique performances (mechanical and rheological) of the BBPs are significantly dominated by this determinant. To calculate the initiation efficiency of BBPs, direct cleavage of brushes from the backbone is essential, which has been

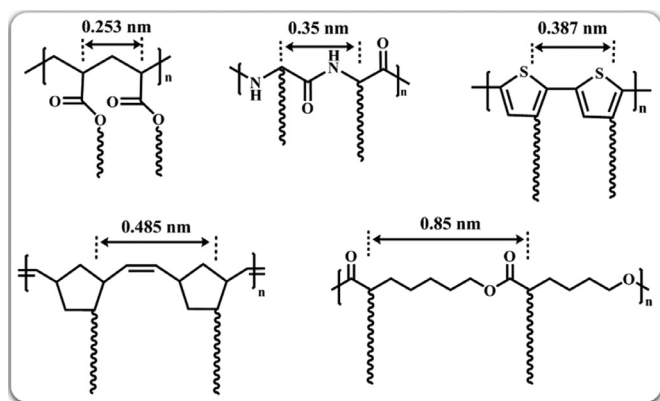


Fig. 2. Illustration of various lengths for repeating unit in bottlebrush polymers.

achieved through an acid [70] or base [72] solvolysis reaction. For instance, a BBP, poly(2-(2-bromopropionyl)oxyethyl methacrylate)-*g*-poly(butyl acrylate) (denoted as PBPEM-*g*-PBA), was used as a model to calculate the initiation efficiency [70]. The PBA side chains were obtained after acid cleavage, and its true MW was determined using nuclear magnetic resonance (NMR) spectroscopy. The corresponding monomer conversion could be determined by NMR or gas chromatography, thereby affording the theoretical MW of the side chains (assuming quantitative initiation). The ratio of the theoretical and true MWs of the side chains can be considered as the initiation efficiency. Two approaches have been employed to increase the initiation efficiency to decrease the monomer attachment in each activation/deactivation process in the ATRP, i.e., by an increase in the amount of CuX_2 and addition of solvent to decrease the monomer concentration [70].

Owing to the characteristics of the vinyl monomers, most BBPs possess side chain crowding with a spacing (repeat unit length is 0.253 nm) of two C-C bonds along the backbone (Fig. 2). The side chain crowding typically induces a high stretching of the backbone and side chains, which forces the entire BBP to adopt an entropically unfavorable extended shape. However, densely packed polyinitiator sites on the backbone can hinder the initiation efficiency during side chain growth, as discussed previously. Alternatively, other backbone monomers with large spacing between the neighboring brushes (e.g., PLA has a spacing of 0.36 nm [73] and poly(L-lysine) (PLL) has a spacing of 0.35 nm [74]) provide a more kinetically active environment for chain propagation, which may be readily converted into the BBPs with high grafting density. PLL-based BBP was prepared through the ROP of α -amino acid N-carboxyanhydride (NCA) and then, the PS side chain was synthesized by ATRP, with alkyl-bromine on the backbone as an initiator [58]. Thereafter, another type of BBP with a polythiophene (repeating unit length of 0.387 nm [75]) backbone was synthesized by oxidative polymerization with FeCl_3 , followed by the growth of poly(N-isopropyl acrylamide) (PNIPAM) arms via ATRP [61]. Recently, BBP architectures containing 2-oxazoline inimers were obtained using ROP, and the initiators on the backbone were employed to grow the side chains [76]. Notably, the ROMP of norbornyl monomers can afford a large spacing (0.485 nm for the repeating unit length) with five C-C bonds among the adjacent brushes [77]. A combination of ROMP and NMP was applied for preparing a precisely designed PNB-based BBP via the “grafting-from” approach [78]. To further increase the initiation efficiency, poly(ϵ -caprolactone) (PCL) with a spacing of 0.85 nm between the adjacent brushes was selected as the backbone, [75] as it provided more space to grow the brushes. The BBP, PCL-*g*-PBA, was prepared via the ATRP of *t*-butyl acrylate (tBA) and exhibited a worm-like morphology [62]. Alternatively, the copolymerization of dif-

ferent comonomers has also been applied to increase the spacing among the side chains. The backbones can be produced by the copolymerization of monomers such as styrene (St), [79] NCA, [80] and 3-hexylthiophene, [81] to form brush- or comb-shaped polymers. However, as the partial repeating units have initiators that are randomly distributed along the backbone, closely grafted BBPs are not formed. Even though a decreased essential grafting density due to the incorporation of the external moiety in the repeating units may result in loosely-packed brushes, all BBPs have high initiation efficiency, forming worm-like structures. However, when the main chain length is comparable to that of the side chain, BBPs do not afford worm-like morphology [82,83].

Till date, BBPs with polyacrylate backbone are mostly studied via the “grafting-from” strategy, where ATRP-initiating groups are introduced directly or through post-modification. The BBPs with high grafting density are obtained by the combination of ATRP and “grafting-from” approaches (Fig. 3a) [13,84]. The linear polymer PHEMA-TMS was prepared by the ATRP of HEMA-TMS. After cleavage of the TMS group and subsequent esterification with 2-bromopropionyl bromide under catalysts, the macroinitiator PBPEM was readily obtained. In a seminal work, BBPs containing PS or PBA side chains (PHEMA-*g*-PS or PHEMA-*g*-PBA) with low \bar{D} were synthesized via ATRP and stopped at monomer conversions of < 20% to prevent undesirable side reactions. Notably, low temperature, low Cu^{I} concentration, and Cu^{II} addition were also employed to decrease the radical amounts during the ATRP process. Thereafter, BBPs bearing various side chains such as photo-responsive poly(4-methacryloyloxyazobenzene), [85] thermal-responsive PNIPAM [86] and poly(2-(2-methoxyethoxy) ethyl methacrylate) (PMEOMA), [87] pH-responsive polyacrylic acid (PAA) [88], poly(styrenesulfonate), [89] and poly(dimethylaminoethyl methacrylate) (PDMAEMA), [90,91] etc. [92,93] were crafted using this strategy. In addition, well-defined BBPs with crystallizable side chains such as PCL, [94,95] poly(L-lactide) (PLA), [96] and peptides with secondary structure [97,98] were also synthesized using ROP, with PHEMA as the macromolecular initiator.

The controlled synthesis of BBPs via the “grafting-from” strategy employing ATRP or other CRP techniques was successfully achieved in extremely dilute systems with low monomer conversions to prevent the macroscopic gel formation during polymerization. However, a significant decrease in the polymerization rate in a highly diluted system and wastage of monomers in bulk polymerization are some drawbacks of this approach. An alternative solution to resolving this issue is the use of miniemulsion system to synthesize BBPs. A miniemulsion is a miniaturized bulk system with the reaction compartmentalized into small stable monomer droplets, where macroscopic gelation cannot occur. Worm-like BBPs are obtained in a miniemulsion system through the activators generated by electron transfer (AGET) ATRP with high monomer conversion [99]. Nonetheless, cross-linking still exists in the miniemulsion particles because of inevitable radical coupling. Furthermore, the $\text{L}/\text{Cu}^{\text{II}}\text{-P}_n$ organometallic intermediate can react with the active hydrogen species, producing a dead polymer chain. This copper-catalyzed radical termination (CRT) process facilitates the chain termination in the ATRP of acrylates [100]. Nonetheless, CRT is favorable for suppressing gelation during the preparation of densely grafted BBPs via the “grafting-from” approach because of the absence of the usual bimolecular radical coupling [101].

Another method to suppress cross-linking during the preparation of BBPs involves the use of Cu-mediated, photoinduced, controlled ATRP (photoATRP), which is based on the photoinduced reductive quenching mechanism between an electron donor (a tertiary amine or excess ligands) and excited $\text{Cu}^{\text{II}}\text{X}/\text{L}$ deactivator. This reaction affords $\text{Cu}^{\text{I}}/\text{L}$ activator (re)generation by direct reduction

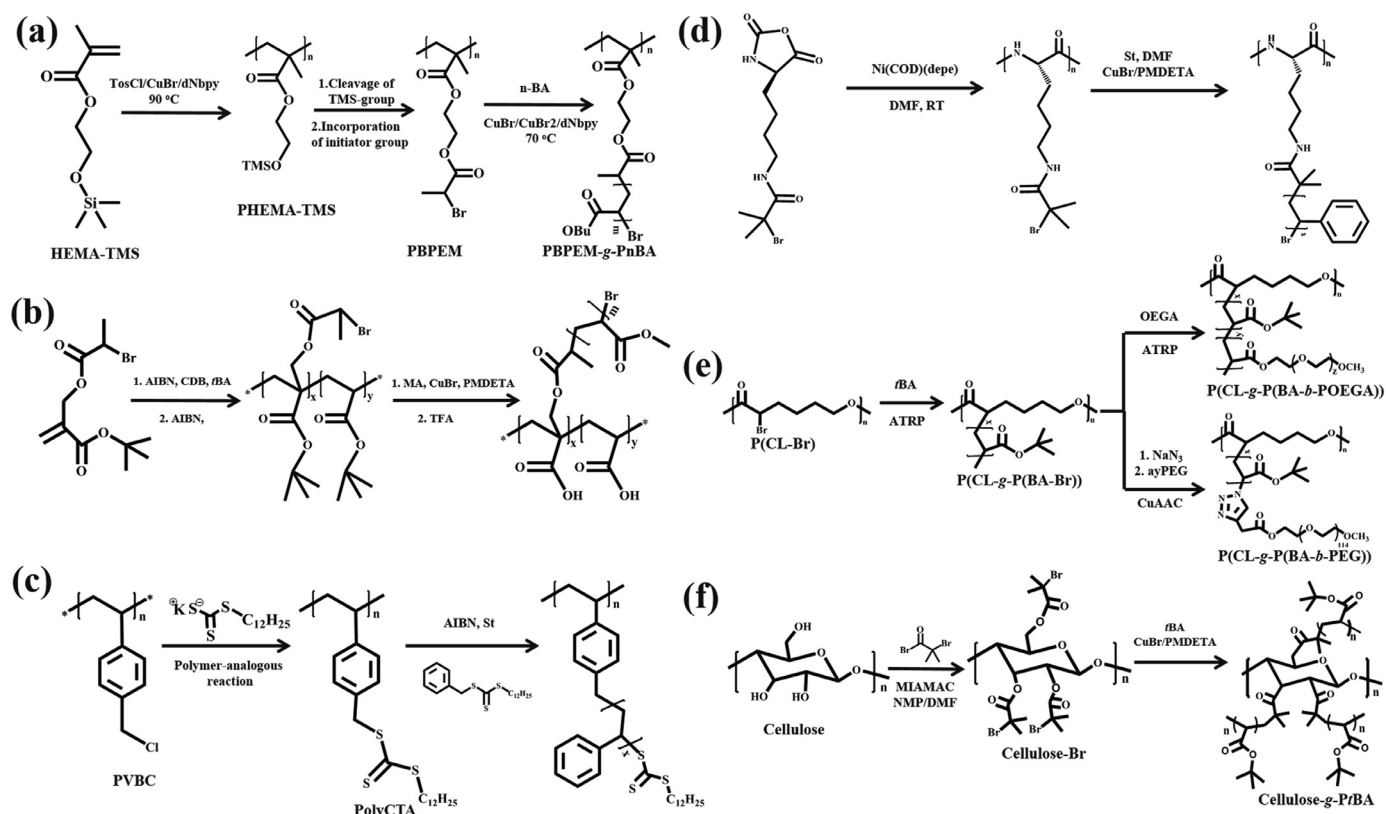


Fig. 3. Synthesis of BBPs with various backbones via the “grafting-from” approach. (a) PHEMA-based BBPs. [13], Copyright 2001. Adapted with permission from the American Chemical Society. (b) PtBA-based BBPs. [103], Copyright 2010. Adapted with permission from American Chemical Society. (c) PS-based BBPs. [56], Copyright 2014. Adapted with permission from John Wiley and Sons Inc. (d) Polypeptide-based BBPs. [58], Copyright 2012. Adapted with permission from John Wiley and Sons Inc. (e) PCL-based BBPs. [62], Copyright 2018. Adapted with permission from Elsevier Science Ltd. (f) Cellulose-based BBPs. [12], Copyright 2016. Adapted with permission from the American Association for the Advancement of Science.

[102]. The photoreduction rate constant increases with a decrease in the $\text{Cu}^{\text{II}}\text{X}/\text{L}$ concentration owing to the decreased absorbance or enhanced transmittance of the solution. In addition, the rate of polymerization (R_p) in the system with activator regeneration depends significantly on the rate of reduction. A high ATRP activity of catalyst affords a low photoreduction rate constant. This discrepancy is compromised in the photoATRP process, where a high reduction rate is achieved because high activity results in a significantly high $[\text{Cu}^{\text{II}}\text{X}_2/\text{L}]/[\text{Cu}^{\text{I}}\text{X}/\text{L}]$ concentration ratio, which allows rapid overall photoreduction, promotes CRT, and thus allows the preparation of brushes with high grafting densities and monomer conversions [103].

Recently, Huang and coworkers reported a new synthetic methodology for preparing well-controlled BBPs with PtBA as the backbone (Fig. 3b) [104]. A novel acrylate iminer containing ATRP initiating site was first synthesized, followed by RAFT polymerization to afford the backbone. The initiation groups on the backbone remained intact during polymerization and could be used to initiate ATRP of methyl methacrylate (MMA) to obtain BBP (e.g., PtBA-g-PMMA) without post-modification [104]. Thereafter, in the following works, they expanded this approach to grow different side chains with high MW and low \bar{D} on the BBPs, such as thermoresponsive poly(N-vinyl caprolactam), [105] PNIPAM, [106] poly(ethylene glycol) methyl ether methacrylate, [107] and pH-responsive PDMAEA, [108] etc [109–112]. Furthermore, the tBA moieties on BBP backbone were selectively hydrolyzed using trifluoroacetic acid (TFA) to yield BBPs with acid groups anchored on their backbones [104].

However, it is challenging to grow less-active monomers (e.g., vinyl acetate (VOAc) and N-vinyl pyrrolidone (NVP)) on the back-

bone with ATRP macroinitiators because of a very low ATRP equilibrium constant [113]. In contrast, RAFT polymerization has been used to prepare BBPs with an expanded range of monomers, including less reactive vinyl esters (e.g. vinyl acetate) and vinyl amides [40]. Xanthate-containing CTAs were used to esterify the hydroxyl groups on the PHEMA backbone, forming macromolecular multifunctional CTAs (i.e., PPXEM). PVOAc [51] and PNVP [114] side chains with high MWs were then grown from the PPXEM to generate BBPs through RAFT polymerization, and the BBPs exhibited excellent worm-like morphology.

Although RAFT polymerization has been successfully employed to synthesize BBPs through the “grafting-from” strategy to grow less-active-monomer-based side chains, this methodology often suffers from limited control over the branch grafting and \bar{D} [41]. For instance, PS branches were obtained from dense CTA-functionalized poly(p-chloromethylstyrene) (PCMS) backbone linked via the R-group approach, but the resting brush polymer showed multimodal MW distribution [115]. During this RAFT polymerization, active radicals transferred via the intramolecular and intermolecular transfer processes. The intramolecular transfer was achieved by transferring to the neighboring CTAs existed on the same BBP, whereas the latter case involved the transfer to CTAs on another BBP. These two processes fulfill the addition-fragmentation equilibrium resembling the conventional RAFT process and ensure that all polymer chains grow at the same rate. However, the latter transfer is critically limited owing to the densely grafted side chains of the BBPs. In addition, the sparse radicals are stuck within an independent BBP rather than adding to the CTAs on other BBPs, thus resulting in BBPs with high \bar{D} because of the absence of deactivation. Müller and co-workers developed a CTA-shuttled R-group

methodology to increase the radical concentration, where the low-MW CTAs were applied as CTA shuttles to enhance the radical transfer pathways (Fig. 3c) [56]. With the efficient transfer of active radicals by the surrounding CTA shuttles, BBPs afford a homogeneous propagation of the side chains and low \bar{D} [56]. Thereafter, with this CTA-shuttle-tuned RAFT methodology, BBPs with alternating diblock poly(4-N-acryloylmorpholine) and poly(dimethyl acrylamide) (PDMA) side chains and alternating multi-segmented copolymer side chains were synthesized [116]. Although the shuttled CTA R-group approach provided better control over the BBP structure, the free CTA shuttle produced inevitable linear polymers and fractional precipitation was required to separate it. You and coworkers reported the preparation of BBPs using tandem RAFT polymerizations with two disparate RAFT agents in one pot [117]. The backbone was synthesized by the selective cationic RAFT polymerization of the inimer carrying a dormant RAFT agent. Then, the brushes were obtained by capitalizing on conventional RAFT polymerization initiated by AIBN. This tandem orthogonal polymerization did not require the purification of intermediate products and final linear polymers.

In the aforementioned reports, the backbones of BBPs are involved petroleum-based synthetic polymers that were not biocompatible. It is appealing to expand the range of biodegradable polymeric materials because of the depletion of fossil fuel reserves. Synthetic polypeptides are promising biomaterials that display unprecedented properties such as biocompatibility and the capability to form higher-order structures. Additionally, biomimetic polypeptides have inherent chiral structure and intramolecular or intermolecular hydrogen bonding that can afford them tunable secondary structures (e.g., α -helix or β -sheet) [118]. The controlled synthesis of a polypeptide with predictable MW and low \bar{D} has been achieved at high vacuum and low temperature. With the living character in the ROP of the NCAs monomers, well-defined polypeptide-based BBPs with different side chains have been obtained, such as poly(L-glutamic acid) (PLG)-*g*-PEG, [119] PLL-*g*-PS and PLL-*g*-PEGMA (Fig. 3d), [58] PLG-*g*-POMEOMA, [80] and PLG-*g*-PLA, [120] which have been synthesized via ATRP or ROP through the “grafting-from” approach. Recently, human serum albumin was used as a natural backbone to systematically construct uniform anisotropic BBPs using ATRP via the “grafting-from” approach [121]. In parallel, new BBPs bearing functional, natural polypeptide side chains were also synthesized [122]. Notably, the polypeptides can form secondary structures, and the incorporation of polypeptide brushes can predictably broaden the scope of BBP-based materials with remarkable performances [97,123–125]. Complex and hierarchical structures that mimic globular proteins were obtained by capitalizing on the precise molecular structure and specific intermolecular interactions of the polypeptide-based BBPs [126]. Moreover, BBPs with peptides as side chains endowed the materials with enhanced biological activities, such as high binding affinities to the targets and increased cell penetration [127].

PCL is an example of a synthetic biodegradable polymer, which can be obtained via the ROP of ϵ -caprolactone (CL). However, PCL exhibits inherent functional group paucity, which diminishes the possibilities for grafting side chains. Modified CL monomers bearing pendant functionalized sites have been reported in the past decades [128,129]. An elegant strategy that yielded halide ϵ -caprolactone was reported and subsequently applied to synthesize PCL-based BBPs. For example, the PCL backbone was crafted via random copolymerization of γ -(2-bromo-2-methylpropionate)- ϵ -caprolactone (BMPCl) and CL monomers [130]. The pendant initiation groups were used as initiators for the ATRP of DMAEMA to form PCL-*g*-PDMAEMA BBPs with different grafting densities. Thereafter, poly(4-vinylpyridine) (P4VP) and PDMAEMA brushes were fabricated via anionic polymerization with PCL macroinitia-

tors to yield PCL-*g*-P4VP, and PCL-*g*-PDMAEMA BBPs, respectively [131,132]. However, with the partial anionic activation produced by a non-nucleophilic lithium diisopropyl amide on the backbone, the obtained BBPs had low grafting densities. It could be reasonably that they self-assembled into spherical morphologies [133]. To further improve the steric repulsions effect within these brush polymers, amphiphilic core-shell BBPs were synthesized with PCL-Br as the backbone, and the side chain PBA-*b*-POEGA was then prepared by the sequential ATRP of *t*BA and oligo (ethylene glycol) acrylate (OEGA) (Fig. 3e) [62]. The second bulky block of POEGA enhanced the steric effect among the side chains. The effect of the backbone DP on the BBP conformation was investigated, and with an increase in the backbone DP, the lengths of BBPs gradually increased and exhibited a worm-like morphology.

Cellulose is a long-chain, high-MW polysaccharide [134]. Cellulose nanocrystals have diameters at the range of nano-scale, and lengths at the micron scale. Both intramolecular and intermolecular hydrogen bonding coexist in cellulose, which causes the cellulose chains to assemble into close-packed bundles. One of the most unique characteristics of cellulose is that every repeating unit has three hydroxyl groups. Cellulose has particular superiority for ROP in comparison to other polymerization methods, and many polymers have been successfully grafted from cellulose via surface-initiated ROP [135–137]. However, these celluloses were solid bundles with large sizes and thus, could not be considered as BBPs. Esterification is another important method to chemically modify the cellulose structure. Various polymers have been grafted from cellulose using the CRP techniques [138–140]. However, grafting from cellulose yields poor grafting density because of difficulties in separating the cellulose bundle chains and anchoring nonpolar initiators on their highly polar surfaces. To achieve better control of the grafting density of the initiators on cellulose, ionic liquids have been used as the reaction media to perform esterification. Ionic liquid is a desirable green and recyclable medium with many advantages such as broad liquid range and excellent dissolution capability [12,141,142]. Nevertheless, even in ionic liquids, the complete conversion of -OH groups into initiators is difficult to achieve [142,143]. Cellulose-based macroinitiators with almost 100% ATRP initiator density after two esterification processes with ionic liquid as the solvent have been reported (Fig. 3f) [12]. Although cellulose-Br macroinitiators can easily dissolve in organic solvents, their MWs exhibit broad \bar{D} owing to the intrinsic variation in the lengths of their cellulose backbones. To synthesize high-quality BBPs with uniform cellulose backbone lengths, fractional precipitation with acetone as the solvent and deionized water as the precipitator is employed. A series of pure linear macroinitiators with different MWs and low \bar{D} were obtained. Various side chains were subsequently grown from the cellulose backbone with ATRP of the monomers. A variety of monomers were also sequentially grown via ATRP to obtain cellulose-based core-shell BBPs such as cellulose-*g*-[P4VP-*b*-PS], cellulose-*g*-[PtBA-*b*-PS], and cellulose-*g*-[PS-*b*-PtBA] [12]. Notably, the main chain of cellulose is considered to be significantly stiffer than those of the common vinyl polymers [144]. The diblock copolymer brushes not only increase the steric repulsions among the side chains but also afford new properties and conformations. For instance, the core-shell structure of cellulose-*g*-[PAA-*b*-PS] exhibited rigid rod-like morphology, [12] while a characteristic worm-like structure of cellulose-*g*-PBA was observed by AFM [145]. Considering the complicated synthetic process and difficulty in purification, the preparation of BBPs bearing triblock copolymer side chains has rarely been reported, but the successful synthesis of triblock-copolymer-grafted BBPs such as cellulose-*g*-[P4VP-*b*-PtBA-*b*-PS] and cellulose-*g*-[PS-*b*-PAA-*b*-PS] have been reported by the Lin group [12]. The hydrophilic core block PAA or P4VP can coordinate with the metal ions, which suggests the application potential of BBPs as nanoreactors.

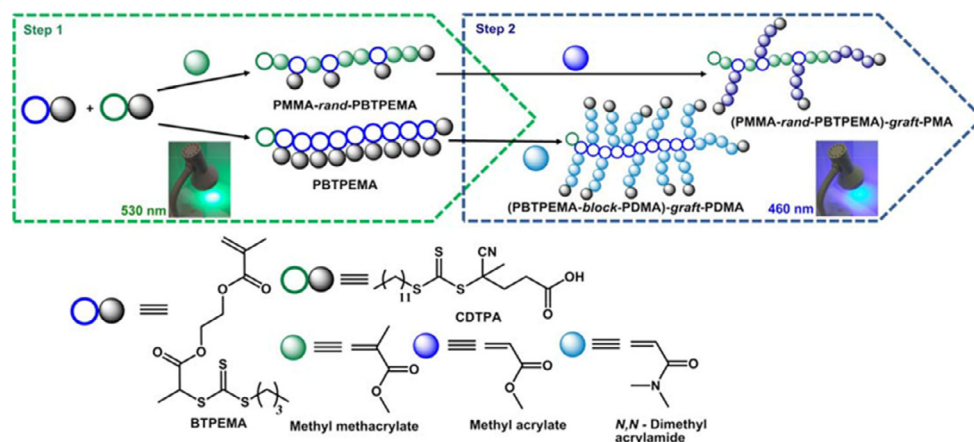


Fig. 4. Two-step synthesis of BBPs via photo-mediated RAFT in two different wavelengths of light. [149], Copyright 2018. Reproduced with permission from the American Chemical Society.

These aforementioned methodologies for preparing BBPs have some disadvantages such as harsh reaction conditions, tedious separating processes, and the use of harmful metals. Photo-mediated RDRP is an emerging technique to prepare well-defined architectures under mild conditions and with flexible implementation [146–148]. In comparison to other common triggers for polymerization, light provides mild reaction conditions without the need for additional reactive molecules. Moreover, light-mediated RAFT polymerization provides an alternative methodology to prepare well-defined polymers without requiring heating and slow decomposition of the thermal initiators. Matson and coworkers reported the preparation of BBPs via the ROMP of a norbornene (NB)-based photoiniferter, followed by the photoiniferter polymerization of side chains under visible light [64]. This method affords a high monomer conversion without coupling reactions and linear polymers, in comparison to those encountered in conventional RAFT polymerization. In addition, the light source can prevent the formation of possible initiator-derived chains, maintain high chain-end fidelity and low radical concentration, and allow operation at low reaction temperatures that can prevent chain coupling and β -scission. However, the two-step method requires a photocatalyst and ruthenium catalysts for RAFT polymerization and ROMP. Orthogonal RAFT polymerizations can be implemented in one pot to prepare polymers with various architectures. For instance, facile photo-mediated RAFT polymerizations induced by chemoselective lights were used to prepare BBPs under mild reaction conditions (Fig. 4) [149]. In this work, two different types of RAFT agents (e.g., CDTA and BTPEMA) with different photolysis capabilities at different wavelengths were selected as photoiniters without addition of photocatalysts. The inimer, BTPEMA, was homopolymerized to form PBTPEMA under green light-mediated RAFT polymerization with CDTA as the CTA, while the pendant CTA remained intact during the process. By capitalizing on blue-wavelength irradiation, the RAFT polymerization of DMA monomer using PBTPEMA was achieved, yielding PBTPEMA-g-PDMA within a short duration. This photoiniferter approach afforded the synthesis of complex macromolecular architectures through copolymerization with other monomers by adjusting the grafting densities without any intermediate steps [149].

It is necessary to use nontoxic catalysts in the synthesis of BBPs for biomedical applications. Enzyme-catalyzed polymerizations have attracted great interest in the past decade owing to the high selectivity, mild reaction conditions, recyclability, and biocompatibility [150]. For instance, Moeller and coworkers successfully prepared linear polyglycidol (PG) macroinitiators bearing primary hydroxyl groups were successfully prepared via the anionic ROP of

a glycidol, followed by the Novozyme435-catalyzed ROP of CL to yield the brush polymer PG-g-PCL [151]. Interestingly, the chemical structure of the obtained polymer was different from that of the polymer obtained via chemical catalysis with the same ratio of repeating units to monomers. The initial efficiency of the hydroxyl groups on the backbone with enzyme catalysis was low because of the steric hindrance of enzyme, which resulted in many free hydroxyl groups in the brush polymer. Thereafter, random (heterografted) BBPs were prepared with consecutive enzymatic and chemical ROP of CL and LA monomers, respectively, using PG as the multifunctional initiator. CL was first grafted enzymatically to a PG backbone via ROP with Novozyme435 as the catalyst. The remaining (~50%) hydroxyl groups on the PG backbone were then used as initiators for the chemically catalyzed ROP of the LA monomers, yielding heterografted a BBP bearing PCL and PLA side chains [152]. In an alternative method, the end hydroxyl groups on the PCL side chains were selectively acetylated, and the residual hydroxyl groups were then brominated using an ATRP initiator. After the growth of the side chains by ATRP, heterografted BBPs were obtained in two-step polymerization [153]. However, it is challenging to achieve an esterification efficiency of 100% with BBP backbone, indicating that free initiating sites remain available on the backbone, which could be used for post-modification. In this manner, heterografted BBPs with two different polymer chains on the same backbone have been achieved through simultaneously the ROP of LA and ATRP of St in one pot [154].

2.3.2. Grafting-through

The “grafting-through” strategy is employed to polymerize the macromonomers through appropriate techniques. As opposed to the “grafting-from” approach, which often suffers from a low initiation efficiency, macromonomer polymerization ensures good efficiency because of the intrinsic features [1,34]. The key feature of this strategy is that each repeating unit contains a pre-attached side chain, which ensures 100% grafting density of the resulting BBPs. Here, the side chains are prepared and completely characterized prior to the formation of backbone. It is well known that grafting density plays a significant role in controlling the properties of BBPs [1]. Therefore, BBPs with precisely controlled dimensions and architectures prepared via the “grafting-through” approach are widely used as model samples to investigate their structure-dependent properties, including grafting density, diameter, length, and dispersed state vs. assembled states and properties. Owing to the inherent macroscopic properties (i.e., high viscosity and steric hindrance because of high MW), the polymerization conditions for the macromonomers and small monomers are

different. For example, the reaction medium exhibits high viscosity and limited solubility of the macromonomers with the progress of the polymerization, which restricts the macromonomer conversion. BBPs with high DP values can be prepared via the “grafting-through” approach at low concentration, but the reaction requires a long time. In general, the “grafting-through” approach produces BBPs containing backbones with low DP values because of less polymerizable end groups and high steric hindrance of the brush around the propagation sites. Furthermore, the low conversion of the macromonomers leads to the coexistence of linear and brush polymers in the solution. Therefore, tedious fractional precipitation or dialysis are often needed to remove the unreacted linear macromonomers, which can be laborious and time-consuming.

Free radical polymerization is generally used in the “grafting-through” approach to prepare BBPs because the side chains can be considered as monomers. For instance, methacrylate-terminated PS was synthesized by the living ionic polymerization of St and followed by esterification. Subsequently, BBPs with well-defined PS side chains were obtained by free radical polymerization several decades ago [38]. Thereafter, BBPs bearing diblock copolymers, PS-*g*-[PI-*b*-PS], were synthesized using a combination of stepwise living anionic and free radical polymerizations with a similar process [155]. The optimized polymerization conditions such as concentration, MWs of macromonomers, and solvents were identified to successfully prepare the BBPs. BBP synthesis with high-MW macromonomers is extremely challenging because of the enhanced steric hindrance, such that polymerization may not occur at all. Notably, the chemical characteristics of the side chains, significantly affect the main chain flexibility of the brushes [156].

Macromonomers can also comprise two oligomer chains attached onto one terminal group. In one case, an ATRP initiator carrying two initiating sites afforded polymers with two PS or PrBA side chains [157]. In another case, an initiator containing both ATRP and RAFT sites was used individually to grow the PMMA and PDMA side chains [158]. The hydroxyl group was then converted to a polymerizable methacryloyl group through esterification, and finally, BBPs with two side chains attached onto each repeating unit were obtained by free radical polymerization of these macromonomers [157,158]. In addition to the attachment of two side chains on the backbone, dendronized macromonomers were also used as side chains to prepare BBPs via free radical polymerization. However, high steric hindrance of the dendronized side chain prevented the growth of the backbone. It is reported that only BBPs bearing G1 or G2 dendrons exhibit worm-like morphology [159]. An increase in the spacer length between the polymerizable end group and dendrons may facilitate an growing of the backbone length. Unfortunately, it is challenging to synthesize BBPs using macromonomers bearing G4 brush via the “grafting-through” approach.

Although well-controlled brushes can be engineered through living polymerization techniques, the BBP backbone may lack a precise structure because of the relatively poor control over the MW and chain-end functionality in free radical polymerization. Fortunately, recent advancements in CRP have facilitated the development of well-defined BBPs via the “grafting-through” approach. As CRP techniques result in relatively low radical concentrations in the system, termination coupling during polymerization can be effectively prevented.

ATRP is the most widely used CRP technique to prepare precisely designed BBPs via the “grafting-through” approach. As steric hindrance can severely impede the construction of BBPs with high DP, ATRP has been used to polymerize the macromonomers with short side chains [160] or thin polyethylene glycol (PEG) segments [161,162]. In one case, less bulky PEG was selected as macromonomer to perform ATRP via the “grafting-through” approach. A high conversion up to 90% was readily achieved within

two hours, yielding BBPs containing backbones with DP up to 425, but the \bar{D} of the resulting polymers were broad [161]. Thereafter, well-controlled BBPs with relatively high MW and narrow \bar{D} at high conversions were achieved using the aqueous AGET ATRP of oligo (ethylene glycol) methyl ether methacrylate (OEGMA) with ascorbic acid as the reductant at room temperature [162]. This approach has also been used to successfully fabricate heterografted BBPs. It can be achieved by copolymerizing PEG-based macromonomers with other thin macromonomers, such as poly(dimethylsiloxane) (PDMS) and PLA [163,164]. An additional merit of the PEG-based heterografted BBPs is that PEG side chains occupy less space, such that another side chain can be attached onto the backbone to form Janus BBPs. Huang and coworkers synthesized PEGMA with the “grafting-through” approach, and then covalently bonded an ATRP initiator onto each repeating unit on the backbone. After the ATRP of PS side chain, an amphiphilic Janus BBP containing PEG and PS brushes was synthesized [165]. This method can also be extended to introduce other side chains, however, the backbone DP of BBP is very low because of the steric hindrance. Therefore, optimizing the reaction parameters of macromonomer polymerization is urgently required.

It has been reported that macromonomer polymerization does not occur at concentrations below the equilibrium monomer concentration ($[M]_e$) due to thermodynamic limitations under heating or pressuring conditions [28]. A decrease temperature or increase pressure can shift $[M]_e$ to low values and allow polymerization [28]. However, low temperature not only decreases the polymerization rate but also reduces polymer solubility. High pressure increases the propagation rate coefficient and the ATRP equilibrium constant (in the case of copper catalysis), and simultaneously decreases the rate coefficient of termination. This favorable effect can lead to a higher monomer conversion in a shorter time, while maintaining a narrow \bar{D} . For instance, the polymerization of the macromonomer OEGMA with M_n of 950 or 2080 g mol⁻¹ was investigated at different concentrations (e.g., 50, 75, and 300 mM) using ATRP under ambient or high pressure (Fig. 5a). With low-MW OEGMA, the preparation of star-like and brush-like polymers at high concentrations (e.g., 75 and 300 mM) were easily achieved at ambient or high pressure, but polymerizations with an initial concentration of 50 mM showed no monomer conversion. With high-MW OEGMA, high pressure allowed the polymerization of essentially all types of OEGMA, even at low concentration, but the \bar{D} remained broad [28].

The toolbox of CRP techniques for preparing BBPs is expanding, particularly with the emergence of RAFT and photo-electron transfer (PET)-RAFT which does not require metal catalysts. Furthermore, the active dithioester or trithiocarbonate moieties for RAFT can be completely removed from the polymer chain end by reacting with a range of nucleophilic reducing reagents [166] or excess of radical initiators [104]. Schubert and coworkers synthesized well-controlled oxazoline-based macromonomers by living cationic ROP and in situ end-termination [167]. Then, a set of BBPs were prepared by RAFT polymerization, which exhibited lower critical solution temperature (LCST) behavior [167]. As PET-RAFT is performed under mild conditions, side reactions are minimized, and the integrity of the biomolecules can be retained during polymerization. Enzyme-responsive and pro-apoptotic peptide-based BBPs were successfully synthesized from peptide macromonomers using 450-nm light by metal-free PET-RAFT copolymerization with the comonomers in organic and aqueous phases (Fig. 5b) [127]. In view of the steric effect of peptide brushes, a comonomer was introduced and copolymerized with the macromonomer to successfully yield polypeptide brushes with different grafting densities and narrow \bar{D} . Furthermore, a significantly high DP of a polypeptide-based BBP can be achieved in water because of the enhanced solubility of the brush polymers in an aqueous solu-

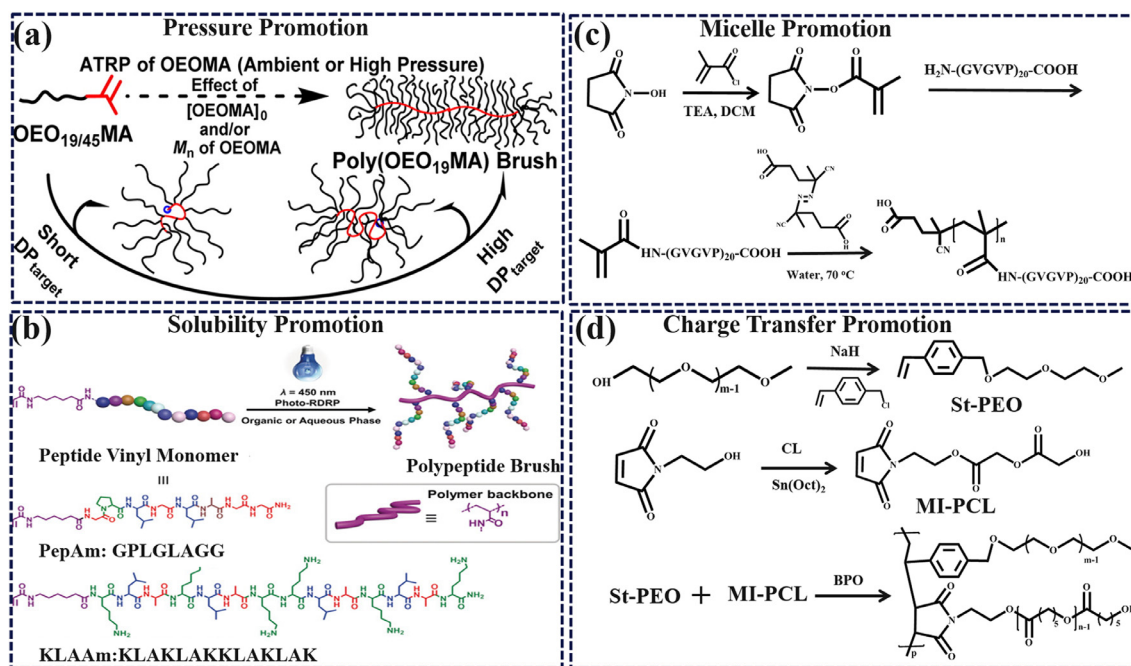


Fig. 5. Strategies for promotion of monomer conversion via the “grafting-through” approach. (a) Schematic illustration of the preparation of BBPs through ATRP under ambient or high pressure. [28], Copyright 2015. Reproduced with permission from the American Chemical Society. (b) Preparation of peptide-based BBPs via photo-RDRP in water. [127], Copyright 2019. Adapted with permission from John Wiley and Sons Inc. (c) Preparation of cylindrical BBPs bearing ELP brushes in phase-separated regime. [169], Copyright 2013. Adapted with permission from the American Chemical Society. (d) Synthesis of amphiphilic alternating brush polymers. [170], Copyright 2015. Adapted with permission from Elsevier Science Ltd.

tion [127]. This phenomenon is consistent with the conclusion of a previous study which reported that the bulky side chains such as PBA as macromonomers cannot afford a high DP because of significantly enhanced steric hindrance [168].

As mentioned above, high-MW BBPs can be readily prepared using copolymerization or by increasing the solubility of polymers via the “grafting-through” approach. High monomer conversion can also be achieved using a high concentration of the macromonomer. To verify this hypothesis, Schmidt and coworkers prepared cylindrical polymer brushes using elastin-like polypeptide (ELP) macromonomers (Fig. 5c) [169]. ELP is a monodisperse macromonomer and possesses easily controllable chain length and end-functionality. In addition, ELP exhibits LCST behavior, which provides an additional variable to further tune the architecture of the BBPs. The macromonomers were synthesized by coupling NHS-activated methacrylate to the ELP. Then free radical polymerization was performed in water, where highly concentrated macromonomer solution underwent phase separation. Polymerization was found to primarily proceed in the highly concentrated gel phase and yield high-MW cylindrical brushes. They concluded that when the macromonomers formed cylindrical micelles at high concentrations and/or temperatures, the macromonomers aggregated toward the active propagating radicals, which in turn facilitated the polymerization of high-MW BBPs, as speculated based on the extremely high-MW ELP macromonomers [169].

Additionally, highly active macromonomers can also facilitate monomer conversion. Macromonomers with electron-donating (vinyl benzyl-based macromonomers) and electron-accepting (maleimide-based macromonomers) polymerizable end-groups have been used to prepare BBPs with high monomer conversions in a relatively short time [170,171]. Chen and coworkers synthesized alternating amphiphilic BBPs bearing PEO and PCL brushes using this methodology (Fig. 5d) [170]. Maleimide-based macromonomer was synthesized via the ROP of CL with N-(2-hydroxyethyl) maleimide as the initiator, while vinyl benzyl-based

macromonomer was prepared by the substitution reaction between PEO and p-chloromethylstyrene. The macromonomers were copolymerized under thermal conditions using BPO or AIBN as initiators to yield alternating copolymer brushes with backbone DP of 310. Notably, the copolymerization of styrene and maleimide produced alternating copolymers through the formation of a charge-transfer complex (CTC). The electron donor moiety on the styryl macromonomers with para substituents could enhance the electron density of the monomer. Thus, monomer showed a high alternating tendency for copolymerization with the maleimide derivatives through CTC formation to produce high-MW BBPs. In addition, the reactivity ratios ($r_1 = r_2 = 0.1$) of the two macromonomers close to those of their corresponding small molecules [170].

Alternatively, an increase in the spacing of the adjacent repeating units can also facilitate the preparation of BBPs with high DP [172]. It is notable that the BBPs with either styryl or methacrylate backbones have a space of two C-C bonds among the pendant side chains. As the previously grafted bulky side chains surround the propagating center of the backbone, it is kinetically unfavorable to propagate the macromonomers because they need to extend their conformation and diffuse to the active center. Therefore, when the polymerizable end groups form a large unit length after polymerization, it can alleviate the steric hindrance of the grafted brushes and promote polymerization. The norbornenyl group was exclusively selected as the polymerizable moiety of the macromonomers in the “grafting-through” approach owing to its quantitative monomer conversion catalyzed by the Grubbs’ catalyst [34]. The high reactivity and large spacing of the NB group can compensate for the high steric hindrance of the side chains, allowing high conversion of the macromonomers into BBPs.

There are two general synthetic strategies to prepare NB-terminated macromonomers to grow BBPs via the “grafting-through” approach: direct polymerization with a functional NB initiator or CTA (i.e., direct-growth method) and post-coupling reactions of the premade polymers with terminal functionaliza-

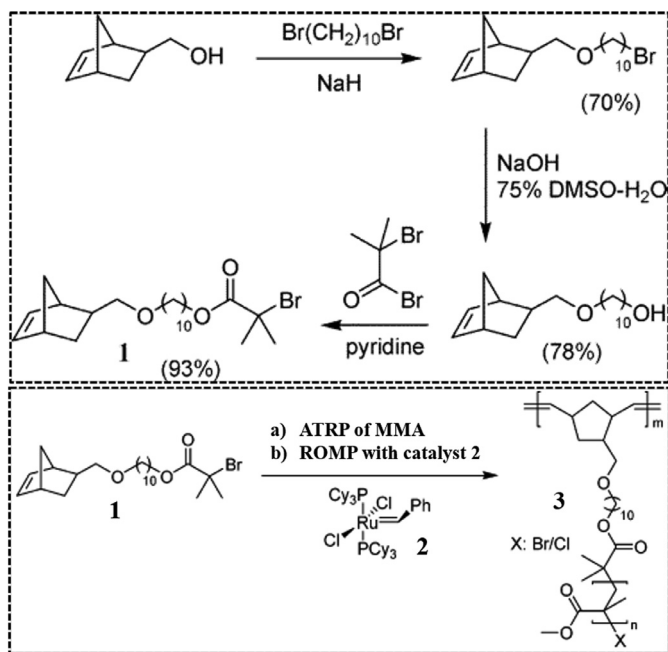


Fig. 6. Synthesis of NB-based initiator, macromonomers, and bottlebrush polymer. [63]. Copyright 2006. Adapted with permission from the American Chemical Society.

tion (i.e., growth-then-coupling method). In the former case, the macromonomers with quantitative functionalization after polymerization with the initiator can be obtained, and the side chains possess living characteristics. Moreover, the versatility of aluminum alkoxide catalysts for the ROP of lactones and L-lactides (LA), has facilitated macromolecular engineering of biodegradable polyesters in the BBPs via the “grafting-through” approach [173]. With the development of CRP techniques, parallel progress has been reported for synthesizing NB-based macromonomers via ROMP. It is well-known that *exo*-norbornenyl stereochemical configuration shows a significantly higher reactivity in ROMP than *endo*-norbornenyl monomers because it provides the C=C bond with less steric hindrance for the reaction [174]. In addition, the norbornenyl group shows low reactivity in radical polymerization. Because of these distinct advantages, NB-based macromonomers have been prepared via ATRP, [63,175] RAFT, [176] and NMP [78] techniques. For example, NB-functionalized ATRP initiator was synthesized via a three-step process (Fig. 6) [63,175]. The relatively long spacer reduced the unfavorable steric effect on the norbornenyl functionality and was beneficial in maintaining the high ROMP reactivity of the *exo*-norbornenyl macromonomer. Thereafter, various NB-functionalized macromonomers were synthesized via the ATRP of monomers, followed by subsequent ROMP to afford the formation of BBPs [175]. Recently, Grubbs' catalyst was employed to mediate the ROMP and ATRP of the backbone and side chain formation through tandem catalysis in one pot [63]. This two-step method was simple, consisting of four components in one pot, without requiring complicated and time-consuming procedures. Furthermore, this method showed excellent compatibility between ROMP and RAFT polymerization or NMP. Therefore, BBPs with block copolymer side chains can be easily obtained because of the living character of the end group on the macromonomer.

The second strategy to prepare NB-terminated macromonomers involves the covalent bonding of the polymers to the norbornenyl moiety via high-efficiency coupling reactions. Copper(I)-catalyzed azide-alkyne cycloaddition (CuAAC) reaction was first applied to prepare NB-based macromonomers using azide-terminated poly-

mers and alkyne-functionalized norbornene [177]. Unfortunately, various side reactions decreased the purity of the macromonomers [39]. Functional anionic initiators have shown significant potential as designed end groups for polymers. Particularly, nucleophilic acyl substitution reaction with acyl chlorides has been applied to the coupling reaction, but lengthy purification procedures are required for isolation [178–180]. Recently, Lee *et al.* synthesized a set of polymer side chains such as PS with a terminal 1,1-diphenylethyllithium ($\text{PSt}(\text{DPE})^-\text{Li}^+$), P2VP with a terminal 2-pyridinylethyllithium ($\text{P2VP}^-\text{Li}^+$), and poly(benzyl methacrylate) with a terminal lithium ester enolate ($\text{PBzMA}^-\text{Li}^+$) via living anionic polymerization, and then NB-substituted pentafluorophenyl (PFP) ester was used to cap the polymers with nearly 100% nucleophilic substitution reaction, forming NB-based macromonomers (Fig. 7) [179]. Finally, the ROMP of the macromonomers was carried out to synthesize BBPs with high DP as well as predictable MW and low Đ. Notably, the spacer length has a significant effect on BBP synthesis. A long flexible alkyl spacer can alleviate steric hindrance and separate the propagating active centers from the sterically demanding pendants which consequently increases the DP of the BBPs [179]. Furthermore, premade conjugated poly(3-hexylthiophene) (P3HT), [181] polyolefins, [182] and PEO [183] have also been attached onto the norbornenyl group for preparing of BBPs via ROMP.

The aforementioned synthetic strategies are convenient methods to covalently couple the polymer chains onto norbornyl groups, and then use the macromonomers to prepare BBPs via the “grafting-through” approach. The anchor groups located between the side chain and NB group are commonly derived from carboxylic acid, [183] norbornenol, [63,175,176] or norbornene anhydride [179,180] derivatives. Ultimately, NB-based macromonomers afford a carbonyl site near the catalytic center. The catalyst activities are compromised due to the formation of a stable ruthenium carbene complex [83]. The mechanism describing the effect on propagation rate in the ROMP of macromonomers is in stark contrast to that of the small monomers. It is notable that the reactivities of NB-based small-molecule monomers decrease with an increase in the substituent size, and *exo* isomers show higher reactivities than their *endo* counterparts on their anchor groups [174]. However, steric congestion has a minor effect on the reactivities of the macromonomers. The anchor groups can affect the electronic structure of the macromonomers, which in turn modulate the reaction rate, i.e., the monomers with electron-donor anchor groups that increase the HOMO energy can increase the propagation rate and promote the formation of high-MW BBPs via the “grafting-through” approach, and the density functional theory (DFT) calculations verify this conclusion (Fig. 8) [83].

The “grafting-through” approach can be used to synthesize BBPs, which resemble linear BCPs synthesized using small monomers. Miktoarm BBPs with randomly distributed brushes can be readily obtained by the copolymerization of two different macromonomers. For instance, Hudson and coworkers synthesized miktoarm copolymer brushes via the ROMP of NB-functionalized macromonomers that were premade by the ATRP of the acrylic monomers [10]. The unbalanced heterografts BBPs with incompatible brushes often self-assemble into irregular morphologies rather than well-ordered conformation. Specifically, heterografted BBPs with two different PS and PLA grafts on each repeating unit, with equivalent distributions facilitate the formation of a well-ordered Janus morphology [184,185]. BBPs can be readily obtained via the “grafting-through” approach with the sequential polymerization of two different macromonomers with the CRP or ROMP technique [2]. Diblock and triblock BBPs bearing miktoarm copolymer side chains have been synthesized via this approach [22]. Furthermore, multiblock BBPs with precise, well-defined structures have also been prepared by the sequential addition of macromonomers

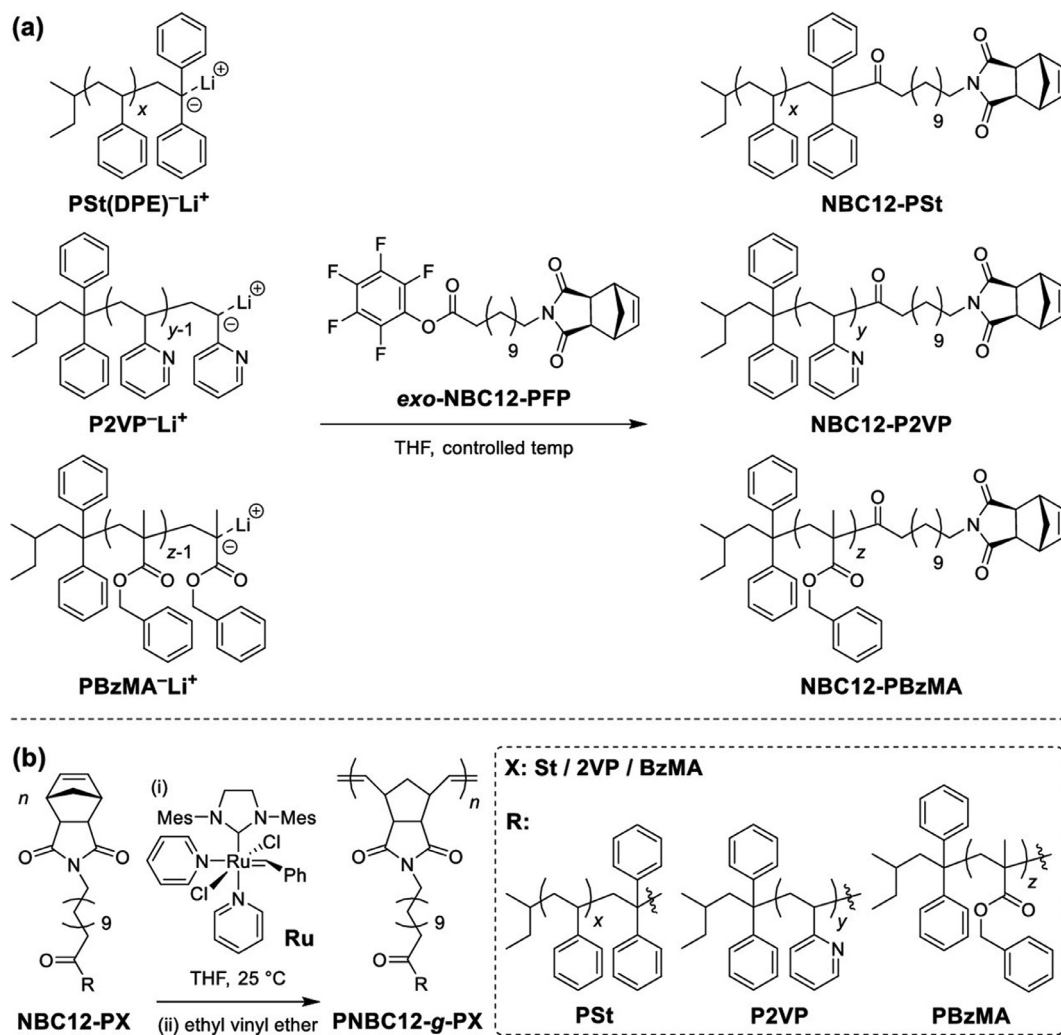


Fig. 7. (a) End-capping reaction of three different types of living anionic polymers with *exo*-NBC12-PFP and (b) corresponding BBPs via ROMP. [179], Copyright 2019. Reproduced with permission from the American Chemical Society.

strategy. When macromonomers with different MWs were added during ROMP in different manners (i.e., different molar ratios of monomer to catalyst to control the length), cone-shaped, three-dimensional BBPs were obtained [186].

2.3.3. Grafting-to

The “grafting-to” strategy involves the pre-synthesized polymers with reactive functional moieties and subsequent attachment to reactive sites on the prepared polymer backbones via highly effective coupling reactions. As the polymers are independently pre-synthesized using appropriate polymerization techniques independently, the precise control of MWs and narrow \bar{M}_w/\bar{M}_n can be achieved as the polymers can be characterized before coupling. Although the “grafting-to” strategy is straightforward, it typically suffers the low grafting density issue due to the unfavorable kinetic and thermodynamic barriers. With more side chains grafted on backbone, steric repulsion between the brushes prevents the movement of brushes toward active moieties on the backbone, leading to low grafting densities with loosely grafted polymer brushes. This effect is more prominent for grafting polymers with high MWs. In addition, the grafted side chains need to change from a random coil to an entropically unfavorable stretched conformation upon grafting brushes to the backbone with a high grafting density [172]. Free active sites likely exist on the backbone during grafting, and thus, limited grafting density on the BBPs is often obtained using

this approach. Generally, an excess of the pre-prepared polymers is added to promote the coupling reaction to a high extent. Thus, an additional separation process such as fractional precipitation is required to remove the unreacted polymers after the reaction. This process is tedious, time-consuming, and costly, and sometimes the purification is incomplete. These factors have limited negative effects when high-efficiency coupling reactions (e.g., CuAAC reaction) are used to craft BBPs via the “grafting-to” approach.

Nucleophilic substitution. Chemoselective coupling reactions (e.g. nucleophilic substitution/exchange) have laid the foundation for modern polymer analogous reactions, particularly for the post-modification of polymers. The activated ionic polymer end groups obtained after living anionic polymerization can nucleophilically react with various functional moieties [187]. Deffieux and co-workers reported the synthesis of BBPs with high grafting density via the coupling reaction of polystyryllithium or polyisoprenyllithium with the chlorine moieties on the poly(chloroethyl vinyl ether) backbone [188,189]. Alternatively, Gromadzki and coworkers obtained amphiphilic molecular brushes by preparing well-defined linear PCMS backbone with NMP and then attaching the anion-terminated PEG to the active sites on the backbone via Williamson etherification reaction [190]. In addition, N-hydroxysuccinimide (NHS)-activated amine exchange or pentafluorophenyl (PFP)-activated ester exchange has attracted tremendous interests from the synthetic standpoint because of the abundant

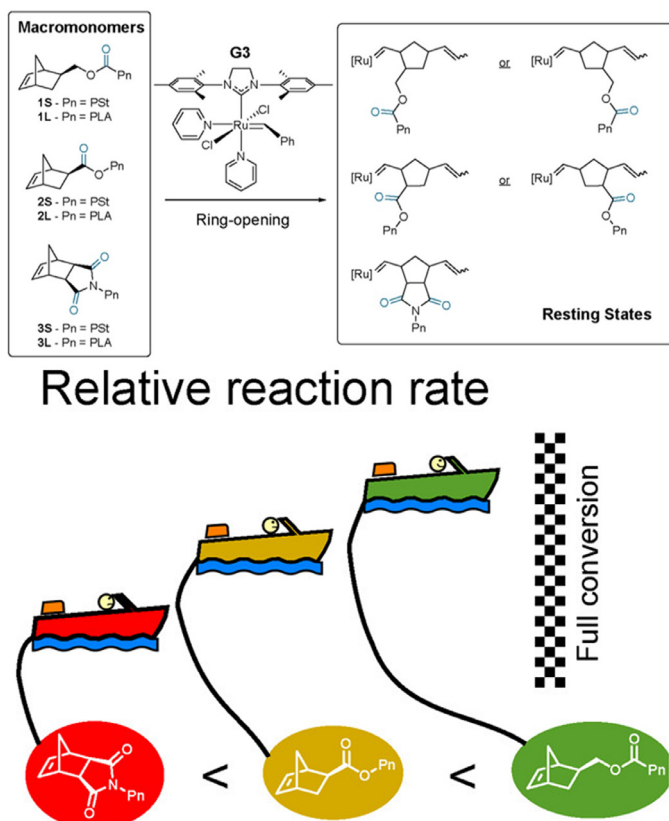


Fig. 8. Structures of macromonomers with different anchor groups and the corresponding relative reaction rate. [83], Copyright 2016. Adapted with permission from the American Chemical Society.

availability of most amines from natural or commercial sources and a lack of toxic metal catalysts usage [191]. For example, well-established poly(pentafluorophenyl methacrylate) (PPFPMA) reactive ester polymer was synthesized by RAFT polymerization, and it showed selective reactivity toward primary amines. BBPs bearing hyperbranched PG that has precisely one focal amino functionality were prepared via the “grafting-to” approach through selective nucleophilic exchanges (Fig. 9a) [192].

In addition, DNA-attached BBP conjugates have been reported using nucleophilic-activated amine exchange between the amino groups on DNA and the dangling reactive NHS sites on the polymer backbone (Fig. 9b) [193,194]. However, the harsh reaction conditions of living anionic polymerization lead to the inevitable deactivation of the end anionic groups. Moreover, the exchange reactions show low grafting efficiency of < 32% [193]. Therefore, it is highly desirable to develop mild coupling reactions for preparing densely grafted BBPs via the “grafting-to” approach with high efficiency.

CuAAC reaction. Click reactions are robust, highly efficient, and orthogonal organic coupling reactions for engineering complex polymer architectures in various fields [195,196]. Among the versatile click reactions, the CuAAC reaction is extensively employed in post-polymerization [197–200]. Matyjaszewski and coworkers first reported the synthesis of BBPs using click reaction via the “grafting-to” strategy (Fig. 10a) [201]. In their study, PHEMA bearing the pendant alkynyl sites was obtained after the ATRP of HEMA and subsequent esterification to examine the dependency of grafting density on the chemical composition and MW of side chains during click reaction. Azido-terminated polymeric side chains (e.g., PEO, PS, PBA, and diblock copolymer PBA-*b*-PS) were employed for the CuAAC reaction. BBPs with grafting density up to 88% were obtained when “thin” and low-MW PEO- N_3 was utilized as the side

chain. Conversely, when bulky side chains with high MW were grafted, a low grafting density (< 50%) was obtained because of the steric effect. This phenomenon was more obvious in the synthesis of all-conjugated BBPs using this strategy. For instance, during the grafting of acetylene-terminated polyselenophene to the azide-functionalized polythiophene backbones, low grafting density and Glaser terminal alkyne homocoupling were observed in the system, and fortunately, the side reaction (homocoupling) could be suppressed using an organic-soluble copper catalyst [202]. Therefore, it was favorable to prepare densely grafted BBPs with thin and short side chains. This conclusion was also verified using bulky alkyne-terminated PMMA as the brush, which afforded only 50% grafting under the same conditions [203]. Very recently, Zhao and coworkers also investigated the effect of the backbone composition on the grafting efficiency [204,205]. They prepared hetero-grafted BBPs bearing PMMA backbone and two distinct bulky side chains (i.e. PDEGEA and PEO) through the combination of ATRP and CuAAC reaction. The flexible tri(ethylene glycol) spacer between the backbone and side chain improved the grafting density because it alleviated the steric effect during CuAAC reactions (Fig. 10b) [204]. Thereafter, Hammond and coworkers prepared polypeptide-based BBP with almost 100% grafting density using the CuAAC reaction [206]. The α -helical backbone made the pendant alkyne-terminus protrude for a favorable side chain coupling, and the steric exclusion among the grafted brushes maintained the symmetrical backbone conformation [206]. Recently, Wu and coworkers synthesized densely packed BBPs with helical polyisocyanide as both backbone and side chain [207]. They also demonstrated that a helical backbone promoted an increase in the grafting density of the BBPs through polyisocyanide consisting of a C-C single bond.

In general, alkyne functional groups are placed on the backbone or side chain end via the direct polymerization of alkyne-containing monomers and initiators or post-modification. It has been reported that the positions of functional moieties significantly affect the grafting density. For example, Gao and coworkers synthesized BBPs with ultrahigh crowded brushes (~ 2.68 PEO per repeating unit) through the accelerated CuAAC “grafting-to” strategy (Fig. 10c). Here, azido- and alkynyl-functionalized side chains with different chemical structures (e.g., PEG, PMMA, and PDMA) were synthesized and employed to couple PMMA bearing pendant multialkynyl or multiazido functional moieties, respectively [208]. PMMA backbones bearing multiazido dangling groups could improve the grafting efficiency of CuAAC reaction with alkynyl-terminated PEO as side chains because the formed triazole moieties could complex with the CuX catalyst and proximal chelation accelerated the catalysis of adjacent azido moieties on the backbone during CuAAC reaction.

DNA molecules have been used to build highly sophisticated architectures with excellent precision because of their remarkable structural features and unique molecular recognition properties [209]. Researchers have attempted to tether DNA brushes onto an artificial polymer main chain. For example, DNA-grafted BBPs were synthesized via the “grafting-through” approach and the precise control of DNA could be achieved by varying the monomer-to-catalyst ratio [210]. However, the tedious process of preparing DNA-based macromonomers adversely affects the DNA structure. Click reactions allow easy grafting of the side chain under mild conditions even in water solution. Das and coworkers used macroinitiator as the backbone to initiate the PEO monomer as the first block to increase the solubility in aqueous solutions. Then, the halide terminus on side chain was substituted with azides. Finally, 5-hexynyl-modified DNA oligonucleotide was grafted onto the termini of the clickable BBPs through CuAAC reaction in buffer solution to obtain core-shell BBPs [211,212]. However, the initiation efficiency was 50% because of the presence of a bulky monomer on the first block, which led to the low grafting density of the DNA

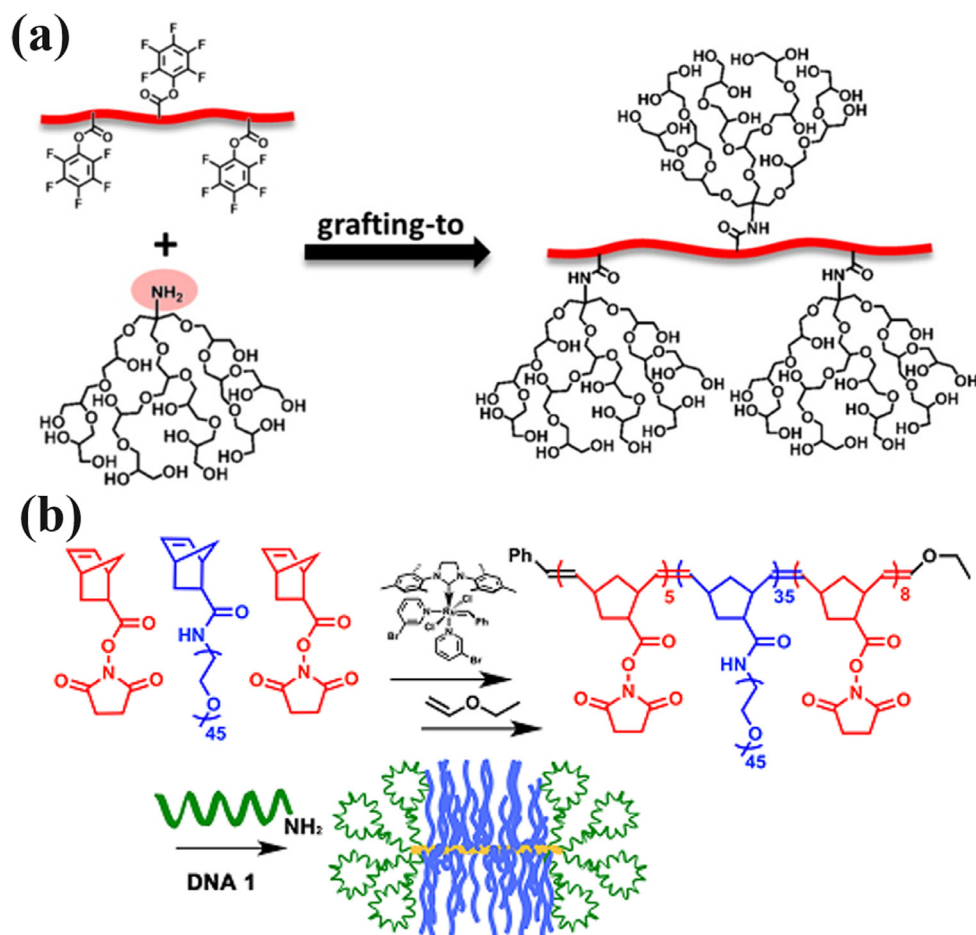


Fig. 9. Preparation of BBPs via the "grafting-to" approach. (a) Amino nucleophilic substitution of PFP. [192], Copyright 2012. (b) Amino nucleophilic substitution of NHS. [193], Copyright 2014. Reproduced with permission from the American Chemical Society.

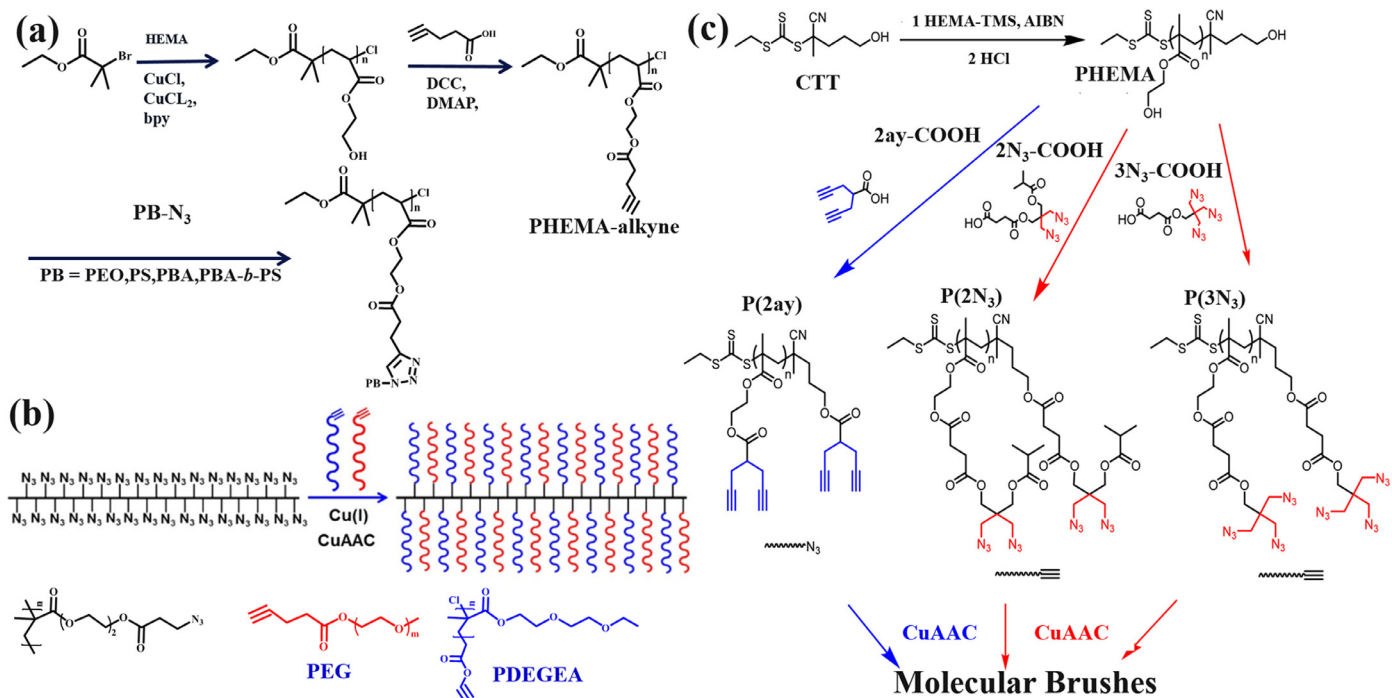


Fig. 10. Schematic illustration of synthesis for bottlebrush polymers via a combination of CRP and click reactions. (a) Homografted bottlebrush polymer. [201], Copyright 2007. (b) Binary heterografted bottlebrush polymer. [204], Copyright 2017. (c) Multigrafted bottlebrush polymers. [208], Copyright 2017. Adapted with permission from the American Chemical Society.

bristles. To increase hydrophilicity and biocompatibility, the BBPs with biomimetic polypeptides as the backbones were also prepared using click chemistry [120,206,213]. Polypeptide-g-DNA BBPs containing complementary DNA side chains were synthesized via the CuAAC reaction, and core-shell supermolecular bottlebrushes were easily prepared through specific DNA hybridization [214]. Although BBPs with high grafting densities have been achieved using CuAAC reaction, the azide groups could decompose because of their UV sensitivities and thermal instabilities, such that extra precautions were needed during the preparation.

Thiol-ene/yne reaction. This hydrothiolation reaction can proceed via a radical mechanism under UV irradiation, using an initiator with thermal heating, or via a base/nucleophile-mediated addition [215]. Recently, Saito and coworkers reported the synthesis of BBPs, PDMS-g-PEGMEA, with a photo-irradiated thiol-ene reaction. In their work, they used a (mercaptopropyl)methylsiloxane homopolymer (thiol-PDMS) bearing pendant thiol groups as the backbone, an OEGMA as the side chain, BBPs with different backbone lengths were obtained after UV irradiation [216]. However, thiol-ene polymerization between the thiols and acrylates often results in a mixed-mode polymerization, i.e., thiol-ene coupling reaction and acrylate homopolymerization, and thus, linear polymers are inevitably formed during the reaction [216,217]. Alternatively, Renard and coworkers synthesized amphiphilic BBPs using thiol-terminated polymers as side chain, and vinyl moieties-containing polymers as backbone via photochemical thiol-ene addition [218]. The methodology prevented the formation of linear polymers by employing a monomer with a low-activity double bond. However, thiol-ene additions suffer from low coupling efficiencies because of their intrinsic two-step reaction mechanism [215]. Thiol-yne reactions can be explained using the generally accepted mechanisms of propagation and chain transfer steps in the thiol-ene reaction, improving the grafting efficiency in preparing BBPs. For instance, PS-based brush polymers were achieved using photochemical thiol-yne reaction between the thiol-PS backbone and phenylacetylene-terminated PS side chain [219].

Diels-Alder cycloaddition reaction. Diels-Alder (DA) cycloaddition reaction is performed between a conjugated diene and alkene to afford an unsaturated ring upon heating without any catalysts. DA reactions allow the formation of a dynamic bond and without any byproducts. It is favorable to prepare BBPs for applications in biomedical and photoelectronic fields [215]. Yagci and coworkers reported the preparation of well-defined brush copolymers using anthracene-maleimide-based DA “click reaction” via the “grafting-to” approach [220]. The backbone was synthesized by the copolymerization of St and CMS via NMP, followed by the attachment of the anthracene functionality to the CMS units, and then maleimide-functionalized brushes (e.g., PS and PEG) were covalently attached to the pendant anthryl moieties at elevated temperatures. Thereafter, well-defined heterograft BBPs were prepared using CuAAC and DA reactions in one pot [221,222]. Notably, the conventional DA reactions are performed at elevated temperatures, which is an energy-consuming process and can have adverse effects on the BBPs. The triazolidinedione (TAD)-diene DA reaction has been extensively studied in organic synthesis and can be performed at room temperature in metal-free condition with high efficiency [223]. Recently, Zhang and coworkers reported the preparation of BBPs employing TAD-diene DA reaction under mild conditions [224,225]. The TAD-diene coupling reaction was applied to quantitatively yield the corresponding BBPs and the process was accomplished in 10 min [224].

2.3.4. Other routes

The “grafting-from,” “grafting-through,” and “grafting-to” strategies have been extensively investigated to synthesize various well-defined BBPs with different sub-architectures and chemical com-

positions. However, it is difficult to prepare complex-structured BBPs using only one strategy owing to their intrinsic features. Recent developments in the advanced polymerization techniques have afforded various polymer architectures with incredible control and simple operations through different strategies. Combining two or three strategies with complementary features in one method can produce well-designed BBPs and facilitate the straightforward preparation of complicated BBPs.

A unique promising strategy to synthesize BBPs, known as the “transfer-to” polymerization, is the hybrid of “grafting-from” and “grafting-to” strategies [41]. RAFT CTAs possess an R-group and a Z-group, and the CTAs can be attached onto the backbone through these two moieties. Most reported methods to synthesize BBPs using RAFT polymerization via the “grafting-from” approach are based on the R-group method, in which the brushes grow from the periphery of the main chain. In contrast, during polymerization in the Z-group method, the Z-group-derived radicals remain tethered on the backbone during CTA fragmentation, whereas the detached initiating radicals grow freely in the media and transfer to the pendant CTA on the backbone for deactivation [41]. In this method known as the “transfer-to” strategy, the chain grows freely in solution. It can eliminate the side reactions such as intermolecular and intramolecular couplings that lead to defects on the substrates via the “grafting-from” strategy. However, the grafting density may be severely affected by the steric shielding phenomenon as in the case of the “grafting-to” strategy. Matson and coworkers reported the synthesis of BBPs via the “transfer-to” strategy [226]. PNB backbone bearing the CTA sites that were connected with the Z-group method were synthesized via ROMP, and the brushes were then grown via RAFT polymerization initiated by the pendant CTAs. This strategy afforded the preparation of high-MW BBPs without radical coupling during polymerization.

Notably, the alternating block BBPs can be synthesized by the copolymerization of styrenic and maleimide (macro)monomers with an equimolar feed ratio [170]. Liu and coworkers reported the preparation of well-controlled amphiphilic Janus BBPs bearing alternative PMMA and PNIPAM brushes via the “grafting-from” strategy in conjunction with the “grafting-to” approach [227]. Inspired by the mechanism of ATRP and CuAAC click reaction using the same catalytic system (i.e., CuX/PMDETA), Huang and coworkers reported the synthesis of Janus BBPs employing the orthogonal reactions of ATRP and CuAAC in one pot [3]. They synthesized a tri-functional inimer and used it to prepare a backbone macroinitiator through RAFT polymerization, where the 2-bromopropionate initiator was used for ATRP via the “grafting-from” approach and the alkynyl moiety was used for CuAAC via the “grafting-to” approach. Subsequently, asymmetric brushes were attached onto the PMMA main chain through tandem CuAAC reaction and ATRP using the same catalyst. This facile methodology provided a versatile pathway to prepare various Janus BBPs with high controllability and compatibility. However, the backbone length was short because of the intrinsic steric hindrance of specific monomers [3].

Brush-on-brush BBPs are brush polymers that have secondary side chains on the primary side chains directly attached onto the backbone [228,229]. These have not been extensively studied, because the synthetic pathways are limited, complicated, and time-consuming. In addition, as most of the BBPs include two C-C bonds among the adjacent side grafts, the intrinsic steric hindrance prevents the grafting of the secondary brush on the grafted side chains. On the one hand, as mentioned before, copolymerizing with other comonomers can relieve steric crowding. On the other hand, loose grafting may affect the conformation and morphology. Introducing bulky side chains such as dendrons into the BBPs with low grafting densities allows stretching of the backbone and affords more control over their structures and dimensions. Chen and coworkers designed PCL as the backbone to prepare polymers

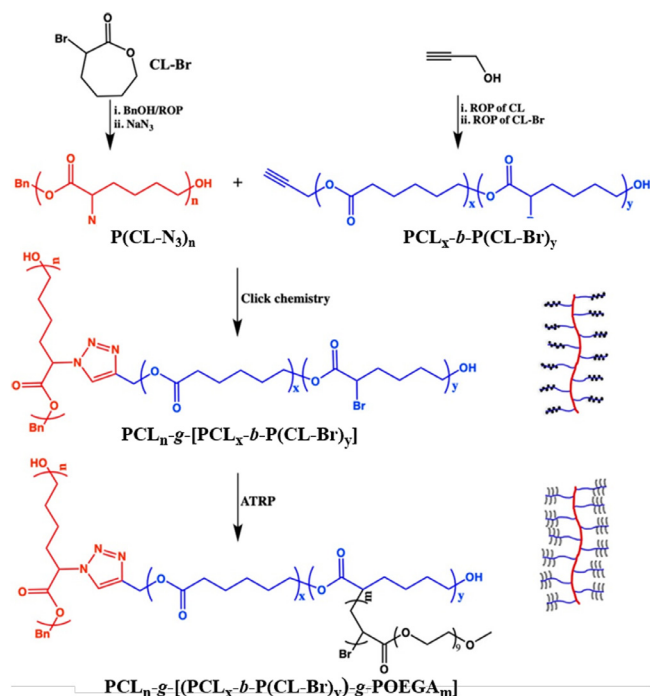


Fig. 11. Schematic illustration for the synthesis of brush-on-brush BBPs. [229]. Copyright 2019. Reproduced with permission from the American Chemical Society.

with brush-on-brush architecture (Fig. 11) [229]. They synthesized the P(CL-Br) backbone via the ROP of CL-Br and subsequently converted the pendant bromines on the backbone into azido groups via a substitution reaction. Then, the alkyne-terminated diblock primary side chain was grafted onto the backbone by a CuAAC reaction to afford PCL-g-(PCL-b-P(CL-Br)) BBPs. Finally, the secondary POEGA brushes were grown from the primary brush via the ATRP of OEGA, yielding an amphiphilic core-shell BBPs, PCL-g-(PCL-b-(P(CL-Br)-g-POEGA)). Interestingly, both PCL-g-(PCL-b-P(CL-Br)) and brush-on-brush PCL-g-(PCL-b-(P(CL-Br)-g-POEGA)) polymers showed worm-like morphology with “hairy” brushes [229].

3. Self-assembled architectures of bottlebrush polymers

The steric effect arising from densely-grafted and constrained side chains forces the BBPs to form a cylindrical architecture. This conformation of BBPs is significantly affected by the grafting density and sizes of the main chain and side chain. Many anticipated properties of the BBPs arise from their unique molecular structures. BBPs exhibit a distinct lack of entanglement in comparison to the linear polymers with the same composition due to the steric repulsion among the dense brushes. This absence of entanglement in the BBPs leads to low energy barriers for structural reorganization and rapid assembly in the concentrated solution and melt [230]. In addition, the worm-like BBPs can be visualized using AFM or scanning force microscopy (SFM) [1,10]. Moreover, small-angle neutron scattering (SANS) or small-angle X-ray scattering (SAXS) measurements have been used to accurately characterize the stretched conformations of the polymeric main chain and brushes, which can address the full form factors of BBPs in solution [231]. Furthermore, theoretical simulations have also been employed to study the self-assembly of BBPs in solution or bulk state with self-consistent-field, [27,232] analytical theory, [233] and scaling theory [234]. However, most of the information discussed herein is based on the cylindrical morphology of the BBPs. BBPs exhibit different self-assembly behavior with different structural parameters. Moreover, BBP copolymers (e.g., BBPs

and Janus BBPs) with high or ultrahigh MWs (>1MDa) can readily assemble into well-ordered structures arising from the high MW and extended conformation of the BBP blocks [15]. It is worth noting that solvent quality significantly affects the polymer conformation, and it can also be employed to tune the assembled morphologies of the BBPs. By varying these parameters, together with the stiffness of the polymer side chains, various sophisticated self-assembled nanostructures have been prepared with variable dimensions and functionalities [197,235,236]. Recent studies have reported that by increasing the DP of the backbone, BBPs can achieve the conformational transition from star-like to brush-like polymers under appropriate solvent conditions [28,30,231]. When the lengths of their backbones are similar to those of the side chains, BBPs behave as star-like polymers exhibiting spherical morphologies, whereas these behave as semiflexible cylinders when their backbone lengths are larger than those of the side chains (Fig. 12) [231]. This conformational transformation of the BBPs has been theoretically and experimentally verified by simulation [237] and SANS [231] measurements. The self-assembly behavior of the BBPs bearing poly(oxanorbornene) backbones and PS brushes was investigated by SANS and transmission electron microscopy (TEM) [231]. With an increase in the backbone length, a conformational transition from sphere to cylinder occurred, which was observed by the SANS measurement. For the BBPs with short backbones, plateaus were observed in the low-*q* range in the SANS curves, indicating that these showed globular or spherical morphology in toluene. The extended rod-like conformations of the BBPs with long backbones were characterized by an increased slope in the low-*q* range (Fig. 12) [231]. The BBP size and conformation in solution can be quantitatively measured using the Guinier-Porod model to fit the SANS data, which affords a small dimension parameter, indicating the spherical morphology of the molecules. The TEM results of the BBPs with low backbone DP also exhibit spherical shape despite the incomparable size with the SANS measurements [231].

3.1. Spherical nanostructures

Amphiphilic linear BCPs can self-assemble into a wide range of well-ordered morphologies to minimize the energetically unfavorable interactions. The inherent interfacial curvature of the BCP significantly affect the formation of predictable conformations and properties. Various reported morphologies have been obtained by manipulating the packing of copolymer chains [238]. The packing parameter, *p*, can be expressed by Equation (1):

$$p = \frac{v}{al} \quad (1)$$

where *v* and *l* are the volume and length of the hydrophobic tail chain, respectively, and *a* is the section area per polymer chain [238]. Therefore, self-assembled geometrical morphology can be predicted by *p*. A guiding principle has been proposed to tune the self-assembly behaviors of the amphiphilic BCPs in solution. For *p* < 1/3, a spherical morphology is preferred, while the cylindrical morphology is preferred for 1/3 < *p* < 1/2, and enclosed membrane morphology (e.g., vesicles) is preferred for 1/2 < *p* < 1.

BBPs show cylindrical shapes because of the densely grafted brushes. The persistence lengths of the BBPs can be easily manipulated by varying the DP of their backbones, while the cross-sectional diameter is determined by the length of the brush. The dimensions of the BBPs can be readily tuned by controlling the above structural parameters. Amphiphilic bottlebrush copolymers with different sub-architectures including core-shell, [12,62,214,229] blocky, [10,55,239] and Janus-like [3,158,165,184] structures have been prepared via the aforementioned strategies. Therefore, by manipulating the lyophilic and lyophobic properties of the bottlebrush copolymers, precise self-assembled morpholo-

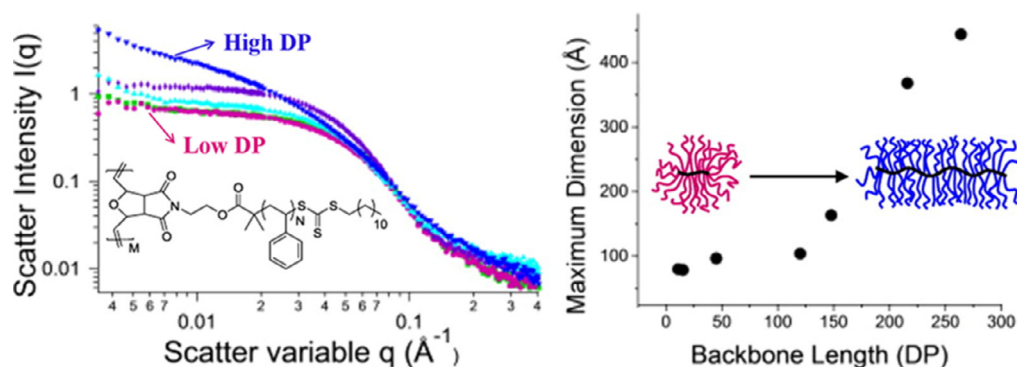


Fig. 12. SANS measurements for BBPs with various backbone length and corresponding relationship of the conformation of BBPs with backbone DP. [231], Copyright 2013. Adapted with permission from the American Chemical Society.

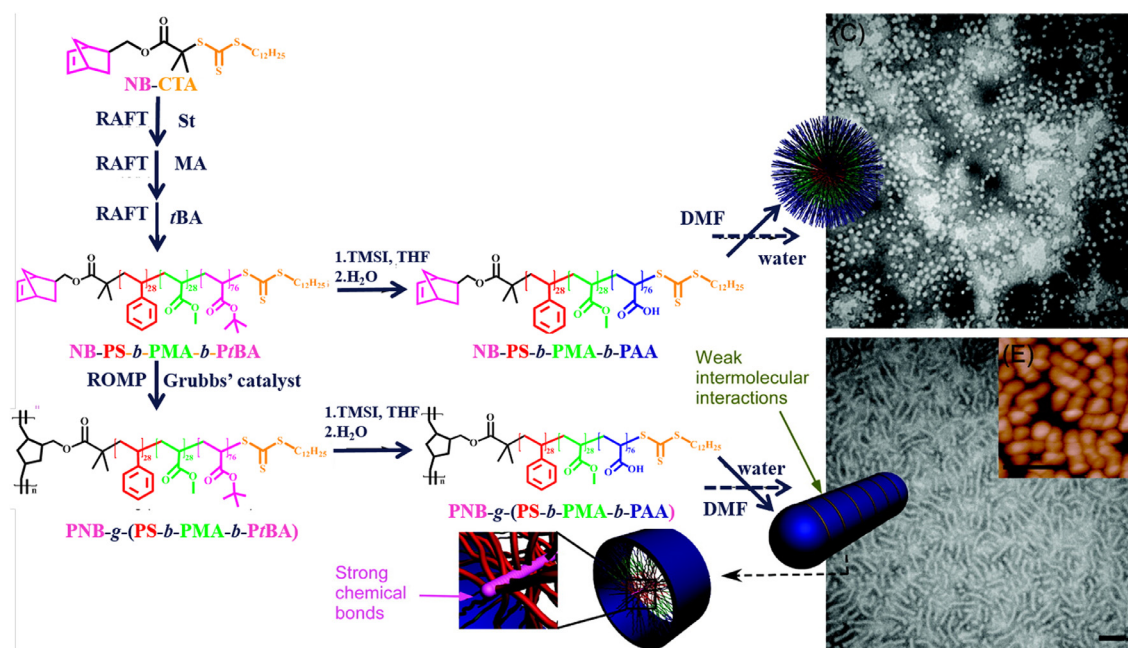


Fig. 13. TEM and AFM images of the self-assembly of concentrically amphiphilic triblock-grafted BBP and linear amphiphilic macromonomer. [240], Copyright 2011. Adapted with permission from the American Chemical Society.

gies can be obtained in selected solvents based on the packing parameter.

In an extraordinary case, self-assembled spherical aggregates acted as unstable intermediates, which continued to grow and form stable aggregates. Amphiphilic triblock-grafted BBP PNB-g-(PS-*b*-PMA-*b*-PAA) was prepared by the ROMP of a triblock macromonomer, NB-PS-*b*-PMA-*b*-PtBA, via the “grafting-through” approach after converting the tBA portion of the PtBA chain segments to PAA (Fig. 13) [240]. When the BBP solution in dimethylformamide (DMF) dialyzed with water, a long cylindrical shape was formed and its diameter was similar to that of the spherical morphology formed by the corresponding linear copolymer amphiphiles. The outer PAA block in the molecular brush framework could stabilize the cylindrical micelles in aqueous dispersions, but only to a limited extent. Another interaction owing to the assembly of multiple molecular brushes was observed through the contact of the hydrophobic interior (PS and PMA) counterparts. Thus, unidirectional self-assembly could decrease the exposure of the active end caps and lower the intrinsic energy of the cylindrical micelles. After heating the solution, cylindrical morphologies disassembled into globular entities because of the breakage of weak supermolecular interactions. Unfortunately, cooling could not re-

sult in the reversible recovery of the cylindrical morphology because of the formation of stable spherical micelles surrounded by hydrophilic shells [240].

Amphiphilic brush-linear copolymers can also self-assemble into structures with different morphologies. Brush-linear copolymers have the advantage of more functional groups at the ends of their brushes. For instance, a copolymer consisting of a brush and linear polymer segment exhibited a tadpole-like conformation in good solvents [17]. Upon changing the polymeric tail structure, the block copolymer transformed into worm-like micelles with a collapsed tail morphology [16,17]. However, in another case, brush-linear copolymers self-assembled into a spherical shape [241]. Recently, a fascinating brush-star architecture was obtained by covalently cross-linking the self-assembled brush-linear copolymers containing PMMA side chains and linear poly(glycidyl methacrylate) (PGMA) end blocks [242].

Amphiphilic diblock BBPs with symmetric side chain lengths can form crew-cut aggregates that resemble linear BCPs with high block asymmetry. For example, amphiphilic diblock BBPs bearing hydrophilic PAA and hydrophobic PS side chains were prepared by sequential ROMP and RAFT polymerization, and globular aggregates were obtained with phase-segregation micellization meth-

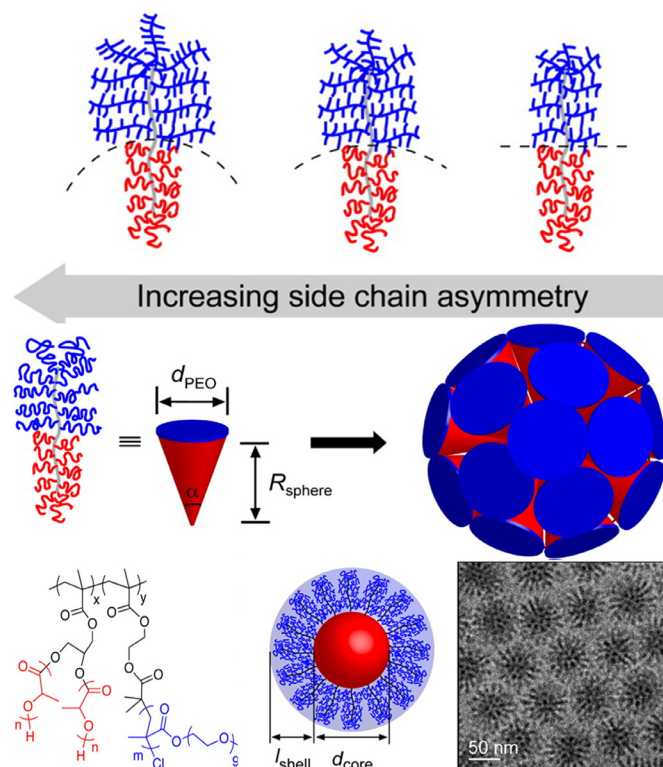


Fig. 14. Schematic illustrations of interfacial curvature and self-assembly of BBPs with different side chain and corresponding TEM image. [239], Copyright 2014. Adapted with permission from the American Chemical Society.

ods and characterized using TEM and AFM [243]. Notably, the self-assembly of linear BCPs in solution is driven by a decrease in free energy. Several variables can change these parameters and lead to various self-assembled morphologies [238]. However, linear BCPs with very high MWs (> 200 kDa) are not easily thermodynamically stabilized during self-assembly because of extensive entanglements in the condensed phase, whereas BBPs can afford the thermodynamically stable morphologies by forming kinetically favored intermediate morphologies owing to limited entanglements. Kim and coworkers reported the self-assembly of PNB-based BCP with PEG and PS side chains [244]. A gradual decrease in the weight fraction of the hydrophilic PEG brushes (W_{PEG}) was found to translate the morphology of amphiphilic BBPs from spherical micelles to vesicles in a mixture of 1,4-dioxane and water. When the W_{PEG} values were decreased to 6 wt%, the BBPs could self-assemble into inverse cubosomes, a morphology that is challenging to achieve in linear BCPs, considering the kinetic trapping of self-assembly in solution. In addition, with an increase in the rate of water addition from 0.5 to 1 mL/h, the internal cubic order of the polymer cubosomes deteriorated significantly, owing to the kinetic effect of self-assembly. When solvent evaporation was used to extend the self-assembly time, cubosomes with single symmetry were achieved with this BCP [244]. Furthermore, complex spherical nanostructures with coaxial lamellae were obtained using the BBPs bearing incompatible PS and PLA brushes in the confined nanoemulsion droplets [245].

The preparation of BBPs with different side chain lengths can lead to conical morphologies [186]. In this context, the cone height is approximately equal to the micelle radius, forming molecular-shape-mediated morphology. To understand the native micelle compositions of the amphiphilic BBPs, Rzaev and coworkers synthesized amphiphilic BBPs containing PLA and PEGMA brushes via the “grafting-from” strategy (Fig. 14) [239]. The assembled mor-

phologies of the bottlebrush amphiphiles verified the above hypothesis. The protruding brush length in the micelles measured using cryogenic (cryo-TEM) was 19 ± 1 nm, which was comparable to the backbone length of the PEGMA-containing brush block in a highly extended conformation. With identical PLA side chain lengths and fixed DP of the two blocks, the short PEO branches led to reduced interfacial curvature, forming large spherical micelles. The packing parameter for BCP calculated using Equation (1) was approximately 0.3, such that spherical micelles were favorably formed during self-assembly. Furthermore, photoactive coumarin groups could be introduced into the inner PLA side chain ends and core-cross-linked PLA micelles were obtained under UV irradiation, which could be used for drug release [246].

Janus-like amphiphilic macromolecular brushes can spontaneously self-assemble into stable spherical micelles via the cosolvent approach [11,227]. By varying the self-assembly conditions, identical materials can show different morphologies. Janus BBPs with hydrophilic PEG and hydrophobic PS brushes were prepared via a combination of CuAAC and ROP techniques. The self-assembly behaviors of the amphiphilic BBP containing different weight fractions of PEG (W_{PEG}) were investigated in a mixture of H_2O (non-solvent) and tetrahydrofuran (THF; good solvent) (Fig. 15) [247]. The system with the highest W_{PEG} was observed to form homogeneous spherical micelles. A decrease in W_{PEG} in the BBPs resulted in the formation of a cornucopia of toroidal morphology coexisting with other morphologies. Vesicles were formed at the lowest W_{PEG} via rapid assembly, while giant vesicles were observed by dialysis for the same amphiphiles. The morphological diversity resulted from the interfacial curvature or the interaction between the immiscible blocks. In a selected solvent, the hydrophobic backbone and PLA collapsed to form the core while the hydrophilic PEG stretched out acting as a steric stabilizing layer to minimize the energy. An increase in the PLA content was insufficient to stabilize the unimolecular structures, and these changed into a cylindrical morphology through intermolecular association. Additionally, local concentration in conjunction with the solvent quality directed cylinder growth over the end-to-end connection, forming toroid micelles. This phenomenon has also been reported in the BBPs consisting of rigid polypeptide backbones and flexible PEG side chains, which is consistent with the simulation [248]. Vesicles are formed with a further decrease in W_{PEG} , as hydrophilic PEG blocks preferentially migrate to the outer surface to stabilize the hydrophobic interlayer. Similar mechanisms of vesicle micelle formation were reported for asymmetric BBPs, PGMA-*g*-(PEO/PS-*b*-PNIPAM), bearing PEO and diblock PS-*b*-PNIPAM brushes [249]. In addition, extrinsic constraints, such as annealing at elevated temperatures above the melting temperature promote the chain motions. For instance, Janus BBP PNB-*g*-PS/PLA was first found to self-assemble into particle-like morphologies. The BBPs were then observed to form “gradual-Janus” conformations when annealed at 150°C because it slightly promoted the chain motion in amorphous domains forming parallel domains. Further annealing at 180°C , transformed the BBPs into round particles because of the free movement of brushes [184].

3.2. Cylindrical nanostructures

BBPs can adopt worm-like morphology in a good solvent with lengths and diameters controlled by the DP of backbone and side chains, respectively. In principle, cylindrical morphology can be characterized using the parameters such as length per monomeric unit of backbone (l_m ($l_m = L/n_{\text{bb}}$, where L is the contour length of a bottlebrush macromolecule), diameter of cylindrical brush (D), persistence length of the cylindrical brush (l_p (or Kuhn segment length b), particularly, $b = 2l_p$, grafting density (σ), and DP of the backbone (N_{bb} or n_{bb}) and side chain (N_{sc} or n_{sc}), where n_g is num-

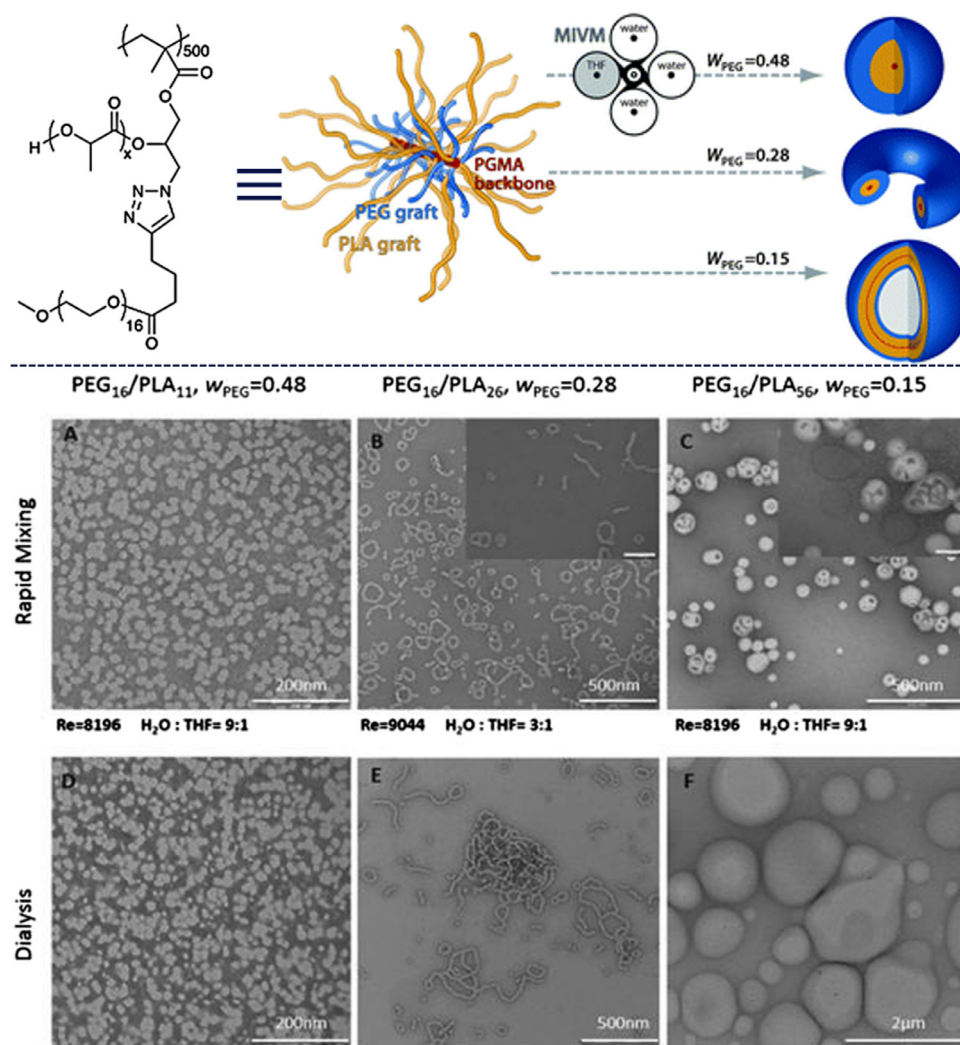


Fig. 15. Schematic illustrations of self-assembly mechanism and aggregate morphologies of amphiphilic Janus BBPs under various conditions. [247], Copyright 2014. Adapted with permission from the Royal Society of Chemistry.

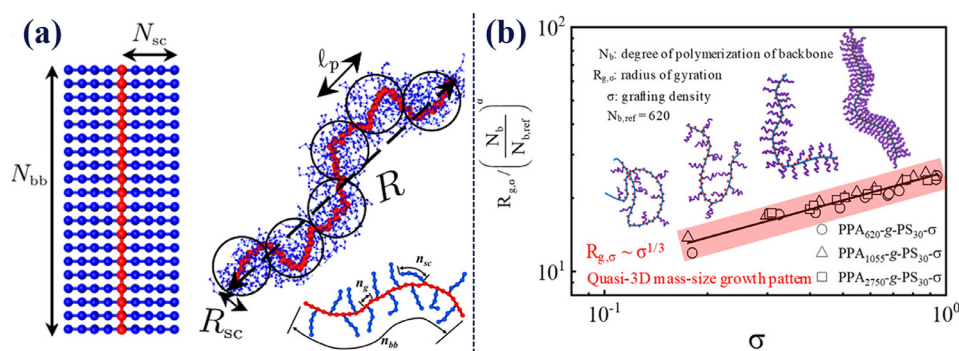


Fig. 16. (a) Molecular architecture and conformation of a BBP with different grafting densities. [251], Copyright 2016. Reproduced with permission from the American Association for the Advancement of Science. (b) Grafting density dependence of the normalized chain size for brush-like polymer. [255], Copyright 2019. Reproduced with permission from the American Chemical Society.

ber of bonds on backbone between the adjacent grafting points [8,250]. When $n_{bb} < b/l_m$, the backbone can be regarded as rigid backbone, whereas it is flexible backbone [8]. In addition, a brush macromolecule can be considered as a bead chain with a diameter of R_{sc} that hosts the monomeric units of the surrounding macromolecules, and its value is of the order of the length, l_p (Fig. 16a) [251]. The DP of the side chain and grafting density of the BBPs

can increase the l_p value [252]. For PS-based BBP, with an increase in the MW of the side chain, l_p increases from $l_m = 0.1$ nm with M_n of 1.4 k Da to $l_m = 0.21$ nm with M_n of 4.9 k Da in a good solvent [253]. The l_p originating from the spherical chain model can be characterized by the radius of gyration R_g and hydrodynamic radius R_h . The length of the cylindrical brush is different from the contour length measured for the polymer in Brownian motion. Fur-

thermore, BBPs exhibit distinct excluded volume effects, which significantly affect the structural parameters and experimental results. It is extremely challenging to accurately predict the scaling between l_p and N_{bb} or N_{sc} . Although several theories have been proposed to establish the relationship between these chemical structural parameters, [250] discrepancy in the simulations and experimental results still exists, which is attributed to several phenomena. First, BBPs afford various structural conformations on different length scales [250]. On a small length scale, the backbone behaves flexibly, and on a large length scale, the backbone is extended and rigid. Nevertheless, it is difficult to separate the scattering signals from the main chain and branched chains. Second, it is challenging to obtain an extremely long backbone ($> 10\text{--}100 l_p$) to satisfy the ordinary self-avoiding walk model [254]. Third, the assumed structural parameters of the BBPs are different in different experiments.

Notably, l_m is dependent on the solvent quality [253]. For BBPs bearing the PMMA main chain and PS branched chains, the increase in l_m in a good solvent (e.g., toluene) for the side chains is greater than that in a poor solvent (e.g., cyclohexane). This difference in l_m is attributed to the weak excluded volume effects among the side chains, forming local coiled backbone in cyclohexane. In addition, an increase of solubility of BBPs increases the l_m to that for a fully extended vinylic main chain conformation with $l_m \approx 0.253 \text{ nm}$, regardless of the side chain length [253]. Furthermore, the main chain transforms from the coiled to the extended state with an increase in the grafting density owing to the enhanced steric repulsion among the side chains. Lodge and coworkers made significant experimental progress in determining the effect of grafting density on the excluded volume theory [256]. They prepared a set of comb-like brush polymers by grafting short PEG onto methylcellulose backbones in the low- σ regime ($\sim 0.01 < \sigma < \sim 0.33$). The size of the resulting brush-like polymer increased monotonically with an increase in the grafting density, and it was consistent with the classical excluded volume theories by neglecting the branch-branch excluded volume interaction. In agreement with Flory's argument, three types of excluded volume interactions (e.g., repeating unit-repeating unit, repeating unit-branch, and branch-branch) are involved in the free energy of a BBP. Li and coworkers successfully synthesized four sets of brush-like polymers with poly(propargyl acrylate) (PPA) as the backbone bearing PS side chains with $0 < \sigma < 0.97$ [255]. The branch-branch excluded volume interactions still contributed to the free energy of the BBPs even with low σ . In addition, the backbone length significantly affected the excluded volume interactions and morphology of the BBP. In particular, scaling equations of $R_g \sim \sigma^{1/3}$ and $[\eta] \sim \sigma^\circ$ for the BBPs were obtained, this conclusion was experimentally confirmed by rational design and preparation of BBPs (Fig. 16b) [255].

As mentioned above, the dimensions of the main chain and brushes can be independently characterized by X-ray scattering and AFM in the solution state. Unlike the BBPs in solution, the conformations of the BBPs on the surface can only be visualized by AFM, which can afford intermolecular resolution. By combining the Langmuir Blodgett (LB) technique, which provides the mass density of the monolayer, with AFM that affords the molecular density information, the absolute value for the number-average MW and length distribution of the BBPs can be accurately determined [257].

It is worth noting that the conformations of the BBPs adsorbed on a substrate are significantly affected by the surrounding environment [1]. The cylindrical shape of BBP can break into sectionalized side chains when adsorbed on the surface. The fraction of the adsorbed side chains (φ_a) on the surface dominates the conformation of BBP on the substrate. In good solvents, BBPs can adopt a ribbon-like conformation, which allows a large surface contact with $\varphi_a \approx 1$ (Fig. 17b). When the side chains are weakly adsorbed

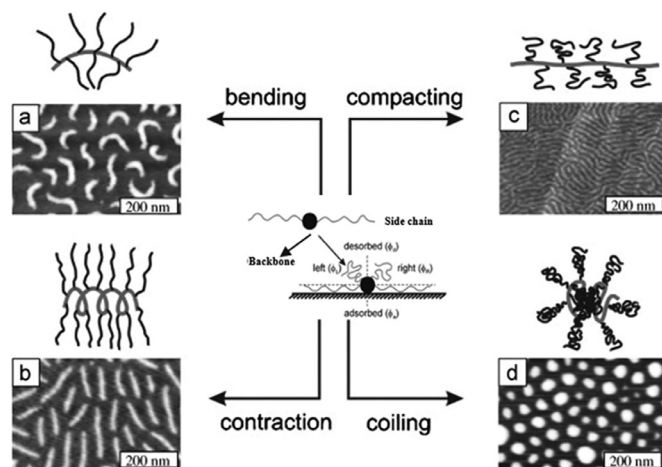


Fig. 17. AFM images along with schematic illustrations of BBPs adsorbed on different substrates. (a) Curving cylindrical shape ($\varphi_a \neq \varphi_b$). (b) Ribbon shape ($\varphi_a \approx 1$, $\varphi_L \approx \varphi_R = 0.5$). (c) Cylindrical shape ($\varphi_a < 1$, $\varphi_L \approx \varphi_R = 0.5$). (d) Spherical shape ($\varphi_a < 1$, $\varphi_L \approx \varphi_R = 0.5$, attraction among desorbed branches). [1]. Copyright 2008. Adapted with permission from Elsevier Science Ltd.

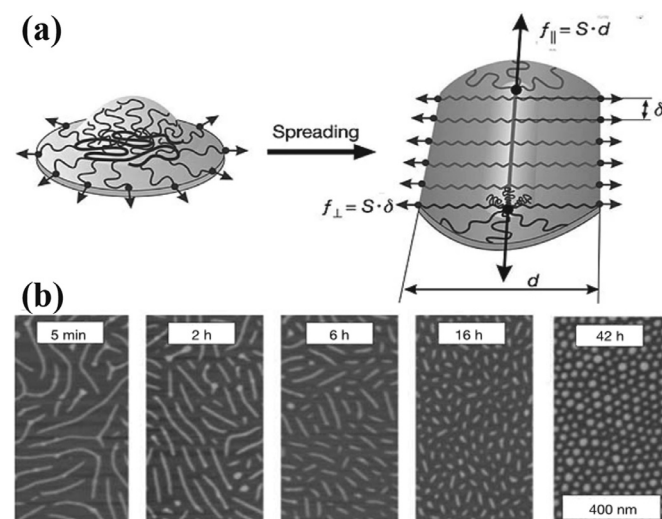


Fig. 18. (a) Schematic illustration of the tensile force distribution for BBPs on high-energy substrates. (b) AFM images for molecular degradation of BBPs on water and propanol surface for various incubation times. [252]. Copyright 2006. Reproduced with permission from the Nature Publishing Group.

on a substrate ($\varphi_a < 1$), the morphologies of the BBPs depend on the surrounding environments. These exhibit spherical shape (Fig. 17d) due to the attraction of the desorbed side chains in a poor solvent, resulting in a coiled main chain on the substrate. In a good solvent with $\varphi_a < 1$, the steric repulsion of the desorbed branches promotes the formation of compacting worm-like conformation (Fig. 17c). In some cases, the distribution of the adsorbed branches on substrate also dominates the conformations of BBPs. With an unbalanced distribution, i.e., $\varphi_R \neq \varphi_L$, the BBPs can spontaneously afford a curved worm-like morphology because of the uneven steric repulsions (Fig. 17a). This morphological transformation from a stretched to a curved cylinder has been experimentally achieved by compression and the subsequent expansion of the LB monolayer [258].

The grafted brushes of the BBPs are spread to cover on an attractive substrate (such as mica), resulting in the stretching of polymers in all dimensions (Fig. 18a) [252]. The backbone experiences a wetting-induced tensile force ($f \approx S \cdot d$), which increases with an increase in the side chain length. In the direction parallel

to the side chains, all grafted brushes evenly distribute the tensile force, $f \approx S\delta$, where S is the coefficient related to the substrate, d is the diameter of the side chain, and δ is the distance between the adjacent side chains. Therefore, the force value is proportional to the side chain length and substrate spreading coefficient [252]. Moreover, the solvent quality dominantly affects the tension of the BBPs on the substrates [259]. The stretching of individual polymer chains requires a tensile force in the range of 10–100 pN. The adsorption of the BBPs on a surface can increase the steric repulsion among the adsorbed side chains and generate a tensile force of the order of 1 nN along the backbone. It exceeds the strengths of the typical stretched polymer chains and leads to a spontaneous spatial bond scission in the backbones of the BBPs. The spontaneous scission process can be monitored by AFM. BBPs bearing a polyacrylate backbone and long PBA ($N_{sc} = 140$) side chains are spread on the surface of water and propanol mixture. With an increase in the incubation time, the BBP backbones get progressively shorter and their number densities increase, suggesting the occurrence of scission (Fig. 18b) [252]. This rate of bond scission shows an anti-Arrhenius behavior because an increase in the substrate temperature decreases the surface energy and rate [260,261]. Additionally, bond scission has been observed in the macroscopic spreading BBP melt films. The addition of a linear polymer to the BBP melt can position the bond-scission zone in the film during spreading [262].

The block copolymer brushes of the core-shell BBPs provide a new regulatory parameter to modulate their self-assembly on the surfaces. When one block of the side chain has a stronger attraction to the substrate than that of another block, the BBPs prefer to decrease the interfacial energy by folding back the side chains with weak absorption. This can form unusual morphologies, and the location of a more attractive block has a significant effect on the morphologies. In one case, BBPs with PBA-*b*-PS side chains showed a necklace-like morphology on mica (Fig. 19a) [13]. The inner PBA blocks with polar acrylic groups exhibited strong affinity for the substrate, while the outer blocks repelled the substrate, resulting in aggregation to decrease the interfacial energy. In another case, BBPs with the same backbone but PCL-*b*-PBA side chains showed completely different spine-like conformation (Fig. 19b) [263]. This was attributed to the strong adsorption of the outer PBA blocks, and they could partially fold back to cover the underlying surface of the PCL blocks. In addition, the PCL blocks crystallized into bundles during self-assembly. When the outer block was hydrophilic PEGMA, the BBPs exhibited a worm-like morphology with more rigidity compared to that of the BBPs without the PCL core compartment [264].

Diblock BBCPs are suitable for achieving well-defined architectures because of the low entropy and stretched conformations. PNB-based BBPs prepared via ROMP in earlier studies afforded low DP of the backbone because of the short C2 linker in the macromonomers. Hudson and coworkers reported the preparation of BBPs with long backbones by the incorporation of a long C11 spacer between the NB moiety and side chain [10]. In their work, the macromonomers comprising dimethylacridine chromophore (ACR-MM), triazine chromophore (TRZ-MM), or equal parts of the two by mass (ACRTRZ-MM) were prepared by ATRP. Subsequently, a set of BBPs were synthesized by ROMP with distinct donor (D) and acceptor (A) interface types and a target backbone length of 150 via the “grafting-through” approach. For example, the ROMP of the macromonomer, ACRTRZ-MM, afforded a homopolymer bottlebrush (ACRTRZ150-BB) containing random polymer side chains. Miktoarm BBP (ACR75-*co*-TRZ75-BB) formed through the random copolymerization of macromonomers, ACR-MM and TRZ-MM, giving a bottlebrush with homopolymer side chains. Diblock BBCP (ACR75-*b*-TRZ75-BB) was obtained by the sequential ROMP of the macromonomers, ACR-MM and TRZ-MM. All three BBPs exhibited worm-like morphology for up to several hundred nanometers on

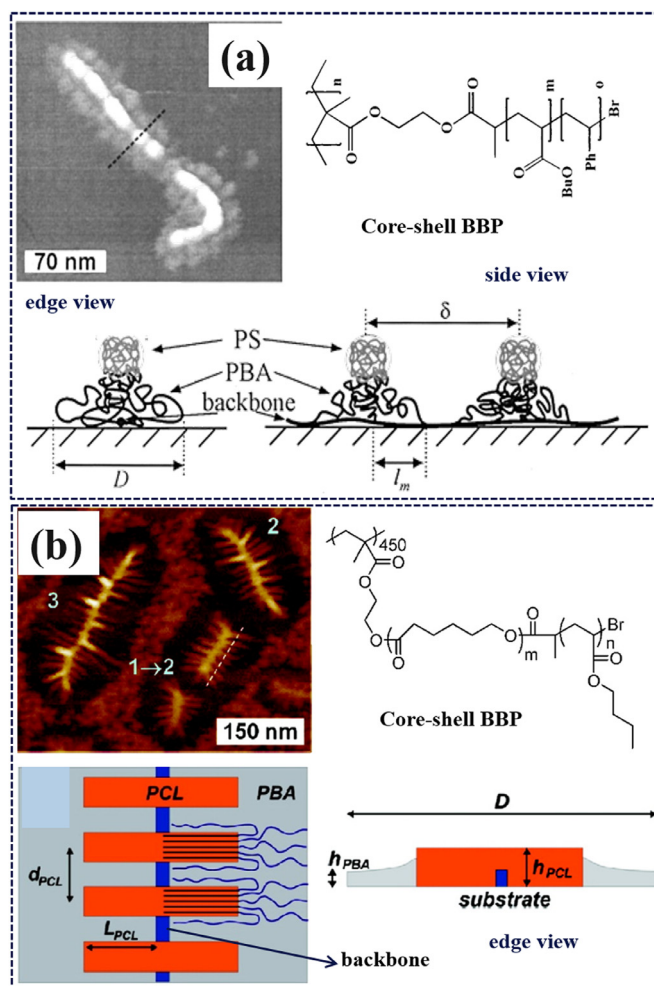


Fig. 19. AFM images of single molecules of core-shell BBP and the corresponding schematic illustrations. (a) Necklace-like morphology. [13], Copyright 2001. (b) Spine-like morphology. [263], Copyright 2009. Adapted with permission from the American Chemical Society.

the graphene substrates (Fig. 20) [10]. Worm-like BBCPs containing different semiconducting building blocks were also synthesized [22,265].

Organic tubular structures obtained by the self-assembly of small building blocks or BCPs have been studied and inspired future endeavors. However, these methods often suffer from the issue of finite length or polydisperse tubular morphology because of poor length control. BBPs adopt cylindrical shapes in solution, which can be used as molecular templates for the preparation of organic nanotubes in solution. Rzaev and coworkers synthesized BBP precursors containing triblock copolymer side chains, in which the inner block was degradable PLA, the middle block was PtBA that decorated the nanotube interior surface, and the outer cross-linkable block was poly(styrene-*r*-(4-(3-butenyl)styrene)). The shell of the BBP was then cross-linked using Grubbs' catalyst. Finally, 1D amphiphilic nanotubes were obtained in solution after the removal of the PLA core and tert-butyl groups by acidic hydrolysis [18]. The exposed PAA coating on the nanotube interior increased the dispersibility and enhanced the dye uptake. In addition, the shell could be cross-linked by other covalent cross-linking units [266] or dynamic covalent bonds [236,267]. Organic nanotubes with controlled open ends were also obtained by incorporating the segmented PLA side chains into triblock BBCPs and cross-linking the shell of the middle brush block [268].

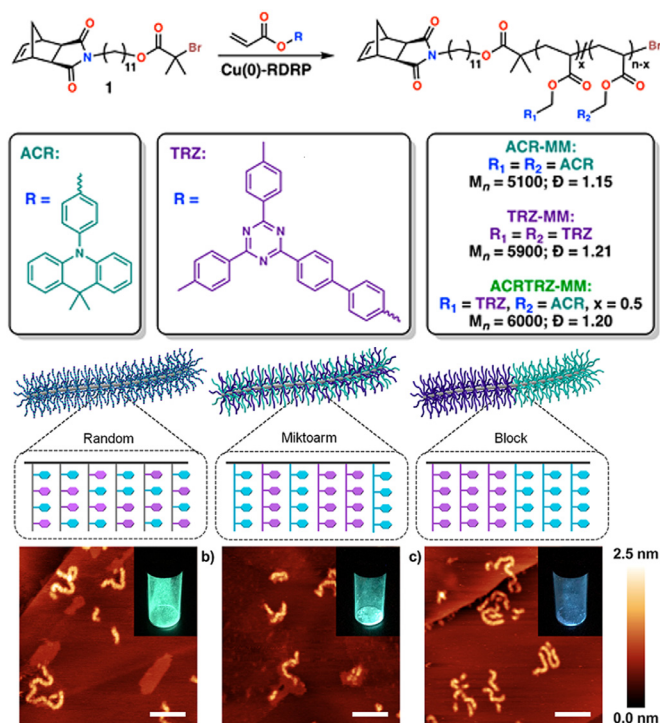


Fig. 20. Synthesis of norbornene-functionalized macromonomers and the corresponding schematic illustrations and AFM height traces of BBPs. Scale bars = 200 nm [10]. Copyright 2019. Adapted with permission from the American Chemical Society.

Interpolyelectrolyte complexation (IPEC) of the cylindrical BBPs can be used to promote the preparation of 1D architectures with multicompartments in solution. Müllner and coworkers synthesized core-shell BBPs bearing PCL-*b*-PMAA brushes through sequential ROP of CL and ATRP of MAA via the “grafting-from” approach [269]. The BBP showed distinct pearl-necklace morphology

in cryo-TEM, suggesting the formation of core compartmentalization along the backbone direction in solution. This conformation was attributed to the hydrophobicity of the PCL block on the side chain, and its assembly into a spherical shape was required to minimize the surface energy in water. IPEC in the BBPs was formed by coordinating the positively charged diblock copolymers with the negatively charged polyelectrolyte brush. These formed centipede-like nanowires, where the IPEC in the branch preferred to form a lamellar disc separated by PEO blocks. (Fig. 21).

To understand the mechanism of cooperative supramolecular polymerization and produce well-ordered helical superstructures, PNB-graft-polypeptide such as PN-g-PLG was synthesized via ROMP and followed by the ROP of NCAs (Fig. 22) [126]. At an appropriate pH, the PLG side chains were partially protonated and water-soluble, which decreased the charge repulsion and facilitated intermolecular PLG-chain intercalation. Thus, a more favorable antiparallel β -sheet conformation provided the driving forces for supramolecular polymerization. Three steps were involved during this process, namely, monomeric dispersion in solution at pH 7, followed by slow nucleation growth from the oligomers with the first turn of the helix, and a subsequent increase in the number of interactions generated upon monomer addition. This allowed cooperative growth into tubular supramolecular structures with distinct handedness, which could be observed in the TEM images. Similar experiments were also reported recently, where the polyisocyanide side chains were grafted onto the BBPs [207]. Triblock BBCPs bearing DNA side chains on both the outer blocks were prepared, and these exhibited spherical morphologies in solution because of their short backbones. Under suitable conditions, the DNA-based BBCPs self-assembled to form 1D worm-like morphology due to intramolecular DNA hybridization [193].

3.3. Lamellar nanostructures

Two-dimensional (2D) lamellar nanostructures have been obtained by the self-assembly of amphiphilic BCPs or small bolaamphiphiles in selective solvents [37,238,270]. Amphiphilic BCPs assemble into vesicles with bilayer structured membranes to de-

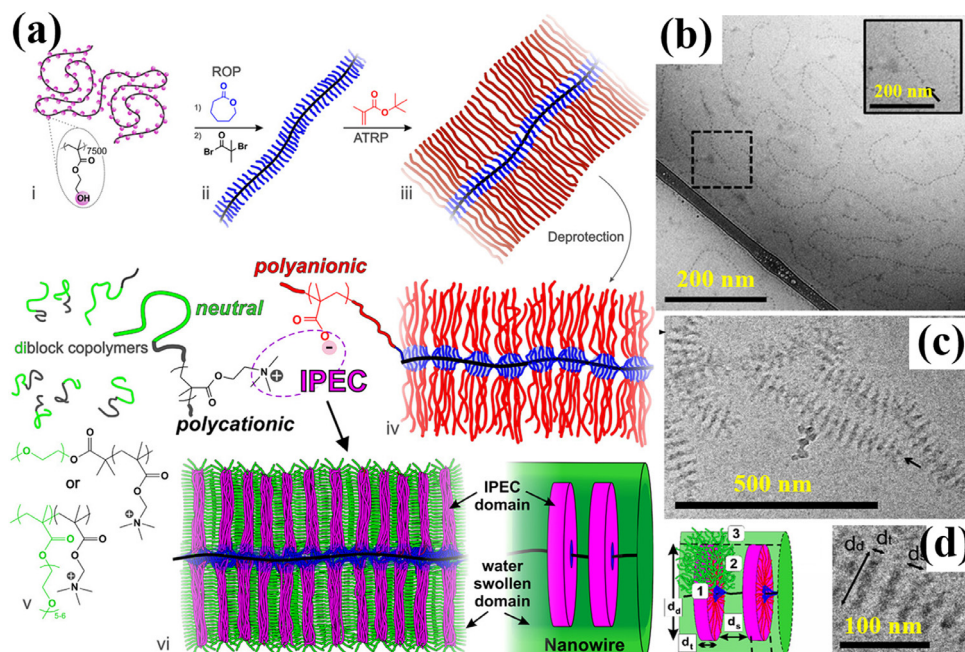


Fig. 21. (a) Design process of producing IPEC-structured, centipede-like polymer nanowires and (b, c, d) the corresponding cryo-TEM images. [269]. Copyright 2018. Adapted with permission from the American Chemical Society.

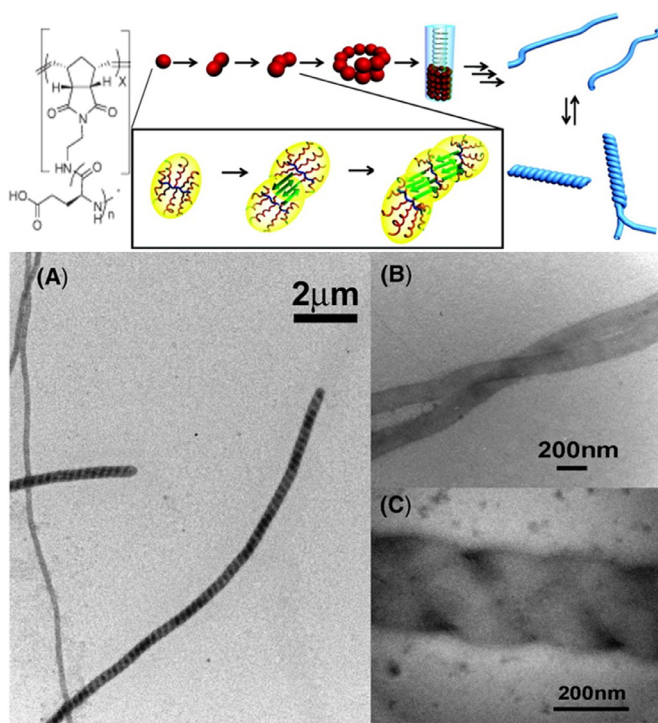


Fig. 22. Schematic illustration and corresponding TEM images of supramolecular polymerization of polypeptide-based BBP into tubular superstructures. [126]. Copyright 2011. Adapted with permission from the American Chemical Society.

crease the free energy of the hydrophobic edges [238]. It is believed that the rim-capping energy of the lamellae is lower than the curvature energy; vesicle morphologies are more thermodynamically favorable [238]. When subjected to a high bending modulus, planar lamellae nanostructures can be obtained through self-assembly. As the BBPs have rigid cylindrical shapes owing to their densely-grafted side chains, these show significant promise as building blocks for constructing lamellar morphologies.

Chen and coworkers developed a method using well-defined rigid molecular bottlebrushes with two terminals tethered with coil-like polymers, i.e., linear-brush-linear copolymer, to afford disk-like micelles [14]. In their work, amphiphilic AbBA BBPs were synthesized by CuAAC via the “grafting-to” approach, where the middle bB segment was the molecular bottlebrush bearing the densely-packed PtBA-*b*-PS side chains, while the A segments were the linear polymers. The AbBA BBPs showed 1D worm-like morphologies in good solvent, suggesting that the middle block had a rigid rod-like shape. In a selective solvent for the coiling A block, rod-like bB blocks were densely hexagonally packed in two directions, resulting in the formation of monolayer disk-like micelles stabilized by the A blocks. The well-ordered hexagonal pattern in the disk-like micelles was characterized by TEM using RuO₄ vapor to stain the PS domains (Fig. 23) [14]. In addition, the sizes of the disks increased with an increase in time because of merging. Remarkably, prolonged incubation time led to vesicle formation, suggesting that the curvature energy dominated the micellization of vesicles. In a related study, this method was extended to prepare disk-like platelets with an internal lamellar structure using the AbBA triblock bottlebrushes with a microphase-separation of side chains [271]. In this case, they used PDMA as the A block and molecular bottlebrush carrying densely-grafted PAA-*b*-PS as the bB block. The PS and PAA blocks in the brush were thermodynamically incompatible, which led to microphase separation among the neighboring PAA-*b*-PS segments, forming ribbon patterns along with the disk platelets [271].

Long-range structural periodicities on the scale of 100 nm are harder to control and achieve with linear BCPs because the DP determines the domain size, and its microdomain scale is approximately two-third power of the DP. In addition, the DP contributes to the segregation strength during self-assembly [272]. It is challenging to prepare linear BCPs with ultrahigh MWs, and the self-assembly process requires an extended period. These limitations can be typically overcome using BBPs. The highly stretched backbones of the BBPs are beneficial in preventing chain entanglement, which is the major kinetic barrier for chain orientation during the self-assembly. BBPs (e.g., Janus BBPs, random BBPs, and block BBPs) can readily self-assemble to form large domains (d_{lam}) in a more rapid process than those typically observed in linear BCPs in the bulk state (Fig. 24) [15,96,273].

Brush-linear copolymer was used to determine the self-assembly behavior in a solid film. Runge and coworkers identified the self-assembly mechanisms of brush-linear copolymers in the solid state, [274] which could self-assemble into various morphologies (e.g., sphere, lamella, and cylinder) by tuning their chemical parameters. In addition, the large domain sizes of 132–258 nm were observed in well-ordered structures. The lamellar morphology for asymmetric brush-linear copolymers was observed at low volume fractions of grafts (< 50 %), which suggested that the linear blocks must have MW comparable to that of the brush block. With an increase in the side chain length, their morphologies changed from lamellar to cylindrical, and finally to disordered spheres. The domain sizes were highly dependent on the backbone length, suggesting that their self-assembly behavior was similar to those of the linear BCPs with backbones aligned perpendicularly to the substrate (Figs. 25a and 25b).

Janus-like asymmetric BBPs self-assembled into cylindrical morphology in a bulk film owing to the microphase separation of the side chains [275]. Notably, the nanostructure patterns with nanodomain sizes (e.g., < 10 nm) are of particular interest for the separation engineering applications and micro-electronics industry in the continuous pursuit of increased chip density. The self-assembled phase behavior of the linear BCPs can be predicted in terms of the segregation strength parameter (χN), where χ is the Flory-Huggins segmental interaction parameter and N is the total DP of the BCP [272]. Microphase separation and self-assembly can only occur when χN is larger than the threshold of the order-disorder transition (χN)_{ODT} [272]. There are three strategies to achieve this goal (Figs. 25a–25c) [276]. The introduction of high- χ segments can compensate for the loss of driving force for self-assembly in BCPs with low DP. However, when N is too low to provide a sufficiently large thermodynamic driving force for the formation of well-ordered nanostructures, the samples afford a disordered morphology. In addition, the low N value may interfere with other properties (e.g., mechanical properties) of the materials.

Janus BBPs self-assemble into long-range ordered lamellar morphology with ultra-small domain sizes dominated by the side chain length. For instance, Johnson and coworkers prepared Janus BBPs bearing PDMS and PLA branches with different lengths via the “grafting-through” approach [276]. In the self-assembly of lamellar structures in bulk state, the incompatible side chains are segregated on the opposite two sides of the main chain to decrease the free energy and the backbone connects the two brush interfaces (Fig. 25c). The lamellar micro/nanodomains formed by Janus BBPs were found to be oriented perpendicular to the substrate without any surface modification. This is attributed to the surface energy difference between the two blocks and the high-polarity branch (e.g., PLA) that preferentially interacts with the substrate. This proposal is strongly supported by the findings that with a sufficiently large MW, both the brush macromonomers (BMM; PDMS-branch-PLA) and the corresponding Janus BBPs afford long-range ordered lamellar structures with small domain size of down to

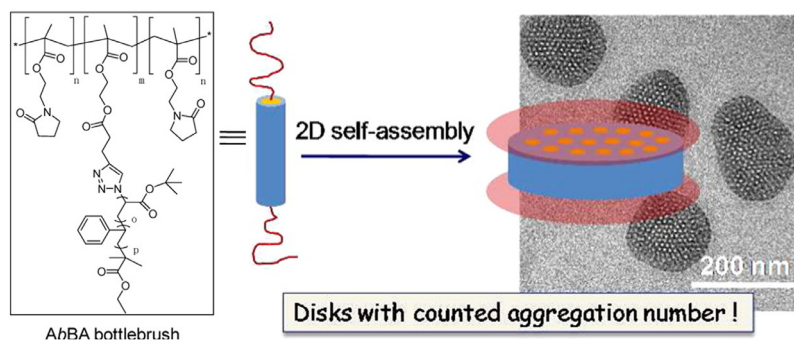


Fig. 23. Schematic illustration of packing molecular structure of amphiphilic AbBA triblock BBP and corresponding TEM image. [14], Copyright 2014. Reproduced with permission from the American Chemical Society.

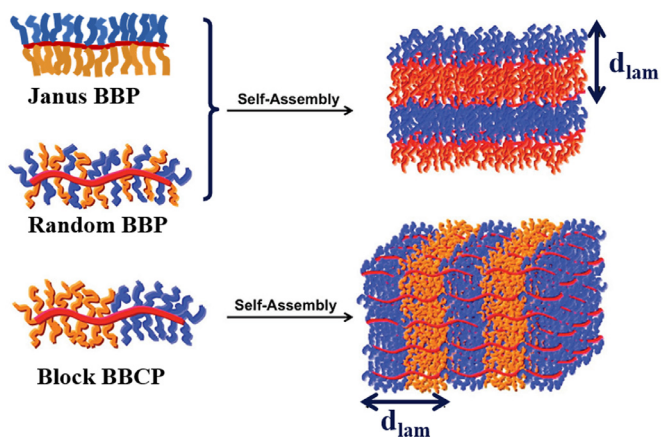


Fig. 24. Proposed self-assembly of symmetric Janus BBP, random BBP, and block BBP with 2D lamellar morphology. [273], Copyright 2009. Adapted with permission from the American Chemical Society.

5.6 nm, which are consistent with the SAXS patterns (Fig. 25e) [276]. Moreover, with an increase in the MW, an expanded ordered phase region is observed in the phase diagram for the Janus BBPs. This is because a slight chain stretching compensates for the effect of the decrease in the critical N value, which is verified by a slight decrease in the d -spacing. Under optimized processing conditions, the Janus BBPs are more favorable for forming well-ordered structures, and solvent or thermal annealing can facilitate the formation of well-ordered structures [277].

Block BBPs are similar to linear BCPs in structure that have two or more blocks along the backbone, yet ultra-high MWs can be easily achieved, which are more favorable to form long-range, well-ordered morphologies in the bulk state [15,272]. Grubbs and coworkers investigated the self-assembly of the block and random BBPs bearing PLA and PBA side chains [177]. With symmetric volume fractions of the side chains, random BBPs exhibited lamellar morphology, as indicated by the sharp integer multiples of the SAXS peaks. The d -spacing was independent of the backbone length, suggesting that the microphase separation was simi-

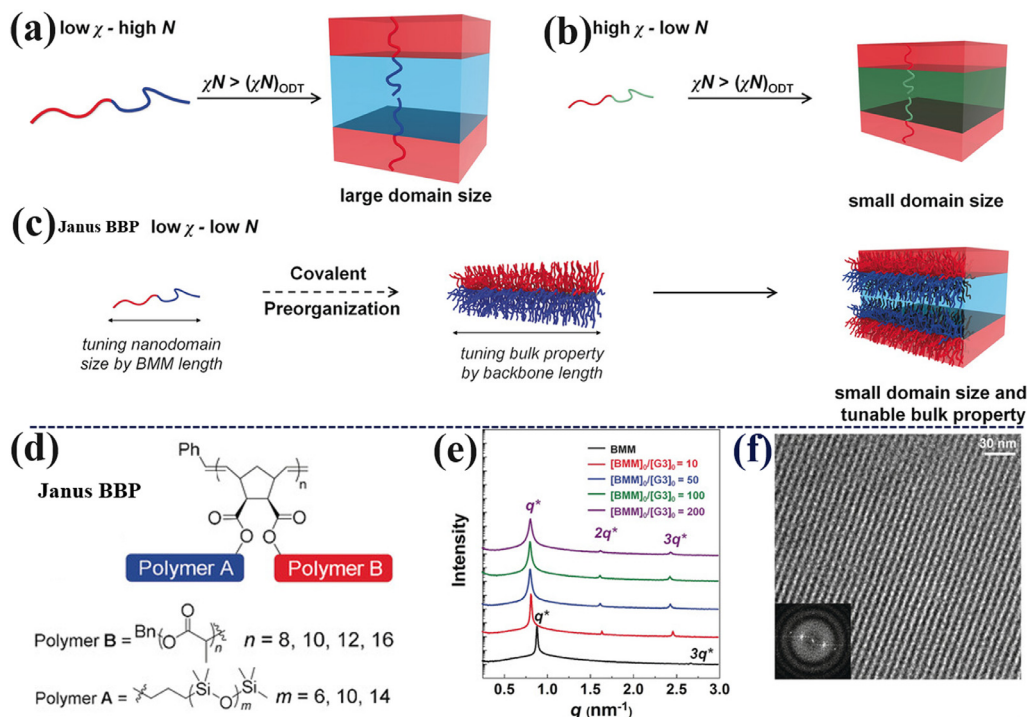


Fig. 25. Idealized illustrations of self-assembly of linear BCPs with a) low χ -high N and b) high χ -low N , c) Janus BBPs with low χ -low N in ordered small domain sizes nanostructures; (d) Chemical structure of Janus BBPs with different composition and corresponding (e) SAXS patterns and (f) TEM image. [276], Copyright 2018. Adapted with permission from John Wiley and Sons Inc.

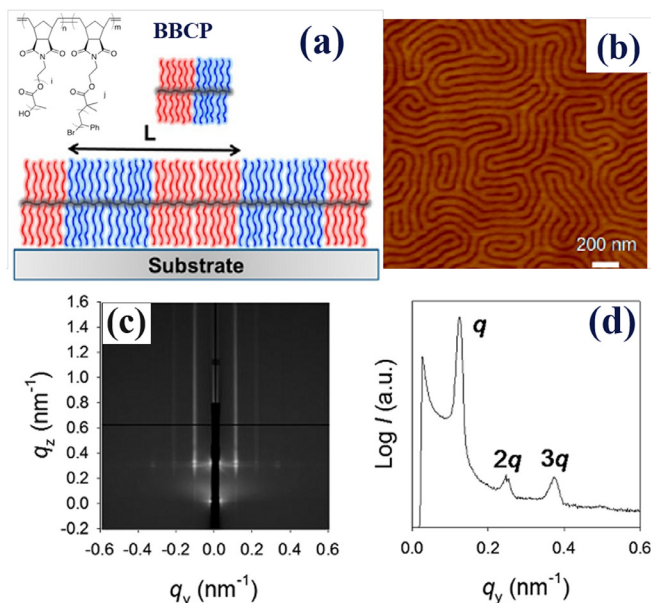


Fig. 26. (a) Schematic illustration of lamellar microdomains orientation from the self-assembly of BBCP and corresponding (b) AFM image, (c) GI-SAXS pattern and (d) 1D GI-SAXS profile along the in-plane (q_y) direction. [280]. Copyright 2013. Adapted with permission from the American Chemical Society.

lar to that in the Janus BBPs, where the backbone was confined in the segregated brush domains (Fig. 24). The BBPs self-assembled into disordered morphologies with ultra-asymmetric random side chains, whereas the high-MW BBCPs with symmetric side chain distributions were self-assembled into lamellar morphologies with large domain sizes [177]. Green color spontaneously appeared in the bulk film upon slow solvent evaporation [177]. In addition, a large lamellar d-spacing that was approximately equal to the extended PNB main chain length was observed [177]. Here, the orientation of the backbone perpendicular to the substrate and side chains parallel to the substrate resembled linear BCP self-assembly in the bulk state (Fig. 24), i.e., the high-polarity had strong preferential interactions with the substrate and another block interdigitally packed together to minimize the interfacial energy [15,230]. Block BBCPs, [PNB-g-PS]-*b*-[PNB-g-PLA], can self-assemble into a lamellar structure in the bulk state with extremely fast kinetics in one minute at 130 °C, as indicated by the multi-reflections in the SAXS patterns owing to low entanglement among the side chains [230]. In addition, the incorporation of rigid side chains in the BBPs can enhance the steric repulsion and decrease the entanglement, and thus, can significantly facilitate the formation of large domain size. Grubbs and coworkers also prepared block BBCPs bearing helical polyisocyanate side chains. The block BBCPs rapidly self-assembled into lamellar morphologies with large d-spacings through simple controlled evaporation, which was independent of the solvent effect [278,279].

Block BBCPs in thin films possess more conformational degrees of freedom because many side chain ends of the brush preferentially segregate to the surface and substrate interfaces, and the backbones are oriented parallel to the substrate (Fig. 26a) [280]. The film showed well-developed lamellar microdomains throughout the entire film (Fig. 26b). This phenomenon is different from the assembly of the BBCPs in a thick film [230]. Russell and coworkers characterized the self-assembly kinetics and morphology of symmetric BBCP, [PNB-g-PS]-*b*-[PNB-g-PLA], in a thin film by employing grazing-incidence small-angle X-ray scattering (GI-SAXS) [280]. Well-ordered lamellar microdomains perpendicular to the substrate were verified by the multiple orders of scattering in

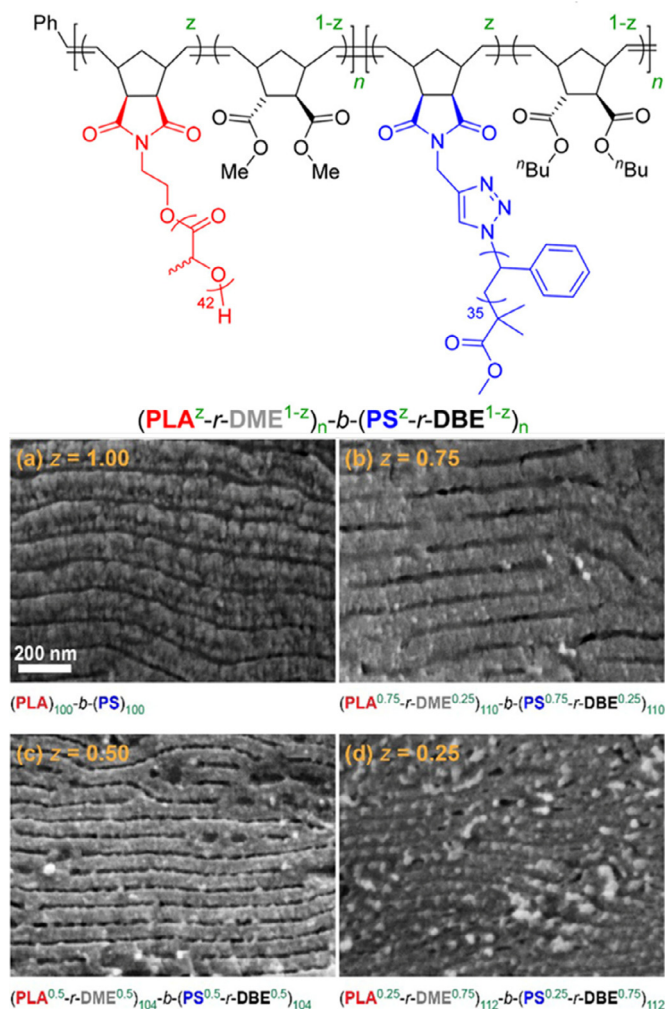


Fig. 27. Chemical structure of BBCP with different grafting density and corresponding SEM images of self-assembled samples. [283]. Copyright 2017. Adapted with permission from the American Chemical Society.

the q_y direction (Figs. 26c and 26d). Meanwhile, distinguishable multiple ring patterns originating from the randomly distributed side chains were observed in the grazing-incidence wide-angle X-ray scattering (GI-WAXS) result [280]. The lamellar period, L , increased almost linearly with the DP of the backbone, following a scaling relationship of $L \sim \text{DP}^{0.99}$ [280]. This scaling dependence of [PNB-g-PS]-*b*-[PNB-g-PLA] was similar to that in the bulk state [230]. Notably, the volume fraction of the block dominates the self-assembly behavior of the asymmetric block BBCP. With an increase in the volume fraction of one block, the BBPs self-assemble from disordered morphology to lamellar, and finally to cylindrical structures [281].

Although backbone length significantly affects the domain size, the grafting density dictates the backbone conformation. The morphologies of self-assembled BBPs can be tuned by varying the grafting densities of the random binary branches [282]. Grubbs and coworkers systematically investigated the dependency of the self-assembly of BBPs on the grafting density [283]. They prepared diblock BBCPs, $(\text{PLA}^\sigma\text{-}r\text{-DME}^{1-\sigma})_n\text{-}b\text{-}(\text{PS}^\sigma\text{-}r\text{-DBE}^{1-\sigma})_n$, by copolymerizing NB-based macromonomers with dilute comonomers through ROMP (Fig. 27). It is favorable to precisely manipulate the grafting density (σ) and MW by tuning the feed ratio. The diblock BBCPs formed well-ordered lamellar morphologies regardless of copolymerization with the same or different diluent comonomers at σ

values of > 0.2 (Fig. 27a) [283]. This morphological transformation was intrinsically related to the conformational changes because of the cylindrical architectures rather than the segregation strength. The scaling relationship of backbone stiffness (C^∞) to grafting density and backbone length can be expressed by the equation, $C^\infty \sim DP^{f(\sigma)}$ [283].

3.4. Other self-assembled nanostructures

Multiblock BBCPs with controlled functionalities provide a versatile pathway to prepare hierarchical nanostructures in the bottom-up approach. Generally, BBPs have a cylindrical molecular geometry, whose size can be manipulated by varying the main chain and side chain lengths. Heterografted BBPs bearing symmetric brushes show well-defined morphologies. By controlling the monomer connectivity, different desired architectures of the BBCPs can be indirectly controlled by the polymerization of macromonomers with varying side chain lengths. For instance, novel triblock dumbbell-shaped molecular brushes were obtained by sequential ROMP via the sequential-addition of macromonomers (SAM) [284]. In this case, PLA-containing macromonomers bearing terminal norbornenyl groups with different lengths were prepared via the ROP of LA. Subsequently, PLA-containing macromonomers were consecutively added into a solution containing Grubbs' catalyst and polymerized for different time intervals. During sequential additions, the first and third additions constituted the same macromonomer with high MW, and the second one comprised a short PLA. Notably, the side chains must have the same composition to prevent potential side-chain phase separation during AFM measurements. Dumbbell-shaped morphology with "balls" consisting of the high-MW macromonomer and "bars" made of the low-MW macromonomer was visualized using AFM (Fig. 28a) [284]. The sizes of the dumbbell-shaped brushes could be readily manipulated by controlling the macromonomer length and feed ratio. Asymmetrical cone-shaped multiblock BBCPs with precisely defined structures were prepared by sequential ROMP via SAM [186]. A series of NB-functionalized PS with different MWs were synthesized by ATRP, and the SAM for ROMP was then performed to yield tapered BBPs. It was critically important to achieving complete conversion of each macromonomer to ensure efficient blocking. Direct visualization of the AFM image of the tapered BBCP revealed cone-shaped nanostructures (Fig. 28b). In addition, gradient sequences (brush polymers) can be prepared by one-pot copolymerization of a macromonomer and different types of comonomers via ROMP. Tapered, non-cylindrical molecular shapes with different cross-sectional radii (R_c) can be manipulated by controlling the discrete comonomer distribution. This is attributed to the different steric repulsions among the side chains with different percentages of the incorporated diluent along the backbone. The side chain distribution was characterized using synchrotron-SAXS (Fig. 28c) [174].

Linear-brush-linear BBPs with rigid cylindrical shapes have been used as molecular building interconnectors with directional interactions for constructing 3D porous materials. These BBPs can serve as connectors in all directions because of the inherent flexibility of the linear polymers that promote the self-assembly of coiling conformation. Linear-brush-Linear copolymers consisting of reactive linear end blocks were prepared [285]. Ru-catalyzed cross-metathesis cross-linking of the olefinic double bonds at the two linear blocks allowed the preparation of 3D mesoporous polymer networks. The porosity could be conveniently manipulated by altering the length of the middle brush building block, and it showed a logarithmic scaling relationship with the DP of the bottlebrush backbone [285]. Notably, side chains in the brush block should be cross-linked to increase the inherent stiffness.

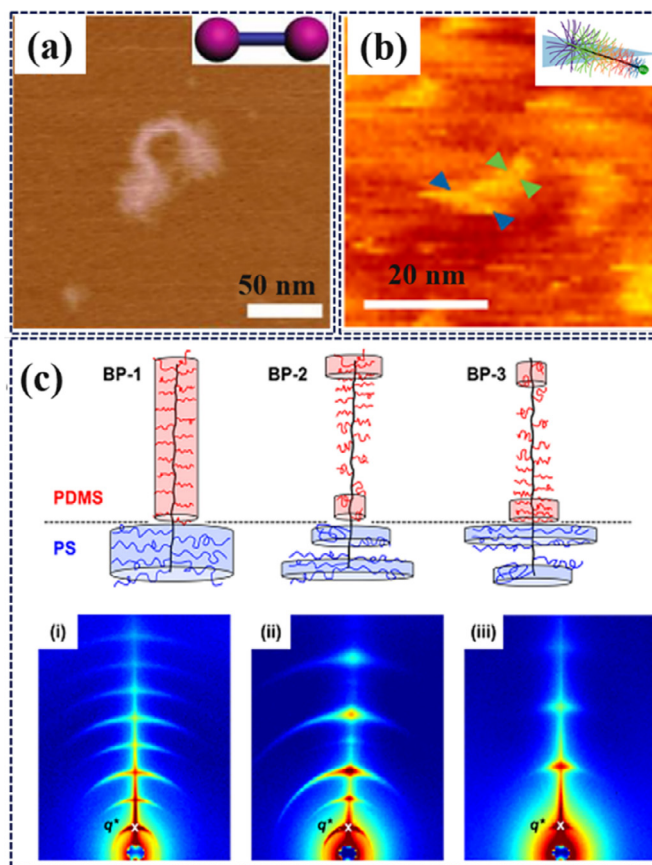


Fig. 28. (a) Dumbbell-shaped molecular brushes and AFM image. [284], Copyright 2012. (b) Cone-shaped molecular brushes and AFM image. [186], Copyright 2017. (c) Illustrations of three types of brush copolymers with different shapes and corresponding 2D SAXS patterns. [174], Copyright 2017. All adapted with permission from the American Chemical Society.

Although extensive efforts have been directed towards obtaining complex architectures by the SAM, these have been hindered by the tedious synthetic processes and limited morphological controllability. Flow chemistry is a promising methodology that can improve productivity of synthetic chemistry. The flow stream is uniformly mixed and heated or cooled, and the reactions are precisely and reproducibly controlled in the flow systems. Using an automated synthesis platform, the shapes and sizes of the BBPs were programmed by implementing a computer-controlled semibatch reactor set up in conjunction with the "grafting-through" polymerization (Fig. 29) [286]. In the first vessel, a syringe/syringe pump was used as the reaction set-up to synthesize the macromonomers, where 5-norbornene-2-methanol served as an initiator for the ROP of LA catalyzed by 1,8-diazabicyclo [5.4.0]undec-7-ene (DBU) for the brush synthesis. The resulting NB-based macromonomer solution was then continuously fed into the second reaction vessel for the growth of the BBPs via ROMP. Meanwhile, the brush growth was immediately quenched upon the addition of boric acid, which could quantitatively scavenge out DBU without affecting the ROMP. The flowrate profile of the solution containing the growing macromonomers was found to directly translate into the shapes of the BBPs (i.e., each flow rate profile resulted in a unique polymer shape). Specifically, the BBPs with conical, ellipsoidal, and concave architectures were synthesized through ROP in tandem with ROMP [286]. Ellipsoidal particles with multilayer structures were obtained by the self-assembly of diblock BBCPs with the aid of surfactants in the emulsion [287]. In addition, high-MWs and low- \bar{D} BBPs with hourglass, football,

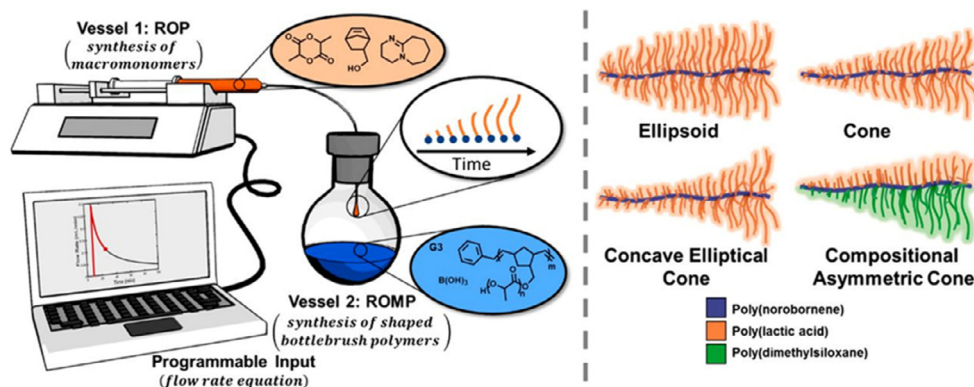


Fig. 29. (Left) Schematic illustration of the programmable semibatch reactor system and (Right) shaped bottlebrush polymers. [286], Copyright 2020. Reproduced with permission from the National Academy of Sciences.

spherical, and bowtie architectures were synthesized by leveraging this versatile automated synthesis approach [288]. For the synthesis of BBPs with different architectures, it is necessary to consider the following selection criteria. First, the two reactions must be fully compatible and orthogonal. Second, macromonomer synthesis should be easily quenched in the second vessel. Third, macromonomer polymerization should be highly efficient to prevent the accumulation and scrambling of macromonomers of different lengths.

It is challenging to obtain hierarchical structures via the spontaneous self-assembly of the block BCP because of thermodynamic variables, whereas solvent evaporation on the substrates typically results in the formation of randomly assembled structures [289]. Controlled evaporative self-assembly (CESA) of nonvolatile solutes in confined geometries has been used to afford intriguing complex structures with high fidelity and regularity via the evaporation of a sessile droplet [290, 291]. Hierarchically organized structures of the BBPs have been prepared by the Lin group using CESA on Si substrates (Fig. 30) [292]. This process was implemented by dropping BBP toluene solution in a confined geometry on a Si substrate (i.e., wedge-on-Si geometry). During solvent evaporation, the confined geometry induced the self-assembly of BBPs into hierarchical nanostructures [292]. This could be attributed to the competition between the unfavorable interfacial interaction that suppresses the stabilization of self-assembly and solvent-induced regeneration of nanodomains on the substrate [292]. Finally, concentric straight and jagged stripes were constructed through repeated “stick-slip” processes in confined geometry by manipulating the wedge height [292,293]. With THF-vapor annealing for different times, the morphological transition from featureless topology to mixed perpendicular and parallel cylinders was achieved (Fig. 30b). When cylinder-on-flat geometry was employed, a hierarchical structure was also be obtained using the block BCP bearing PS and PLA side chains [289].

4. Properties of bottlebrush polymers

The structures of the materials direct their properties and further determine their applications. BBPs exhibit intrinsic extended 1D conformations because of the steric repulsions among their crowded branches. In addition, diverse assembled conformations have been achieved by the self-assembly of BBPs in solution or film states. The hierarchically organized conformations afford BBPs with interesting properties. Furthermore, by the rational design and use of state-of-the-art synthetic techniques, BBPs with precisely well-defined architectures have been achieved. All these features are difficult to achieve in other systems. Therefore, many distinctive

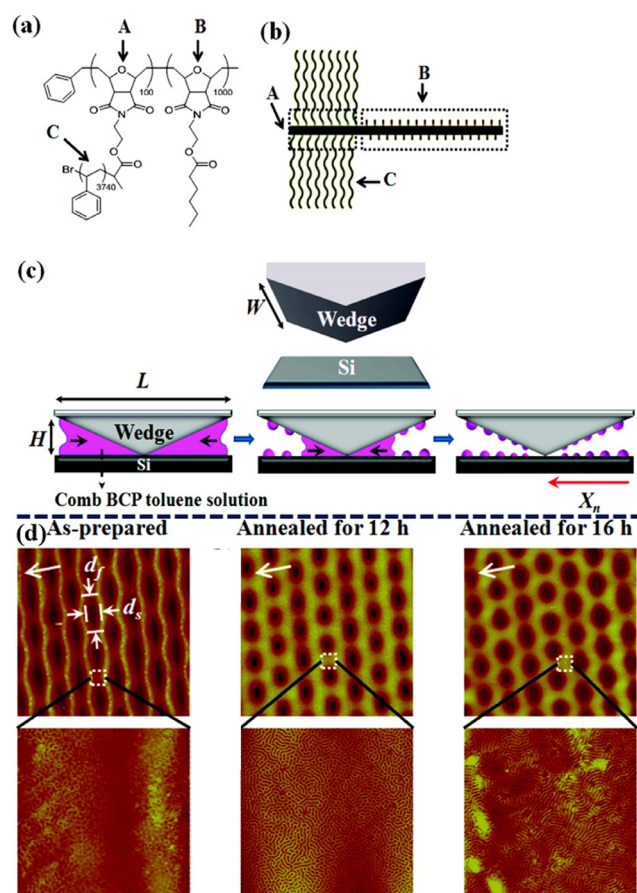


Fig. 30. (a) Chemical structure and (b) schematic illustration of BBP. (c) Schematic illustration of CESA process. (d) AFM images for the assembled morphological transformation with different annealing times. [292], Copyright 2010. Adapted with permission from the American Chemical Society.

properties of BBPs can be achieved by manipulating their chemical parameters.

4.1. Crystalline property of bottlebrush polymers

Unlike linear polymers, the high steric crowding of the crystalline side chains in BBPs can facilitate crystal nucleation but retard its growth [294–297]. The main chain along with the spacer groups between the backbone and side chain comprises the amorphous layer, whereas the side chains are incorporated into the

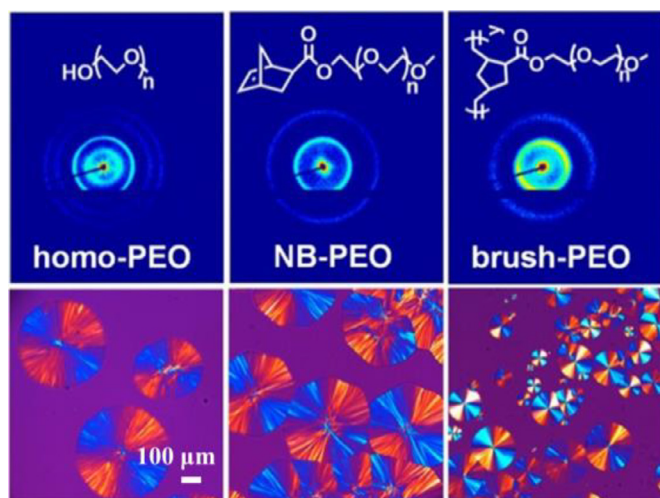


Fig. 31. Representative 2D SAXS patterns and polarized optical micrographs of homo-PEO, NB-PEO and brush-PEO ($M_{n,sc} \approx 3$ K; $M_{n,bb} \approx 35$ K, $D=1.36$; grafting density $\sigma = 100\%$; $n_g = 6$). Samples were crystallized at 40°C for 100 s. [299], Copyright 2019. Reproduced with permission from the American Chemical Society.

crystalline lamella [263,298]. Russell and coworkers anchored crystallizable PEO to the PNB backbone and studied the effect of the constraints imposed by the chain architecture on the crystallization of PEO [299]. In contrast to the macromonomers, NB-PEO and homo-PEO, which can crystallize, brush-PEO was observed to only form small crystals with a high nucleation density. The backbone anchored the side chain PEO phase and restricted the mobility of the PEO side chain, thereby increasing the defect density of the PEO crystals through heterogeneous nucleation (Fig. 31). This effect was also supported by the decrease in the nucleation density of NB-PEO, where the foreign NB components served as the defects, lowering the nucleation barrier. In addition, increasing constraints from the backbone decreased the spherulitic growth rate, crystallization rate, and crystal thickness. For the brush-PEO, a well-ordered microphase structure was formed isotropically in the lamella and observed in the 2D SAXS result, as indicated by the appearance of two ring patterns. [299] Furthermore, an increase in the crystalline side chain length and annealing temperature promoted the crystalline behaviors of the BBPs [299,300].

Translational symmetry is a fundamental law of the crystallization of materials, which can be broken under intrinsic or extrinsic constraints. Very recently, Li and coworkers reported the spontaneous formation of spherical hollow crystals with controlled openings using BBPs bearing crystalline PEO side chains [301]. They grafted alkyne-functionalized PEO to a polymer backbone bearing azide pendants via the CuAAC reaction to form crystalline BBPs (BB-PEO) with different grafting densities. A unique molecular bottlebrush crystalsome (mBBC) was obtained through self-seeding solution crystallization [302]. In the self-seeding process, the growth from a slightly curved lamellar crystal to a spherical shell with an open structure was observed. Closing the shell crystalsome was difficult because of the intrinsic shapes and large sizes of individual mBB molecules (Fig. 32) but the incorporation of linear PEO was found to effectively facilitate the formation of a closed mBB crystal structure. In addition, a decrease in the grafting density resulted in a gradual increase in the mBBC diameter, and a flat crystal with ultra-low grafting density was eventually formed. The formation mechanism of mBBC with the breakage of translational asymmetry was attributed to the local overcrowding-induced bending of the lamella and immiscibility of the side chain and backbone. Thus the backbone and spacers were excluded to both or one side of the lamellar crystal, which formed symmet-

ric lamella with the three-layer structure or asymmetric crystal in solution. In the latter case, the asymmetric crystal consisted of one PEO lamella and mBB backbone/spacer layer. An increase in the grafting density enhanced the steric overcrowding in the PEO lamella, which was alleviated by further bending the crystal toward the backbone layer [301].

As mentioned above, the BBP backbone constrained the mobility of the crystalline side chains. The distribution of crystalline phase significantly affects the crystalline behaviors, as reported for linear polymers [303]. For the core-shell BBPs with crystallizable block linked to the backbone while the amorphous block located towards the outer side in the side chain, a similar crystallization behavior as that of the corresponding linear crystallizable block is observed, but these exhibit higher crystalline temperatures due to the constraints of the backbone. The inverse block sequence in the side chain of core-shell BBP significantly affects the thermal behavior and structure because of the constraints to the motions of the side chain arm, which hinder the crystallization of the crystallizable block domains [304]. Furthermore, when the crystalline block (i.e., A block) is located on the linear tails of the linear-brush-linear copolymers (ABA), these exhibit different crystalline behaviors, and network formation depends on the brush side chain length [305]. With a short side chain in brush B domain, the ABA copolymer forms a hard crystalline scaffold because the A block screens the mechanical performances of the soft brush B. Soft brush networks were obtained by grafting medium side chains onto brush B, which were reversibly cross-linked by the crystalline linear blocks. However, the crystallization of A blocks was suppressed for brush B bearing long side chains; it decreased the cross-linking of the brush blocks. [305].

4.2. Stimuli-responsive bottlebrush polymers

Smart polymeric materials respond to external stimuli signals by regulating their performances (e.g., ion and molecule transport, wettability, and conformational and chemical changes) to adapt to the surrounding environment [306]. Stimuli-responsive behaviors of the polymers can be readily achieved in solution because the Brownian motion of the solvent molecules requires relatively low energies for the displacement of macromolecular segments. Stimuli-responsive materials have been extensively explored in many emerging fields such as self-healing, self-cleaning, drug delivery, bioengineering, and other systems. BBPs are unique polymers with unique morphological conformations. As discussed in the previous sections, BBPs can self-assemble into various architectures with a single molecular component by simply tuning their structural parameters. Hence, any parameter that changes the morphologies or properties of the BBPs can be used as a regulatory parameter. In addition, the energy required to induce changes in the external environment of the assembled aggregates is significantly lower than that for the covalently bonded species [307]. In combination with other stimuli-responsive parameters such as temperature, light, pH, and mechanical forces, BBPs can rapidly transform based on surrounding environments. Therefore, by varying the stimuli, trigger-induced morphology transformations of single-macromolecule brushes in solution have been investigated. The corresponding morphologies and properties changes can be beneficial in diverse applications [308].

4.2.1. Temperature-responsive bottlebrush polymers

Temperature is the most commonly used trigger in biocompatible responsive polymers. Thermal change is easy to implement in the in vitro and in vivo systems. The unique feature of temperature-responsive polymers is their solubility variation at the critical temperature [309]. Two typical phenomena are exhibited by thermal-responsive polymers at the critical temperature of

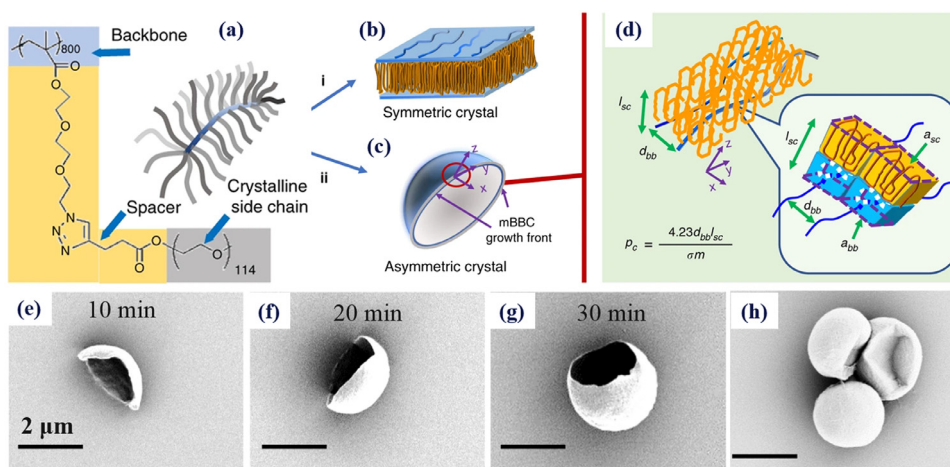


Fig. 32. mBBC formation mechanism (a–d). An mBB (a) could crystallize following pathway i to form a flat symmetric crystal (b). Pathway ii leads to an asymmetric crystal (c, d), where (d) is an enlarged view of c. *x* and *z* denote growth direction and the PEO axis, respectively. The blue shaded areas denote mBB backbones/spacers. Two mBB molecules are shown in (d). (e–g) SEM images of mBB crystallized at 20 °C for different times. (h) SEM image of mBB crystals after adding the linear PEO to preformed crystalline shells. [301], Copyright 2020. Adapted with permission from the Nature Publishing Group.

the cloud point (T_{cp}), where phase separation occurs. A key feature of phase separation is the visual transparency change due to an increase in the light scattering in solution [48]. Lower critical solution temperature (LCST) is the temperature above which the polymer is completely immiscible in a solvent at all proportions and the individual polymer chain collapses, and below which the polymers are in a monodisperse state [310]. In contrast, the polymer chains and solvent are in a homogenous mixing phase with favorable free energy above the upper critical solution temperature (UCST) [310]. PNIPAM is the most commonly used thermal-responsive polymer. It experiences water-swelling to undergo a globular transition in aqueous solution at an LCST of 32 °C, which is close to the human body temperature; [48,311] this key feature is promising for biomedical applications. Therefore, thermal-responsive PNIPAM-containing BBPs have been extensively explored for application in drug delivery [86,312,313].

Water-soluble BBPs exhibit worm-like morphology because the PNIPAM side chains are fully stretched and enhance the steric repulsions. When the temperature reaches the LCST, the PNIPAM side chains become dehydrated and collapse on the backbone with compact morphologies, and the solution changes from clear to turbid with a light blue color. More importantly, for the BBPs with side chains that are sufficiently long to allow such mobility, the side chains only interpenetrate at the outermost periphery during aggregation above the LCST. BBPs have been reported to exhibit concentration-dependent thermal transformation (Fig. 33a) [314]. At low concentrations, intramolecular collapse occurs at a temperature above the LCST because of a larger average distance between the molecules than its hydrodynamic diameter. When the concentration increases to a critical range, the intermolecular aggregation of BBPs occurs at a temperature above the LCST (Fig. 33a) [314]. Dynamic light scattering (DLS) has been used to detect transformation tendencies (Fig. 33b). At low concentrations, the hydrodynamic diameter decreases with an increase in temperature above the LCST due to the intramolecular collapse. In contrast, the hydrodynamic diameter increases with an increase in temperature at high concentrations [314]. Recently, ELP-based BBPs also exhibited a low value of LCST in water with the rapid formation of hydrodynamic radius at $T > 37$ °C due to intermolecular aggregation [169]. This phenomenon was also reported by Verduzco and coworkers, who used applied SANS to quantitatively estimate the BBP size and anisotropy. BBPs with long PNIPAM side chains formed a lyotropic liquid crystal phase upon cylindrical packing above the

LCST. This phase transition was characterized by the absence of a plateau at low *q* and the presence of peaks in the SANS data [315]. Additionally, the BBPs have been reported to undergo a conformational change from cylindrical to spherical shape upon heating above the LCST of PNIPAM. For instance, Zhang and coworkers synthesized BBPs P(oABA-g-PNIPAM) via the acid-catalyzed polymerization of the macromonomer o-aminobenzyl alcohol-g-poly(N-isopropyl acrylamide) (oABA-g-PNIPAM) [313]. P(oABA-g-PNIPAM) and oABA-g-PNIPAM exhibited different dependences of transmittance on temperature (Fig. 33c). The BBPs showed higher LCST values than those of the linear macromonomers because of the strong steric congestion among the PNIPAM branches, which suppressed their soluble-to-insoluble transition. In addition, the PNIPAM branches were constrained by the backbone, which retarded their free motion. The LCST values of both the BBPs and macromonomers increased with an increase in the DP due to the weakening of solvophobic effect of the CTA terminal [313].

Conjugated polymers such as polythiophene, poly(fluorene), and polyaniline have been used as BBP backbones. These afford efficient transport of excited states (excitons) along the polymer chain. Notably, the capability of intramolecular energy migration is highly dependent on the planarized extent of the conjugated backbone. Nesterov and coworkers synthesized BBPs, polythiophene-g-PNIPAM, via the “grafting-from” approach employing a combination of the Grignard metathesis method and ATRP [312]. With Ni(dppp)Cl₂ catalyst, regioregular polymers (head-to-tail coupled repeating units) could be obtained, and regiorandom polythiophene was achieved under the same conditions using Ni(PPh₃)₂Cl₂ instead of Ni(dppp)Cl₂. An increase in temperature above the LCST resulted in significant hypsochromic shifts in both the absorption and fluorescence spectra of the grafted BBPs (Fig. 33d) and increased the intensity of fluorescence emission. This phenomenon was attributed to the conformational twisting of the conjugated backbone as the PNIPAM side chains collapsed into a bulky hydrophobic globular phase at temperatures above the LCST, which resulted in a decrease in the conjugation length of the BBPs [61,312]. In addition, the regioregularity of polythiophene significantly affected the extent and appearance of conformational twisting. BBPs with high regioregularity afforded a large conformational twisting, which further decreased the planarized conformations of the backbone and resulted in larger spectral changes in absorption and fluorescence [312].

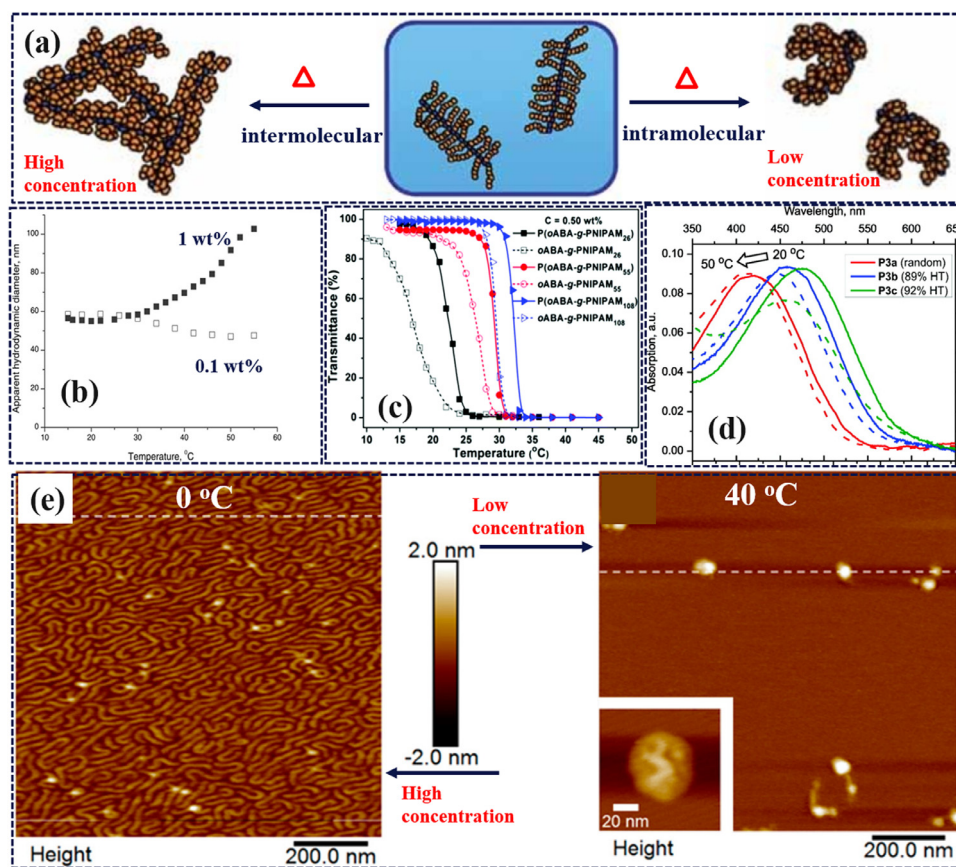


Fig. 33. (a) Schematic illustration and (b) DLS measurement for thermal-responsive BBPs with LCST characteristic at various concentrations. [314], Copyright 2007. Adapted with permission from John Wiley and Sons Inc. (c) Temperature-dependent transmittance of the oABA-g-PNIPAM and P(oABA-g-PNIPAM) with different side chain length. [313], Copyright 2017. Reproduced with permission from the Royal Society of Chemistry. (d) Absorption spectra of PNIPAm-grafted conjugated BBP with regioregularity of polythiophene in aqueous solution at various temperatures. [312], Copyright 2010. Reproduced with permission from the American Chemical Society. (e) AFM images of heterografted BBPs from aqueous solutions with different concentrations. [204], Copyright 2017. Adapted with permission from the American Chemical Society.

Spherical nanoaggregates are unstable above the LCST, and eventually, precipitate out of the solution [86]. Zhao and coworkers synthesized thermosensitive binary heterografted BBPs consisting of PDEGEA and PEG side chains via the “grafting-to” approach [204]. PDEGEA exhibited an LCST of 9 °C in an aqueous solution, and the PEG chains served as stabilizers to prevent the precipitation of the collapsed BBPs. The heterografted BBP exhibited a reversible LCST transition at 10 °C in an aqueous solution. These underwent the conformational transformation from extended worm-like to stable globular shapes with unimolecular collapse at both high and low concentrations. In addition, this transformation was clearly visualized by AFM, exhibiting a unique worm-like morphology at 0 °C and spherical conformation with a coiled main chain at 40 °C (Fig. 33e) [204].

The chemical composition of the side chain can be used to manipulate the LCST of the BCP. The random copolymerization of the monomers with different properties of the side chains resulted in BBPs that exhibited intermediate characteristics as those of the constituent components [316–318]. The LCST value increased by incorporating more water-soluble PEGMA into the random copolymer side chains comprising PMEO2MA and PEGMA [318]. Moreover, when the diblock copolymer side chains containing two different blocks with distinct LCST behaviors were selected as branches, the BBPs showed two stages of aggregation upon heating owing to intermolecular and intramolecular aggregation. Additionally, the sequence of the two blocks can significantly affect the thermal dehydration behavior and associated structural changes [87,319,320]. More recently, this concept was applied to BBPs by

Papadakis and coworkers [319]. The BBPs bearing statistical PrE (random copolymer of poly(propylene oxide) (PPO) and PEG) or diblock PbE (block copolymer of PPO and PEG) were prepared via the “grafting-from” approach [319]. The PPO exhibited LCST behavior at approximately 8 °C, while the cloud point of PEG was > 100 °C. The BBP containing PrE side chains showed a T_{CP} of 38 °C, while a value of 60 °C was observed for the BBP bearing PbE side chains; both exhibited worm-like morphology in water below the LCST. Upon heating above the LCST, the BBP bearing PbE side chains experienced severe and slight dehydration of the core and shell, respectively, and formed aggregates with strong connections among the swollen shells. Conversely, the PrE side chains showed severe dehydration together with a cylinder-to-disk transformation [319]. Furthermore, the LCST behaviors of the BBPs were strongly dependent on the hydrophilic or hydrophobic comonomer content, with the LCST shifting toward a lower temperature upon the introduction of more hydrophobic units [87]. Interestingly, homopolymer BBPs exhibited an anti-Arrhenius behavior with the spontaneous degradation of the backbone on aqueous substrates. With an increase in the temperature of the substrate, the cleavage of the BBP backbones was significantly suppressed, as clearly observed clearly from the AFM results [260].

All the aforementioned analyses of the conformation states of thermosensitive BBPs are based on the experimental results. However, it is challenging to experimentally understand the individual BBPs at a molecular level due to the structural complexity of the thermally responsive BBPs. Deshmukh and coworkers identified the backbone and side chain conformations in thermo-responsive BBPs

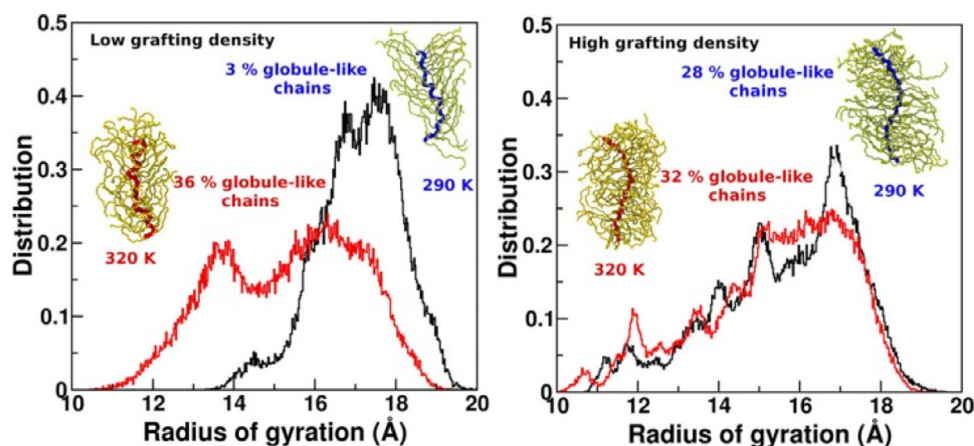


Fig. 34. Normalized distribution of R_g , averaged over all the grafted brushes in the BBPs with different grafting densities at different temperatures. [321], Copyright 2019. Adapted with permission from the American Chemical Society.

using coarse-grained molecular dynamics (MD) simulations [321]. This method preserved the important and critical information regarding the BBP conformations without the negative influence of the solvents. BBPs with backbones of 72 beads were grafted with 12 (grafting density ~16%), 24 (~33%), 36 (~50%), and 72 (~100%) PNIPAM side chains of different lengths, and their conformations were investigated at 320 K and 290 K. With grafting densities of $\leq 50\%$, the PNIPAM side chains showed coil-like and globule-like conformations below and above their LCST, respectively, leading to a cylindrical-to-spherical shape change of the BBP. For BBPs with high grafting densities, most PNIPAM side chains were in the collapsed conformations during LCST transition because of the dehydration of BBP cores, while the BBPs also underwent a cylindrical-to spherical- transformation due to the coil-to-globule transition of PNIPAM. The backbones of the BBPs formed coiled-coil conformations and became stiffer with an increase in the grafting density in all systems. These conclusions were drawn from the evaluation of the radius of gyration (R_g) of the BBPs under various conditions (Fig. 34).

Self-immolative polymers are a subset of end-to-end depolymerizable polymers [322]. The depolymerization can occur following an unzipping process that is often triggered by an external stimulus such as thermal, chemical, and irradiative triggers. BBP-based self-immolative polymers containing poly(benzylether) backbones end-capped with tert-butyldimethylsiloxy or allyl chloroformate have been synthesized and shown to undergo an irreversible degradation with a decapping reagent ($\text{Pd}(\text{O})$ or F^-) [323]. Recently, Kennemur and coworkers investigated the depolymerization of BBPs with varying lengths of polycyclopentene backbones and PS grafts [324]. With high temperatures and catalyst trigger, ring closing metathesis depolymerization of BBPs occurred, affording quantitative cyclopentene bearing original PS grafts from the BBPs [324]. Notably, the lengths of the backbone and side chains did not play a significant role in the depolymerization kinetics.

4.2.2. Photo-responsive bottlebrush polymers

Light is a distinct and highly effective stimulus that can be easily and rapidly applied and removed. Furthermore, light can be delivered remotely and instantaneously to the targeted locations in a noninvasive manner. Light of varying intensities and wavelengths can be readily used to precisely control the assembly and disassembly of nanoobjects with engineered structures and properties [270,325,326]. Photochromic compounds such as azobenzene, coumarin, cinnamate, and those with o-nitrobenzyl group exhibit isomerization between the two chemical structures with different physical and chemical properties in response to light illumination

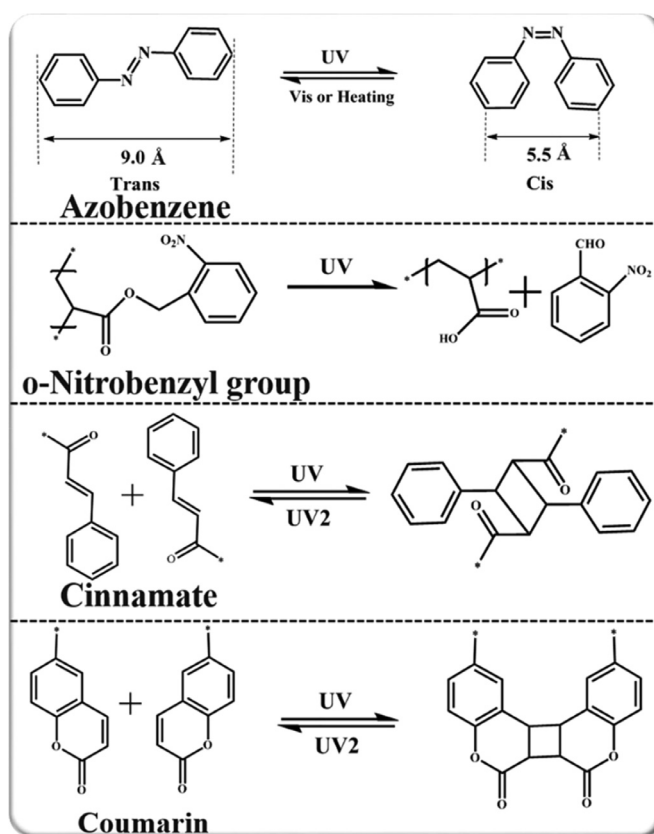


Fig. 35. Schematic illustration of photochromic compounds and corresponding photo-responsivities mechanism.

(Fig. 35). These have been incorporated into the side chains to prepare photo-responsive BBPs.

Azobenzene chromophore undergoes photoisomerization from *trans*- to *cis*-form and vice versa under alternative irradiation of visible light or heating. During isomerization, a high polarity change of the chromophore occurs, which is derived from the dipole moment variation during photoisomerization, and affects polymer-solvent interaction during photoisomerization [310]. Therefore, photo-responsive azobenzene pendants were incorporated into the BBPs to tune the self-assembled morphology. BBPs with azobenzene moieties in the side chains were first prepared via the “grafting-through” approach [85]. The *trans*- to *cis*- iso-

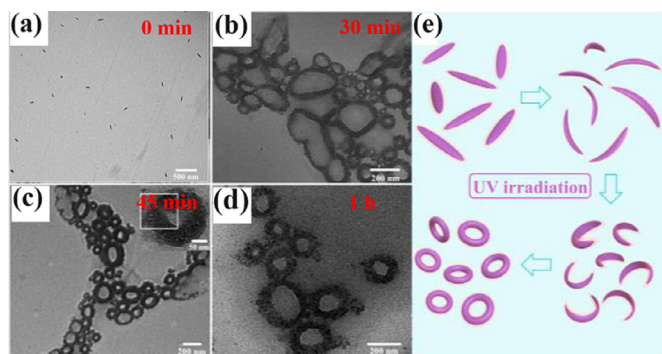


Fig. 36. TEM images (a–d) and schematic illustration (e) of morphology transition for Janus BBPs under UV irradiation. [327], Copyright 2020. Adapted with permission from the American Chemical Society.

merization of the azo chromophores was confirmed by the spectra changes. In addition, the onset temperature for a decrease in the hydrodynamic diameter of the BBP containing the *cis*-isomer is higher than that bearing the *trans*-isomer due to the decreased hydrophobicity of the *cis*-isomer, which increases the LCST of the polymer side chains. Recently, Lin and coworkers synthesized Janus BBPs consisting of PEO and azobenzene-containing side chains using a combination of ATRP and CuAAC in a one-pot method [327]. The BBPs could self-assemble into a rod-like morphology in THF/H₂O (Fig. 36a). With an increase in water content, the increased alignment among azobenzene-containing side chains on the BBPs enhanced the π - π stacking, leading to a transition from rod-like to spindle-like micelles. However, Janus BBP required a prolonged time to reach the photostationary state in comparison to the linear azobenzene-containing polymers because of the constrained motions of azobenzene moieties in the side chain. In addition, a reversible spindle-toroid-spindle transformation was observed upon alternative UV and visible light irradiation (Fig. 36) [327]. The nonplanar *cis*-azobenzene induced the curvature of the spindle micelle during photoisomerization. Moreover, the photoisomerization also broke the original symmetric side chain distribution and arrangement on the Janus BBPs. To minimize the interfacial energy during the photoisomerization of spindle micelles, BBPs adopted a toroid conformation through the toroid-closure process [327].

The photosensitive *o*-nitrobenzyl group has been widely used as a protecting and cleaving unit in the polymers for photodegradation and protection [328,329]. Upon UV irradiation, the *o*-nitrobenzyl group cleaves from its ester derivatives, manipulating the chemical structures of the polymer chains [330,331]. However, unlike other light-responsive moieties, this photosensitive unit exhibits an irreversible light-responsive behavior. A brush-linear copolymer consisting of a polyacrylate-based brush with PBA side chains and a linear block bearing the *o*-nitrobenzyl protecting group on the ureido-pyrimidinone (UPy) unit shows a worm-like morphology with a linear-chain tail in a good solvent (e.g., THF). After cleavage of the protecting group, it exhibits a coiled tail due to the intramolecular H-bonding of the UPy-UPy dimers [17]. In another case, *o*-nitrobenzyl moiety was incorporated into the side chains of the BBPs via the “grafting-to” approach. The cleavage of the hydrophobic *o*-nitrobenzyl group upon UV irradiation induced the formation of the hydrophilic side chain. The increased solubility of the BBPs promoted the conformational changes from spherical-like to worm-like morphology after UV irradiation [332].

In other cases, light was used to trigger the reversible cross-linking reactions based on dimerization. Coumarin moieties can undergo [2+2] photodimerization at 365 nm and photocleavage under 254 nm. Reversible photodimerization of coumarin has been

employed in the side chains of BBPs and applied to cross-link their shells, leading to the formation of organic nanotubes after the hydrolysis of the inner block on the side chains in solution [285,333,334]. Recently, this photo-crosslinking reaction was used to fix a spherical micelle transformed from the worm-like BBPs [335]. In addition to its usage for cross-linking the micelle at a microscale, it can also be applied to macroscopic materials. Super-soft elastomers based on the BBPs bearing PBA side chains and coumarin chain end groups were prepared [336]. The coumarin-functionalized BBPs exhibited a liquid-like behavior with G'' values greater than the G' values. The rubbery plateau of G' at high temperature was observed upon UV irradiation due to intramolecular or intermolecular dimerization under 365-nm light irradiation. In addition, when 254-nm light was used to photocleave the cross-linked BBPs, the G' value in the rubbery plateau gradually decreased with time [336].

4.2.3. pH-responsive bottlebrush polymers

The conformations of the weak polyelectrolytes such as PAA, [88] PSS, [79,337] and PDMAEMA [205] can be reversibly transformed from an expanded state to a collapsed state by adjusting the environmental pH value. This change can alter the steric hindrance, solubility, and light scattering properties of the molecular conjugates. The changes in the ionization state caused by pH variation are often accompanied by the morphological changes of the individual BBPs [338–340]. Conformational transformation of densely grafted BBPs is difficult to observe with AFM or TEM because of the slight changes in steric repulsion upon pH variation. Therefore, the effect of pH on the individual conformational change of the loosely grafted BBPs should be investigated. For instance, the loosely grafted BBPs bearing PAA side chains underwent a sphere to cylinder conformational transition with an increase in pH from 4.8 to 8.9 because the enhanced steric congestion among the side chains extended the backbone [88]. Conversely, 100% grafted BBPs were observed to maintain the fully stretched worm-like conformations independent of the pH values. PDMAEMA can be permanently quaternized and converted into zwitterionic structures. The BBPs bearing PDMAEMA side chains with 50% grafting density exhibited worm-like conformations under acidic conditions. These transformed into highly contracted morphologies owing to the coiled side chains under basic conditions [90]. In some cases, the BBPs bearing PDMAEMA-based BCP side chains fully collapsed into a spherical shape upon a further increase in pH [205]. In addition, the PDMAEMA segments on the BBPs could affect the interaction of the BBPs with the substrate because of the variable protonation degree. For instance, cylindrical core-shell BBPs bearing POEGMA-*b*-PDMAEMA side chains exhibited slight scission of the backbone at pH of 10. In contrast, upon a decrease in the pH to 1.9, the severe rupture was observed on mica due to the protonation of PDMAEMA [341]. However, quaternary ammonium BBPs were produced by two-step post-quaternization [90]. Recently, cationic BBPs were prepared using a straightforward ROMP of the quaternary ammonium macromonomers in one step [342].

As the pH-responsive moieties in the BBPs are based on zwitterionic electrolytes, such as acidic and quaternary ammonium units, the potential applications of the pH-responsive BBPs are limited. Notably, the facile incorporation of various pH-responsive carbon-nitrogen double bonds such as hydrazone, imine, and oxime bonds [343] or hydrogen bond [344–346] has been achieved in the BBPs. Thus, the responsiveness can be tuned for specific applications. For instance, pH-responsive hydrazone bonds were incorporated in dextran (DEX) polysaccharide bottlebrush-architecture to conjugate doxorubicin (DOX) on the side chain [347]. The DEX pro-drug with bottlebrush architecture was shown to release DOX in an acidic endo/lysosomal microenvironment (pH ~5.0) due to the

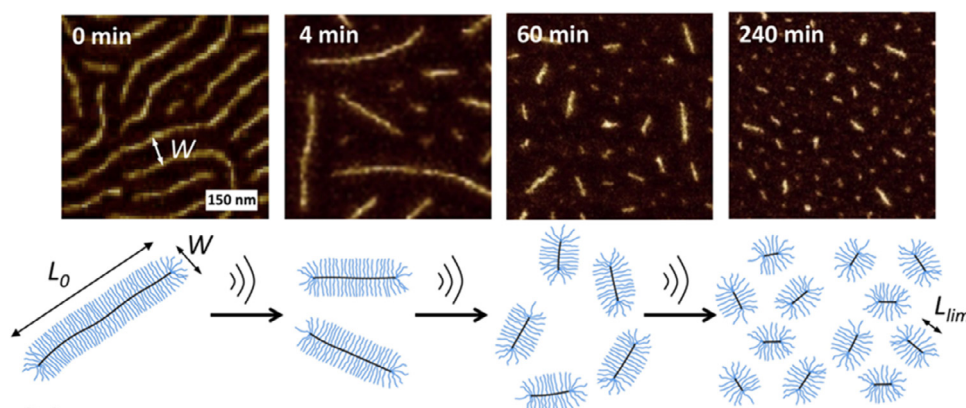


Fig. 37. AFM height micrographs of BBP and cartoon displaying fragmentation of bottlebrushes during sonication. [353]. Copyright 2016. Reproduced with permission from Elsevier Science Ltd.

hydrolysis of the hydrazone bond, leading to a real-time release of DOX.

Despite the widespread use of organic fluorescein as a pH-responsive chromophoric group in linear polymers, the application of fluorescein in BBPs for responsiveness had not been demonstrated until recently. Matyjaszewski and coworkers synthesized pH-sensitive molecular bottlebrushes, in which the side chains were the random copolymers containing the fluorescein moiety [348]. The fluorescent BBPs exhibited worm-like morphologies but showed no fluorescence under neutral conditions. A strong fluorescent emission and the presence of green color in the BBP solution were observed at alkaline pH. This was attributed to the ionization of the fluorescein moiety. In addition, by varying the solution pH, the fluorescence of the BBPs was reversibly toggled on and off.

4.2.4. Mechanically responsive bottlebrush polymers

The intrinsic tension of the BBP can be precisely controlled by manipulating its chemical structure. The external force can dominate the conformation changes of the BBPs during their spreading on a substrate via the LB method [308]. AFM has been applied to trace the in-situ shape transformation in response to the force induced by the substrates. Along the spread flow direction of the drop on the substrates, the BBPs exhibited an extended worm-like morphology [349]. In addition, the flow-induced scission of the individual BBP was confirmed by a decrease in its contour length along the flow direction. When the fractured backbone was shorter than the side chain, the mid-chain fracture of the backbone was dominant [262]. Furthermore, an increase in the substrate surface energy increased the scission rate, which led to the severe spontaneous breakage of the covalent BBP backbone [350].

Mechanochemistry induced by grinding or sonication with a destructive force has been extensively investigated in recent years [351]. It allows the management of bond tension on molecular length scales, enabling a mechanical force to break specific bonds [352]. Thus, an applied external force may effectively mediate the BBP architectures. Sonication is the most convenient and simplest dynamic force that can be applied to determine the mechanical responsiveness of the BBPs [352]. Sheiko and coworkers synthesized BBP, PHEMA-g-PBA, with identical backbones and different side chain lengths, and investigated the backbone scission by ultrasonication [353]. Significant scission occurred on the backbone because the drag force along the backbone was larger than that along the side chain. Long BBPs underwent progressive fragmentation into smaller species (short contour length) with an increase in time (Fig. 37). An increase in the grafted brush length increased the scission rate [353]. It is noteworthy that the radicals generated during backbone scission were spontaneously shielded by the

side chains, preventing intermolecular coupling. Recently, Choi and coworkers used BBPs, PNB-g-PCL and PNB-g-PS, as models to determine the exact relationship between the chain-scission rate enhancement and side chain length [354]. The contour lengths of the arms at the termini of the PNB backbone and extended polymer conformation affected the degradation rates. The degradation rates increased with an increase in the arm length when both the backbone length and arm composition (PLA or PS) were constant. Moreover, backbone scission exhibited first-order rate constant, and the rate constant for backbone scission was significantly higher than that for arm scission [354].

Mechanoresponsive polymers with bond scission can also induce mechanophore responses. However, multimechanophore polymers suffer from low percentages of activated mechanophores in their backbone owing to the length dependency of mechanochemical reaction rate [355]. BBPs with a drag force on the backbones induced by the densely-grafted side chains and elongated conformations underwent faster ultrasonic degradation than their linear counterparts. Therefore, the BBPs, PNB-g-PS, were synthesized by incorporating maleimide-anthracene cycloadducts at the backbone-arm junctions to activate the mechanophores [356]. Mechanophore activation was dependent on the arm or the spanning length, and relatively independent of the initial backbone length. This phenomenon was different for the BBPs without the cycloadduct junctions in their side chains, affording a faster scission of the backbone, which was attributed to the weak dynamic cycloadduct bonds [299] and spanning length dependency [356]. Furthermore, BBPs exhibited mechanoresponsiveness as indicated by their fluorescence upon sonication in a solution or grinding in the solid state [356].

4.2.5. Other responsive bottlebrush polymers

As discussed previously, the conformation of a BBP is highly dependent upon the dispersed state of the grafted brushes. BBPs exhibit longer backbone and side chain lengths in good solvents compared to the poor solvents. Thus, any stimulus that can trigger the side chain solubility can change the BBP conformation. By varying the ratio of good to poor solvents, BBPs can self-assemble into spherical, cylindrical, lamellar, and other complex architectures. A unique pear-necklace morphology was achieved for the core-shell BBPs when the inner (solvophobic) and outer (solvophilic) blocks showed different solubilities in selective solvents [357]. As the salt ions can substantially change the phase behavior of a polyelectrolyte solution, salt concentration (ionic strength) is an effective stimulus for polymer solutions. For a cationic polyelectrolyte, the addition of monovalent salt induced a conformation change from extended worm-like to collapsed form due to electrostatic screen-

ing [358]. Similarly, anionic surfactant could trigger a worm-to-sphere transition in the cationic BBPs due to the formation of insolubilized side chains [91]. Notably, the addition of di- or trivalent salt in the BBP solution, resulted in a helical conformation in the intermediate state [359]. In addition, the BBPs bearing peptide side chains underwent coil to helix transition with the addition of NaClO_4 owing to the twist of the β -sheet side chains [97]. The incorporation of other stimuli-responsive moieties into BBPs has been shown to alter their external responsiveness without changing their conformations. For instance, BBPs with a redox-responsive poly(ferrocenylsilane) (PFS) backbone [360] or redox-responsive nitroxide in the side chains have been prepared for MRI and fluorescence imaging [361]. Multi-responsive BBPs were also obtained and their conformation changes could be varied at multi-scales [205,332]. The BBPs also exhibited solvent responses of the cross-linking density during swelling and were more resistant to swelling compared to their linear analogs [362].

4.3. Mechanical and rheological properties of bottlebrush polymers

Due to the sterically hindered conformations of the BBPs, their side chains cannot pass through the occupied volume of the neighboring side chains, which significantly hinders the chain packing and prevents entanglement. Even though linear polymers of the same composition encounter entanglement, it is prevented in BBPs [1]. The mechanical and rheological properties of the BBPs can be expressed in terms of viscoelastic characteristics, which depend on the formation of entanglements as well as structures [21]. At ultra-low grafting densities, BBPs form comb-like polymers with unperturbed side chains in a random Gaussian conformation. In this topology, the chains can easily overlap physically with each other. This phenomenon is distinctly different from that observed for densely grafted BBPs, in which the side chains are segregated and penetrate weakly [21]. Therefore, the mechanical and rheological properties of the BBPs can be manipulated by varying both the grafting density and length of the backbone or side chains.

In an affine network model, the shear modulus of an elastomer can be estimated by the equation, $G \approx \nu RT = \rho RT/M$, where ρ is the density, M is the molar mass of a network strand, and R and T are constants at room temperature [363]. Thus, softer materials with low moduli can be readily prepared by increasing M . However, for linear polymer chains, an intrinsic entanglement in the melt states is observed above the entanglement molecular weight, $M_e \approx 10^3 \sim 10^4 \text{ g mol}^{-1}$, which leads to an intrinsic plateau modulus (entanglement modulus) $G_N^0 \approx 10^5 \sim 10^6 \text{ Pa}$. For the BBPs with high grafting densities, no entanglement (i.e., MW should be very large to achieve entanglement, $> 10^7 \text{ g mol}^{-1}$) is observed. Therefore, the entanglement moduli of the BBP melts decrease with an increase in the DP of side chain. A BBP with a plateau modulus as low as $10^2 \sim 10^3 \text{ Pa}$ can be obtained even in the absence of solvent [363]. Notably, the incorporation of the solvents or oligomers in the melts can further increase the entangled MWs and consequently decrease the plateau modulus of the system. Particularly, the side chains of the BBPs relax faster than the backbones and behave as solvents to dilute the tube diameter of the backbone [21]. Therefore, the BBPs exhibit low mechanical and shear moduli compared to those of the linear polymers owing to their unique extended cylindrical shapes without intermolecular entanglement [363–365].

Sheiko and coworkers systematically explored the mechanical performances of the BBP materials. They synthesized a series of bottlebrush elastomers bearing PDMS side chains with different cross-linking densities [363,365]. With a decrease in the cross-linking density, the consistent modulus of the bottlebrush elastomers decreased to 520 Pa, implying a significantly softer material than the linear PDMS melts (Fig. 38a) [363]. The elonga-

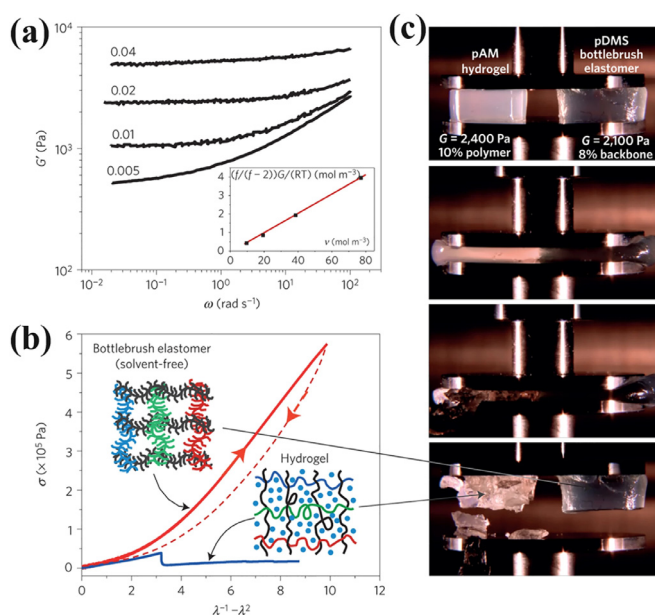


Fig. 38. (a) Rheological performances of PDMS-based BBP elastomer with variable cross-linking density. (b) True stress compression of PDMS-based BBP elastomer and PAM hydrogel with similar volume fractions of backbone and polymer chain, respectively, and (c) corresponding compression behaviors. [363]. Copyright 2016. Reproduced with permission from the Nature Publishing Group.

tion-at-break (λ_{\max}) showed a different dependency on the polymer volume fraction for the BBPs and conventional polymeric materials. For the BBPs, $\lambda_{\max} \sim \phi_{bb}^{3/4}$, while for the conventional polymers, $\lambda_{\max} \sim \phi_0^{5/8}$, where ϕ_{bb} is the volume fraction of bottlebrush backbone in the gel and ϕ_0 is the polymer concentration in an as-prepared gel [363]. With similar backbone volume fractions, solvent-free PDMS BBP elastomer exhibited significantly higher fracture energy and larger elongation than those of the poly(acrylamide) (PAM) hydrogel in compression performance (Fig. 38b). BBP elastomers exhibited inherent strain-stiffening behavior in the tensile performance because of the intrinsic extended cylindrical shapes without entanglement. This behavior was similar to those of the conventional prestrained elastomers owing to the finite extensibility of the network strands in the swelled state. However, the performance was different from those of the conventional elastomers, which exhibited linear elasticity over elongation due to the coiled strands in the network but did not exhibit strain-stiffening behavior (Fig. 38c) [365].

To quantify the viscoelastic behaviors of the BBPs, several independent molecular characteristics for the cylindrical shape such as n_g and n_{sc} are employed (Fig. 16a) [251]. The volume fraction of the backbone monomers in a graft macromolecule is expressed as $\phi_{bb} = n_g/(n_g + n_{sc})$. The inverse, ϕ_{bb}^{-1} , is equivalent to the “swelling ratio” of the polymer gel [366]. Sheiko and co-workers determined the influence of grafting density on the conformation through MD simulations and experimental measurements [251]. They found that increase in grafting density and side chain length resulted in the extension of the backbone and long-range interactions among the backbone monomers. With scaling analysis, they distinguished the diagram of conformational states into four different regimes based on the parameters of the grafted polymer (ϕ_{bb} , and n_{sc}), i.e., comb regime, which is further divided into loosely-grafted comb-like (LC) and densely-grafted comb-like (DC) polymers, stretched backbone (SBB) regime, stretched side chain (SSC) regime, and rod-like side chain (RSC) regime [251]. In the comb regime, the BBP main chain and branches exhibit random Gaussian conformations and the branches can interpenetrate the neighboring side chains,

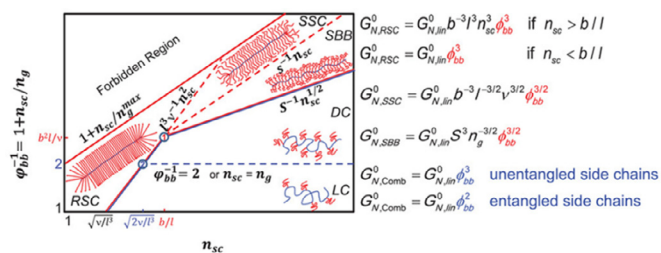


Fig. 39. Molecular conformations of comb-like and brush-like polymers and their corresponding expressive equations with parameters, among which $s = v/(bl^2)$ and $S = v/(bl)^{3/2}$. [21], Copyright 2019. Reproduced with permission from John Wiley and Sons Inc.

indicating the presence of entanglements in these polymers. The plateau modulus of the entangled comb-like polymer can be expressed as $G_{N,comb}^0 = G_{N,lin}^0 \phi_{bb}^3$, where $G_{N,lin}^0$ is the plateau modulus for the corresponding linear side chain with entanglement [363]. Further increase in the grafting density with a constant side chain length decreases the penetration among the BBPs. In the SBB subregime, the backbone was stretched because of the steric repulsion among side chains. However, the side chains in this regime still exhibit unperturbed conformations. In the SSC and RSC subregimes, both the main chain and branches were in stretched conformations, and the side chains cannot theoretically interpenetrate the adjacent BBPs, indicating a lack of entanglement in the BBPs. The corresponding rubber plateau moduli in each regime are shown in Fig. 39 [21].

It is notable previous models for scaling analysis are based on the BBPs with unentangled branches because the entanglement of these side chain polymers requires very high MWs [367]. Bates and coworkers systematically investigated the effects of the main chain and side chain lengths on the linear rheological behaviors, particularly in the range where entanglement could occur among the side chains [368]. The extensive understanding of the Rouse-like dynamics was achieved by applying time-temperature superposition. They synthesized two sets of BBPs with different side chains (Fig. 40a and 40b). In one case, the side chain, poly(ethylene-alt-propylene) macromonomers (PEP-NB), had MW above the M_e of the linear PEP [368]. The BBPs showed sequential relaxation which could be readily observed in the master curves with three regimes (e.g. segmental regime, arm regime (intermediate region), and terminal regime) (Fig. 40c). In the segmental regime, chain segments relaxed with Zimm-like dynamics during the viscous response and the glassy moduli were independent of the side chain length [369,370]. In the arm regime, the side chains began to relax and the addition of the rubbery plateau regions confirmed the formation of side chain entanglements among the PEP branches in the curve. Additionally, the plateau shoulder length increased with an increase in the side chain length in this regime [367]. In the terminal regime, the relaxation behavior of the whole brush molecules (global chain relaxation) was observed and the relaxation time (dynamics are Rouse-like model) was significantly dependent on the main chain length. In another case, the BBPs bearing atactic polypropylene (aPP-NB) side chains with lengths shorter than those necessary for side chain entanglement (linear aPP, $M_n/M_e \approx 0.5$) were prepared [368]. No rubbery plateau was observed in the dynamic master curve, indicating that the side chains remained unentangled even at high MWs for the BBP, poly(aPP-NB) (Fig. 40d). This was attributed to steric crowding among the densely-packed branches that suppressed the flexibility of the backbone and formed persistent brush molecules with large cross-sectional areas. Furthermore, poly(aPP-NB) exhibited a more pronounced Rouse-like relaxation in the arm region and the breadth also increased with an increase in backbone length [368].

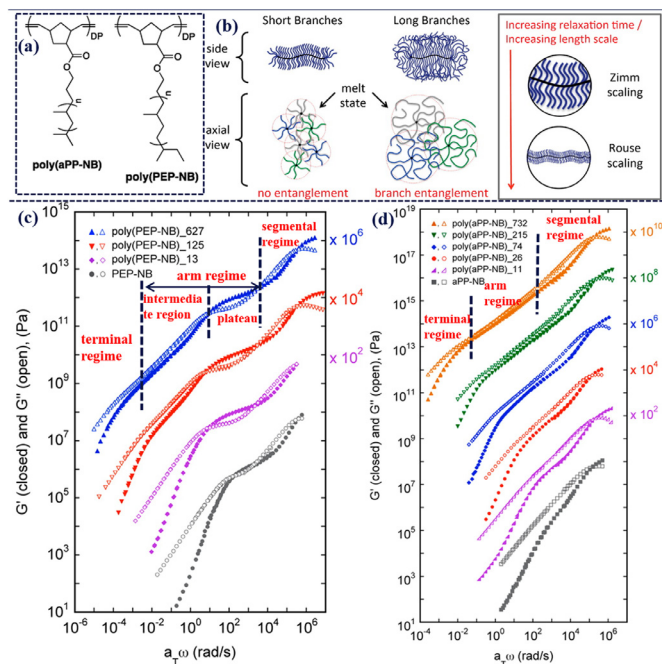


Fig. 40. (a) Chemical structures of BBPs. (b) Dynamic relaxation behaviors for BBPs with different side chain length. (c) Dynamic master curves of G' (closed symbols), G'' (open symbols) for BBPs and macromonomers at a reference $T_{ref} = T_g + 34$ °C. Curves vertically shifted using the indicated scale factors. [368], Copyright 2015. Adapted with permission from the American Chemical Society.

Notably, the linear viscoelastic properties of the BBPs were highly dependent on the grafting density despite the side chain length. The grafted branches in the loose bottlebrush topologies penetrated the side chains of the neighboring molecules during deformation [371].

Zero-shear rate viscosity, η_0 , is another characteristic parameter for evaluating the linear viscoelastic properties of the BBPs, and is defined as the complex viscosity (η^*) at infinitesimal frequency [372]. Bates and coworkers systematically determined the effect of the backbone DP on zero-shear viscosity. They synthesized two series of BBPs using norbornenyl-terminated macromonomers with fixed side chain lengths via the “grafting-through” approach [368,372]. Poly(aPP-NB) contained side chains with lower MWs than the M_e of the corresponding linear aPP, while poly(PEP-NB) consisted of longer side chains (higher than the M_e of the linear PEP). These showed a Rouse relaxation mechanism for η_0 , owing to the backbone relaxation in the terminal regime, regardless of the side chain length (with or without side chain entanglement). The η_0 of the polymer melt is correlated to the weight-average molecular weight (M_w) by the expression: $\eta_0 \sim M_w^\alpha$. Based on the empirical studies, $\alpha \approx 1$ for the polymer chains in the Rouse model, and $\alpha \approx 3.4$ for polymers with MW above the critical M_e with side chain entanglement [372]. Linear aPP molecule exhibited two distinct relaxation mechanisms based on the curves of the reduced zero-shear viscosity as a function of M_w , which was attributed to the entanglement of the polymer chains at high MWs. In contrast, α was approximately 1 for BBPs, poly(aPP-NB) and poly(PEP-NB), indicating that the viscosity was weakly dependent on M_w (Fig. 41a) [372]. This was ascribed to the limited penetration of the densely-grafted side chains and the extended cylindrical shapes of the BBPs that relaxed with undisturbed conformations [368,372]. As mentioned above, the grafting density significantly affects the conformations of the BBPs and apparent M_e , which can lower the viscosity and affect the processing of BBPs. Bates and coworkers further investigated the dependency of

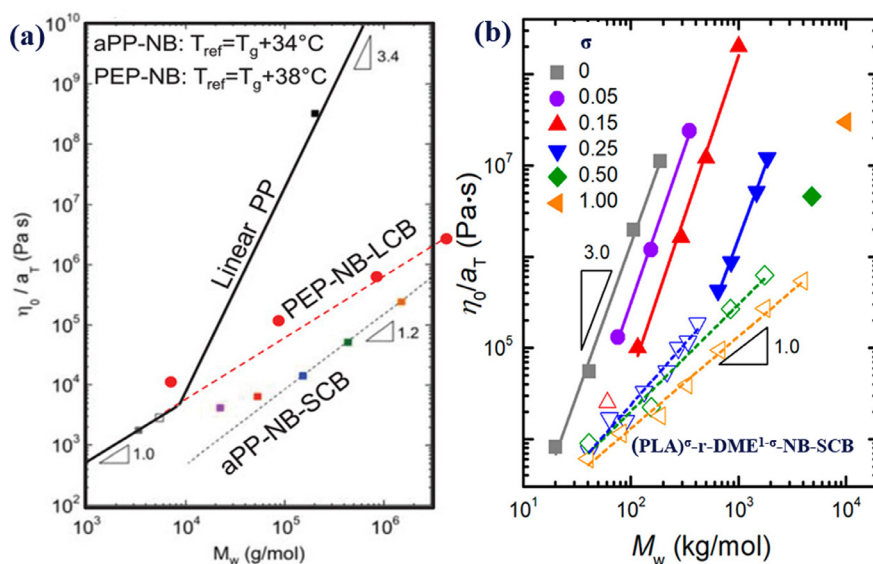


Fig. 41. Reduced zero-shear viscosity as a function of M_w for BBPs. (a) BBPs with different side chain lengths. [368,372], Copyright 2014 and 2015. (b) BBPs with different grafting densities. [373], Copyright 2018. All adapted with permission from the American Chemical Society.

zero-shear viscosity on grafting density. BBPs (PLA-*r*-DME-NB-SCB) with variable grafting densities ($0 < \sigma < 1$) were synthesized by the ROMP of a macromonomer (NB-PLA with short length) and a comonomer, dimethyl ester (DME), in a one-pot method [373]. At a low grafting density, the BBPs showed similar relaxation behaviors as those of the linear polymers and exhibited typical reptation scaling with an α value of 3. With $\sigma = 0.25$, the BBPs underwent an abrupt transition from the Rouse to reptation model due to entanglement among the side chains. With a high grafting density, the BBPs exhibited a Rouse relaxation mechanism with an α value of 1 without side chain entanglement because of the densely-packed branches even when their M_w s exceeded the M_e of the corresponding linear polymers (Fig. 41b) [372]. In contrast, the side chains could penetrate the neighboring side chains in loosely grafted BBPs and show high side chain entanglement [373]. In addition, other viscoelastic properties of the BBPs were tuned by varying the structural parameters of the synthesized BBPs [21,371].

5. Applications of bottlebrush polymers

Novel materials with excellent performances have been continuously pursued by researchers in recent years. The BBPs with accurate cylindrical structures are highly desirable for preparing advanced materials with new or improved properties. By precisely crafting BBPs with well-designed architectures and chemical components, excellent performances for an array of potential applications such as templates, elastomers, organic optoelectronic materials, and energy storage can be achieved (Fig. 42).

5.1. Templates

High controllability of the dimensions can be achieved in polymers, which allows the fabrication of different architectures. Therefore, polymers show great potential applications in the nanoreactor-directed synthesis of nanomaterials with different structures and compositions. Linear polymers were first developed and applied as nanoreactors to prepare nanocrystals (NCs) [374–376]. In addition to the linear polymers, cyclodextrin-based star-like polymers have served as nanoreactors to prepare nanoparticles with various structures [198,377–379]. Different morphologies such as solid nanoparticles with optical, [199,380] and plasmonic properties, [381,382] as well as upconversion, [383] and ferroelectric

performances, [384,385] core-shell nanoparticles, [352,386–388] and hollow nanoparticles, [200,381] have been obtained through nanoreactor-directed methods. Although 0D inorganic nanomaterials with diverse morphologies have been prepared utilizing BCPs or star-like polymers as nanoreactors, the preparation of 1D nanomaterials with BCPs as templates is challenging because of the limited formation of 1D morphology. One-dimensional nanomaterials such as nanorods and nanowires afford a unique platform for tailoring and utilizing the properties of metals or metal oxides, which have been applied in diverse applications [389]. Therefore, it is highly desirable to develop straightforward methods for preparing 1D nanomaterials with variable compositions and morphologies. The conceptually intuitive 1D structures of the BBPs provide unprecedented access to unimolecular and anisotropic nanoreactors to allow straightforward preparation of 1D nanomaterials. A 1D cylindrical BBP with core-shell structure not only provides an excellent compartmentalized domain in the inner block among the side chains to load the precursors but also allows confinement to grow nanomaterials along the backbone. The outer chains allow solubility of the resulting 1D nanomaterial and prevent agglomeration and precipitation in solution. The obtained 1D hybrid nanomaterials prepared via the nanoreactor-directed method exhibit superior properties such as stability, flexibility, and lack of physically absorbed ligands because of the use of organic components, over other methods. In addition, the precise controllability of the BBP parameters such as aspect ratio, side chain blocks, and functionalities allows the BBPs to act as uniform nanoreactors for the template-directed preparation of 1D nanomaterials. Although the adsorption of pre-synthesized nanoparticles along 1D micelle surfaces can allow the fabrication of the 1D hybrid materials, [390,391] this aspect is not discussed in this review. The straightforward and versatile nanoreactor method for the preparation of 1D nanomaterials can be employed through two major routes: (1) in-situ formation via the hydrolysis or pyrolyzation of the precursor-containing side chain blocks, or (2) by loading the precursors followed by reactions.

The in-situ build-up of 1D nanomaterials with BBPs is a straightforward method, which can prevent the pre-loading of metal precursors. Müllner and coworkers reported a proof-of-concept demonstration of the formation of 1D nanomaterials using blocks that contained inorganic precursors [392–

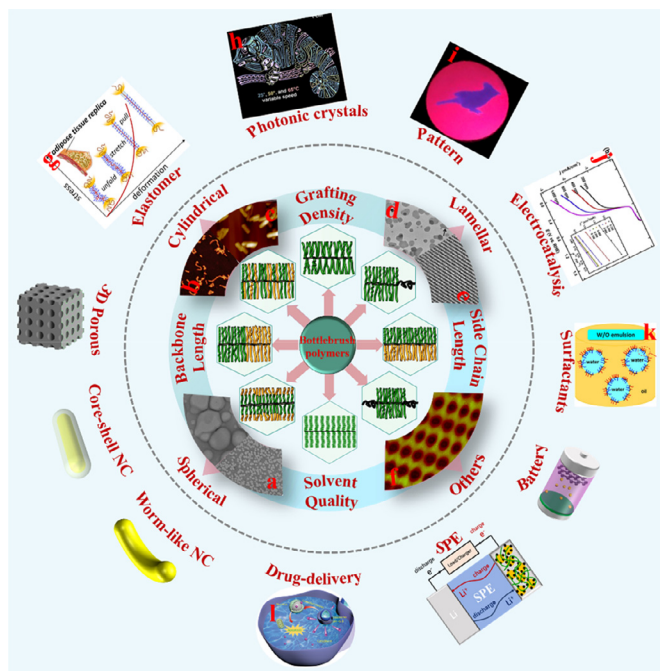


Fig. 42. Various types of BBPs, self-assembly morphologies, and their applications. (a) spherical assembled morphology. [247], Copyright 2014. (l) Drug-delivery. [347], Copyright 2020. All adapted with permission from the Royal Society of Chemistry. (b) Cylindrical morphology. [265], Copyright 2018. (d) Disk-like morphology. [14], Copyright 2013. (f) Hierarchically organized structures. [292], Copyright 2010. (g) Hierarchical deformation of BBPs elastomer. [427], Copyright 2020. (i) Fluorescence pattern from BBPs. [22], Copyright 2019. (k) Surfactants from Janus BBPs. [477], Copyright 2017. All adapted with permission from the American Chemical Society. (c) Rod-like morphology. [12], Copyright 2016. (h) Photonic crystals. [442], Copyright 2020. All adapted with permission from the American Association for the Advancement of Science. (e) Lamellar structures from Janus BBPs. [276], Copyright 2018. Adapted with permission from John Wiley and Sons Inc. (j) Electrocatalysis from BBP-based nanomaterials. [456], Copyright 2017. Adapted with permission from Elsevier Science Ltd.

395]. They synthesized BBPs by the sequential ATRP of 3-acryloxypropyltrimethoxysilane (APTS) and OEGMA in the side chains, which were used as the silsesquioxane precursors. Under basic conditions, the inner condensation led to a cross-linked silsesquioxane core, which was further pyrolyzed into inorganic silica nanowires. During condensation, the solubilized POEGMA shell sufficiently prevented the intermediates from precipitation. With a precise design and control of the backbone and side chain lengths, the length and diameter of the worm-like nanowire were easily tailored, and the variation in the dimensions was verified by AFM and TEM. When a third block was introduced in the innermost part, worm-like nanotubes were directly obtained after the condensation of the middle block [393]. However, this in-situ method was hindered by the availability of limited monomers and easy hydrolysis of the precursor-containing block (e.g., APTS), which restricted further applications.

The latter approach in which the precursors are pre-loaded in the BBP templates is a general methodology for preparing 1D nanomaterials. To provide a domain for precursors loading and immobilization, the interior blocks are typically weak polyelectrolytes such as positively charged P4VP or PDMAEMA and negatively charged PAA, which can coordinate to the metal precursors. In the subsequent step, the precursors are reduced or sulfidated to form 1D nanomaterials exhibiting excellent stability in solution owing to the exterior side chains. With the precise synthesis of BBP templates, 1D nanomaterials with various compositions including Au, [396,397] SiO₂, [397] TiO₂, [394,398,399] Fe₃O₄, [400] ZnO, [401] CdS, [402] and CdSe [403] have been obtained. In

a unique case, Müllner and coworkers grafted diblock copolymer, PAA-*b*-PDMAEMA, in the BBPs and incorporated rare-earth metal cations such as Ln³⁺, Gd³⁺, and Tb³⁺ into the core. Thereafter, tetramethyl orthosilicate (TMOS) was loaded on the outer shell domain, and subsequent condensation of the exterior shell resulted in silica-coated 1D hybrid nanomaterial exhibiting visible photoluminescence and magnetic resonance [404]. Notably, when the backbone length was approximately the same as the side chain lengths, the BBP template adopted a star-like morphology and tended to form spherical micelles [398]. Although various 1D nanomaterials have been prepared using BBPs as nanoreactors, the worm-like structure of the BBP is difficult to employ in the preparation of rigid rod-like 1D nanomaterials.

As mentioned previously, cellulose has a rigid 1D morphology, and cellulose-based BBPs exhibit rigid rod-like morphology. By capitalizing on functional unimolecular BBPs with well-defined structures and low \bar{D} as the nanoreactors, diverse 1D inorganic plain or core-shell nanorods and nanotubes have been prepared (Fig. 43a) [12]. With the core-shell cellulose-*g*-[PAA-*b*-PS] as the unimolecular nanoreactor, various plain nanorods with different various compositions including a single component (i.e., Au and Ag), two components (e.g., CdSe, Fe₃O₄, PbTe, and TiO₂), and multi-components (e.g., BaTiO₃, NaYF₄:Yb/Tm, NaYF₄:Yb/Er) have been readily obtained after a sequential two-step process of loading and the corresponding reduction or hydrolysis. Au nanotubes soluble in organic solvents were prepared using cellulose-*g*-[PS-*b*-PAA-*b*-PS] as a unimolecular nanoreactor under similar conditions (Fig. 43b). For the cellulose-*g*-[PS-*b*-PAA-*b*-PS] BBP nanoreactor, the inner PS block was used as the metal-free domain, which was unfavorable for loading. The outer PS had the same functionality as discussed above, and the PAA block provided a domain to load the precursor. When a unimolecular template, e.g., cellulose-*g*-[P4VP-*b*-PtBA-*b*-PS], containing two domains that could load precursors served as a nanoreactor, core-shell nanorods were prepared (Fig. 43c). In this case, Au precursors were first anchored to the P4VP domain and reduced using tert-butylamine borane to form core Au nanorods. Subsequently, the middle PtBA block was hydrolyzed or pyrolyzed into active PAA that loaded the second precursor such as iron ions or titanium(IV) tetraisopropoxide, thus allowing the formation of uniform Au@Fe₃O₄ or Au@TiO₂ core-shell nanorods capped by PS. The length and diameter of the nanorod or nanotube were rationally tuned by varying the cellulose intrinsic backbone and side lengths. The aspect ratio of the 1D Au nanomaterials was highly dependent on the size, aspect ratio, and shape (e.g., hollow and core-shell) [405]. Furthermore, when the outer PS block was changed to hydrophilic PEG via a click reaction, water-soluble 1D (core-shell) nanorods and nanotubes were readily synthesized.

In addition to the preparation of hybrid 1D nanomaterials with BBPs as the nanoreactors, these themselves can serve as templates for fabricating functional materials without hybridization with inorganic materials. In a literature report, organic nanotubes were formed owing to their intrinsic structural diversity [236]. BBPs bearing diblock side chains with cross-linkable corona and degradable core segments self-assembled into cylindrical morphology. After cross-linking the corona shell and removing the inner part, organic nanotubes were obtained [236,268,334]. These organic nanotubes showed significant application potential as selective carriers for therapeutic agents and cellular uptake [406]. In an additional report, BBPs bearing PtBA-*b*-PS side chains were synthesized via the “grafting-from” approach. Then, FeCl₃-catalyzed Friedel-Crafts reaction was used to cross-link the outer PS blocks on cylindrical BBPs. After the in-situ hydrolysis of the resulting porous functional nanonetwork-structured polymers, 3D porous carbon materials with enhanced adsorption performance were obtained [407,408]. In addition, the BBPs can serve as sacrificial domains to fabricate ordered porous materials with tailored pore sizes [409].

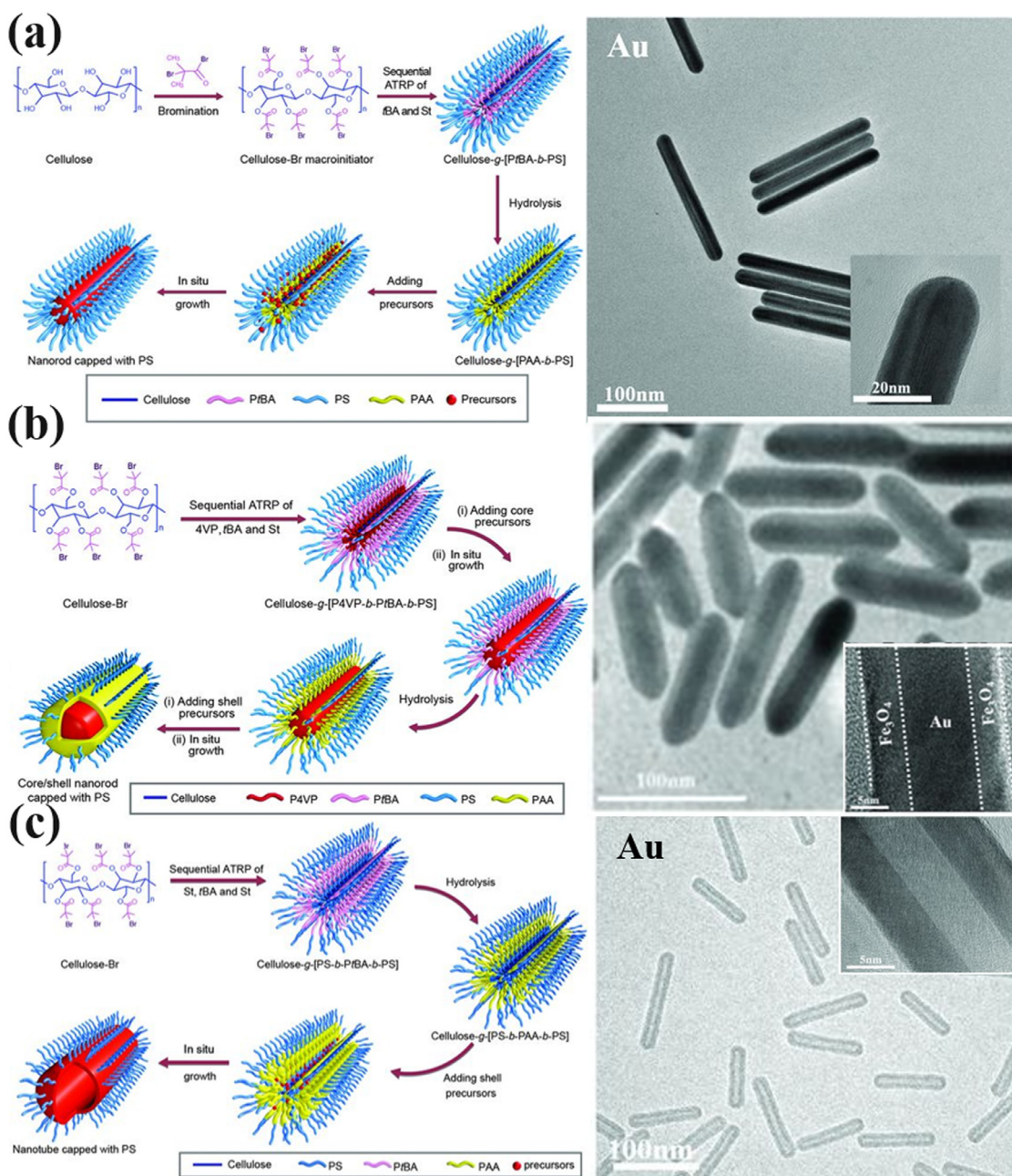


Fig. 43. Schematic illustration for crafting 1D nanocrystals with BBPs as unimolecular nanoreactors (a) Cellulose-g-[PAA-b-PS]-directed plain nanorods, (b) Cellulose-g-[P4VP-b-PBA-b-PS]-directed core-shell nanorods, (c) Cellulose-g-[PS-b-PAA-b-PS]-directed nanotubes. [12], Copyright 2016. Adapted with permission from the American Association for the Advancement of Science.

Linear BCPs can self-assemble into micelles with sizes of approximately 2 and 35 nm and polymer colloids with sizes of > 100 nm [238]. These structures serve as soft templates to fabricate porous carbon materials. However, a wide gap in the accessible pore sizes between 35 and 100 nm exists, which limits their widespread usage. BBPs can self-assemble into spherical morphology with uniform domain sizes between 15 and 150 nm, and these are used to fill the gap, thereby effectively bridging the meso- and macropores. Watkins and coworkers synthesized block BBCPs, (PNB-g-PDMS)-*b*-(PNB-g-PEO), where PEO selectively interacted with the hydrogen bond donors and PDMS reduced the energy penalties to form high-curvature morphologies [409]. The BBPs formed uniform spherical morphologies and then served as soft templates to form a hybrid with the phenol-formaldehyde resin. Porous carbons with pore sizes of 16–108 nm were readily obtained after carbonization.

Additionally, the pore size followed a linear relationship with the M_w of BBP, and therefore it could be readily manipulated by varying the MW of the BBPs.

5.2. Elastomers

BBPs have a major advantage of significantly reduced chain entanglements due to the large volume of the bottlebrush strand, which leads to a unique viscoelastic behavior compared to that of their linear analogs. Additionally, solvent-free BBP elastomers exhibit low shear moduli of $10^2 \sim 10^3$ Pa (discussed in Section 4). This presents significant opportunities to control the macroscopic performances of BBP superelastomers with an unprecedented tenability by manipulating the chemical structures [363,410]. BBP-based ultra-soft elastomers with low moduli and high deformability have

been widely investigated and synthesized by cross-linking the side chains with a cross-linker during polymerization [161,363,410] or post-synthesis [411,412]. Even with a low cross-linking density in the elastomer, it allows the accessibility of entanglements caused by intermolecular or intramolecular cross-linking. This cross-linked conformation was clearly verified by the appearance of a rubbery plateau in the linear scaling of the middle-frequency plateau modulus [363]. The G' value increased with an increase in the cross-linker concentration, but the elastomer exhibited a large deformation during stretching [363]. To specifically target biomedical soft materials, PDMS-based BBP elastomers without entanglement were recently developed. Notably, linear PDMS showed entanglement at M_e of $> 10^4$ g mol $^{-1}$, while the BBP has an M_e value of $> 10^7$ g mol $^{-1}$. Thus, entanglement-free elastomer can be readily fabricated by covalently cross-linking the difunctionality-terminated PDMS cross-linker through hydrosilylation [413] or copolymerization [216,414].

However, the cross-linking densities in these systems are difficult to control, and therefore, the development of a universal synthetic platform is highly desirable. Beers and coworkers prepared the BBP networks with PBA side chains via the ROMP of NB-containing macromonomers and cross-linker. ROMP can quantitatively polymerize the monomers, and it is thus favorable to tune the cross-linking density by controlling the feed ratio [415]. With precise control of the ratio, all networks yielded $> 90\%$ gel fractions. The swelling ratio, Q , increased with an increase in the cross-linking density. Contact adhesion testing demonstrated that the BBP networks exhibited low shear moduli (G), in the dry state, and a scaling relationship of $G \sim Q^{-1.71}$ was established [415].

Although in-situ cross-linking during polymerization with multifunctional cross-linkers can simultaneously construct a backbone and connections in a BBP network, the necessity of air-free conditions is unfavorable to analyze BBP molecules before cross-linking. In addition, the tedious deoxygenation process limits this approach [416]. Photo-cross-linking provides a possible ex-situ method to cross-link the BBPs in the bulk state. Photo-cross-linkable bis-benzophenone cross-linker with PDMS spacer was prepared by esterification. The benzophenone moiety promoted the promiscuous C-H abstraction to form active radicals and underwent cross-linking reactions [417]. To extend the scope of telechelic polymers (i.e., cross-linkers) with reactive benzophenone functionality, a library of cross-linkers bonded by small-molecule alkyl derivatives or polymers was synthesized [418]. Homogeneous BBP components exhibited entanglement-free relaxation in the viscoelastic behavior before UV irradiation. After UV cross-linking, all BBP networks exhibited $G' > G''$, suggesting a viscoelastic liquid-to-solid transition during UV exposure. Previous BBP elastomers prepared by in-situ polymerization exhibited characteristics corresponding to the phantom network model, where all added cross-linkers were elastically effective. In contrast, the ex-situ photo-cross-linking led to elastically effective and ineffective cross-links (cross-linked in intermolecular BBP) in the BBP elastomers, which showed characteristics consistent with the affine network model [418]. A distinct phenomenon was observed in the ex-situ photo-cross-linked elastomers; the cross-linking density showed a limited effect on G'' because the pendant chain ends were intact during photo-cross-linking [418].

The aforementioned BBP networks are cross-linked with nondynamic covalent bonds and thus, the traditional approaches do not allow the self-healing of elastomers, which is vital to mitigate device damage [419]. Dynamic covalent adaptable networks (CANs) have been applied in BBP elastomers to tailor their self-healing performances [420,421]. CANs that maintain constant cross-linking densities and desirable mechanical properties throughout the exchange process are also known as vitrimers [422]. Recently, dynamic bond exchange via transesterification catalyzed by Lewis

acids was applied to the BBP elastomers to obtain soft self-healing materials [423]. BBPs bearing poly(4-methylcaprolactone) side chain were synthesized via the “grafting-through” approach using ROMP. The resulting materials exhibited dynamic stress-relaxation rates at elevated temperatures due to the transesterification of dynamic ester bonds with the residual hydroxyl groups (Fig. 44). The G' increased with a decrease in the backbone length or increase in the side chain length. Furthermore, the BBP networks exhibited excellent self-healing performances with strains of up to 350%.

Similar to the BBPs cross-linked via dynamic covalent bonding, the networks formed by physical bonds in the BBPs typically result in super-soft elastomers with low moduli, high stretchability, and distinct strain-stiffening characteristics. Among the various BBP architectures, linear-brush-linear triblock copolymers (ABA) with microphase separation that form physically cross-linked networks, represent an emerging system for preparing ultrasoft elastomers [305,364,424–426]. Sheiko and coworkers synthesized linear-brush-linear copolymers bearing crystalline linear blocks [305]. With an appropriate side chain length, the crystallization of the linear block facilitated the formation of reversible physical networks, while the bottlebrush segment served as a connector to bridge the crystalline phase. The dependency of mechanical properties on the branch length and grafting density was evaluated [364]. In addition, a three-step fitting, modeling, and synthesis process was employed to mimic the biological stress-strain behavior of the prototypical PDMS-based elastomers [364]. Recently, chameleon-like elastomers with structural coloration were reported using linear-brush-linear triblock copolymers (PMMA-bbPDMS-PMMA) with microphase separation [424]. The rigid crystalline domains formed by the linear block dispersed in the supersoft bottlebrush matrix with a low modulus because of the absence of entanglement (Fig. 45a). Characteristic coloration during solvent evaporation originated from the periodic domain induced by microphase separation (Fig. 45b). The domain was found to transform from spherical to worm-like morphology with an increase in the PMMA volume fraction (ϕ_A) (Fig. 45c). The elastomers showed a low initial moduli and intense strain stiffening with strain extension. These performances were significantly affected by structural parameters, such as brush backbone length and ϕ_A (Figs. 45d and 45e) [424]. The deformation mechanism for the soft-to-firm transition in the BBP networks is shown in Fig. 45f, which constitutes: (1) the unfolding of bottlebrush filaments, (2) stretching of backbones inside the brush envelopes, and (3) pulling of the linear chains from the microdomains to create a new interface between exposed linear block segments and the bottlebrush matrix [427]. In addition, the elastomer film exhibited a blue shift of color during stretching due to a decrease in the interdomain distance (d_3) [424]. Owing to the initial softness and intrinsic intense strain-stiffening at large deformations, free-standing and solvent-free elastomers have been used in dielectric actuators that can prevent the occurrence of electrical breakdown [365,428].

5.3. Organic optoelectronic materials

5.3.1. Photonic crystals

PCs have periodic structures with periodicity on the same length scale as the wavelength of light that forbids light propagation [429]. The simplest structure is periodic alternating layers with domain sizes larger than 100 nm, where some of the incident light is reflected. The thickness of each layer dominates the reflected light peak position. The wavelength of the reflected light (λ) can be predicted from the equation: $\lambda = 2(d_1n_1 + d_2n_2)$, where d and n are the domain size and refractive index of each layer, respectively [15]. The self-assembly of linear BCPs provides a promising approach to fabricate the PCs due to their cost but is lim-

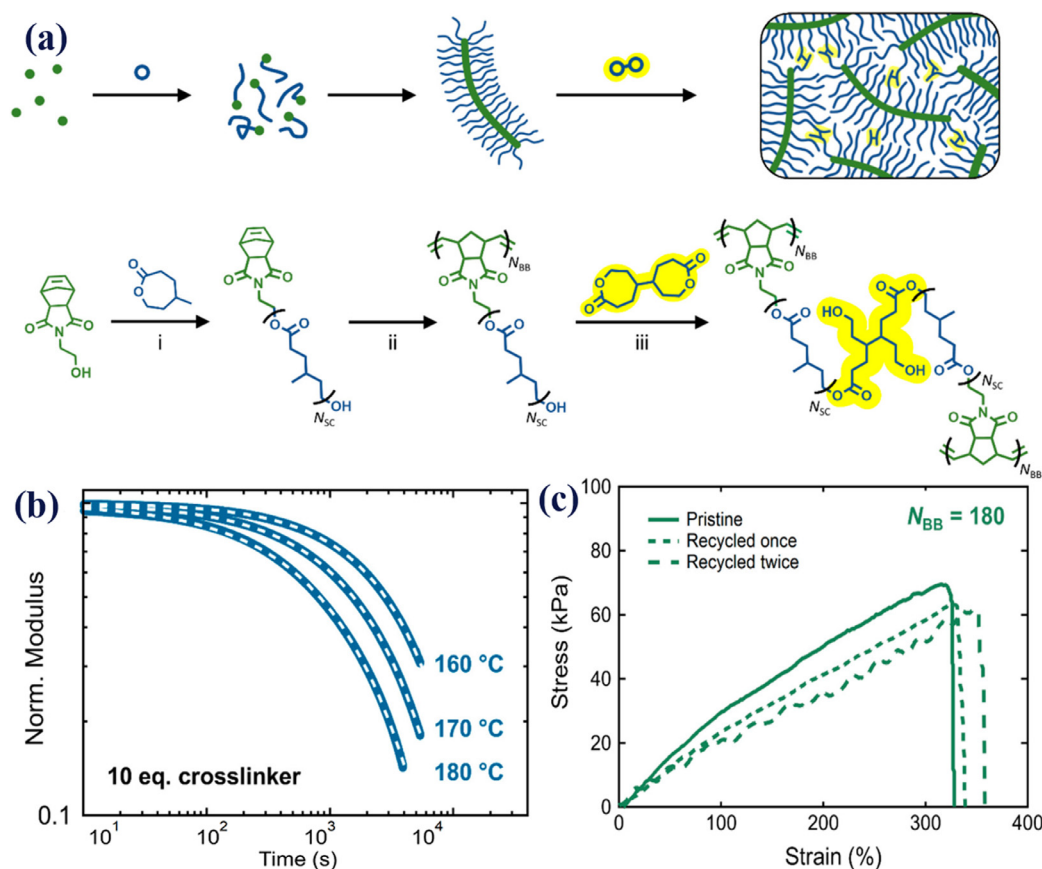


Fig. 44. (a) Reaction scheme for generating dynamic BBP networks that undergo associative transesterification. (b) Stress-relaxation experiments of BBP elastomers under elevated temperature with constant cross-linking density. (c) Stress-strain curves of self-healing BBP elastomers. [423], Copyright 2020. Adapted with permission from the American Chemical Society.

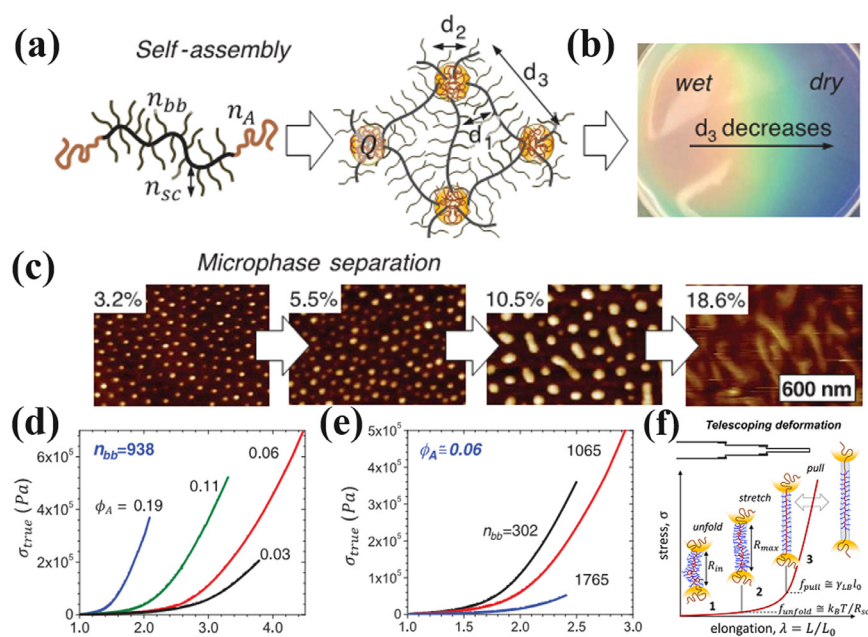


Fig. 45. (a) Schematic illustration of physical networks formed from linear-brush-linear copolymers. (b) The structural coloration of elastomer film during solvent evaporation. (c) AFM images of linear-brush-linear BBPs with variable linear volume fraction. (d, e) The dependency of mechanical performances of elastomers on structural parameters. [424], Copyright 2018. Adapted with permission from the American Association for the Advancement of Science. (f) The deformation mechanisms of linear-brush-linear elastomer during uniaxial extension. [427], Copyright 2020. Reproduced with permission from the American Chemical Society.

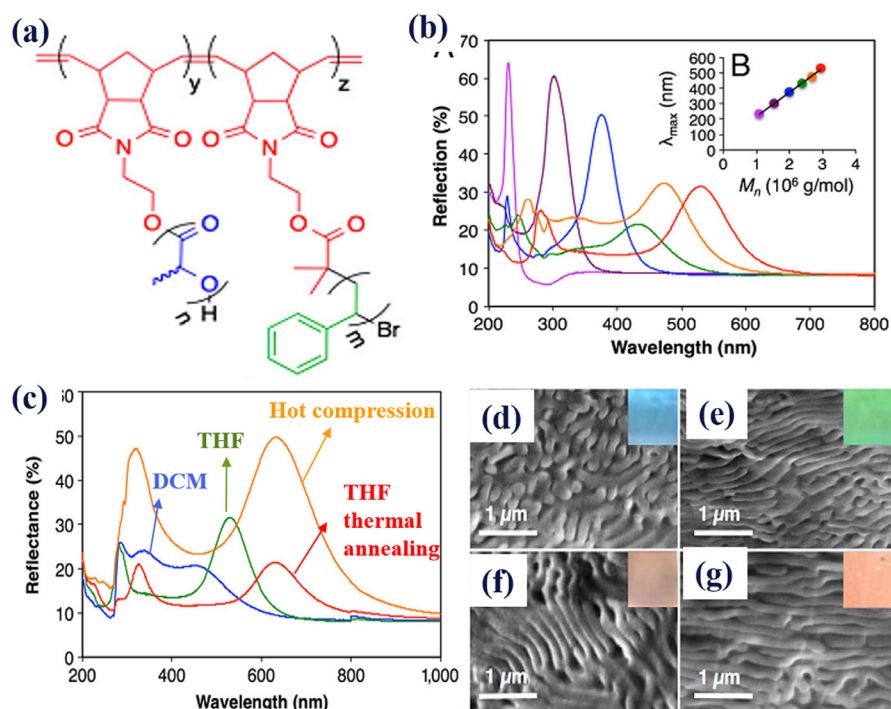


Fig. 46. (a) Chemical structure of BBCP. (b) The dependency of the wavelength of light on MW of BBCPs. (c) Reflection spectra and (d–g) corresponding cross-sectional SEM images for the BBCP films under different processing conditions, insets are photographs of the samples. [431], Copyright 2012. Adapted with permission from the National Academy of Sciences.

ited by the domain size because of relatively low MWs. High-MW BCPs exhibit high polymer chain entanglements, which severely impede the generation of ordered morphologies with large sizes. The BBCPs with ultrahigh MWs can be readily synthesized using advanced polymerization techniques. In addition, no backbone and side chain entanglements are observed in the BBCPs even with ultrahigh MWs, benefiting from the intrinsic cylindrical morphology with densely-grafted side chains [15]. Both these virtues promote the rapid self-assembly of the BBCPs into large ordered structures that strongly reflects in the visible spectrum without suffering from kinetic barriers during the reorganization.

Bowden and coworkers first demonstrated the fabrication of large domain sizes and ordered films that exhibited visible color using comb-like BCPs [430]. Thereafter, Grubbs and coworkers systematically investigated the effects of chemical structure, component, solvent quality, and processing conditions on the photonic properties of the assembled BBCPs [278,279,431–433]. They synthesized a set of PNB-based BBCPs bearing PS and PLA brushes with identical side chain lengths via the “grafting-through” approach (Fig. 46a) [431]. The peak wavelength of reflection is proportional to the M_n of the BBCP owing to an increase in the thickness. A broad range from visible light across ultraviolet (UV) to near-infrared (NIR) was readily achieved with increasing MWs (Fig. 46b). Therefore, the main chain and side chain lengths of the BBCPs have been used to manipulate the wavelength of the reflected light [230,283]. This was consistent with the redshift observed in the solvent-swollen BBCP films [430]. By employing different solvents for film casting, different reflection colors from blue (dichloromethane, DCM) to green (THF) were observed. THF shows good solubility for the BBPs and low volatility, which can afford larger and better ordered domains than those obtained with DCM (Figs. 46c–46g). Thermal annealing and direct hot pressing of the polymer powders under compression promoted the formation of well-ordered lamellae with long-wavelength reflection [431,434]. Moreover, the rigid-rod, helical polyisocyanate side chain was also

incorporated to facilitate the rapid self-assembly of the BBCPs with uniform lamellar structures, and these exhibited a controllable reflecting light with fast self-assembly [278]. Notably, the introduction of dendronized side chains significantly narrowed bandwidths of the PCs [432]. Recently, BBCPs bearing the crystalline polyhedral oligomeric silsesquioxane (POSS) moiety in one side chain were synthesized via the “grafting-through” approach. The POSS pendants in the BBCPs played a critical role in microphase separation. In addition, these promoted the formation of structural colors with extremely narrow bandwidths of high intensities [435].

Although BBCP has been extensively used to prepare the PCs, BBCPs with specific MWs are needed to reflect the target wavelengths of light. Similar to the linear BCPs, the blends of BBCPs with different MWs can adopt similar conforming morphologies with large domain sizes. Tuning of the weight fractions of two the BBCPs with high and low MWs facilitated the formation of uniform self-assembled domains that could reflect the light wavelengths ranging from the visible spectrum to NIR [279]. In addition, the peak reflection showed a linear relationship with the composition content. To manipulate the photonic bandgap in the telecommunication regime ($\lambda \approx 1200$ – 1650 nm), low-MW linear polymers were blended with the block BBCPs. The result was consistent with that of blending two different BBCPs because of the swelling of the lamellar periodicity. The linear polymers dispersed in the side-chain domain of the BBCPs with identical compositions and expanded the domain size [433]. Wavelengths of up to ~ 1410 nm were readily achieved by increasing the linear polymer amount. Additionally, the functional groups on linear polymers have been used to dynamically manipulate the optical properties of the BBCP films, [433] but the functional groups (hydrogen bonding) negatively affect the ability of the BBCPs to form ordered arrays [436]. Furthermore, inorganic nanoparticles (NPs) such as gold, ZrO_2 , and CdSe NPs have been introduced into the ordered domains of the BBCP films. The optical performances were tuned by regulating the loading [437–439] or refractive index contrast [437,440] of the NPs.

The film geometry has been extensively investigated to determine the photonic properties of the BBCPs in prior researches. Recently, the preparation of photonic pigment particles was achieved by the self-assembly of BBCPs in confined emulsion microdroplets using a flow-focusing microfluidic device [287,441]. In the monodisperse monochromatic microdroplets suspended in water, poly(vinyl alcohol) acted as the aqueous surfactant and BBCPs in chloroform as the droplets. The structural coloration was attributed to the formation of highly ordered concentric lamellae upon solvent evaporation [441]. Additionally, the bright colors of the individual microspheres showed a structural change from blue to red upon varying the backbone lengths of the BBCPs. The color reflection was further varied by changing the weight ratio between the two different BBCPs in the microdroplets [441]. Dendronized bottlebrush block copolymers (den-BBCPs) assembled into striped ellipsoids by the precise modulation of interfacial properties [287]. The highly ordered axially stacked lamellae within an ellipsoid afforded near-perfect PCs with reflection wavelength across the entire visible spectrum. Moreover, when Fe_3O_4 NPs were incorporated into the ellipsoid, these exhibited particle orientation-dependent photonic behavior [287]. To expand the industrial relevance of the PCs, a rapid, scalable, and highly customizable 3D printing technology was used to print complex BBCP PC patterns with tunable structural colors [442].

5.3.2. Organic electronic materials

To mimic the energy- and electron-transfer processes in the light-harvesting systems, chromophores were incorporated into cylinder-shaped BBPs [443,444]. Long-range exciton transport along the 1D objects played a critical role in light-harvesting and optoelectronic devices [445,446]. P3HT is among the most extensively used organic semiconducting polymers in the organic field-effect transistor (OFET) and organic photovoltaic devices [447–449]. The charge carrier mobility in OFET is highly dependent on the MW of linear P3HT [449]. Thelakkat and coworkers synthesized a BBP, PS-g-P3HT, with variable side chain lengths via the “grafting-to” approach [450]. BBPs with short side chain lengths exhibited an amorphous phase and poor electronic properties. Charge carrier mobility increased by five orders of magnitude with an increase in the side chain length because of the crystalline lamellar structure formations. Furthermore, conjugated side chains in the BBPs have also been used to manipulate the dielectric response [451].

To construct 1D nanoobjects with the structures of phosphorescent OLEDs on single macromolecules, Hudson and coworkers synthesized block BBCPs bearing organic semiconductor moieties. The segments in the BBCPs acted as emissive layer (EML), hole-transport layer (HTL), and electron-transport layer (ETL), which were typically observed in the OLEDs [265,452]. In addition, the BBCP bearing discrete p- and n-type semiconductor side chains was used to mimic the structure of the diode structures, and these could achieve ambipolar charge transport [265]. Thereafter, triblock BBCP was synthesized as an optoelectronic material with each block containing the representative materials used in the OLEDs: HTL, ETL, and a two-component EML (e.g., IrPPY) (Figs. 47a–47c). This material showed bright green phosphorescence and reversible reduction and oxidation. In addition, the matched energy levels of each block in the BBCP promoted the charge transport of donors (D) and acceptors (A) along a non-conjugated backbone to the central active block [265]. To further investigate charge transfer at the nanoscopic interface between the D and A segments in the BBCPs, i.e., through-space charge transfer (TSCT) effect, homopolymer BBP ACRTZ150-BB, miktoarm BBP ACR75-co-TRZ75-BB, and diblock BBCP ACR75-b-TRZ75-BB were synthesized (Fig. 20) [10]. Miktoarm BBP, ACR75-co-TRZ75-BB, showed fluorescent emission in both the monodispersed and powder states due to the blocking of TSCT. Conversely, ACRTZ150-BB and ACR75-b-TRZ75-BB exhib-

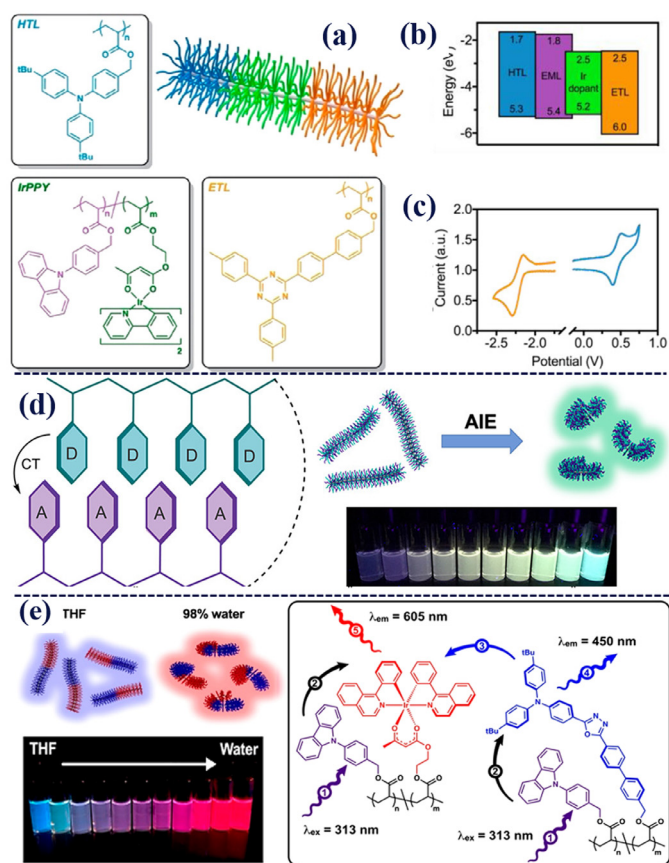


Fig. 47. (a) Schematic illustration, (b) energy level diagram and (c) cyclic voltammogram for triblock BBCPs. [265], Copyright 2018. (d) Aggregation-induced space charge transfer mechanism and corresponding fluorescence emission of miktoarm BBP ACR75-co-TRZ75-BB. [10], Copyright 2019. (e) Aggregation-induced energy transfer processes and fluorescence emission of diblock BBCP. [22], Copyright 2019. All adapted with permission from the American Chemical Society.

ited no fluorescence in solution and red-shifting fluorescent emission in the solid state because of the TSCT effect (Fig. 47e). Additionally, thermally activated delayed fluorescence was further enhanced by activating the TSCT effect induced by the aggregation of the nanofibers into a globular form in the solution [10,453].

Recently, multiple organic semiconductors have been introduced into the BBPs to tune the fluorescence resonance energy transfer (FRET) by varying the distance between the donor and acceptor segments via a variation of the chain length [50]. Thereafter, to regulate the energy transfer processes in the BBCP nanofibers, chromophores with red, green, and blue luminescence were incorporated into the discrete blocks along the BBCP backbones (Fig. 47e) [22]. In a good solvent, the BBCP solution exhibited a strong blue fluorescence. By increasing the nonsolvent in the system, BBCPs began to collapse, initiating the formation of small aggregates and the color change due to an increase in the FRET rate. Energy transfer among the intermolecular and intramolecular side chains was significantly enhanced during the self-assembly of the BBCP. The aggregation induced the fluorescence transition from blue to red in a solution, and this phenomenon was used for fluorescent sensing. Furthermore, the pentablock BBCP containing ETL, HTL, and red-, green-, and blue-emissive segments was prepared to mimic the white OLED device [22].

5.4. Energy storage

As previously mentioned, BBPs can act as templates to prepare organic 1D nanomaterials. The cross-linking of the outer shells

of the BBPs can enhance the cylindrical shape during the transfer process for characterization [454]. PAN is a widely used polymeric precursor for the preparation of carbon fibers and has been used as a nitrogen-doping source to increase electrocatalysis performances [455]. Recently, BBPs bearing PBA-*b*-PAN brushes were prepared by ATRP. Thereafter, porous nitrogen-doped carbon material was obtained after two-step carbonization at elevated temperature [456]. With an increase in the outer PAN lengths, the specific surface area gradually increased and accompanied by an increase in the mesopore size from 4.3 to 6.8 nm. Nitrogen-doped carbon materials have been extensively used for electrocatalysis such as oxygen reduction reaction (ORR) in alkaline and acid electrolytes [457]. The N-doped carbon exhibits excellent ORR performance with an onset over potential at 0.87 V via efficient 4e⁻ transfer process [456]. As discussed above, the BBPs can self-assemble into a spherical morphology and have been used to fabricate porous carbons with hierarchical pores generated through template degradation. The interconnectivity of the porous structure with enhanced SSA makes these promising candidates for supercapacitor applications. These exhibited excellent performances as supercapacitor electrodes with capacitances of up to 254 F/g [409]. The porous nanonetwork-structured carbons obtained via the carbonization of porous functional nanonetwork-structured polymers, demonstrated excellent electrochemical performances in lithium-sulfur batteries [24].

Recently, our research group synthesized a hydrophilic brush-like polymer, HPC-*g*-PAA, with hydroxypropyl cellulose (HPC) as the backbone via ATRP [458]. Then, the precursors were loaded on PAA blocks owing to the strong coordinative interaction of the acid groups [459]. The SnO₂ nanoparticles were formed in-situ after the hydrothermal reaction. As PAA compartments were discretely anchored along the cellulose backbone, the corn-on-the-cob nanostructures were obtained with loosely grafted BBPs. Thereafter, the polydopamine (PDA) layer was covered on the SnO₂ nanoparticles by a simple polymerization of dopamine, which could suppress the formation of solid-electrolyte interphase layer. PDA-coated SnO₂ in lithium-ion batteries afforded a better long-term stability and higher capacity in the entire cycle life.

Solid polymer electrolyte (SPE) has promising potential in replacing liquid electrolytes as it can suppress the growth of lithium dendrite [460]. Ideal polymer electrolytes should have a high fraction of heteroatoms (such as oxygen) to promote salt dissociation, and a low *T_g* to increase the segment mobility and ion transport [461]. PEO has been extensively studied because of its excellent ability to form complexes with alkali metal salts [462,463]. Notably, high-MW PEO increases the coordinated Li⁺ content and ionic conductivity. However, high MW increases the crystallinity, which has a negative effect on the conductivity [463,464]. During the breaking/forming of Li-O bonds in the Li-PEO complex, the transportation of Li⁺ occurs in intrachain and/or interchain hopping [462]. Interchain hopping is difficult to achieve because of the severe entanglement of long PEO chains. The BBPs can attain high MWs without entanglement, which afford high ion conductivity due to the facilitation of intrachain Li⁺ hopping. Short PEO side chains can afford high Li⁺ mobility as the avoidance of the center-of-mass motion can be prevented [463]. Recently, BBPs grafted with PEO side chains were synthesized and coordinated to the lithium salt to fabricate polymer electrolytes [464-467]. BBP-based polymer electrolytes displayed excellent ionic conductivities and higher thermal stabilities. However, PEO crystallinity remained an issue in these polymer electrolytes. Recently, well-defined BBPs bearing densely-grafted PEO side chains were synthesized via the ATRP of PEGMA. After hydrolysis with TFA, the exposed acid groups anchored on the backbone reacted with Li⁺ to yield brush polymer electrolytes with single-ion structures (Fig. 48a) [23]. In addition, this single-ion polymer electrolyte could prevent the se-

vere concentration polarization and capacity loss arising from the accumulation of anions. Therefore, the acid groups anchored on the BBP backbone promoted the transport of Li⁺ and improved the Li⁺-ion transference number. The resulting SPE displayed high potential for application in lithium-ion batteries with high capacities and excellent cycle performances (Figs. 48b and 48c).

5.5. Other applications

5.5.1. Biomedical applications

Various micelles of different sizes have been obtained during the self-assembly of the BBPs. In addition, the sizes of the spherical micelles are larger than those of their linear amphiphilic analogs, and functionalities can be anchored on the side chains. BBPs have been extensively used in the biological fields (e.g., drug delivery, fluorescence imaging, and biodetection). Recently, acid activatable supramolecular nanodrugs (DOM@DOX) based on the polysaccharide-containing BBPs were prepared through a two-step polymerization (Fig. 49) [347]. BBP contained diblock copolymer side chain, in which the hydrophobic anticancer drug doxorubicin (DOX) was conjugated with the hydrazine bonds. The hydrophilic POEGMA block in combination with hydrophilic dextran endowed the BBPs with amphipathicity, resulting in self-assembly in aqueous solution. In addition, BBPs-based micelles provided steric shielding for the loaded drugs because of the densely-grafted side chains. Furthermore, the shielding POEGMA layer enhanced the solubility and stability of prodrugs in blood. The DOM@DOX micelles were then entered into the cells via the enhanced permeability and retention (EPR) effect. In the acidic tumor cells, the nanodrugs are released from the brush-based spherical micelles due to the pH-sensitive decomposition of hydrazine bonds in the acidic endo/lysosomal microenvironment (Fig. 49). The DOM@DOX prodrug exhibited excellent intratumoral permeability and significant tumor suppression efficiency.

The cylindrical nanostructures exhibited longer residence times in the body than those of the spherical micelles of equivalent MWs [468]. The polymer chains adopted random-coil conformations that rendered bioactive moieties inaccessible toward the biologically active sites. The effect of shape anisotropy on drug delivery capability was recently explored using BBPs with different topologies, which were easily obtained by varying the backbone lengths of the BBPs with identical side chains [469]. Rod-like micelles exhibited preferential association and penetration into the multicellular tumor spheroids. Thus, the performance of the drug carrier systems was readily manipulated by controlling the structural parameters [469]. Core-shell worm-like BBPs with carriers loaded into their cores through hydrophobic interactions were employed for drug delivery [470,471]. Moreover, the BBPs were used for magnetic resonance imaging (MRI) and fluorescence imaging, [361,472] as well as electrochemiluminescence detection of proteins with high sensitivity [211,473]. Notably, paramagnetic nitroxides have been extensively explored as "organic radical contrast agents" (ORCAs) for MRI due to their minimal toxicity and diamagnetic property induced by physiological reducing agents [474]. However, they suffer from low relaxivity and fast reduction. BBP-based ORCAs could overcome these limitations because they have dense side chains that could carry multiple nitroxides and impede the diffusion of reductant to the reactive sites. For instance, redox-responsive branched-bottlebrush copolymer NPs (ORCAFluors) were synthesized via ROMP of NB-terminated branched macromonomers bearing reduction-resistant spirocyclohexyl nitroxide and Cy5.5. These materials showed enhanced MRI and NIR fluorophore for optical imaging [361]. Furthermore, DNA can be readily grafted onto BBPs via click reactions under mild conditions. The dense array of DNA on BBPs could prevent the dissociation of the intercalating dyes. Nonetheless, the DNA duplex bristles on the BBP simultaneously

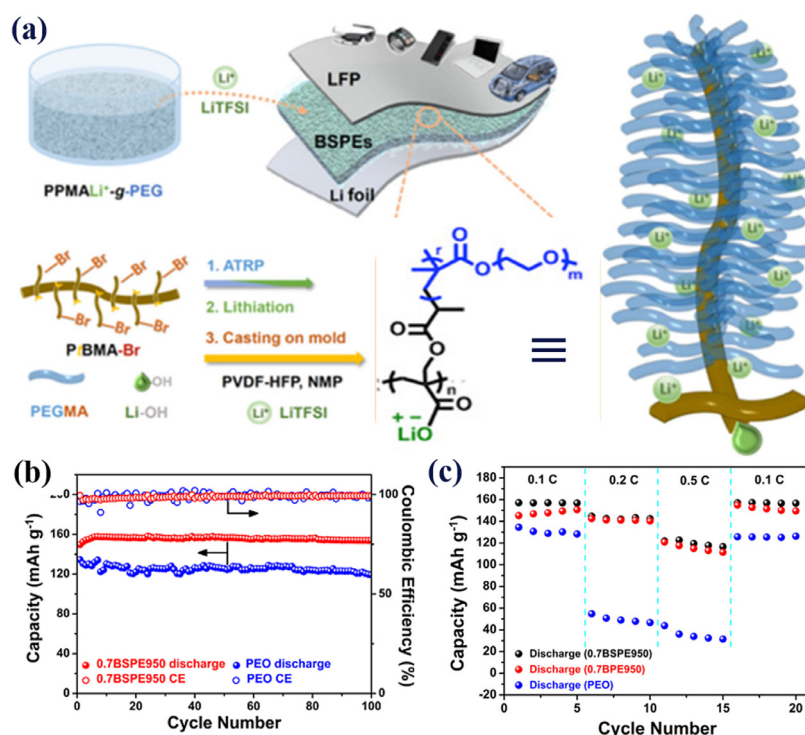


Fig. 48. (a) Schematic illustration of brush polymer electrolyte. (b) Cycle performances and (c) specific capacities at varied current density for brush polymer electrolyte-based cells. [23], Copyright 2019. Adapted with permission from the American Chemical Society.

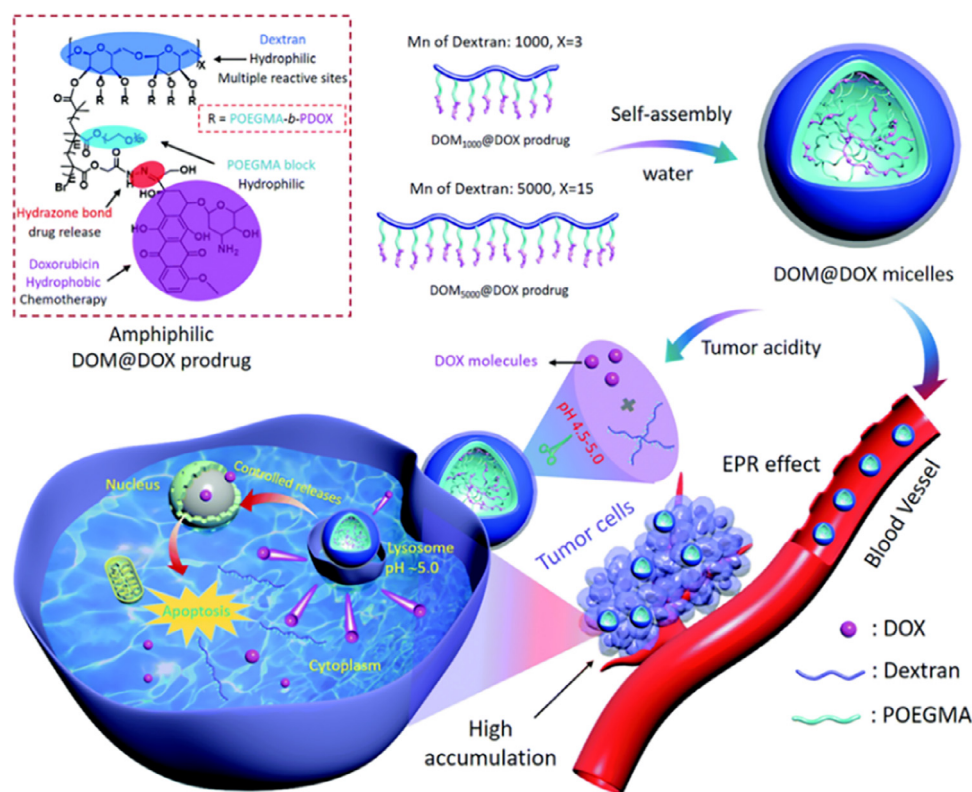


Fig. 49. Schematic illustration of the synthetic route of DOM@DOX micelles, drug accumulation via the EPR effect, cell internalization process, and pH-responsive drug release mechanism. [347], Copyright 2020. Reproduced with permission from the Royal Society of Chemistry.

maintained their intrinsic ability to undergo strand hybridization and enzymatic degradation owing to the stretched side chain conformations [122,212].

5.5.2. Surfactants

Macromolecules bearing both hydrophilic and hydrophobic parts resemble small molecular surfactants and are generally known as polymeric surfactants [475]. Amphiphilic double-brush diblock and symmetrical triblock copolymers containing hydrophilic PEO and hydrophobic PS side chains have been used as “giant surfactants” [475]. Janus BBPs bearing a hydrophilic PEO branch and hydrophobic PLA or PS branch on each repeating unit could stabilize the biphasic emulsion droplet [185,476]. This was because numerous amphiphilic segments were covalently bonded together to form a robust individual macromolecular surfactant that withstood high interfacial tension. When it was added into a water-oil (W/O) system, the resulting miniemulsions exhibited remarkably enhanced stability [185]. The surfactants on the miniemulsion surfaces were further used for crosslinking or polymerization [158,476]. Recently, it was reported that random BBPs containing hydrophilic PEO and hydrophobic PBA grafts with controlled dimensions could serve as surfactants to stabilize the emulsions at extremely low concentrations (0.005 wt %) [477]. Furthermore, the heterografted BBP surfactants showed enhanced adsorption on the interfaces and higher emulsifying efficiency compared to those of the diblock analogs [477].

5.5.3. Antifouling

Healthcare-associated infection is a major public health issue. This situation is more severe in 2020 because of the worldwide outbreak of coronavirus disease (COVID-19). The COVID-19 is caused by severe acute respiratory syndrome coronavirus 2 (SARS-CoV-2) and affects the immune system of the body [478]. In addition, the virus is stable for several hours to days in aerosols and on surfaces such as plastic, stainless steel, and cardboard [478]. Therefore, it is urgent to prevent nonspecific microorganism adsorption on surfaces. Protein-repelling polymers such as PEG, polysarcosine, and zwitterionic polymers have been extensively used to decrease bacterial adhesion owing to their excellent antifouling properties [479]. BBPs bearing poly(2-oxazoline) [480] and antimicrobial peptide [479,481] side chains have been anchored on different substrates with excellent antimicrobial activities. However, the BBPs are covalently grafted onto the surfaces with their backbones, which limit the antifouling events due to the limited loading of the BBPs. Spin-coating an amphiphilic polymer film onto a substrate is the most convenient and scalable strategy to enhance the antifouling efficiency of the surface. Amphiphilic BBPs can increase the biofouling efficiency, because the hydrophilic side chains prevent the proteins from penetrating the substrate surface and the hydrophobic side chains show low interfacial energy with proteins and excellent fouling release properties [482]. Furthermore, the side chains were densely grafted onto the backbone, which assisted in resisting the protein adsorption. Janus-like asymmetric BBPs bearing PS and PEO side chains with low protein adsorption and excellent HaCaT cell inhibition were prepared, and BBPs with long PEO and short PS side chains showed better antifouling properties [482]. Fluorinated polymers have low surface energies and have been incorporated into the BBPs to replace the hydrophobic PS side chains via a facile one-pot strategy [110,483–485]. The fluorinated Janus BBP film showed significantly better antifouling properties in comparison to those of the non-fluoropolymers. Additionally, consistent with the prior report, long PEO side chains afforded enhanced antifouling property [484]. Notably, the introduction of organic cations into the side chains endowed the BBP films with antimicrobial properties [481,486–488]. Inspired by lubricin (LUB), linear-brush-linear BBCPs bearing quaternized PDMAEMA

coil blocks and polyzwitterionic branches were prepared [488]. The charged coil blocks were used to increase the adsorption and stability via electrostatic interactions, while the neutral middle brush improved their antiadhesive properties and biocompatibility. The LUB-inspired BBPs exhibited superior antifouling properties and slow adsorption rates for proteins and bacteria [488].

6. Conclusion and outlook

Bottlebrush polymers are an appealing class of polymers with nonlinear architectures. They are high-MW polymers because of the densely-grafted branches along the linear backbone. With the development of advanced polymerization techniques, researchers have synthesized cylindrical BBPs with diverse sub-architectures (e.g., block, random, double-brush, Janus, core-shell, brush-linear, linear-brush-linear, and brush-on-brush BBPs) using different strategies (i.e., grafting-from, grafting-through, and grafting-to methods). Such unique architectures render the BBPs to adopt extended cylindrical shape due to the steric repulsions among the adjacent densely-grafted branches. The steric repulsion also imparts a peculiar nonoverlapping characteristic of the side chains, thus governing the viscoelastic properties and alignment of BBPs in both the solution and bulk states. By manipulating the chemical structures, compositions, and solvent quality, the resulting BBPs can self-assemble into diverse hierarchical architectures (i.e., spherical, worm- or rod-like, lamellar structure, etc.) with rapid self-assembly behaviors, particularly, in the bulk state. In addition, the BBPs exhibit high crystal nucleation but retarded crystal growth ability due to the external backbone constraint. Furthermore, BBPs demonstrate excellent rheological and mechanical performances with low shear moduli because of the absence of entanglements. The ability to tune self-assembled structures and length scales over a wide range while maintaining their excellent melt processability affords BBPs with an array of applications, including as supersoft elastomers, organic optoelectronic materials, templates for preparing 1D nanomaterials, and energy storage and biomedical materials. It is also notable that the conformation of BBPs can be readily tailored by tuning the backbone and side chain lengths, grafting density, and the number of side chains per repeating unit. Furthermore, smart materials triggered by external stimuli (e.g. temperature, light, pH, etc.) have been achieved by introducing stimuli-responsive moieties in the backbones or side chains.

Despite many effective strategies (particularly CRPs and ROMP methods) have been extensively developed to synthesize BBPs of interest, some challenges remain in the synthesis of BBPs with completely controlled architectures. Accomplishing these objectives can afford state-of-the-art BBP-based materials with hierarchical structures.

- (a) **Controllability of grafting density in BBPs.** “Grafting-from” and “grafting-to” approaches afford limited control over the grafting density due to the steric hindrance from the densely-grafted side chains. Some strategies have been exploited to increase the grafting densities (its value is the same as initiation efficiency in the “grafting-from” approach) of the BBPs, which are listed as follows. The first strategy includes an increase in the concentration of Cu^{II}X or a decrease in the monomer concentration during ATRP in the “grafting-from” approach. Second, the addition of CTA-shuttles (i.e., free CTAs) to tune the radical concentration in the RAFT polymerization with the “grafting-from” approach. Third, grafting alkynyl-terminated side chain with multi brushes (e.g., dendrons) and performing several grafting reactions in the “grafting-to” approach. Fourth, employing brush-on-brush BBPs with densely-grafted side chains that introduce secondary conformations. However, achieving

100% grafting density for all types of polymeric side chains remains challenging, leading to loosely packed conformations that may affect the rheological and mechanical properties of the BBPs. A preferred method to increase the grafting density is increasing the spacing among the adjacent side chains with suitable backbone repeating unit length.

- (b) **Preparation of BBPs with long backbones via the “grafting-through” method.** The backbone length of a BBP plays a critical role in forming a cylindrical shape. It is challenging to prepare BBPs with long backbones via the “grafting-through” approach because of severe steric hindrance around the propagating sites. To obtain backbones via the “grafting-through” approach, introducing long and flexible spacers between the side chains and polymerizable end groups or using highly active catalysts are the preferred strategies. In addition, applying high pressure can increase the propagation rate coefficient and ATRP equilibrium constant, which increases the backbone length. Furthermore, by increasing the solubilities of the macromonomers and BBPs, forming micelles for macromonomers, and using macromonomer pairs with electron-donating (vinyl benzyl-based macromonomers) and electron-accepting polymerizable end-groups, the backbone length can be increased by enhancing the local propagation ability. It is necessary to develop a universal methodology to prepare BBPs with high DP via the “grafting-through” approach.
- (c) **Simplicity of the synthetic method.** Most previous strategies involve tedious multistep synthesis (e.g., purifying intermediate macromonomers and macroinitiators) and/or post-processing of metal catalysts with chromatographic column. Newly emerging strategies that are simple as well as time- and cost-effective should be widely employed in the BBPs synthesis in the future. Potential methods include (i) photo-mediated RAFT polymerizations, (ii) electrochemically-mediated CRP, (iii) enzyme-catalyzed polymerization or click reactions, and (IV) programmable flow chemistry methodologies. These emerging reactions can be implemented under mild conditions with ppm-level catalysts (e.g., electrochemically-mediated CRP) or without any catalyst (e.g., photo-mediated RAFT polymerization). In addition, enzyme catalysts are biocompatible and easy to be removed by filtration after polymerization. Furthermore, photo-mediated RAFT polymerization and programmable flow reaction have been applied to synthesize BBPs with well-controlled structures in one pot without separation processes of intermediates. The fourth methodology is a scalable synthetic strategy to manipulate polymer synthesis via a computer-controlled flow reactor system without involving any tedious separation process. This method is also superior for preparing new materials in both academia and industry because it can allow the control of the polymer architecture (e.g., shape and size controlled by the sequence of macromonomers) and is compatible with various chemistries.
- (d) **Preparation of BBPs with aerobic radical polymerization.** Current advanced polymerization techniques (e.g., CRPs and living anionic/cationic polymerization) for preparing BBPs require strict anoxic and thermal conditions prior to initiation because of the oxygen sensitivity of the living end groups. External purging steps (e.g., bubbling with N₂ or degassing via freeze-pump-thaw cycle) are needed for deoxygenation before polymerization. This significantly limits their widespread implementation on large scales. Therefore, it is highly desirable to develop a versatile technique for the preparation of BBPs with high oxygen tolerance. Recently, oxidation using glucose oxidase (GOx) [489] and microbial

metabolism [490] have been applied in ATRP and/or RAFT polymerization to rapidly deplete the dissolved oxygen for preparing linear polymers at room temperature. These in-situ oxygen scrubbing techniques can also be used to prepare BBPs and address deoxygenation issues in the BBP synthesis. Such a breakthrough can expand the implementation of BBPs to other fields, and render the development of microbial metabolism-mediated radical polymerization.

- (e) **Metal-free synthesis of BBPs.** Most of the current techniques for synthesizing BBPs necessitate the use of metal catalysts to promote the reaction. The metal contamination of the polymers hinders their application in bio-related areas and optoelectronic devices. Therefore, metal-free CRPs and click reactions are highly desirable to synthesize BBPs with controlled architectures and MWs. This can eliminate metal contamination in the traditional systems and expand the applications of BBPs in biomedical fields.
- (f) **Sustainable BBPs.** The most widely studied BBPs are based on the PNB or polyacrylate backbone obtained from petrochemical resources. The backbone containing the C-C covalent bond is difficult to degrade under natural conditions. In addition, the usage of petrochemical resources increases carbon emissions and deteriorates the petroleum crisis. From the standpoint of a sustainable economy, biodegradable and biocompatible polypeptide-, PLA-, and cellulose-based BBPs should be developed to expand the diversity of the properties of BBPs.

The structure-property relationship of the BBPs has been summarized to guide the molecular design for various applications. Highly tunable properties and widespread applications of BBPs with different sub-architectures should be explored in the following emerging areas.

- (i) **Nanoreactor-directed fabrication of nanomaterials with other 1D morphologies and functionalities.** Inspired by the nanoreactor functionality and diverse architectures of the BBPs, different inorganic compositions should be introduced into one molecular brush. Suitable Janus BBPs or diblock BBPs can provide two different compartmentalized domains on the opposite sides or opposite directions (backbone parts) of the backbone, respectively [491]. Such an asymmetric architecture can be used to sequentially grow two different compositions within one structure, for example, one composition for the hydrogen evolution reaction and the other composition for the oxygen evolution reaction. Thus, 1D hybrid nanomaterial as an electrocatalyst for the overall water splitting can be achieved within one material [492]. In addition, stimuli-responsive inorganic nanomaterials can be readily prepared using BBP templates that bear responsive-polymer chains on their outer blocks and the properties of the obtained nanomaterials can be tuned by environmental triggers (e.g., temperature, pH, light, etc.). Furthermore, the surfaces of the 1D nanomaterials are permanently ligated by polymer chains, which can direct the formation of the colloidal assembly into monolayers with superlattice structures on the solution surfaces. Notably, cylindrical micelles have been used as sacrificial templates for the preparation of mesoporous 2D conducting polymer monolayer nanosheets, where the micelles are prepared using linear BCPs [493]. However, the micelle size is difficult to control. BBPs have intrinsic cylindrical shapes that allow these to be readily assembled on the nanosheet surfaces and used as sacrificial templates for preparing mesoporous 2D conductive polymer nanosheets or mesoporous 2D carbon nanosheets. Chiral functional materials, particularly, the chiral perovskite materials with optoelectronic performances,

have emerged as promising materials for high-performance optoelectronic devices [494]. When chiral BBPs (such as chiral polypeptide-based BBPs) act as templates, hybrid chiral perovskite nanocrystals can be readily obtained via a facile and rapid coprecipitation reaction. The hairy polymer chains on the perovskite nanocrystal surface can enhance its stability to moisture and light [380].

(ii) **Self-assembly of BBCPs in confined geometries.** A confined geometry affords good controllability for the self-assembly of polymers with well-ordered structures. Self-assembly of BBCPs in confined emulsified microdroplets can result in concentric lamellae PCs, yet the self-assembly of BBPs in other confined geometries has not been investigated. The self-assembly of brush-linear BBPs confined in a cylinder-on-flat or wedge-on-flat geometry with CESA resulted in the formation of lamellar nanodomains within the thin stripes [292,293]. However, the size of the nanodomain in the stripe was < 100 nm. When thick stripes were prepared with concentrated BBCP solution, a lamellar structure with a domain size > 100 nm was formed within the stripes and colorful reflected light could be observed in the stripes [495]. Meniscus-assisted self-assembly (MASA) is another confined geometry that can be used to tune the self-assembly of the BBPs. The MASA approach is implemented by constraining the evaporation of the polymer solution between two almost parallel plates. The upper blade is fixed, while the lower movable substrate is controlled by a computer program in the stop-and-move mode motion [326,496,497]. Thick stripes will show different colors when their domain sizes (> 100 nm) are altered. When printing the stripes in different directions for the multilayers, the patterns with structural color will be achieved via the MASA approach with the BBCPs, which is similar to the recently reported 3D printing PCs [442].

(iii) **Quantification of the rheological properties of BBPs.** BBPs have distinct rheological properties compared to those of the linear polymers. The equations used to quantify their rheological properties vary based on different models (such as the dependency of plateau modulus on the MWs of the BBPs). The quantification of the effects of chemical composition and structure parameters on the conformation as well as rheological and mechanical performances of BBPs using common methods such as the scaling analysis of relaxation times remains challenging. It is highly desirable to develop a universal model to quantify the rheological properties based on the experimental data obtained from the BBPs prepared via the “grafting-through” approach. In addition, most of the rheological studies are based on the polyacrylate-based BBPs, while polyolefin materials are commercially viable and used in society. Therefore, quantifying the rheological properties of polyolefin-based bottlebrush polymeric materials can be beneficial in diverse applications such as self-healing wearable devices.

(iv) **Energy and electron transport in 1D nanomaterials.** Previous studies on the charge or electron transfer are based on the BBPs with worm-like or star-like (short backbone length) morphologies. Long-range energy and electron transport along with the rigid 1D or all conjugated BBPs (both backbone and side chains are conjugated) can be examined using precisely designed BBPs. Understanding the mechanism of energy and charge transport in the BBPs can be beneficial for the rational design of BBPs with desirable optical and electronic properties. In addition, the BBP-based polymer electrolytes described in prior studies have short backbones because of the intrinsic steric effects of the iminers. Therefore, additional studies are needed to scrutinize the

transport of Li⁺ ions in BBP-based polymer electrolytes with long backbone.

(v) **Other potential applications of Janus BBPs.** To date, Janus BBPs have only been used in a limited number of applications (e.g. surfactants and coatings); however, as most of the coatings are physically adsorbed on the substrates, the coating layer is not stable and easily rinsed away, which severely limits their potential applications. Therefore, additional potential applications of Janus BBPs remain to be explored. Janus BBPs possess two different properties (e.g., hydrophilicity/hydrophobicity and positive/negative charges) in one object. For example, silsesquioxane precursors incorporated in one side block of the Janus BBPs can be covalently grafted onto the substrates. The other block can be judiciously selected to provide the desired functionality. For instance, pH-, thermal-, light-, or salt-responsive polymeric brushes can be transferred from hydrophobic into hydrophilic coating under external triggers. When fluorinated polymers are located on the opposite side, anti-fog and oil-repellent coating can be achieved, while the incorporation of positive charges in the opposite side chains can afford antifouling and antibacterial properties. In addition, Janus membranes have been used as an emerging class of materials for oil/water separation, and have been fabricated by the sequential casting of two composites, followed by the cross-linking of the two layers or asymmetric decoration of the surfaces; however, these two methods are tedious [498]. Cross-linked Janus BBPs with hydrophilicity/hydrophobicity or positive/negative charges on the opposite side chains can be readily utilized to construct a Janus membrane due to the phase separation among the opposite side chains. Furthermore, Janus BBPs bearing immiscible side chains can serve as compatibilizers to bind the immiscible phases in the polymer composites and enhance the performances of the blends. This strategy of using Janus BBP as a binder can be extended to other multiphase devices/mixtures such as solar cells, LEDs, and OFET. Janus BBPs bearing PDMS side chains can serve as excellent matrices for fabricating thermal and electrical conducting materials because of their excellent resistance against air and moisture arising from the densely-grafted side chains.

The recent advances in BBPs in terms of their controlled synthesis, self-assembly, and beneficial properties for various applications have been highlighted in this review. Despite the remaining challenges, BBPs are unique nonlinear polymers that have been widely studied and exhibit many remarkable properties that are different from those of the other polymers. As BBPs are in their initial stages of development, these are expected to have untapped potential applications and opportunities considering their diverse sub-architectures.

Declaration of Competing Interest

The authors declare that they have no known competing financial interests or personal relationships that could have appeared to influence the work reported in this paper.

Acknowledgements

This work is supported by the AFOSR (FA9550-19-1-0317), the NSF (DMR1903990, and Chemistry 1903957) and the National Natural Science Foundation of China (Grant No: 21922503).

References

- [1] Sheiko SS, Sumerlin BS, Matyjaszewski K. Cylindrical molecular brushes: Synthesis, characterization, and properties. *Prog Polym Sci* 2008;33:759–85.

- [2] Sharma A, Pande P. Recent advancement in comb-like polymers: a review. *J Polym Mater* 2019;36:175–94.
- [3] Xu B, Feng C, Huang X. A versatile platform for precise synthesis of asymmetric molecular brush in one shot. *Nat Commun* 2017;8:333.
- [4] Lazzari M, Scalapone D, Vazquez-Vazquez C, López-Quintela MA. Cylindrical micelles from the self-assembly of polyacrylonitrile-based diblock copolymers in nonpolar selective solvents. *Macromol Rapid Commun* 2008;29:352–7.
- [5] Hsiao M-S, Yusoff SFM, Winnik MA, Manners I. Crystallization-driven self-assembly of block copolymers with a short crystallizable core-forming segment: controlling micelle morphology through the influence of molar mass and solvent selectivity. *Macromolecules* 2014;47:2361–72.
- [6] Ganda S, Stenzel MH. Concepts, fabrication methods and applications of living crystallization-driven self-assembly of block copolymers. *Prog Polym Sci* 2019;101:101195.
- [7] Foster JC, Varlas S, Couturaud B, Coe Z, O'Reilly RK. Getting into shape: reflections on a new generation of cylindrical nanostructures' self-assembly using polymer building blocks. *J Am Chem Soc* 2019;141:2742–53.
- [8] Liang H, Cao Z, Wang Z, Sheiko SS, Dobrynin AV. Combs and bottlebrushes in a melt. *Macromolecules* 2017;50:3430–7.
- [9] López-Barrón CR, Brant P, Eberle AP, Crowther DJ. Linear rheology and structure of molecular bottlebrushes with short side chains. *J Rheol* 2015;59:865–83.
- [10] Tonge CM, Hudson ZM. Interface-dependent aggregation-induced delayed fluorescence in bottlebrush polymer nanofibers. *J Am Chem Soc* 2019;141:13970–6.
- [11] Palacios-Hernandez T, Luo H, Garcia EA, Pacheco LA, Herrera-Alonso M. Nanoparticles from amphiphilic heterografted macromolecular brushes with short backbones. *Macromolecules* 2018;51:2831–7.
- [12] Pang X, He Y, Jung J, Lin Z. 1D nanocrystals with precisely controlled dimensions, compositions, and architectures. *Science* 2016;353:1268–72.
- [13] Börner HG, Beers K, Matyjaszewski K, Sheiko SS, Möller M. Synthesis of molecular brushes with block copolymer side chains using atom transfer radical polymerization. *Macromolecules* 2001;34:4375–83.
- [14] Shi Y, Zhu W, Yao D, Long M, Peng B, Zhang K, et al. Disk-like micelles with a highly ordered pattern from molecular bottlebrushes. *ACS Macro Lett* 2014;3:70–3.
- [15] Liberman-Martin AL, Chu CK, Grubbs RH. Application of bottlebrush block copolymers as photonic crystals. *Macromol Rapid Commun* 2017;38:1700058.
- [16] Neiser MW, Muth S, Kolb U, Harris JR, Okuda J, Schmidt M. Micelle formation from amphiphilic "cylindrical brush"-coil block copolymers prepared by metallocene catalysis. *Angew Chem Int Ed* 2004;43:3192–5.
- [17] Stals PJ, Li Y, Burdzyńska J, Nicolaÿ R, Nese A, Palmans AR, et al. How far can we push polymer architectures? *J Am Chem Soc* 2013;135:11421–4.
- [18] Huang K, Rzaevyev J. Charge and size selective molecular transport by amphiphilic organic nanotubes. *J Am Chem Soc* 2011;133:16726–9.
- [19] Pietrasik J, Budzalek K, Zhang Y, Halagan K, Kozanecki M. Macromolecular templates for synthesis of inorganic nanoparticles. *Reversible Deactivation Radical Polymerization: Materials and Applications*. ACS Publications; 2018. p. 169–200.
- [20] Müllner M, Müller AH. Cylindrical polymer brushes—anisotropic building blocks, unimolecular templates and particulate nanocarriers. *Polymer* 2016;98:389–401.
- [21] Abbasi M, Faust L, Wilhelm M. Comb and Bottlebrush Polymers with Superior Rheological and Mechanical Properties. *Adv Mater* 2019;31:1806484.
- [22] Sauv   ER, Tonge CM, Hudson ZM. Aggregation-induced energy transfer in color-tunable multiblock bottlebrush nanofibers. *J Am Chem Soc* 2019;141:16422–31.
- [23] Li S, Jiang K, Wang J, Zuo C, Jo YH, He D, et al. Molecular brush with dense PEG side chains: design of a well-defined polymer electrolyte for lithium-ion batteries. *Macromolecules* 2019;52:7234–43.
- [24] Lin X, Xie G, Liu S, Martinez MR, Wang Z, Lou H, et al. Fabrication of porous nanonetwork-structured carbons from well-defined cylindrical molecular bottlebrushes. *ACS Appl Mater Interfaces* 2019;11:18763–9.
- [25] Ilgach D, Meleshko T, Yakimansky A. Methods of controlled radical polymerization for the synthesis of polymer brushes. *Polym Sci Ser C* 2015;57:3–19.
- [26] Matyjaszewski K. Advanced materials by atom transfer radical polymerization. *Adv Mater* 2018;30:1706441.
- [27] Feuz L, Leermakers FA, Textor M, Borisov O. Bending rigidity and induced persistence length of molecular bottle brushes: A self-consistent-field theory. *Macromolecules* 2005;38:8891–901.
- [28] Cho HY, Kryz P, Szcze  niak K, Schroeder H, Park S, Jurga S, et al. Synthesis of poly(OEOMA) using macromonomers via "grafting-through" ATRP. *Macromolecules* 2015;48:6385–95.
- [29] Lecommandoux S, Ch  cot F, Borsali R, Schappacher M, Deffieux A, Br  let A, et al. Effect of dense grafting on the backbone conformation of bottlebrush polymers: Determination of the persistence length in solution. *Macromolecules* 2002;35:8878–81.
- [30] Juhari A, Mosn   ek J, Yoon JA, Nese A, Koynov K, Kowalewski T, et al. Star-like poly(n-butyl acrylate)-b-poly( -methylene- -butyrolactone) block copolymers for high temperature thermoplastic elastomers applications. *Polymer* 2010;51:4806–13.
- [31] Yagci Y, Tasdelen MA. Mechanistic transformations involving living and controlled/living polymerization methods. *Prog Polym Sci* 2006;31:1133–70.
- [32] Aoshima S, Kanaoka S. A renaissance in living cationic polymerization. *Chem Rev* 2009;109:5245–87.
- [33] Dechy-Cabaret O, Martin-Vaca B, Bourissou D. Controlled ring-opening polymerization of lactide and glycolide. *Chem Rev* 2004;104:6147–76.
- [34] Choinopoulos I. Grubbs' and schrock's catalysts, ring opening metathesis polymerization and molecular brushes—synthesis, characterization, properties and applications. *Polymers* 2019;11:298.
- [35] Nair DP, Podgorski M, Chatani S, Gong T, Xi W, Fenoli CR, et al. The thiol-Michael addition click reaction: a powerful and widely used tool in materials chemistry. *Chem Mater* 2014;26:724–44.
- [36] Uhrig D, Mays JW. Synthesis of combs, centipedes, and barbwires: poly(isoprene-graft-styrene) regular multigraft copolymers with trifunctional, tetrafunctional, and hexafunctional branch points. *Macromolecules* 2002;35:7182–90.
- [37] Li Z, Tang M, Dai J, Wang T, Wang Z, Bai W, et al. Preparation of covalent pseudo-two-dimensional polymers in water by free radical polymerization. *Macromolecules* 2017;50:4292–9.
- [38] Tsukahara Y, Mizuno K, Segawa A, Yamashita Y. Study on the radical polymerization behavior of macromonomers. *Macromolecules* 1989;22:1546–52.
- [39] Matyjaszewski K. Atom transfer radical polymerization (ATRP): current status and future perspectives. *Macromolecules* 2012;45:4015–39.
- [40] Keddie DJ. A guide to the synthesis of block copolymers using reversible-addition fragmentation chain transfer (RAFT) polymerization. *Chem Soc Rev* 2014;43:496–505.
- [41] Foster JC, Radzinski SC, Matson JB. Graft polymer synthesis by RAFT transfer-to. *J Polym Sci, Part A: Polym Chem* 2017;55:2865–76.
- [42] Nicolas J, Guillauneuf Y, Lefay C, Bertin D, Giges D, Charleux B. Nitroxide-mediated polymerization. *Prog Polym Sci* 2013;38:63–235.
- [43] Hirao A, Goseki R, Ishizone T. Advances in living anionic polymerization: from functional monomers, polymerization systems, to macromolecular architectures. *Macromolecules* 2014;47:1883–905.
- [44] Zhang S, Tezuka Y, Zhang Z, Li N, Zhang W, Zhu X. Recent advances in the construction of cyclic grafted polymers and their potential applications. *Polym Chem* 2018;9:677–86.
- [45] Kolb HC, Finn M, Sharpless KB. Click chemistry: diverse chemical function from a few good reactions. *Angew Chem Int Ed* 2001;40:2004–21.
- [46] Tiwari VK, Mishra BB, Mishra KB, Mishra N, Singh AS, Chen X. Cu-catalyzed click reaction in carbohydrate chemistry. *Chem Rev* 2016;116:3086–240.
- [47] Li Z, Tang M, Dai J, Wang T, Bai R. Effect of multiwalled carbon nanotube-grafted polymer brushes on the mechanical and swelling properties of polyacrylamide composite hydrogels. *Polymer* 2016;85:67–76.
- [48] Li Z, Tang M, Bai W, Bai R. Preparation of hydrophilic encapsulated carbon nanotubes with polymer brushes and its application in composite hydrogels. *Langmuir* 2017;33:6092–101.
- [49] Cheng G, B  ker A, Zhang M, Krausch G, M  ller AH. Amphiphilic cylindrical core-shell brushes via a "grafting from" process using ATRP. *Macromolecules* 2001;34:6883–8.
- [50] Ling J, Zheng Z, K  hler A, M  ller AH. Rod-Like Nano-Light Harvester. *Macromol Rapid Commun* 2014;35:52–5.
- [51] Nese A, Kwak Y, Nicolay R, Barrett M, Sheiko SS, Matyjaszewski K. Synthesis of poly(vinyl acetate) molecular brushes by a combination of atom transfer radical polymerization (ATRP) and reversible addition–fragmentation chain transfer (RAFT) polymerization. *Macromolecules* 2010;43:4016–19.
- [52] Fan X, Wang G, Zhang Z, Huang J. Synthesis and characterization of amphiphilic heterograft copolymers with PAA and PS side chains via "grafting from" approach. *J Polym Sci, Part A: Polym Chem* 2011;49:4146–53.
- [53] Lederle F, H  bner EG. Radical polymerization of styrene in presence of poly(2, 2, 6, 6-tetramethylpiperidine-N-oxyl-4-yl methacrylate)-formation of polymer brushes. *Polymer* 2017;111:258–64.
- [54] Vivek A, Dhamodharan R. Grafting of methacrylates and styrene on to polystyrene backbone via a "grafting from" ATRP process at ambient temperature. *J Polym Sci, Part A: Polym Chem* 2007;45:3818–32.
- [55] Tong M, An X, Pan W, Liu H, Zhao Y. Synthesis and properties of stimuli-sensitive heterografted toothbrush-like terpolymers with a linear handle and two types of V-shaped grafts. *Polym Chem* 2016;7:2209–21.
- [56] Zheng Z, Ling J, M  ller AH. Revival of the R-group approach: a "CTA-shuttled" grafting from approach for well-defined cylindrical polymer brushes via RAFT polymerization. *Macromol Rapid Commun* 2014;35:234–41.
- [57] Wei Z, Zhu S, Zhao H. Brush macromolecules with thermo-sensitive coil backbones and pendant polypeptide side chains: Synthesis, self-assembly and functionalization. *Polym Chem* 2015;6:1316–24.
- [58] Liu Y, Chen P, Li Z. Molecular bottlebrushes with polypeptide backbone prepared via ring-opening polymerization of NCA and ATRP. *Macromol Rapid Commun* 2012;33:287–95.
- [59] Rhodes AJ, Deming TJ. Tandem catalysis for the preparation of cylindrical polypeptide brushes. *J Am Chem Soc* 2012;134:19463–7.
- [60] Gadwal I, Rao J, Baettig J, Khan A. Functionalized molecular bottlebrushes. *Macromolecules* 2014;47:35–40.
- [61] Balamurugan SS, Bantchev GB, Yang Y, McCauley RL. Highly water-soluble thermally responsive poly(thiophene)-based brushes. *Angew Chem Int Ed* 2005;44:4872–6.
- [62] Chen Y, Zhou H, Sun Z, Li H, Huang H, Liu L, et al. Shell of amphiphilic molecular bottlebrush matters as unimolecular micelle. *Polymer* 2018;149:316–24.
- [63] Cheng C, Khoshdel E, Wooley KL. Facile one-pot synthesis of brush polymers through tandem catalysis using Grubbs' catalyst for both ring-opening metathesis and atom transfer radical polymerizations. *Nano Lett* 2006;6:1741–6.

- [64] Arrington KJ, Matson JB. Assembly of a visible light photoreactor: an inexpensive tool for bottlebrush polymer synthesis via photoiniferter polymerization. *Polym Chem* 2017;8:7452–6.
- [65] Bernard J, Favier A, Davis TP, Barner-Kowollik C, Stenzel MH. Synthesis of poly(vinyl alcohol) combs via MADIX/RAFT polymerization. *Polymer* 2006;47:1073–80.
- [66] Zhang N, Steenackers M, Luxenhofer R, Jordan R. Bottle-brush brushes: cylindrical molecular brushes of poly(2-oxazoline) on glassy carbon. *Macromolecules* 2009;42:5345–51.
- [67] Miwa Y, Yamamoto K, Sakaguchi M, Shimada S. Well-defined polystyrene grafted to polypropylene backbone by “living” radical polymerization with TEMPO. *Macromolecules* 2001;34:2089–94.
- [68] Morandi G, Pascual S, Montebault V, Sp Legoupy, Delorme N, Fontaine L. Synthesis of brush copolymers based on a poly(1, 4-butadiene) backbone via the “grafting from” approach by ROMP and ATRP. *Macromolecules* 2009;42:6927–31.
- [69] Raus V, Hološ A, Kronek J, Mosnáček J. Well-defined linear and grafted poly(2-isopropenyl-2-oxazoline)s prepared via copper-mediated reversible-deactivation radical polymerization methods. *Macromolecules* 2020;53:2077–87.
- [70] Sumerlin BS, Neugebauer D, Matyjaszewski K. Initiation efficiency in the synthesis of molecular brushes by grafting from via atom transfer radical polymerization. *Macromolecules* 2005;38:702–8.
- [71] Zhang Z, Wang X, Tam KC, Sèbe G. A comparative study on grafting polymers from cellulose nanocrystals via surface-initiated atom transfer radical polymerization (ATRP) and activator re-generated by electron transfer ATRP. *Carbohydr Polym* 2019;205:322–9.
- [72] Neugebauer D, Sumerlin BS, Matyjaszewski K, Goodhart B, Sheiko SS. How dense are cylindrical brushes grafted from a multifunctional macroinitiator? *Polymer* 2004;45:8173–9.
- [73] Cheng B, Qian L, Qian H-j, Lu Z-y, Cui S. Effects of stereo-regularity on the single-chain mechanics of poly(lactic acid) and its implications on the physical properties of bulk materials. *Nanoscale* 2017;9:14312–16.
- [74] Wang Y, Chang YC. Synthesis and conformational transition of surface-tethered polypeptide: poly(L-lysine). *Macromolecules* 2003;36:6511–18.
- [75] Surin M, Coulembier O, Tran K, De Winter J, Leclère P, Gerbaux P, et al. Regioregular poly(3-hexylthiophene)-poly(ϵ -caprolactone) block copolymers: controlled synthesis, microscopic morphology, and charge transport properties. *Org Electron* 2010;11:767–74.
- [76] Beyer VP, Cattoz B, Strong A, Schwarz A, Becer CR. Brush Copolymers from 2-Oxazoline and Acrylic Monomers via an Inimer Approach. *Macromolecules* 2020;53:2950–8.
- [77] Dutertre F, Bang K-T, Loppinet B, Choi I, Choi T-L, Fytas G. Structure and dynamics of dendronized polymer solutions: gaussian coil or macromolecular rod? *Macromolecules* 2016;49:2731–40.
- [78] Cheng C, Qi K, Khoshdel E, Wooley KL. Tandem synthesis of core-shell brush copolymers and their transformation to peripherally cross-linked and hollowed nanostructures. *J Am Chem Soc* 2006;128:6808–9.
- [79] Lienkamp K, Noé L, Breniaux M-H, Lieberwirth I, Groehn F, Wegner G. Synthesis and characterization of end-functionalized cylindrical polyelectrolyte brushes from poly(styrene sulfonate). *Macromolecules* 2007;40:2486–502.
- [80] Ding J, Xiao C, Zhao L, Cheng Y, Ma L, Tang Z, et al. Poly(L-glutamic acid) grafted with oligo (2-(2-(2-methoxyethoxy) ethoxy) ethyl methacrylate): Thermal phase transition, secondary structure, and self-assembly. *J Polym Sci, Part A: Polym Chem* 2011;49:2665–76.
- [81] Economopoulos SP, Chochos CL, Gregoriou VG, Kallitsis JK, Barrau S, Hadziioannou G. Novel brush-type copolymers bearing thiophene backbone and side chain quinoline blocks. Synthesis and their use as a compatibilizer in thiophene-quinoline polymer blends. *Macromolecules* 2007;40:921–7.
- [82] Wang M, Zou S, Guerin G, Shen L, Deng K, Jones M, et al. A water-soluble pH-responsive molecular brush of poly(N, N-dimethylaminoethyl methacrylate) grafted polythiophene. *Macromolecules* 2008;41:6993–7002.
- [83] Radzinski SC, Foster JC, Chapleski Jr RC, Troya D, Matson JB. Bottlebrush polymer synthesis by ring-opening metathesis polymerization: the significance of the anchor group. *J Am Chem Soc* 2016;138:6998–7004.
- [84] Beers KL, Gaynor SG, Matyjaszewski K, Sheiko SS, Möller M. The synthesis of densely grafted copolymers by atom transfer radical polymerization. *Macromolecules* 1998;31:9413–15.
- [85] Lee H-i, Pietrasik J, Matyjaszewski K. Phototunable temperature-responsive molecular brushes prepared by ATRP. *Macromolecules* 2006;39:3914–20.
- [86] Li C, Gunari N, Fischer K, Janshoff A, Schmidt M. New perspectives for the design of molecular actuators: thermally induced collapse of single macromolecules from cylindrical brushes to spheres. *Angew Chem Int Ed* 2004;43:1101–4.
- [87] Yamamoto S-i, Pietrasik J, Matyjaszewski K. ATRP synthesis of thermally responsive molecular brushes from oligo(ethylene oxide) methacrylates. *Macromolecules* 2007;40:9348–53.
- [88] Lee H-i, Boyce JR, Nese A, Sheiko SS, Matyjaszewski K. pH-induced conformational changes of loosely grafted molecular brushes containing poly(acrylic acid) side chains. *Polymer* 2008;49:5490–6.
- [89] Lienkamp K, Ruthard C, Lieser G, Berger R, Groehn F, Wegner G. Polymerization of styrene sulfonate ethyl ester and styrene sulfonate dodecyl ester by ATRP: synthesis and characterization of polymer brushes. *Macromol Chem Phys* 2006;207:2050–65.
- [90] Xu Y, Bolisetty S, Drechsler M, Fang B, Yuan J, Ballauff M, et al. pH and salt responsive poly(N, N-dimethylaminoethyl methacrylate) cylindrical brushes and their quaternized derivatives. *Polymer* 2008;49:3957–64.
- [91] Xu Y, Bolisetty S, Ballauff M, Müller AH. Switching the morphologies of cylindrical polycation brushes by ionic and supramolecular inclusion complexes. *J Am Chem Soc* 2009;131:1640–1.
- [92] Xu Y, Becker H, Yuan J, Burkhardt M, Zhang Y, Walther A, et al. Double-grafted cylindrical brushes: synthesis and characterization of poly(lauryl methacrylate) brushes. *Macromol Chem Phys* 2007;208:1666–75.
- [93] Muthukrishnan S, Zhang M, Burkhardt M, Drechsler M, Mori H, Müller AH. Molecular sugar sticks: cylindrical glycopolymer brushes. *Macromolecules* 2005;38:7926–34.
- [94] Yuan W, Yuan J, Zhang F, Xie X, Pan C. Synthesis, characterization, crystalline morphologies, and hydrophilicity of brush copolymers with double crystallizable side chains. *Macromolecules* 2007;40:9094–102.
- [95] Lee H-i, Jakubowski W, Matyjaszewski K, Yu S, Sheiko SS. Cylindrical core-shell brushes prepared by a combination of ROP and ATRP. *Macromolecules* 2006;39:4983–9.
- [96] Rzaevyev J. Synthesis of polystyrene-poly(lactide) bottlebrush block copolymers and their melt self-assembly into large domain nanostructures. *Macromolecules* 2009;42:2135–41.
- [97] Sahl M, Muth S, Branscheid R, Fischer K, Schmidt M. Helix-coil transition in cylindrical brush polymers with poly-L-lysine side chains. *Macromolecules* 2012;45:5167–75.
- [98] Cong Y, Gunari N, Zhang B, Janshoff A, Schmidt M. Hierarchical structure formation of cylindrical brush polymer–surfactant complexes. *Langmuir* 2009;25:6392–7.
- [99] Min K, Yu S, Lee H-i, Mueller L, Sheiko SS, Matyjaszewski K. High yield synthesis of molecular brushes via ATRP in miniemulsion. *Macromolecules* 2007;40:6557–63.
- [100] Ribelli TG, Augustine KF, Fantin M, Krysz P, Poli R, Matyjaszewski K. Disproportionation or combination? The termination of acrylate radicals in ATRP. *Macromolecules* 2017;50:7920–9.
- [101] Xie G, Martinez MR, Daniel WF, Keith AN, Ribelli TG, Fantin M, et al. Benefits of catalyzed radical termination: High-yield synthesis of polyacrylate molecular bottlebrushes without gelation. *Macromolecules* 2018;51:6218–25.
- [102] Ribelli TG, Konkolewicz D, Bernhard S, Matyjaszewski K. How are radicals (re)generated in photochemical ATRP? *J Am Chem Soc* 2014;136:13303–12.
- [103] Martinez MR, Sobieski J, Lorandi F, Fantin M, Dadashi-Silab S, Xie G, et al. Understanding the relationship between catalytic activity and termination in photoATRP: synthesis of linear and bottlebrush polyacrylates. *Macromolecules* 2019;52:59–67.
- [104] Zhang Y, Shen Z, Yang D, Feng C, Hu J, Lu G, et al. Convenient synthesis of PtBA-g-PMA well-defined graft copolymer with tunable grafting density. *Macromolecules* 2010;43:117–25.
- [105] Jiang X, Lu G, Feng C, Li Y, Huang X. Poly(acrylic acid)-graft-poly(N-vinylcaprolactam): a novel pH and thermo dual-stimuli responsive system. *Polym Chem* 2013;4:3876–84.
- [106] Feng C, Lu G, Sun G, Liu X, Huang X. BCPMA: A new trifunctional acrylic monomer for convenient synthesis of a well-defined amphiphilic graft copolymer by successive RDRP. *Polym Chem* 2014;5:6027–38.
- [107] Xu B, Gu G, Feng C, Jiang X, Hu J, Lu G, et al. (PAA-g-PS)-co-PPEGMEMA asymmetric polymer brushes: synthesis, self-assembly, and encapsulating capacity for both hydrophobic and hydrophilic agents. *Polym Chem* 2016;7:613–24.
- [108] Sun F, Feng C, Liu H, Huang X. PHEA-g-PDMAEA well-defined graft copolymers: SET-LRP synthesis, self-catalyzed hydrolysis, and quaternization. *Polym Chem* 2016;7:6973–9.
- [109] Jiang X, Jiang X, Lu G, Feng C, Huang X. The first amphiphilic graft copolymer bearing a hydrophilic poly(2-hydroxyethyl acrylate) backbone synthesized by successive RAFT and ATRP. *Polym Chem* 2014;5:4915–25.
- [110] Shen D, Xu B, Huang X, Zhuang Q, Lin S. (PtBA-co-PPEGMEMA-co-PDMAEA)-g-PPFA polymer brushes synthesized by sequential RAFT polymerization and ATRP. *Polym Chem* 2018;9:2821–9.
- [111] Song X, Yao W, Lu G, Li Y, Huang X. tBHBMA: a novel trifunctional acrylic monomer for the convenient synthesis of PAA-g-PCL well-defined amphiphilic graft copolymer. *Polym Chem* 2013;4:2864–75.
- [112] Qian W, Song X, Feng C, Xu P, Jiang X, Li Y, et al. Construction of PEG-based amphiphilic brush polymers bearing hydrophobic poly(lactic acid) side chains via successive RAFT polymerization and ROP. *Polym Chem* 2016;7:3300–10.
- [113] Wakioka M, Baek K-Y, Ando T, Kamigaito M, Sawamoto M. Possibility of living radical polymerization of vinyl acetate catalyzed by iron (I) complex. *Macromolecules* 2002;35:330–3.
- [114] Nese A, Li Y, Averick S, Kwak Y, Konkolewicz D, Sheiko SS, et al. Synthesis of amphiphilic poly(N-vinylpyrrolidone)-b-poly(vinyl acetate) molecular bottlebrushes. *ACS Macro Lett* 2012;1:227–31.
- [115] Quinn JF, Chaplin RP, Davis TP. Facile synthesis of comb, star, and graft polymers via reversible addition-fragmentation chain transfer (RAFT) polymerization. *J Polym Sci, Part A: Polym Chem* 2002;40:2956–66.
- [116] Kerr A, Hartlieb M, Sanchis J, Smith T, Perrier S. Complex multi-block bottle-brush architectures by RAFT polymerization. *Chem Commun* 2017;53:11901–4.
- [117] Tanaka J, Häkkinen S, Boeck PT, Cong Y, Perrier S, Sheiko SS, et al. Orthogonal cationic and radical RAFT polymerizations to prepare bottlebrush polymers. *Angew Chem Int Ed* 2020;132:7270–5.
- [118] Song Z, Han Z, Lv S, Chen C, Chen L, Yin L, et al. Synthetic polypeptides: from polymer design to supramolecular assembly and biomedical application. *Chem Soc Rev* 2017;46:6570–99.

- [119] Chen C, Wang Z, Li Z. Thermoresponsive polypeptides from pegylated poly-L-glutamates. *Biomacromolecules* 2011;12:2859–63.
- [120] Tang H, Li Y, Lahasky SH, Sheiko SS, Zhang D. Core-shell molecular bottle-brushes with helical polypeptide backbone: synthesis, characterization, and solution conformations. *Macromolecules* 2011;44:1491–9.
- [121] Chen C, Wunderlich K, Mukherji D, Koyunov K, Heck A, Raabe M, et al. Precision anisotropic brush polymers by sequence controlled chemistry. *J Am Chem Soc* 2019;142:1332–40.
- [122] Callmann CE, Thompson MP, Gianneschi NC. Poly(peptide): synthesis, structure, and function of peptide–polymer amphiphiles and protein-like polymers. *Acc Chem Res* 2020;53:400–13.
- [123] Breitenkamp RB, Ou Z, Breitenkamp K, Muthukumar M, Emrick T. Synthesis and characterization of polyolefin-graft-oligopeptide polyelectrolytes. *Macromolecules* 2007;40:7617–24.
- [124] Baumgartner R, Kuai D, Cheng J. Synthesis of controlled, high-molecular weight poly(L-glutamic acid) brush polymers. *Biomater Sci* 2017;5:1836–44.
- [125] Lu H, Wang J, Lin Y, Cheng J. One-pot synthesis of brush-like polymers via integrated ring-opening metathesis polymerization and polymerization of amino acid N-carboxyanhydrides. *J Am Chem Soc* 2009;131:13582–3.
- [126] Wang J, Lu H, Kamat R, Pingali SV, Urban VS, Cheng J, et al. Supramolecular polymerization from polypeptide-grafted comb polymers. *J Am Chem Soc* 2011;133:12906–9.
- [127] Sun H, Choi W, Zang N, Battistella C, Thompson MP, Cao W, et al. Bioactive peptide brush polymers via photoinduced reversible-deactivation radical polymerization. *Angew Chem Int Ed* 2019;58:17359–64.
- [128] Pounder RJ, Dove AP. Towards poly(ester) nanoparticles: recent advances in the synthesis of functional poly(ester)s by ring-opening polymerization. *Polym Chem* 2010;1:260–71.
- [129] Detrembleur C, Mazza M, Halleux O, Lecomte P, Mecerreyes D, Hedrick JL, et al. Ring-opening polymerization of γ -bromo- ϵ -caprolactone: a novel route to functionalized aliphatic polyesters. *Macromolecules* 2000;33:14–18.
- [130] Guo S, Wang W, Deng L, Xing J, Dong A. Poly(ϵ -caprolactone)-graft-poly(2-(dimethylamino) ethyl methacrylate) amphiphilic copolymers prepared via a combination of ROP and ATRP: synthesis, characterization, and self-assembly behavior. *Macromol Chem Phys* 2010;211:1572–8.
- [131] Nottelet B, Vert M, Coudane J. Novel amphiphilic degradable poly(ϵ -caprolactone)-graft-poly(4-vinyl pyridine), poly(ϵ -caprolactone)-graft-poly(dimethylaminoethyl methacrylate) and water-soluble derivatives. *Macromol Rapid Commun* 2008;29:743–50.
- [132] Nottelet B, El Ghzaoui A, Coudane J, Vert M. Novel amphiphilic poly(ϵ -caprolactone)-g-poly(L-lysine) degradable copolymers. *Biomacromolecules* 2007;8:2594–601.
- [133] Ponsart S, Coudane J, Vert M. A novel route to poly(ϵ -caprolactone)-based copolymers via anionic derivatization. *Biomacromolecules* 2000;1:275–81.
- [134] Islam M, Chen L, Sisler J, Tam K. Cellulose nanocrystal (CNC)-inorganic hybrid systems: synthesis, properties and applications. *J Mater Chem B* 2018;6:864–83.
- [135] Carlmark A, Larsson E, Malmström E. Grafting of cellulose by ring-opening polymerisation-A review. *Eur Polym J* 2012;48:1646–59.
- [136] Håfrén J, Córdova A. Direct organocatalytic polymerization from cellulose fibers. *Macromol Rapid Commun* 2005;26:82–6.
- [137] Lizundia E, Fortunati E, Dominici F, Vilas JL, León LM, Armentano I, et al. PLLA-grafted cellulose nanocrystals: role of the CNC content and grafting on the PLA bionanocomposite film properties. *Carbohydr Polym* 2016;142:105–13.
- [138] Habibi Y. Key advances in the chemical modification of nanocelluloses. *Chem Soc Rev* 2014;43:1519–42.
- [139] Rol F, Belgacem MN, Gandini A, Bras J. Recent advances in surface-modified cellulose nanofibrils. *Prog Polym Sci* 2019;88:241–64.
- [140] Thomas B, Raj MC, Joy J, Moores A, Drisko GL, Sanchez C. Nanocellulose, a versatile green platform: from biosources to materials and their applications. *Chem Rev* 2018;118:11575–625.
- [141] Zhang H, Wu J, Zhang J, He J. 1-Allyl-3-methylimidazolium chloride room temperature ionic liquid: a new and powerful nonderivatizing solvent for cellulose. *Macromolecules* 2005;38:8272–7.
- [142] Wang Z, Jiang F, Zhang Y, You Y, Wang Z, Guan Z. Bioinspired design of nanostructured elastomers with cross-linked soft matrix grafting on the oriented rigid nanofibers to mimic mechanical properties of human skin. *ACS Nano* 2015;9:271–8.
- [143] Zhang J, Wang Z, Wang X, Wang Z. The synthesis of bottlebrush cellulose-graft-diblock copolymer elastomers via atom transfer radical polymerization utilizing a halide exchange technique. *Chem Commun* 2019;55:13904–7.
- [144] Kinose Y, Sakakibara K, Ogawa H, Tsujii Y. Main-chain stiffness of cellulosic bottlebrushes with polystyrene side chains introduced regioselectively at the O-6 position. *Macromolecules* 2019;52:8733–40.
- [145] Olszewski M, Li L, Xie G, Keith A, Sheiko SS, Matyjaszewski K. Degradable cellulose-based polymer brushes with controlled grafting densities. *J Polym Sci, Part A: Polym Chem* 2019;57:2426–35.
- [146] Xu J, Shanmugam S, Fu C, Aguey-Zinsou K-F, Boyer C. Selective photoactivation: From a single unit monomer insertion reaction to controlled polymer architectures. *J Am Chem Soc* 2016;138:3094–106.
- [147] Pan X, Fantin M, Yuan F, Matyjaszewski K. Externally controlled atom transfer radical polymerization. *Chem Soc Rev* 2018;47:5457–90.
- [148] Pan X, Tasdelen MA, Laun J, Junkers T, Yagci Y, Matyjaszewski K. Photomediated controlled radical polymerization. *Prog Polym Sci* 2016;62:73–125.
- [149] Shanmugam S, Cuthbert J, Kowalewski T, Boyer C, Matyjaszewski K. Catalyst-free selective photoactivation of RAFT polymerization: a facile route for preparation of comblike and bottlebrush polymers. *Macromolecules* 2018;51:7776–84.
- [150] Xiong Q, Zhang X, Wei W, Wei G, Su Z. Enzyme-mediated reversible deactivation radical polymerization for functional materials: principles, synthesis, and applications. *Polym Chem* 2020;11:1673–90.
- [151] Hans M, Gasteier P, Keul H, Moeller M. Ring-opening polymerization of ϵ -caprolactone by means of mono- and multifunctional initiators: Comparison of chemical and enzymatic catalysis. *Macromolecules* 2006;39:3184–93.
- [152] Hans M, Xiao Y, Keul H, Heise A, Moeller M. Novel biodegradable heterografted polymer brushes prepared via a chemoenzymatic approach. *Macromol Chem Phys* 2009;210:736–46.
- [153] Hans M, Keul H, Heise A, Moeller M. Chemoenzymatic approach toward heterografted molecular bottle brushes. *Macromolecules* 2007;40:8872–80.
- [154] Wu D, Yang Y, Cheng X, Liu L, Tian J, Zhao H. Mixed molecular brushes with PLLA and PS side chains prepared by AGET ATRP and ring-opening polymerization. *Macromolecules* 2006;39:7513–19.
- [155] Christodoulou S, Iatrou H, Lohse DJ, Hadjichristidis N. Anionic copolymerization of styrenic-tipped macromonomers: a route to novel triblock-comb copolymers of styrene and isoprene. *J Polym Sci, Part A: Polym Chem* 2005;43:4030–9.
- [156] Saito Y, Jinbo Y, Kumaki J, Narumi A, Kawaguchi S. Influence of the primary structure of the main chain on backbone stiffness of cylindrical rod brushes. *Polym J* 2013;45:193–201.
- [157] Deng G, Chen Y. Preparation of novel macromonomers and study of their polymerization. *J Polym Sci, Part A: Polym Chem* 2004;42:3887–96.
- [158] Li H, Miao H, Gao Y, Li H, Chen D. Efficient synthesis of narrowly dispersed amphiphilic double-brush copolymers through the polymerization reaction of macromonomer micelle emulsifiers at the oil-water interface. *Polym Chem* 2016;7:4476–85.
- [159] Guo Y, Van Beek JD, Zhang B, Colussi M, Walde P, Zhang A, et al. Tuning polymer thickness: synthesis and scaling theory of homologous series of dendronized polymers. *J Am Chem Soc* 2009;131:11841–54.
- [160] Ayres L, Vos MR, Adams PHM, Shklyarevskiy IO, van Hest JC. Elastin-based side-chain polymers synthesized by ATRP. *Macromolecules* 2003;36:5967–73.
- [161] Neugebauer D, Zhang Y, Pakula T, Sheiko SS, Matyjaszewski K. Densely-grafted and double-grafted PEO brushes via ATRP. A route to soft elastomers. *Macromolecules* 2003;36:6746–55.
- [162] Oh JK, Min K, Matyjaszewski K. Preparation of poly(oligo (ethylene glycol) monomethyl ether methacrylate) by homogeneous aqueous AGET ATRP. *Macromolecules* 2006;39:3161–7.
- [163] Lutz JF, Jahed N, Matyjaszewski K. Preparation and characterization of graft terpolymers with controlled molecular structure. *J Polym Sci, Part A: Polym Chem* 2004;42:1939–52.
- [164] Neugebauer D, Zhang Y, Pakula T, Matyjaszewski K. PDMS–PEO densely grafted copolymers. *Macromolecules* 2005;38:8687–93.
- [165] Gu L, Shen Z, Zhang S, Lu G, Zhang X, Huang X. Novel amphiphilic centipede-like copolymer bearing polyacrylate backbone and poly(ethylene glycol) and polystyrene side chains. *Macromolecules* 2007;40:4486–93.
- [166] Yoo M, Kim S, Lim J, Kramer EJ, Hawker CJ, Kim BJ, et al. Facile synthesis of thermally stable core-shell gold nanoparticles via photo-cross-linkable polymeric ligands. *Macromolecules* 2010;43:3570–5.
- [167] Weber C, Becer CR, Hoogenboom R, Schubert US. Lower critical solution temperature behavior of comb and graft shaped poly(oligo (2-ethyl-2-oxazoline) methacrylate)s. *Macromolecules* 2009;42:2965–71.
- [168] Ohno S, Matyjaszewski K. Controlling grafting density and side chain length in poly(n-butyl acrylate) by ATRP copolymerization of macromonomers. *J Polym Sci, Part A: Polym Chem* 2006;44:5454–67.
- [169] Dse Weller, JR McDaniel, Fischer K, Chilkoti A, Schmidt M. Cylindrical polymer brushes with elastin-like polypeptide side chains. *Macromolecules* 2013;46:4966–71.
- [170] Zhu H, Deng G, Chen Y. Amphiphilic polymer brushes with alternating PCL and PEO grafts through radical copolymerization of styrenic and maleimide macromonomers. *Polymer* 2008;49:405–11.
- [171] Zhang Y, Huang J, Chen Y. Reactive dendronized copolymer of styryl dendron and maleic anhydride: A single molecular scaffold. *Macromolecules* 2005;38:5069–77.
- [172] Yuan J, Müller A, Matyjaszewski K, Sheiko S, Moeller M, Matyjaszewski K. Molecular brushes. In: *Polymer Science: A Comprehensive Reference*. New York: Elsevier Science Ltd; 2012. p. 199–264.
- [173] Fu Q, Ren JM, Qiao GG. Synthesis of novel cylindrical bottlebrush polypseudotaxane via inclusion complexation of high density poly(ϵ -caprolactone) bottlebrush polymer and α -cyclodextrins. *Polym Chem* 2012;3:343–51.
- [174] Chang AB, Lin T-P, Thompson NB, Luo S-X, Liberman-Martin AL, Chen H-Y, et al. Design, synthesis, and self-assembly of polymers with tailored graft distributions. *J Am Chem Soc* 2017;139:17683–93.
- [175] Cheng C, Khoshdel E, Wooley KL. ATRP from a norbornenyl-functionalized initiator: balancing of complementary reactivity for the preparation of α -norbornenyl macromonomers/ ω -haloalkyl macroinitiators. *Macromolecules* 2005;38:9455–65.
- [176] Cheng C, Khoshdel E, Wooley KL. One-pot tandem synthesis of a core-shell brush copolymer from small molecule reactants by ring-opening metathesis and reversible addition-fragmentation chain transfer (co)polymerizations. *Macromolecules* 2007;40:2289–92.

- [177] Xia Y, Kornfield JA, Grubbs RH. Efficient synthesis of narrowly dispersed brush polymers via living ring-opening metathesis polymerization of macromonomers. *Macromolecules* 2009;42:3761–6.
- [178] Seo H-B, Yu Y-G, Chae C-G, Kim M-J, Lee J-S. Synthesis of ultrahigh molecular weight bottlebrush block copolymers of ω -end-norbornyl polystyrene and polymethacrylate macromonomers. *Polymer* 2019;177:241–9.
- [179] Chae C-G, Yu Y-G, Seo H-B, Kim M-J, Wen Z, Lee J-S. End-capping reaction of living anionic poly(benzyl methacrylate) with a pentafluorophenyl ester for a norbornenyl- ω -end macromonomer with a long flexible spacer: advantage in the well-controlled synthesis of ultrahigh-molecular-weight bottlebrush polymers. *Macromolecules* 2019;52:4828–38.
- [180] Kim M-J, Yu Y-G, Chae C-G, Seo H-B, Bak I-G, Mallela YK, et al. ω -Norbornenyl macromonomers: in situ synthesis by end-capping of living anionic polymers using a norbornenyl-functionalized α -phenyl acrylate and their ring-opening metathesis polymerization. *Macromolecules* 2018;52:103–12.
- [181] Ahn S-k, Pickel DL, Kochemba WM, Chen J, Uhrig D, Hinestroza JP, et al. Poly(3-hexylthiophene) molecular bottlebrushes via ring-opening metathesis polymerization: macromolecular architecture enhanced aggregation. *ACS Macro Lett* 2013;2:761–5.
- [182] Yang B, Abel BA, McCormick CL, Storey RF. Synthesis of polyisobutylene bottlebrush polymers via ring-opening metathesis polymerization. *Macromolecules* 2017;50:7458–67.
- [183] Rosenbach D, Mödl N, Hahn M, Petry J, Danzer MA, Thelakkat M. Synthesis and Comparative Studies of Solvent-Free Brush Polymer Electrolytes for Lithium Batteries. *ACS Appl Energy Mater* 2019;2:3373–88.
- [184] Li Y, Themistou E, Zou J, Das BP, Tsianou M, Cheng C. Facile synthesis and visualization of Janus double-brush copolymers. *ACS Macro Lett* 2012;1:52–6.
- [185] Li Y, Zou J, Das BP, Tsianou M, Cheng C. Well-defined amphiphilic double-brush copolymers and their performance as emulsion surfactants. *Macromolecules* 2012;45:4623–9.
- [186] Radzinski SC, Foster JC, Scannelli SJ, Weaver JR, Arrington KJ, Matson JB. Tapered bottlebrush polymers: cone-shaped nanostructures by sequential addition of macromonomers. *ACS Macro Lett* 2017;6:1175–9.
- [187] Ito S, Goseki R, Ishizone T, Hirao A. Synthesis of well-controlled graft polymers by living anionic polymerization towards exact graft polymers. *Polym Chem* 2014;5:5523–34.
- [188] Lanson D, Schappacher M, Borsali R, Deffieux A. Synthesis of (poly(chloroethyl vinyl ether)-*g*-polystyrene) comb-*b*-(poly(chloropyran ethoxy vinyl ether)-*g*-polyisoprene) comb copolymers and study of hyper-branched micelle formation in dilute solutions. *Macromolecules* 2007;40:5559–65.
- [189] Lanson D, Ariura F, Schappacher M, Borsali R, Deffieux A. Comb copolymers with polystyrene and polyisoprene branches: effect of block topology on film morphology. *Macromolecules* 2009;42:3942–50.
- [190] Gromadzki D, Jigounov A, Štěpánek P, Makuška R. Synthesis of thermally responsive cylindrical molecular brushes via a combination of nitroxide-mediated radical polymerization and “grafting onto” strategy. *Eur Polym J* 2010;46:804–13.
- [191] Das A, Theato P. Activated ester containing polymers: opportunities and challenges for the design of functional macromolecules. *Chem Rev* 2016;116:1434–95.
- [192] Schüll C, Nuhn L, Mangold C, Christ E, Zentel R, Frey H. Linear-hyperbranched graft-copolymers via grafting-to strategy based on hyperbranched dendron analogues and reactive ester polymers. *Macromolecules* 2012;45:5901–10.
- [193] Lu X, Watts E, Jia F, Tan X, Zhang K. Polycondensation of polymer brushes via DNA hybridization. *J Am Chem Soc* 2014;136:10214–17.
- [194] Lu X, Tran T-H, Jia F, Tan X, Davis S, Krishnan S, et al. Providing oligonucleotides with steric selectivity by brush-polymer-assisted compaction. *J Am Chem Soc* 2015;137:12466–9.
- [195] Shi Y, Cao X, Gao H. The use of azide-alkyne click chemistry in recent syntheses and applications of polytriazole-based nanostructured polymers. *Nanoscale* 2016;8:4864–81.
- [196] Fournier D, Hoogenboom R, Schubert US. Clicking polymers: a straightforward approach to novel macromolecular architectures. *Chem Soc Rev* 2007;36:1369–80.
- [197] Pang X, Zhao L, Feng C, Wu R, Ma H, Lin Z. Functional copolymer brushes composed of a hydrophobic backbone and densely grafted conjugated side chains via a combination of living polymerization with click chemistry. *Polym Chem* 2013;4:2025–32.
- [198] Pang X, Zhao L, Han W, Xin X, Lin Z. A general and robust strategy for the synthesis of nearly monodisperse colloidal nanocrystals. *Nat Nanotechnol* 2013;8:426–31.
- [199] He Y, Yoon YJ, Harn YW, Biesold-McGee GV, Liang S, Lin CH, et al. Unconventional route to dual-shelled organolead halide perovskite nanocrystals with controlled dimensions, surface chemistry, and stabilities. *Sci Adv* 2019;5:eaax4424.
- [200] He Y, Pang X, Jiang B, Feng C, Harn YW, Chen Y, et al. Unconventional route to uniform hollow semiconducting nanoparticles with tailorable dimensions, compositions, surface chemistry, and near-infrared absorption. *Angew Chem Int Ed* 2017;129:13126–31.
- [201] Gao H, Matyjaszewski K. Synthesis of molecular brushes by “grafting onto” method: combination of ATRP and click reactions. *J Am Chem Soc* 2007;129:6633–9.
- [202] Obhi NK, Peda DM, Kynaston EL, Seferos DS. Exploring the graft-to synthesis of all-conjugated comb copolymers using azide-alkyne click chemistry. *Macromolecules* 2018;51:2969–78.
- [203] Yan Y, Shi Y, Zhu W, Chen Y. Highly efficient synthesis of cylindrical polymer brushes with various side chains via click grafting-onto approach. *Polymer* 2013;54:5634–42.
- [204] Henn DM, Fu W, Mei S, Li CY, Zhao B. Temperature-induced dhaphase changing of thermosensitive binary heterografted linear molecular brushes between extended wormlike and stable globular conformations. *Macromolecules* 2017;50:1645–56.
- [205] Kent EW, Henn DM, Zhao B. Shape-changing linear molecular bottlebrushes with dually pH- and thermo-responsive diblock copolymer side chains. *Polym Chem* 2018;9:5133–44.
- [206] Engler AC, Hi Lee, Hammond PT. Highly efficient “grafting onto” a polypeptide backbone using click chemistry. *Angew Chem Int Ed* 2009;48:9334–8.
- [207] Su Y-X, Xu L, Xu X-H, Hou X-H, Liu N, Wu Z-Q. Controlled synthesis of densely grafted bottlebrushes that bear helical polyisocyanide side chains on polyisocyanide backbones and exhibit greatly increased viscosity. *Macromolecules* 2020;53:3224–33.
- [208] Gan W, Shi Y, Jing B, Cao X, Zhu Y, Gao H. Produce molecular brushes with ultrahigh grafting density using accelerated CuAAC grafting-onto strategy. *Macromolecules* 2017;50:215–22.
- [209] Rogers WB, Shih WM, Manoharan VN. Using DNA to program the self-assembly of colloidal nanoparticles and microparticles. *Nat Rev Mater* 2016;1:1–14.
- [210] Tan X, Lu H, Sun Y, Chen X, Wang D, Jia F, et al. Expanding the materials space of DNA via organic-phase ring-opening metathesis polymerization. *Chem* 2019;5:1584–96.
- [211] Fouz MF, Mukumoto K, Averick S, Molinar O, McCartney BM, Matyjaszewski K, et al. Bright fluorescent nanotags from bottlebrush polymers with DNA-tipped bristles. *ACS Cent Sci* 2015;1:431–8.
- [212] Fouz MF, Dey SK, Mukumoto K, Matyjaszewski K, Armitage BA, Das SR. Accessibility of densely localized DNA on doft polymer nanoparticles. *Langmuir* 2018;34:14731–7.
- [213] Borchmann DE, Tarallo R, Avendano S, Falanga A, Carberry TP, Galdiero S, et al. Membranotropic peptide-functionalized poly(lactide)-graft-poly(ethylene glycol) brush copolymers for intracellular delivery. *Macromolecules* 2015;48:942–9.
- [214] Chen P, Li C, Liu D, Li Z. DNA-grafted polypeptide molecular bottlebrush prepared via ring-opening polymerization and click chemistry. *Macromolecules* 2012;45:9579–84.
- [215] Lowe AB. Thiol-ene “click” reactions and recent applications in polymer and materials synthesis. *Polym Chem* 2010;1:17–36.
- [216] Hong T, Cao P-F, Zhao S, Li B, Smith C, Lehmann M, et al. Tailored CO₂-philic gas separation membranes via one-pot thiol-ene chemistry. *Macromolecules* 2019;52:5819–28.
- [217] Cesana S, Kurek A, Baur MA, Auernheimer J, Nuyken O. Polymer-bound thiol groups on poly(2-oxazoline)s. *Macromol Rapid Commun* 2007;28:608–15.
- [218] Le Fer G, Babinot J, Versace DL, Langlois V, Renard E. An efficient thiol-ene chemistry for the preparation of amphiphilic PHA-based graft copolymers. *Macromol Rapid Commun* 2012;33:2041–5.
- [219] Yang L-C, Han L, Ma H-W, Liu P-B, Shen H-Y, Li C, et al. Synthesis of alkyne-functionalized polymers via living anionic polymerization and investigation of features during the post-“thiol-yne” click reaction. *Chin J Polym Sci* 2019;37:841–50.
- [220] Gacal B, Durmaz H, Tasdelen M, Hizal G, Tunca U, Yagci Y, et al. Anthracene-maleimide-based Diels–Alder “click chemistry” as a novel route to graft copolymers. *Macromolecules* 2006;39:5330–6.
- [221] Durmaz H, Dag A, Cerit N, Sirkecioglu O, Hizal G, Tunca U. Graft copolymers via ROMP and Diels–Alder click reaction strategy. *J Polym Sci, Part A: Polym Chem* 2010;48:5982–91.
- [222] Dag A, Durmaz H, Demir E, Hizal G, Tunca U. Heterograft copolymers via double click reactions using one-pot technique. *J Polym Sci, Part A: Polym Chem* 2008;46:6969–77.
- [223] Billiet S, De Bruycker K, Driessen F, Goossens H, Van Speybroeck V, Winne JM, et al. Triazolinones enable ultrafast and reversible click chemistry for the design of dynamic polymer systems. *Nat Chem* 2014;6:815.
- [224] Xiao L, Chen Y, Zhang K. Efficient metal-free “grafting onto” method for bottlebrush polymers by combining RAFT and triazolinone–diene click reaction. *Macromolecules* 2016;49:4452–61.
- [225] Jia F, Lu X, Wang D, Cao X, Tan X, Lu H, et al. Depth-profiling the nuclease stability and the gene silencing efficacy of brush-architected poly(ethylene glycol)-DNA conjugates. *J Am Chem Soc* 2017;139:10605–8.
- [226] Radzinski SC, Foster JC, Matson JB. Synthesis of bottlebrush polymers via transfer-to and grafting-through approaches using a RAFT chain transfer agent with a ROMP-active Z-group. *Polym Chem* 2015;6:5643–52.
- [227] Yin J, Ge Z, Liu H, Liu S. Synthesis of amphiphilic copolymer brushes possessing alternating poly (methyl methacrylate) and poly(N-isopropylacrylamide) grafts via a combination of ATRP and click chemistry. *J Polym Sci, Part A: Polym Chem* 2009;47:2608–19.
- [228] Fu X, Guo Z-H, Le AN, Lei J, Zhong M. Synthesis and visualization of molecular brush-on-brush based hierarchically branched structures. *Polym Chem* 2020;11:270–4.
- [229] Chen Y, Sun Z, Li H, Dai Y, Hu Z, Huang H, et al. Molecular bottlebrushes featuring brush-on-brush architecture. *ACS Macro Lett* 2019;8:749–53.
- [230] Gu W, Huh J, Hong SW, Sveinbjörnsson BR, Park C, Grubbs RH, et al. Self-assembly of symmetric brush diblock copolymers. *ACS Nano* 2013;7:2551–8.
- [231] Pesek SL, Li X, Hammouda B, Hong K, Verduzco R. Small-angle neutron scattering analysis of bottlebrush polymers prepared via grafting-through polymerization. *Macromolecules* 2013;46:6998–7005.

- [232] Zhulina EB, Sheiko SS, Borisov OV. Theory of microphase segregation in the melts of copolymers with dendritically branched, bottlebrush, or cycled blocks. *ACS Macro Lett* 2019;8:1075–9.
- [233] Zhulina EB, Sheiko SS, Dobrynin AV, Borisov OV. Microphase segregation in the melts of bottlebrush block copolymers. *Macromolecules* 2020;53:2582–93.
- [234] Zhulina EB, Sheiko SS, Borisov OV. Solution and melts of barbwire bottlebrushes: hierarchical structure and scale-dependent elasticity. *Macromolecules* 2019;52:1671–84.
- [235] Zhao L, Byun M, Rzaev J, Lin Z. Polystyrene-poly(lactide) bottlebrush block copolymer at the air/water interface. *Macromolecules* 2009;42:9027–33.
- [236] Rzaev J. Molecular bottlebrushes: new opportunities in nanomaterials fabrication. *ACS Macro Lett* 2012;1:1146–9.
- [237] Hsu H-P, Paul W, Rathgeber S, Binder K. Characteristic length scales and radial monomer density profiles of molecular bottle-brushes: Simulation and experiment. *Macromolecules* 2010;43:1592–601.
- [238] Mai Y, Eisenberg A. Self-assembly of block copolymers. *Chem Soc Rev* 2012;41:5969–85.
- [239] Fenyves R, Schmutz M, Horner IJ, Bright FV, Rzaev J. Aqueous self-assembly of giant bottlebrush block copolymer surfactants as shape-tunable building blocks. *J Am Chem Soc* 2014;136:7762–70.
- [240] Li Z, Ma J, Lee NS, Wooley KL. Dynamic cylindrical assembly of triblock copolymers by a hierarchical process of covalent and supramolecular interactions. *J Am Chem Soc* 2011;133:1228–31.
- [241] Du J-Z, Chen D-P, Wang Y-C, Xiao C-S, Lu Y-J, Wang J, et al. Synthesis and micellization of amphiphilic brush-coil block copolymer based on poly(ϵ -caprolactone) and PEGylated polyphosphoester. *Biomacromolecules* 2006;7:1898–903.
- [242] Altay E, Rzaev J. Synthesis of star-brush polymer architectures from end-reactive molecular bottlebrushes. *Polymer* 2016;98:487–94.
- [243] Li Z, Ma J, Cheng C, Zhang K, Wooley KL. Synthesis of hetero-grafted amphiphilic diblock molecular brushes and their self-assembly in aqueous medium. *Macromolecules* 2010;43:1182–4.
- [244] Ma H, Kim KT. Self-assembly of bottlebrush block copolymers into triply periodic nanostructures in a dilute solution. *Macromolecules* 2020;53:711–18.
- [245] Steinhaus A, Pelras T, Chakraborty R, Gröschel AH, Müllner M. Self-assembly of diblock molecular polymer brushes in the spherical confinement of nanoemulsion droplets. *Macromol Rapid Commun* 2018;39:1800177.
- [246] Unsai H, Onbulak S, Calik F, Er-Rafik M, Schmutz M, Sanyal A, et al. Interplay between molecular packing, drug loading, and core cross-linking in bottlebrush copolymer micelles. *Macromolecules* 2017;50:1342–52.
- [247] Luo H, Santos JL, Herrera-Alonso M. Toroidal structures from brush amphiphiles. *Chem Commun* 2014;50:536–8.
- [248] Chen L, Jiang T, Lin J, Cai C. Toroid formation through self-assembly of graft copolymer and homopolymer mixtures: experimental studies and dissipative particle dynamics simulations. *Langmuir* 2013;29:8417–26.
- [249] Lian X, Wu D, Song X, Zhao H. Synthesis and self-assembly of amphiphilic asymmetric macromolecular brushes. *Macromolecules* 2010;43:7434–45.
- [250] Rathgeber S, Pakula T, Wilk A, Matyjaszewski K, Beers KL. On the shape of bottle-brush macromolecules: systematic variation of architectural parameters. *J Chem Phys* 2005;122:124904.
- [251] Paturej J, Sheiko SS, Panyukov S, Rubinstein M. Molecular structure of bottlebrush polymers in melts. *Sci Adv* 2016;2:e1601478.
- [252] Sheiko SS, Sun FC, Randall A, Shirvanyants D, Rubinstein M, Lee H-i, et al. Adsorption-induced scission of carbon-carbon bonds. *Nature* 2006;440:191–4.
- [253] Zhang B, Gröhn F, Pedersen JS, Fischer K, Schmidt M. Conformation of cylindrical brushes in solution: effect of side chain length. *Macromolecules* 2006;39:8440–50.
- [254] Hsu H-P, Paul W, Binder K. Standard definitions of persistence length do not describe the local “intrinsic” stiffness of real polymer chains. *Macromolecules* 2010;43:3094–102.
- [255] Pan X, Ishaq MW, Umair A, Ali MW, Li L. Evolution of Single Chain Conformation for Model Comb-Like Chains with Grafting Density Ranging from 0 to ~100% in Dilute Solution. *ACS Macro Lett* 2019;8:1535–40.
- [256] Morozova S, Lodge TP. Conformation of methylcellulose as a function of poly(ethylene glycol) graft density. *ACS Macro Lett* 2017;6:1274–9.
- [257] Sheiko SS, da Silva M, Shirvanyants D, LaRue I, Prokhorova S, Moeller M, et al. Measuring molecular weight by atomic force microscopy. *J Am Chem Soc* 2003;125:6725–8.
- [258] Potemkin II, Khokhlov AR, Prokhorova S, Sheiko SS, Möller M, Beers KL, et al. Spontaneous curvature of comblike polymers at a flat interface. *Macromolecules* 2004;37:3918–23.
- [259] Panyukov S, Zhulina EB, Sheiko SS, Randall GC, Brock J, Rubinstein M. Tension amplification in molecular brushes in solutions and on substrates. *J Phys Chem B* 2009;113:3750–68.
- [260] Lebedeva NV, Nese A, Sun FC, Matyjaszewski K, Sheiko SS. Anti-Arrhenius cleavage of covalent bonds in bottlebrush macromolecules on substrate. *Proc Natl Acad Sci* 2012;109:9276–80.
- [261] Li Y, Nese A, Matyjaszewski K, Sheiko SS. Molecular tensile machines: anti-arrhenius cleavage of disulfide bonds. *Macromolecules* 2013;46:7196–201.
- [262] Park I, Nese A, Pietrasik J, Matyjaszewski K, Sheiko SS. Focusing bond tension in bottle-brush macromolecules during spreading. *J Mater Chem* 2011;21:8448–53.
- [263] SY Yu-Su, Sheiko SS, Lee H-i, Jakubowski W, Nese A, Matyjaszewski K, et al. Crystallization of molecular brushes with block copolymer side chains. *Macromolecules* 2009;42:9008–17.
- [264] Müllner M, Dodds SJ, Nguyen T-H, Senyschyn D, Porter CJ, Boyd BJ, et al. Size and rigidity of cylindrical polymer brushes dictate long circulating properties in vivo. *ACS Nano* 2015;9:1294–304.
- [265] Tonge CM, Sauv   ER, Cheng S, Howard TA, Hudson ZM. Multiblock bottlebrush nanofibers from organic electronic materials. *J Am Chem Soc* 2018;140:11599–603.
- [266] Huang K, Canterbury DP, Rzaev J. Organosoluble polypyrrole nanotubes from core-shell bottlebrush copolymers. *Chem Commun* 2010;46:6326–8.
- [267] Huang K, Johnson M, Rzaev J. Synthesis of degradable organic nanotubes by bottlebrush molecular templating. *ACS Macro Lett* 2012;1:892–5.
- [268] Huang K, Canterbury DP, Rzaev J. Synthesis of segmented polylactide molecular brushes and their transformation to open-end nanotubes. *Macromolecules* 2010;43:6632–8.
- [269] To Pelras, CS Mahon, x Nonappa, Ikkala O, Gröschel AH, Müllner M. Polymer nanowires with highly precise internal morphology and topography. *J Am Chem Soc* 2018;140:12736–40.
- [270] Li Z, Tang M, Jiang C, Bai R, Bai W. Photoinduced reversible morphological transformation of azobenzene-containing pseudo-2D polymers. *Macromol Rapid Commun* 2018;39:1700880.
- [271] Long M, Shi Y, Zhang K, Chen Y. Microphase separation within disk shaped aggregates of triblock bottlebrushes. *Macromol Rapid Commun* 2016;37:605–9.
- [272] Sinturel C, Bates FS, Hillmyer MA. High χ -low N block polymers: how far can we go? *ACS Macro Lett* 2015;4:1044–50.
- [273] Xia Y, Olsen BD, Kornfield JA, Grubbs RH. Efficient synthesis of narrowly dispersed brush copolymers and study of their assemblies: the importance of side chain arrangement. *J Am Chem Soc* 2009;131:18525–32.
- [274] Runge MB, Lipscomb CE, Ditzler LR, Mahanthappa MK, Tivanski AV, Bowden NB. Investigation of the assembly of comb block copolymers in the solid state. *Macromolecules* 2008;41:7687–94.
- [275] Bolton J, Bailey TS, Rzaev J. Large pore size nanoporous materials from the self-assembly of asymmetric bottlebrush block copolymers. *Nano Lett* 2011;11:998–1001.
- [276] Guo ZH, Le AN, Feng X, Choo Y, Liu B, Wang D, et al. Janus graft block copolymers: design of a polymer architecture for independently tuned nanostructures and polymer properties. *Angew Chem Int Ed* 2018;57:8493–7.
- [277] Kawamoto K, Zhong M, Gadelrab KR, Cheng L-C, Ross CA, Alexander-Katz A, et al. Graft-through synthesis and assembly of janus bottlebrush polymers from A-branch-B diblock macromonomers. *J Am Chem Soc* 2016;138:11501–4.
- [278] Miyake GM, Weitekamp RA, Pionova VA, Grubbs RH. Synthesis of isocyanate-based brush block copolymers and their rapid self-assembly to infrared-reflecting photonic crystals. *J Am Chem Soc* 2012;134:14249–54.
- [279] Miyake GM, Pionova VA, Weitekamp RA, Grubbs RH. Precisely tunable photonic crystals from rapidly self-assembling brush block copolymer blends. *Angew Chem Int Ed* 2012;51:11246–8.
- [280] Hong SW, Gu W, Huh J, Sveinbjornsson BR, Jeong G, Grubbs RH, et al. On the self-assembly of brush block copolymers in thin films. *ACS Nano* 2013;7:9684–92.
- [281] Gai Y, Song D-P, Yavitt BM, Watkins JJ. Polystyrene-block-poly(ethylene oxide) bottlebrush block copolymer morphology transitions: Influence of side chain length and volume fraction. *Macromolecules* 2017;50:1503–11.
- [282] Hou C, Hu J, Liu G, Wang J, Liu F, Hu H, et al. Synthesis and bulk self-assembly of well-defined binary graft copolymers. *Macromolecules* 2013;46:4053–63.
- [283] Lin T-P, Chang AB, Luo S-X, Chen H-Y, Lee B, Grubbs RH. Effects of grafting density on block polymer self-assembly: From linear to bottlebrush. *ACS Nano* 2017;11:11632–41.
- [284] Li A, Li Z, Zhang S, Sun G, Policarpio DM, Wooley KL. Synthesis and direct visualization of dumbbell-shaped molecular brushes. *ACS Macro Lett* 2012;1:241–5.
- [285] Altay E, Nykypanchuk D, Rzaev J. Mesoporous polymer frameworks from end-reactive bottlebrush copolymers. *ACS Nano* 2017;11:8207–14.
- [286] Walsh DJ, Guirionnet D. Macromolecules with programmable shape, size, and chemistry. *Proc Natl Acad Sci* 2019;116:1538–42.
- [287] He Q, Ku KH, Vijayamohanan H, Kim BJ, Swager TM. Switchable full-color reflective photonic ellipsoidal particles. *J Am Chem Soc* 2020;142:10424–30.
- [288] Walsh DJ, Dutta S, Sing CE, Guirionnet D. Engineering of molecular geometry in bottlebrush polymers. *Macromolecules* 2019;52:4847–57.
- [289] Han W, Byun M, Zhao L, Rzaev J, Lin Z. Controlled evaporative self-assembly of hierarchically structured bottlebrush block copolymer with nanochannels. *J Mater Chem* 2011;21:14248–53.
- [290] Li B, Han W, Jiang B, Lin Z. Crafting threads of diblock copolymer micelles via flow-enabled self-assembly. *ACS Nano* 2014;8:2936–42.
- [291] Han W, Byun M, Li B, Pang X, Lin Z. A simple route to hierarchically assembled micelles and inorganic nanoparticles. *Angew Chem Int Ed* 2012;51:12588–92.
- [292] Byun M, Bowden NB, Lin Z. Hierarchically organized structures engineered from controlled evaporative self-assembly. *Nano Lett* 2010;10:3111–17.
- [293] Byun M, Han W, Qiu F, Bowden NB, Lin Z. Hierarchically ordered structures enabled by controlled evaporative self-assembly. *Small* 2010;6:2250–5.
- [294] Rokhlenko Y, Kawamoto K, Johnson JA, Osuji CO. Sub-10 nm self-assembly of mesogen-containing grafted macromonomers and their bottlebrush polymers. *Macromolecules* 2018;51:3680–90.
- [295] Barnard E, Pfu  wa R, Maiz J, M  ller AJ, Klumperman B. Synthesis, structure, and crystallization behavior of amphiphilic heteroarm molecular brushes

- with crystallizable poly(ethylene oxide) and n-alkyl side chains. *Macromolecules* 2020;53:1585–95.
- [296] Isono T, Kondo Y, Ozawa S, Chen Y, Sakai R, Sato S-i, et al. Stereoblock-like brush copolymers consisting of poly(L-lactide) and poly(D-lactide) side chains along poly(norbornene) backbone: synthesis, stereocomplex formation, and structure-property relationship. *Macromolecules* 2014;47:7118–28.
- [297] López-Barrón CR, Hagadorn JR, Mattler SJ, Throckmorton JA. Syndiotactic α -olefin molecular bottlebrushes: crystallization, melting, and hierarchical microstructure. *Macromolecules* 2020;53:3778–88.
- [298] Inomata K, Sasaki Y, Nose T. Packing manner of graft copolymers with rigid-rod main chains and amorphous-crystalline diblock copolymers as side chains. *J Polym Sci, Part B: Polym Phys* 2002;40:1904–12.
- [299] Sun H, Kabb CP, Sims MB, Sumerlin BS. Architecture-transformable polymers: reshaping the future of stimuli-responsive polymers. *Prog Polym Sci* 2019;89:61–75.
- [300] Li J, Wang H, Kong L, Zhou Y, Li S, Shi H. Phase transition and side-chain crystallization of poly(methyl vinyl ether-alt-maleic anhydride)-g-alkyl alcohol comb-like polymers. *Macromolecules* 2018;51:8922–31.
- [301] Qi H, Liu X, Henn DM, Mei S, Staub MC, Zhao B, et al. Breaking translational symmetry via polymer chain overcrowding in molecular bottlebrush crystallization. *Nat Commun* 2020;11:2152.
- [302] Zhou T, Qi H, Han L, Barbash D, Li CY. Towards controlled polymer brushes via a self-assembly-assisted-grafting-to approach. *Nat Commun* 2016;7:1–8.
- [303] He W-N, Xu J-T. Crystallization assisted self-assembly of semicrystalline block copolymers. *Prog Polym Sci* 2012;37:1350–400.
- [304] Kriptout S, Psylla C, Kyriakos K, Raftopoulos KN, Zhao J, Zhang G, et al. Structure and crystallization behavior of poly(ethylene oxide)(PEO) chains in core-shell brush copolymers with poly(propylene oxide)-block-poly(ethylene oxide) side chains. *Macromolecules* 2016;49:5963–77.
- [305] Daniel WF, Xie G, Vatanikhah Varnosfaderani M, Burdyska J, Li Q, Nykypanchuk D. Bottlebrush-guided polymer crystallization resulting in supersoft and reversibly moldable physical networks. *Macromolecules* 2017;50:2103–11.
- [306] Stuart MAC, Huck WT, Genzer J, Müller M, Ober C, Stamm M, et al. Emerging applications of stimuli-responsive polymer materials. *Nat Mater* 2010;9:101–13.
- [307] Van Zee NJ, Adelizzi B, Mabesoone MF, Meng X, Aloï A, Zha RH, et al. Potential enthalpic energy of water in oils exploited to control supramolecular structure. *Nature* 2018;558:100–3.
- [308] Lee H-i, Pietrasik J, Sheiko SS, Matyjaszewski K. Stimuli-responsive molecular brushes. *Prog Polym Sci* 2010;35:24–44.
- [309] Liu F, Urban MW. Recent advances and challenges in designing stimuli-responsive polymers. *Prog Polym Sci* 2010;35:3–23.
- [310] Jochum FD, Theato P. Temperature- and light-responsive smart polymer materials. *Chem Soc Rev* 2013;42:7468–83.
- [311] Chen Y, Wang Z, Harn YW, Pan S, Li Z, Lin S, et al. Resolving optical and catalytic activities in thermoresponsive nanoparticles by permanent ligation with temperature-sensitive polymers. *Angew Chem Int Ed* 2019;58:11910–11917.
- [312] Choi J, Ruiz CR, Nesterov EE. Temperature-induced control of conformation and conjugation length in water-soluble fluorescent polythiophenes. *Macromolecules* 2010;43:1964–74.
- [313] Wang S, Liu C, Zhou H, Gao C, Zhang W. An efficient route to synthesize thermoresponsive molecular bottlebrushes of poly[o-aminobenzyl alcohol-graft-poly(N-isopropylacrylamide)]. *Polym Chem* 2017;8:1932–42.
- [314] Pietrasik J, Sumerlin BS, Lee RY, Matyjaszewski K. Solution behavior of temperature-responsive molecular brushes prepared by ATRP. *Macromol Chem Phys* 2007;208:30–6.
- [315] Li X, Shamsijazeyi H, Pesek SL, Agrawal A, Hammouda B, Verduzco R. Thermoresponsive PNIPAAm bottlebrush polymers with tailored side-chain length and end-group structure. *Soft Matter* 2014;10:2008–15.
- [316] Wilfert S, Iturmendi A, Henke H, Brüggemann O, Teasdale I. Thermoresponsive polyphosphazene-based molecular brushes by living cationic polymerization. *Macromolecular symposia: Wiley Online Library* 2014:116–23.
- [317] Zhang N, Luxenhofer R, Jordan R. Thermoresponsive poly(2-oxazoline) molecular brushes by living ionic polymerization: kinetic investigations of pendant chain grafting and cloud point modulation by backbone and side chain length variation. *Macromol Chem Phys* 2012;213:973–81.
- [318] Lutz JF. Polymerization of oligo(ethylene glycol)(meth) acrylates: toward new generations of smart biocompatible materials. *J Polym Sci, Part A: Polym Chem* 2008;46:3459–70.
- [319] Kang J-J, Jung FA, Ko C-H, Shehu K, Barnsley LC, Kohler F, et al. Thermoresponsive molecular brushes with propylene oxide/ethylene oxide copolymer side chains in aqueous solution. *Macromolecules* 2020;53:4068–81 487.
- [320] Zhao J, Mountrichas G, Zhang G, Pispas S. Thermoresponsive core-shell brush copolymers with poly(propylene oxide)-block-poly(ethylene oxide) side chains via a “grafting from” technique. *Macromolecules* 2010;43:1771–7.
- [321] Bejagam KK, Singh SK, Ahn R, Deshmukh SA. Unraveling the conformations of backbone and side chains in thermosensitive bottlebrush polymers. *Macromolecules* 2019;52:9398–408.
- [322] Yardley RE, Kenaree AR, Gillies ER. Triggering depolymerization: progress and opportunities for self-immolative polymers. *Macromolecules* 2019;52:6342–60.
- [323] Xiao Y, Li H, Zhang B, Cheng Z, Li Y, Tan X, et al. Modulating the depolymerization of self-immolative brush polymers with poly(benzyl ether) backbones. *Macromolecules* 2018;51:2899–905.
- [324] Neary WJ, Isais TA, Kennemur JG. Depolymerization of bottlebrush polypentenamers and their macromolecular metamorphosis. *J Am Chem Soc* 2019;141:14220–9.
- [325] Chen Y, Wang Z, He Y, Yoon YJ, Jung J, Zhang G, et al. Light-enabled reversible self-assembly and tunable optical properties of stable hairy nanoparticles. *Proc Natl Acad Sci* 2018;115:E1391–E1400.
- [326] Li X, Li B, He M, Wang W, Wang T, Wang A, et al. Convenient and robust route to photoswitchable hierarchical liquid crystal polymer stripes via flow-enabled self-assembly. *ACS Appl Mater Interfaces* 2018;10:4961–70.
- [327] Xu B, Qian H, Lin S. Self-assembly and photoinduced spindle-toroid morphology transition of macromolecular double-brushes with azobenzene pendants. *ACS Macro Lett* 2020;9:404–9.
- [328] Hu X, Chen F, Li N, Bai W, Bai R. One-pot strategy for preparation of photo- and chemo-cleavable polystyrene containing o-nitrobenzyl ester moieties. *Polym Degrad Stab* 2017;142:55–61.
- [329] Shibuya Y, Nguyen HV-T, Johnson JA. Mikto-Brush-arm star polymers via cross-linking of dissimilar bottlebrushes: synthesis and solution morphologies. *ACS Macro Lett* 2017;6:963–8.
- [330] Zhao H, Sterner ES, Coughlin EB, Theato P. o-Nitrobenzyl alcohol derivatives: opportunities in polymer and materials science. *Macromolecules* 2012;45:1723–36.
- [331] Lin W, Sun T, Xie Z, Gu J, Jing X. A dual-responsive nanocapsule via disulfide-induced self-assembly for therapeutic agent delivery. *Chem Sci* 2016;7:1846–52.
- [332] Henn DM, Lau CM, Li CY, Zhao B. Light-triggered unfolding of single linear molecular bottlebrushes from compact globular to wormlike nano-objects in water. *Polym Chem* 2017;8:2702–12.
- [333] Onbulak S, Rzaevyev J. Synthesis and one-dimensional assembly of cylindrical polymer nanoparticles prepared from tricomponent bottlebrush copolymers. *J Polym Sci, Part A: Polym Chem* 2017;55:3868–74.
- [334] Onbulak S, Rzaevyev J. Cylindrical nanocapsules from photo-cross-linkable core-shell bottlebrush copolymers. *Polym Chem* 2015;6:764–71.
- [335] Henn DM, Holmes JA, Kent EW, Zhao B. Worm-to-sphere shape transition of thermoresponsive linear molecular bottlebrushes in moderately concentrated aqueous solution. *J Phys Chem B* 2018;122:7015–25.
- [336] Mukumoto K, Averick SE, Park S, Nese A, Mpoukouvalas A, Zeng Y, et al. Phototunable supersoft elastomers using coumarin functionalized molecular bottlebrushes for cell-surface interactions study. *Macromolecules* 2014;47:7852–7.
- [337] Govindaiah P, Kim YS, Hong JK, Kim JH, Cheong IW. One-pot synthesis of grafted brush copolymers via a chain-growth radical/oxidative dual polymerization system. *RSC Adv* 2015;5:93717–23.
- [338] Yamamoto S-i, Pietrasik J, Matyjaszewski K. Temperature- and pH-responsive dense copolymer brushes prepared by ATRP. *Macromolecules* 2008;41:7013–20.
- [339] Li C, Ge Z, Fang J, Liu S. Synthesis and self-assembly of coil-rod double hydrophilic diblock copolymer with dually responsive asymmetric centipede-shaped polymer brush as the rod segment. *Macromolecules* 2009;42:2916–24.
- [340] Liu W, Liu Y, Zeng G, Liu R, Huang Y. Coil-to-rod conformational transition and single chain structure of graft copolymer by tuning the graft density. *Polymer* 2012;53:1005–14.
- [341] Zheng Z, Müllner M, Ling J, Müller AH. Surface interactions surpass carbon-carbon bond: understanding and control of the scission behavior of core-shell polymer brushes on surfaces. *ACS Nano* 2013;7:2284–91.
- [342] Senkum H, Gramlich WM. Cationic bottlebrush polymers from quaternary ammonium macromonomers by grafting-through ring-opening metathesis polymerization. *Macromol Chem Phys* 2020;221:1900476.
- [343] Zhang Z, He C, Chen X. Hydrogels based on pH-responsive reversible carbon-nitrogen double-bond linkages for biomedical applications. *Mater Chem Front* 2018;2:1765–78.
- [344] Wu Y-C, Bastakoti BP, Pramanik M, Yamauchi Y, Kuo S-W. Multiple hydrogen bonding mediates the formation of multicompartment micelles and hierarchical self-assembled structures from pseudo A-block-(B-graft-C) terpolymers. *Polym Chem* 2015;6:5110–24.
- [345] Allgaier J, Hövelmann CH, Wei Z, Staropoli M, Pyckhout-Hintzen W, Lühmann N, et al. Synthesis and rheological behavior of poly(1,2-butylene oxide) based supramolecular architectures. *RSC Adv* 2016;6:6093–106.
- [346] Staropoli M, Raba A, Hövelmann CH, Krutyeva M, Jr Allgaier, Appavou M-S, et al. Hydrogen bonding in a reversible comb polymer architecture: A microscopic and macroscopic investigation. *Macromolecules* 2016;49:5692–703.
- [347] Zhang T, Wang Y, Ma X, Hou C, Lv S, Jia D, et al. A bottlebrush-architected dextran polyprodrug as an acidity-responsive vector for enhanced chemotherapy efficiency. *Biomaterials science* 2020;8:473–84.
- [348] Nese A, Lebedeva NV, Sherwood G, Averick S, Li Y, Gao H, et al. pH-responsive fluorescent molecular bottlebrushes prepared by atom transfer radical polymerization. *Macromolecules* 2011;44:5905–10.
- [349] Xu H, Sun FC, Shirvanyants DG, Rubinstein M, Shabratov D, Beers KL, et al. Molecular pressure sensors. *Adv Mater* 2007;19:2930–4.
- [350] Lebedeva NV, Sun FC, Lee H-i, Matyjaszewski K, Sheiko SS. Fatal Adsorption” of brushlike macromolecules: high sensitivity of C-C bond cleavage rates to substrate surface energy. *J Am Chem Soc* 2008;130:4228–9.
- [351] James SL, Adams CJ, Bolm C, Braga D, Collier P, Friščić T, et al. Mechanochemistry: opportunities for new and cleaner synthesis. *Chem Soc Rev* 2012;41:413–47.

- [352] Yang D, Pang X, He Y, Wang Y, Chen G, Wang W, et al. Precisely size-tunable magnetic/plasmonic core/shell nanoparticles with controlled optical properties. *Angew Chem Int Ed* 2015;127:12259–64.
- [353] Li Y, Niu Z, Burdyska J, Nese A, Zhou Y, Kean ZS, et al. Sonication-induced scission of molecular bottlebrushes: Implications of the “hairy” architecture. *Polymer* 2016;84:178–84.
- [354] Peterson GI, Noh J, Bang K-T, Ma H, Kim KT, Choi T-L. Mechanochemical degradation of brush polymers: kinetics of ultrasound-induced backbone and arm scission. *Macromolecules* 2020;53:1623–8.
- [355] Bowser BH, Craig SL. Empowering mechanochemistry with multi-mechanophore polymer architectures. *Polym Chem* 2018;9:3583–93.
- [356] Peterson GI, Lee J, Choi T-L. Multimechanophore graft polymers: mechanochemical reactions at backbone–arm junctions. *Macromolecules* 2019;52:9561–8.
- [357] Polotsky A, Charlaganov M, Xu Y, Leermakers FA, Daoud M, Müller AH, et al. Pearl-necklace structures in core–shell molecular brushes: experiments, monte carlo simulations, and self-consistent field modeling. *Macromolecules* 2008;41:4020–8.
- [358] Yao K, Chen Y, Zhang J, Bunyard C, Tang C. Cationic salt-responsive bottle-brush polymers. *Macromol Rapid Commun* 2013;34:645–51.
- [359] Xu Y, Bolisetty S, Drechsler M, Fang B, Yuan J, Harnau L, et al. Manipulating cylindrical polyelectrolyte brushes on the nanoscale by counterions: collapse transition to helical structures. *Soft Matter* 2009;5:379–84.
- [360] Kutnyánszky E, Hempenius MA, Vancso GJ. Polymer bottlebrushes with a redox responsive backbone feel the heat: synthesis and characterization of dual responsive poly(ferrocenylsilane)s with PNIPAM side chains. *Polym Chem* 2014;5:771–83.
- [361] Sowers MA, McCombs JR, Wang Y, Paletta JT, Morton SW, Dreaden EC, et al. Redox-responsive branched-bottlebrush polymers for in vivo MRI and fluorescence imaging. *Nat Commun* 2014;5:5460.
- [362] Mah AH, Mei H, Basu P, Laws TS, Ruchhoeft P, Verduzco R, et al. Swelling responses of surface-attached bottlebrush polymer networks. *Soft Matter* 2018;14:6728–36.
- [363] Daniel WF, Burdyska J, Vatanikhah-Varnoosfaderani M, Matyjaszewski K, Paturel J, Rubinstein M, et al. Solvent-free, supersoft and superelastic bottle-brush melts and networks. *Nat Mater* 2016;15:183–9.
- [364] Vatanikhah-Varnoosfaderani M, Daniel WF, Everhart MH, Pandya AA, Liang H, Matyjaszewski K, et al. Mimicking biological stress-strain behaviour with synthetic elastomers. *Nature* 2017;549:497–501.
- [365] Vatanikhah-Varnoosfaderani M, Daniel WF, Zhushma AP, Li Q, Morgan BJ, Matyjaszewski K, et al. Bottlebrush elastomers: a new platform for freestanding electroactuation. *Adv Mater* 2017;29:1604209.
- [366] Liang H, Morgan BJ, Xie G, Martinez MR, Zhulina EB, Matyjaszewski K, et al. Universality of the entanglement plateau modulus of comb and bottlebrush polymer melts. *Macromolecules* 2018;51:10028–39.
- [367] Hu M, Xia Y, McKenna GB, Kornfield JA, Grubbs RH. Linear rheological response of a series of densely branched brush polymers. *Macromolecules* 2011;44:6935–43.
- [368] Dalsin SJ, Hillmyer MA, Bates FS. Linear rheology of polyolefin-based bottle-brush polymers. *Macromolecules* 2015;48:4680–91.
- [369] Iwawaki H, Inoue T, Nakamura Y. Rheo-optical study on dynamics of bottlebrush-like polymacromonomer consisting of polystyrene. *Macromolecules* 2011;44:5414–19.
- [370] Iwawaki H, Urakawa O, Inoue T, Nakamura Y. Rheo-optical study on dynamics of bottlebrush-like polymacromonomer consisting of polystyrene. II. Side chain length dependence on dynamical stiffness of main chain. *Macromolecules* 2012;45:4801–8.
- [371] Abbasi M, Faust L, Riaz K, Wilhelm M. Linear and extensional rheology of model branched polystyrenes: From loosely grafted combs to bottlebrushes. *Macromolecules* 2017;50:5964–77.
- [372] Dalsin SJ, Hillmyer MA, Bates FS. Molecular weight dependence of zero-shear viscosity in atactic polypropylene bottlebrush polymers. *ACS Macro Lett* 2014;3:423–7.
- [373] Haugan IN, Maher MJ, Chang AB, Lin T-P, Grubbs RH, Hillmyer MA, et al. Consequences of grafting density on the linear viscoelastic behavior of graft polymers. *ACS Macro Lett* 2018;7:525–30.
- [374] Li X, Iocozzia J, Chen Y, Zhao S, Cui X, Wang W, et al. From precision synthesis of block copolymers to properties and applications of nanoparticles. *Angew Chem Int Ed* 2018;57:2046–70.
- [375] Chang Y, Yoon YJ, Li G, Xu E, Yu S, Lu C-H, et al. All-inorganic perovskite nanocrystals with a stellar set of stabilities and their use in white light-emitting diodes. *ACS Appl Mater Interfaces* 2018;10:37267–76.
- [376] Zhang G, Tang S, Li A, Zhu L. Thermally stable metallic nanoparticles prepared via core-cross-linked block copolymer micellar nanoreactors. *Langmuir* 2017;33:6353–62.
- [377] Feng C, Pang X, He Y, Li B, Lin Z. Robust route to unimolecular core-shell and hollow polymer nanoparticles. *Chem Mater* 2014;26:6058–67.
- [378] Feng C, Pang X, He Y, Chen Y, Zhang G, Lin Z. A versatile strategy for uniform hybrid nanoparticles and nanocapsules. *Polym Chem* 2015;6:5190–7.
- [379] Xu H, Xu Y, Pang X, He Y, Jung J, Xia H, et al. A general route to nanocrystal kebabs periodically assembled on stretched flexible polymer shish. *Sci Adv* 2015;1:e1500025.
- [380] Yoon YJ, Chang Y, Zhang S, Zhang M, Pan S, He Y, et al. Enabling tailorable optical properties and markedly enhanced stability of perovskite quantum dots by permanently ligating with polymer hairs. *Adv Mater* 2019;31:1901602.
- [381] Chen Y, Yang D, Yoon YJ, Pang X, Wang Z, Jung J, et al. Hairy uniform permanently ligated hollow nanoparticles with precise dimension control and tunable optical properties. *J Am Chem Soc* 2017;139:12956–67.
- [382] Chen Y, Yoon YJ, Pang X, He Y, Jung J, Feng C, et al. Precisely size-tunable monodisperse hairy plasmonic nanoparticles via amphiphilic star-like block copolymers. *Small* 2016;12:6714–23.
- [383] He M, Pang X, Liu X, Jiang B, He Y, Snaith H, et al. Monodisperse dual-functional upconversion nanoparticles enabled near-infrared organolead halide perovskite solar cells. *Angew Chem Int Ed* 2016;55:4280–4.
- [384] Xu H, Pang X, He Y, He M, Jung J, Xia H, et al. An unconventional route to monodisperse and intimately contacted semiconducting organic-inorganic nanocomposites. *Angew Chem Int Ed* 2015;54:4636–40.
- [385] Jiang B, Pang X, Li B, Lin Z. Organic-inorganic nanocomposites via placing monodisperse ferroelectric nanocrystals in direct and permanent contact with ferroelectric polymers. *J Am Chem Soc* 2015;137:11760–7.
- [386] Zheng D, Pang X, Wang M, He Y, Lin C, Lin Z. Unconventional route to hairy plasmonic/semiconductor core/shell nanoparticles with precisely controlled dimensions and their use in solar energy conversion. *Chem Mater* 2015;27:5271–8.
- [387] Cui X, Chen Y, Zhang M, Harn YW, Qi J, Gao L, et al. Tailoring carrier dynamics in perovskite solar cells via precise dimension and architecture control and interfacial positioning of plasmonic nanoparticles. *Energy Environ Sci* 2020;13:1743–52.
- [388] Wang M, Pang X, Zheng D, He Y, Sun L, Lin C, et al. Non epitaxial growth of uniform and precisely size-tunable core/shell nanoparticles and their enhanced plasmon-driven photocatalysis. *J Mater Chem A* 2016;4:7190–9.
- [389] Huo D, Kim MJ, Lyu Z, Shi Y, Wiley BJ, Xia Y. One-dimensional metal nanostructures: from colloidal syntheses to applications. *Chem Rev* 2019;119:8972–9073.
- [390] Pan S, He L, Peng J, Qiu F, Lin Z. Chemical-bonding-directed hierarchical assembly of nanoribbon-shaped nanocomposites of gold nanorods and poly(3-hexylthiophene). *Angew Chem Int Ed* 2016;55:8686–90.
- [391] Pan S, Fu C, Zhu M, He L, Yang Y, Zhang H, et al. Hierarchical self-assembly of conjugated block copolymers and semiconducting nanorods into one-dimensional nanocomposites. *Macromolecules* 2018;51:8833–43.
- [392] Yuan J, Xu Y, Walther A, Bolisetty S, Schumacher M, Schmalz H, et al. Water-soluble organo-silica hybrid nanowires. *Nat Mater* 2008;7:718–22.
- [393] Müllner M, Yuan J, Weiss S, Walther A, Förtsch M, Drechsler M, et al. Water-soluble organo-silica hybrid nanotubes templated by cylindrical polymer brushes. *J Am Chem Soc* 2010;132:16587–92.
- [394] Yuan J, Lu Y, Schacher F, Lunkenbein T, Weiss S, Schmalz H, et al. Template-directed synthesis of hybrid titania nanowires within core-shell bishydrophilic cylindrical polymer brushes. *Chem Mater* 2009;21:4146–54.
- [395] Yuan J, Schacher F, Drechsler M, Hanisch A, Lu Y, Ballauff M, et al. Stimuli-responsive organosilica hybrid nanowires decorated with metal nanoparticles. *Chem Mater* 2010;22:2626–34.
- [396] Djalali R, Li S-Y, Schmidt M. Amphipolar core-shell cylindrical brushes as templates for the formation of gold clusters and nanowires. *Macromolecules* 2002;35:4282–8.
- [397] Müllner M, Lunkenbein T, Breu J, Caruso F, Müller AH. Template-directed synthesis of silica nanowires and nanotubes from cylindrical core-shell polymer brushes. *Chem Mater* 2012;24:1802–10.
- [398] Xie G, Ding H, Daniel WF, Wang Z, Pietrasik J, Sheiko SS, et al. Preparation of titania nanoparticles with tunable anisotropy and branched structures from core-shell molecular bottlebrushes. *Polymer* 2016;98:481–6.
- [399] Müllner M, Lunkenbein T, Schieder M, Gröschel AH, Miyajima N, Förtsch M, et al. Template-directed mild synthesis of anatase hybrid nanotubes within cylindrical core-shell-corona polymer brushes. *Macromolecules* 2012;45:6981–8.
- [400] Zhang M, Estournes C, Bietsch W, Müller A. Superparamagnetic hybrid nanocylinders. *Adv Funct Mater* 2004;14:871–82.
- [401] Ding H, Yan J, Wang Z, Xie G, Mahoney C, Ferebee R, et al. Preparation of ZnO hybrid nanoparticles by ATRP. *Polymer* 2016;107:492–502.
- [402] Zhang M, Drechsler M, Müller AH. Template-controlled synthesis of wire-like cadmium sulfide nanoparticle assemblies within core-shell cylindrical polymer brushes. *Chem Mater* 2004;16:537–43.
- [403] Yuan J, Drechsler M, Xu Y, Zhang M, Müller AH. Cadmium selenide nanowires within core-shell cylindrical polymer brushes: synthesis, characterization and the double-loading process. *Polymer* 2008;49:1547–54.
- [404] Zheng Z, Daniel A, Yu W, Weber B, Ling J, Müller AH. Rare-earth metal cations incorporated silica hybrid nanoparticles templated by cylindrical polymer brushes. *Chem Mater* 2013;25:4585–94.
- [405] Kravets VG, Kabashin AV, Barnes WL, Grigorenko AN. Plasmonic surface lattice resonances: a review of properties and applications. *Chem Rev* 2018;118:5912–51.
- [406] Huang K, Jacobs A, Rzaev J. De novo synthesis and cellular uptake of organic nanocapsules with tunable surface chemistry. *Biomacromolecules* 2011;12:2327–34.
- [407] Xie G, Lin X, Martinez MR, Wang Z, Lou H, Fu R, et al. Fabrication of porous functional nanonetwork-structured polymers with enhanced adsorption performance from well-defined molecular brush building blocks. *Chem Mater* 2018;30:8624–9.
- [408] Wu D, Nese A, Pietrasik J, Liang Y, He H, Kruk M, et al. Preparation of polymeric nanoscale networks from cylindrical molecular bottlebrushes. *ACS Nano* 2012;6:6208–14.

- [409] Fei H-F, Li W, Bhardwaj A, Nuguri S, Ribbe A, Watkins JJ. Ordered nanoporous carbons with broadly tunable pore size using bottlebrush block copolymer templates. *J Am Chem Soc* 2019;141:17006–14.
- [410] Pakula T, Zhang Y, Matyjaszewski K, Lee H-i, Boerner H, Qin S, et al. Molecular brushes as super-soft elastomers. *Polymer* 2006;47:7198–206.
- [411] Arrington KJ, Radzinski SC, Drummey KJ, Long TE, Matson JB. Reversibly cross-linkable bottlebrush polymers as pressure-sensitive adhesives. *ACS Appl Mater Interfaces* 2018;10:26662–8.
- [412] Slegieris R, Ondrusek BA, Chung H. Catechol-and ketone-containing multifunctional bottlebrush polymers for oxime ligation and hydrogel formation. *Polym Chem* 2017;8:4707–15.
- [413] Cai LH, Kodger TE, Guerra RE, Pegoraro AF, Rubinstein M, Weitz DA. Soft poly(dimethylsiloxane) elastomers from architecture-driven entanglement free design. *Adv Mater* 2015;27:5132–40.
- [414] Duncan TT, Chan EP, Beers KL. Maximizing contact of supersoft bottlebrush networks with rough surfaces to promote particulate removal. *ACS Appl Mater Interfaces* 2019;11:45310–18.
- [415] Sarapas JM, Chan EP, Rettner EM, Beers KL. Compressing and swelling to study the structure of extremely soft bottlebrush networks prepared by ROMP. *Macromolecules* 2018;51:2359–66.
- [416] Sheiko SS, Dobrynin AV. Architectural code for rubber elasticity: from super-soft to superfirm materials. *Macromolecules* 2019;52:7531–46.
- [417] Reynolds VG, Mukherjee S, Xie R, Levi AE, Atassi A, Uchiyama T, et al. Super-soft solvent-free bottlebrush elastomers for touch sensing. *Mater Horiz* 2020;7:181–7.
- [418] Mukherjee S, Xie R, Reynolds VG, Uchiyama T, Levi AE, Valois E, et al. Universal approach to photo-crosslink bottlebrush polymers. *Macromolecules* 2020;53:1090–7.
- [419] Tang M, Zheng P, Wang K, Qin Y, Jiang Y, Cheng Y, et al. Autonomous self-healing, self-adhesive, highly conductive composites based on a silver-filled polyborosiloxane/polydimethylsiloxane double-network elastomer. *J Mater Chem A* 2019;7:27278–88.
- [420] Chen Y, Guan Z. Self-healing thermoplastic elastomer brush copolymers having a glassy polymethylmethacrylate backbone and rubbery polyacrylate-amide brushes. *Polymer* 2015;69:249–54.
- [421] Scheutz GM, Lessard JJ, Sims MB, Sumerlin BS. Adaptable crosslinks in polymeric materials: resolving the intersection of thermoplastics and thermosets. *J Am Chem Soc* 2019;141:16181–96.
- [422] Montarnal D, Capelot M, Tournilhac F, Leibler L. Silica-like malleable materials from permanent organic networks. *Science* 2011;334:965–8.
- [423] Self JL, Sample CS, Levi AE, Li K, Xie R, de Alaniz JR, et al. Dynamic bottlebrush polymer networks: self-healing in super-soft materials. *J Am Chem Soc* 2020;142:7567–73.
- [424] Vatanikhah-Varnosfaderani M, Keith AN, Cong Y, Liang H, Rosenthal M, Sztucki M, et al. Chameleon-like elastomers with molecularly encoded strain-adaptive stiffening and coloration. *Science* 2018;359:1509–13.
- [425] Nian S, Lian H, Gong Z, Zhernenkov M, Qin J, Cai L-H. Molecular architecture directs linear-bottlebrush-linear triblock copolymers to self-assemble to soft reprocessable elastomers. *ACS Macro Lett* 2019;8:1528–34.
- [426] Clair C, Lallam A, Rosenthal M, Sztucki M, Vatanikhah-Varnosfaderani M, Keith AN, et al. Strained bottlebrushes in super-soft physical networks. *ACS Macro Lett* 2019;8:530–4.
- [427] Keith AN, Vatanikhah-Varnosfaderani M, Clair C, Fahimipour F, Dashtimoghadam E, Lallam A. Bottlebrush bridge between soft gels and firm tissues. *ACS Cent Sci* 2020;6:413–19.
- [428] Karimkhani V, Vatanikhah-Varnosfaderani M, Keith AN, Dashtimoghadam E, Morgan BJ, Jacobs M, et al. Tissue-mimetic dielectric actuators: Free-standing, stable, and solvent-free. *ACS Appl Polym Mater* 2020;2:1741–5.
- [429] von Freymann G, Kitaev V, Lotsch BV, Ozin GA. Bottom-up assembly of photonic crystals. *Chem Soc Rev* 2013;42:2528–54.
- [430] Runge MB, Bowden NB. Synthesis of high molecular weight comb block copolymers and their assembly into ordered morphologies in the solid state. *J Am Chem Soc* 2007;129:10551–60.
- [431] Sveinbjörnsson BR, Weitekamp RA, Miyake GM, Xia Y, Atwater HA, Grubbs RH. Rapid self-assembly of brush block copolymers to photonic crystals. *Proc Natl Acad Sci* 2012;109:14332–6.
- [432] Piunova VA, Miyake GM, Daeffer CS, Weitekamp RA, Grubbs RH. Highly ordered dielectric mirrors via the self-assembly of dendronized block copolymers. *J Am Chem Soc* 2013;135:15609–16.
- [433] Macfarlane RJ, Kim B, Lee B, Weitekamp RA, Bates CM, Lee SF, et al. Improving brush polymer infrared one-dimensional photonic crystals via linear polymer additives. *J Am Chem Soc* 2014;136:17374–7.
- [434] Guo T, Wang Y, Qiao Y, Yuan X, Zhao Y, Ren L. Thermal property of photonic crystals (PCs) prepared by solvent annealing self-assembly of bottlebrush PS-*b*-PrBA. *Polymer* 2020;194:122389.
- [435] Chae C-G, Yu Y-G, Seo H-B, Kim M-J, Grubbs RH, Lee J-S. Experimental formulation of photonic crystal properties for hierarchically self-assembled POS-S-bottlebrush block copolymers. *Macromolecules* 2018;51:3458–66.
- [436] Yu Y-G, Seo C, Chae C-G, Seo H-B, Kim M-J, Kang Y, et al. Hydrogen bonding-mediated phase transition of polystyrene and polyhydroxystyrene bottlebrush block copolymers with polyethylene glycol. *Macromolecules* 2019;52:4349–58.
- [437] Song D-P, Shahin S, Xie W, Mehravar S, Liu X, Li C, et al. Directed assembly of quantum dots using brush block copolymers for well-ordered nonlinear optical nanocomposites. *Macromolecules* 2016;49:5068–75.
- [438] Song D-P, Li C, Colella NS, Xie W, Li S, Lu X, et al. Large-volume self-organization of polymer/nanoparticle hybrids with millimeter-scale grain sizes using brush block copolymers. *J Am Chem Soc* 2015;137:12510–13.
- [439] Song DP, Li C, Colella NS, Lu X, Lee JH, Watkins JJ. Thermally tunable met-allo-dielectric photonic crystals from the self-assembly of brush block copolymers and gold nanoparticles. *Adv Opt Mater* 2015;3:1169–75.
- [440] Song D-P, Li C, Li W, Watkins JJ. Block copolymer nanocomposites with high refractive index contrast for one-step photonics. *ACS Nano* 2016;10:1216–23.
- [441] Song D-P, Zhao TH, Guidetti G, Vignolini S, Parker RM. Hierarchical photonic pigments via the confined self-assembly of bottlebrush block copolymers. *ACS Nano* 2019;13:1764–71.
- [442] Patel BB, Walsh DJ, Kim DH, Kwok J, Lee B, Guirionnet D, et al. Tunable structural color of bottlebrush block copolymers through direct-write 3D printing from solution. *Sci Adv* 2020;6:eaa7202.
- [443] Sauvé ER, Tonge CM, Hudson ZM. Organization of Chromophores into multi-block bottlebrush nanofibers allows for regulation of energy transfer processes. *Chem Mater* 2020;32:2208–19.
- [444] Scholes GD, Fleming GR, Olaya-Castro A, Van Grondelle R. Lessons from nature about solar light harvesting. *Nat Chem* 2011;3:763.
- [445] Jin X-H, Price MB, Finnegan JR, Boott CE, Richter JM, Rao A. Long-range exciton transport in conjugated polymer nanofibers prepared by seeded growth. *Science* 2018;360:897–900.
- [446] Xia J, Busby E, Sanders SN, Tung C, Cacciuto A, Sfeir MY, et al. Influence of nanostructure on the exciton dynamics of multichromophore donor-acceptor block copolymers. *ACS Nano* 2017;11:4593–8.
- [447] Zhu M, Kim H, Jang YJ, Park S, Ryu DY, Kim K, et al. Toward high efficiency organic photovoltaic devices with enhanced thermal stability utilizing P3HT-*b*-P3PHT block copolymer additives. *J Mater Chem A* 2016;4:18432–43.
- [448] Wang Y, Cui H, Zhu M, Qiu F, Peng J, Lin Z. Tailoring phase transition in poly(3-hexylselenophene) thin films and correlating their crystalline polymorphs with charge transport properties for organic field-effect transistors. *Macromolecules* 2017;50:9674–82.
- [449] Zhang R, Li B, Iovu MC, Jeffries-El M, Sauvé G, Cooper J, et al. Nanostructure dependence of field-effect mobility in regioregular poly(3-hexylthiophene) thin film field effect transistors. *J Am Chem Soc* 2006;128:3480–1.
- [450] Heinrich CD, Thelakkat M. Poly(3-hexylthiophene) bottlebrush copolymers with tailored side-chain lengths and high charge carrier mobilities. *J Mater Chem C* 2016;4:5370–8.
- [451] Yin X, Qiao Y, Gadinski MR, Wang Q, Tang C. Flexible thiophene polymers: a concerted macromolecular architecture for dielectrics. *Polym Chem* 2016;7:2929–33.
- [452] Wang Y, Shao F, Sauvé ER, Tonge CM, Hudson ZM. Self-assembly of giant bottlebrush block copolymer surfactants from luminescent organic electronic materials. *Soft Matter* 2019;15:5421–30.
- [453] Shao F, Wang Y, Tonge CM, Sauvé ER, Hudson ZM. Self-assembly of luminescent triblock bottlebrush copolymers in solution. *Polym Chem* 2020;11:1062–71.
- [454] Tang C, Dufour B, Kowalewski T, Matyjaszewski K. Synthesis and morphology of molecular brushes with polyacrylonitrile block copolymer side chains and their conversion into nanostructured carbons. *Macromolecules* 2007;40:6199–205.
- [455] Nataraj S, Yang K, Aminabhavi T. Polyacrylonitrile-based nanofibers-A state-of-the-art review. *Prog Polym Sci* 2012;37:487–513.
- [456] Yuan R, Kopeč M, Xie G, Gottlieb E, Mohin JW, Wang Z, et al. Mesoporous nitrogen-doped carbons from PAN-based molecular bottlebrushes. *Polymer* 2017;126:352–9.
- [457] Borchardt L, Zhu Q-L, Casco ME, Berger R, Zhuang X, Kaskel S, et al. Toward a molecular design of porous carbon materials. *Mater Today* 2017;20:592–610.
- [458] Jiang B, He Y, Li B, Zhao S, Wang S, He YB, et al. Polymer-templated formation of polydopamine-coated SnO₂ nanocrystals: anodes for cyclable lithium-ion batteries. *Angew Chem Int Ed* 2017;56:1869–72.
- [459] Zhao S, Sewell CD, Liu R, Jia S, Wang Z, He Y, et al. SnO₂ as advanced anode of alkali-ion batteries: inhibiting Sn coarsening by crafting robust physical barriers, void boundaries, and heterophase interfaces for superior electrochemical reaction reversibility. *Adv Energy Mater* 2020;10:1902657.
- [460] Zhou Q, Ma J, Dong S, Li X, Cui G. Intermolecular Chemistry in Solid Polymer Electrolytes for High-Energy-Density Lithium Batteries. *Adv Mater* 2019;31:1902029.
- [461] Barteau KP, Wolffs M, Lynd NA, Fredrickson GH, Kramer EJ, Hawker CJ. Allyl glycidyl ether-based polymer electrolytes for room temperature lithium batteries. *Macromolecules* 2013;46:8988–94.
- [462] Xue Z, He D, Xie X. Poly(ethylene oxide)-based electrolytes for lithium-ion batteries. *J Mater Chem A* 2015;3:19218–53.
- [463] Zhang H, Li C, Piszcz M, Coya E, Rojo T, Rodriguez-Martinez LM, et al. Single lithium-ion conducting solid polymer electrolytes: advances and perspectives. *Chem Soc Rev* 2017;46:797–815.
- [464] Sun J, Stone GM, Balsara NP, Zuckermann RN. Structure-conductivity relationship for peptoid-based PEO-mimetic polymer electrolytes. *Macromolecules* 2012;45:5151–6.
- [465] Ping J, Pan H, Hou PP, Zhang M-Y, Wang X, Wang C, et al. Solid polymer electrolytes with excellent high-temperature properties based on brush block copolymers having rigid side chains. *ACS Appl Mater Interfaces* 2017;9:6130–7.
- [466] Bates CM, Chang AB, Momčilović Na, Jones SC, Grubbs RH. ABA triblock brush polymers: synthesis, self-assembly, conductivity, and rheological properties. *Macromolecules* 2015;48:4967–73.

- [467] Bates CM, Chang AB, Schulze MW, Momčilović N, Jones SC, Grubbs RH. Brush polymer ion gels. *J Polym Sci, Part B: Polym Phys* 2016;54:292–300.
- [468] Geng Y, Dalhaimer P, Cai S, Tsai R, Tewari M, Minko T, et al. Shape effects of filaments versus spherical particles in flow and drug delivery. *Nat Nanotechnol* 2007;2:249–55.
- [469] Müllner M, Yang K, Kaur A, New EJ. Aspect-ratio-dependent interaction of molecular polymer brushes and multicellular tumour spheroids. *Polym Chem* 2018;9:3461–5.
- [470] Zhao P, Liu L, Feng X, Wang C, Shuai X, Chen Y. Molecular nanoworm with PCL core and PEO shell as a non-spherical carrier for drug delivery. *Macromol Rapid Commun* 2012;33:1351–5.
- [471] Zeng X, Wang L, Liu D, Liu D. Poly(L-lysine)-based cylindrical copolypeptide brushes as potential drug and gene carriers. *Colloid Polym Sci* 2016;294:1909–20.
- [472] Miki K, Kimura A, Oride K, Kuramochi Y, Matsuoaka H, Harada H, et al. High-contrast fluorescence imaging of tumors in vivo using nanoparticles of amphiphilic brush-like copolymers produced by ROMP. *Angew Chem Int Ed* 2011;50:6567–70.
- [473] Sankaran N, Rys AZ, Nassif R, Nayak MK, Metera K, Chen B, et al. Ring-opening metathesis polymers for biodetection and signal amplification: synthesis and self-assembly. *Macromolecules* 2010;43:5530–7.
- [474] Rajca A, Wang Y, Boska M, Paletta JT, Olankitwanit A, Swanson MA, et al. Organic radical contrast agents for magnetic resonance imaging. *J Am Chem Soc* 2012;134:15724–7.
- [475] Raffa P, Wever DAZ, Picchioni F, Broekhuis AA. Polymeric surfactants: synthesis, properties, and links to applications. *Chem Rev* 2015;115:8504–63.
- [476] Li Y, Christian-Tabak L, Fuan VLF, Zou J, Cheng C. Crosslinking-induced morphology change of latex nanoparticles: A study of RAFT-mediated polymerization in aqueous dispersed media using amphiphilic double-brush copolymers as reactive surfactants. *J Polym Sci, Part A: Polym Chem* 2014;52:3250–3259.
- [477] Xie G, Krysz P, Tilton RD, Matyjaszewski K. Heterografted molecular brushes as stabilizers for water-in-oil emulsions. *Macromolecules* 2017;50:2942–50.
- [478] Van Doremalen N, Bushmaker T, Morris DH, Holbrook MG, Gamble A, Williamson BN, et al. Aerosol and surface stability of SARS-CoV-2 as compared with SARS-CoV-1. *N Engl J Med* 2020;382:1564–7.
- [479] Gao Q, Yu M, Su Y, Xie M, Zhao X, Li P, et al. Rationally designed dual functional block copolymers for bottlebrush-like coatings: In vitro and in vivo antimicrobial, antibiofilm, and antifouling properties. *Acta biomater* 2017;51:112–24.
- [480] Zheng X, Zhang C, Bai L, Liu S, Tan L, Wang Y. Antifouling property of monothiol-terminated bottle-brush poly(methylacrylic acid)-graft-poly(2-methyl-2-oxazoline) copolymer on gold surfaces. *J Mater Chem B* 2015;3:1921–30.
- [481] Morgese G, Gombert Y, Ramakrishna SN, Benetti EM. Mixing poly(ethylene glycol) and poly(2-alkyl-2-oxazoline)s enhances hydration and viscoelasticity of polymer brushes and determines their nanotribological and antifouling properties. *ACS Appl Mater Interfaces* 2018;10:41839–48.
- [482] Xu B, Feng C, Hu J, Shi P, Gu G, Wang L, et al. Spin-casting polymer brush films for stimuli-responsive and anti-fouling surfaces. *ACS Appl Mater Interfaces* 2016;8:6685–92.
- [483] Sun X, Wu C, Hu J, Huang X, Lu G, Feng C. Antifouling surfaces based on fluorine-containing asymmetric polymer brushes: effect of chain length of fluorinated side chain. *Langmuir* 2018;35:1235–41.
- [484] Xu B, Liu Y, Sun X, Hu J, Shi P, Huang X. Semifluorinated synergistic nonfouling/fouling-release surface. *ACS Appl Mater Interfaces* 2017;9:16517–23.
- [485] Xu Y, Wang W, Wang Y, Zhu J, Uhrig D, Lu X, et al. Fluorinated bottlebrush polymers based on poly (trifluoroethyl methacrylate): synthesis and characterization. *Polym Chem* 2016;7:680–8.
- [486] Zheng W, Anzaldúa M, Arora A, Jiang Y, McIntyre K, Doerfert M, et al. Environmentally benign nanoantibiotics with a built-in deactivation switch responsive to natural habitats. *Biomacromolecules* 2020;21:2187–98.
- [487] Laroque S, Reifarth M, Sperling M, Kersting S, Klöpzig S, Budach P, et al. The impact of multivalence and self-assembly in the design of polymeric antimicrobial peptide mimics. *ACS Appl Mater Interfaces* 2020;12:30052–65.
- [488] Xia Y, Adibnia V, Huang R, Murschel F, Faivre J, Xie G, et al. Biomimetic bottlebrush polymer coatings for fabrication of ultralow fouling surfaces. *Angew Chem Int Ed* 2019;131:1322–8.
- [489] Chapman R, Gormley AJ, Herpoldt K-L, Stevens MM. Highly controlled open vessel RAFT polymerizations by enzyme degassing. *Macromolecules* 2014;47:8541–7.
- [490] Fan G, Graham AJ, Kolli J, Lynd NA, Keitz BK. Aerobic radical polymerization mediated by microbial metabolism. *Nat Chem* 2020;12:638–646.
- [491] Pang X, Wan C, Wang M, Lin Z. Strictly biphasic soft and hard Janus structures: synthesis, properties, and applications. *Angew Chem Int Ed* 2014;53:5524–38.
- [492] Xue ZH, Su H, Yu QY, Zhang B, Wang HH, Li XH, et al. Janus Co/CoP nanoparticles as efficient Mott-Schottky electrocatalysts for overall water splitting in wide pH range. *Adv Energy Mater* 2017;7:1602355.
- [493] Li C, Li Q, Kaneti YV, Hou D, Yamauchi Y, Mai Y. Self-assembly of block copolymers towards mesoporous materials for energy storage and conversion systems. *Chem Soc Rev* 2020;49:4681–736.
- [494] Shi Y, Duan P, Huo S, Li Y, Liu M. Endowing perovskite nanocrystals with circularly polarized luminescence. *Adv Mater* 2018;30:1705011.
- [495] Han W, Lin Z. Learning from “Coffee Rings”: ordered structures enabled by controlled evaporative self-assembly. *Angew Chem Int Ed* 2012;51:1534–46.
- [496] Li B, Zhang C, Jiang B, Han W, Lin Z. Flow-enabled self-assembly of large-scale aligned nanowires. *Angew Chem Int Ed* 2015;127:4324–8.
- [497] He M, Li B, Cui X, Jiang B, He Y, Chen Y, et al. Meniscus-assisted solution printing of large-grained perovskite films for high-efficiency solar cells. *Nat Commun* 2017;8:16045.
- [498] Yang HC, Hou J, Chen V, Xu ZK. Janus membranes: exploring duality for advanced separation. *Angew Chem Int Ed* 2016;55:13398–407.